Transpiration, Tracheids and Tree rings:

Linking stem water flow and wood formation in high-elevation conifers

---

Inauguraldissertation

zur

Erlangung der Würde eines Doktors der Philosophie

vorgelegt der

Philosophisch-Naturwissenschaftlichen Fakultät

der Universität Basel

von

Richard Louis Peters

von den Niederlanden

Birmensdorf (CH), 2018

Genehmigt von der Philosophisch-Naturwissenschaftlichen Fakultät
auf Antrag von

Prof. Dr. Ansgar Kahmen, Dr. Patrick Fonti and PD Dr. Günter Hoch

Basel, den 22. Mai 2018

Prof. Dr. Martin Spiess

Transpiration, Tracheids and Tree rings:

Linking stem water flow and wood formation
in high-elevation conifers

Richard Louis Peters

Thesis

Submitted in fulfilment of the requirements for the degree of doctor at the University of Basel
in the presence of the Thesis Committee
to be defended in public
on Thursday 31 of May 2018
at 4:15 p.m. in the Botanical Institute

Thesis committee

Faculty representative
Prof. Dr. Ansgar Kahmen
Department of Environmental Sciences – Institute of Botany
University of Basel

Thesis advisor
Dr. Patrick Fonti
Forest Dynamics – Dendrosciences
Swiss Federal Research Institute for Forest, Snow
and Landscape Research (WSL)

Co-referee
PD Dr. Günter Hoch
Department of Environmental Sciences – Institute of Botany
University of Basel

Other members
Dr. David C. Frank – The University of Arizona, USA
Prof. Dr. ir. Kathy Steppe – Ghent University, Belgium
Dr. Kerstin Treydte – WSL

Voor oom Piet

Richard L. Peters
Transpiration, Tracheids and Tree rings: Linking stem water flow and wood formation in high-elevation conifers
240 pages

PhD thesis, University of Basel, Basel, CH (2018)
With references, with a summary in English

Table of Contents

Preface

This thesis is about wood, or more specifically, about how tall woody plants (that we call trees) generate the material that is commonly found in tables, chairs and clogs, besides being valued as a carbon storage to mitigate climate change. Wood is undoubtedly one of the most versatile raw materials available to man. Yet, recent changes in climatic conditions raise many questions about the future fate of wood formation. How is wood formation or "xylogenesis" regulated by climate within our forests? Which mechanism is driving the formation and growth from a single woody cell to the characteristic annual tree rings? What effect will climatic change have on tree growth? This work addresses these questions and aims to provide a "mechanistic perspective" on wood formation.

To me it is fascinating how, although trees appear to be static elements within the landscape, the environment has a significant impact on their "movement". On a daily basis, the tree-stem dimensions shrink due to the usage of water from the stem-storage compartments during the day and swell or refill again during the night. Driven by transpiration, the transported water is used for photosynthesis to produce sugars, which are subsequently crucial for the formation of woody tissue. Additionally, the refilling of the water storage compartments during the evening provides the required turgor pressure for wood formation processes (i.e., wood cell enlargement) and contributes to the generation of the characteristic tree-ring structure. After having worked on long-term growth change patterns in tropical tree rings, I was highly interested to start this PhD and link these physiological mechanisms to explain tree-ring formation.

This thesis synthesises results that were generated in the framework of the four year lasting LOTFOR project, entitled; "Coupling stem water flow and structural carbon allocation in a warming climate: the Lötschental study case". It contains multiple manuscripts in preparation for, submitted to, or accepted in peer-reviewed scientific journals. Besides presenting these results, my goal is to provide the story around and beyond my research interest, namely; tree physiology and wood formation. In addition, I would like to provide readers with my reasoning and perspective on tree physiological research focussing on tree growth and ideally generate future research avenues.

This work (and the LOTFOR project in general) demanded persistence, creativity, goodwill, structure and a healthy dose of humour. It touched upon a large range of research topics, including ring-width studies, wood anatomy, tree hydraulics and mechanistic modelling. From studying highly detailed processes of wood formation, to large scale patterns in tree water use around the Northern Hemisphere. Searching for the mechanistic reasoning behind wood formation was challenging but rewarding, especially when linking wood formation at different temporal scales with tree hydraulics. This project provided me with the unique opportunity to explore many different research directions and further sharpen my research interests.

My current purpose as a researcher is to use models that provide a more physiological basis for wood formation and interplay between growth and climate. To put it bluntly, I want to challenge the current paradigm of "simple" linear climate versus tree-ring width relationships and bridge the gap between rings and the physiological mechanisms driving their formation. In my view, studying trees along environmental gradients is crucial to obtain this knowledge. Furthermore, incorporating a large range of high-resolution measurements on multiple physiological parameters and integrating them with long-term growth proxies should receive more attention. Instead of either viewing a tree as a giant thermometer or focussing on highly controlled and detailed physiological processes, we should combine these approaches into a more holistic scientific research field. I also firmly believe that although models are only simplifications of reality, they provide a vessel in which knowledge of biological processes can be preserved for, and transferred to, future generations. With this thesis, I (hope to) present ways of doing so and stimulate discussion on how to improve the cooperation between mechanistic modellers and the tree-ring community.

Birmensdorf (Switzerland), May 2018

Richard L. Peters

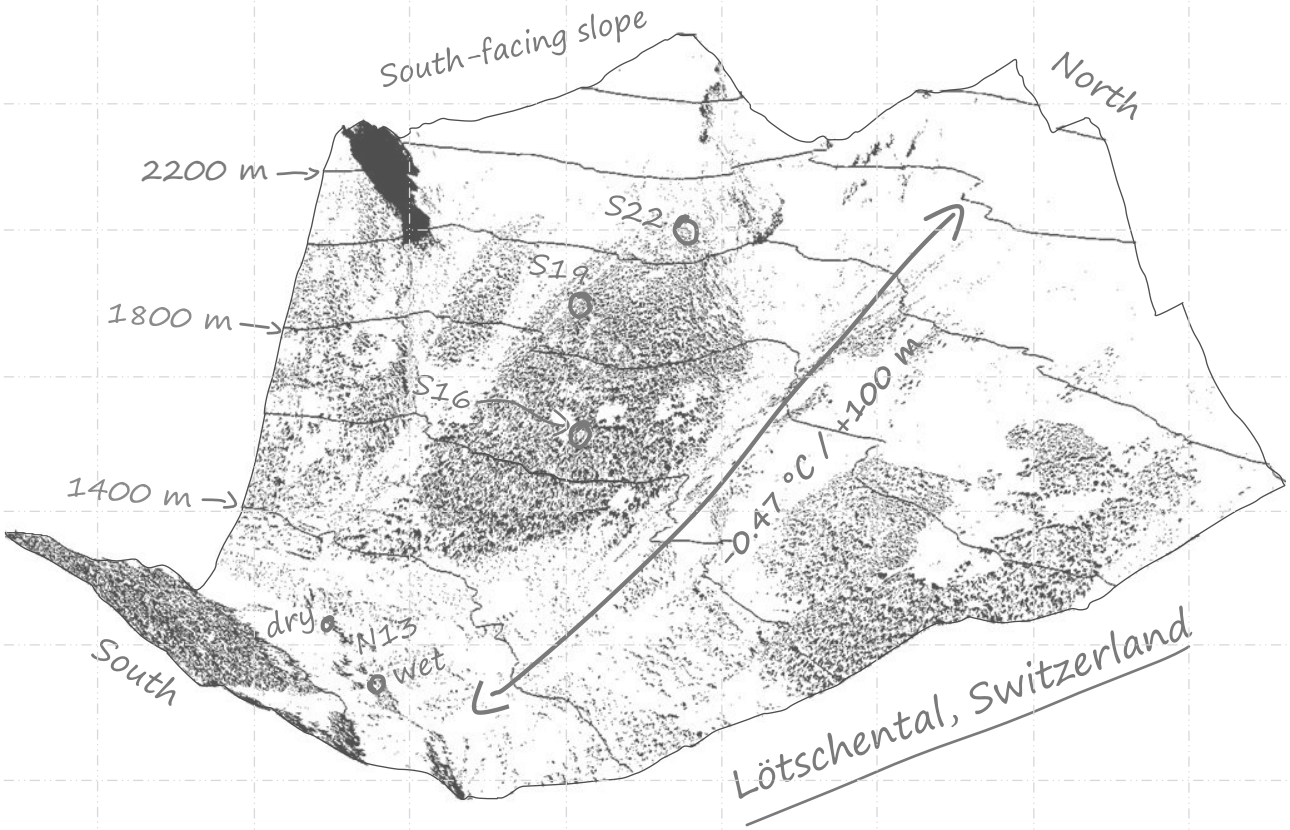
South-facing slope
North
2200 m
1800 m
1400 m
S22
S19
S16
-0.47 °C / +100 m
dry
A13
wet
South
Lötschental, Switzerland

Chapter 1

General introduction

Richard L. Peters

1.1 Interplay between tree growth and climate

Current predictions on climatic change indicate that the global air temperatures can increase with 2.6 to 4.8 °C by the end of the 21st century (compared to 1986-2005; Collins *et al*. 2013). Also, an increase in frequency, duration and magnitude of hot extremes on both daily and seasonal scales is expected (Collins *et al*. 2013). The carbon cycle has been recognized as a key component for better understanding these climate change patterns (Frank *et al*. 2010; Kirtman *et al*. 2013). Yet, uncertainties in these predictions are to a large extend related the capacity of the terrestrial biosphere to capture atmospheric carbon (Friedlingstein *et al*. 2006; Chapin *et al.* 2008). Investigating the effect of climate change on the productivity of the terrestrial vegetation is thus important for improving our understanding of the biogeochemical processes that shape the earth's climate (Bonan 2008).

"Trees are wonderful things" (McCarroll & Loader 2004), or at least remarkable life forms, especially when considering their unique capability of converting CO_2 into large quantities of woody tissue (Pan *et al*. 2011). Trees thus play a key role in the biosphere-atmosphere-climate feedback, as forests store ≈45% of terrestrial carbon within their woody tissue, contribute to ≈50% of terrestrial net primary production, and are a key component within the global hydrological cycle (Hutjes *et al*. 1998; Prentice *et al*. 2000; Myneni *et al*. 2001; Anderson *et al*. 2011). In other words, trees can be considered as the anchor points in the earth climate system where the carbon and the hydrological cycle are coupled. There has consequently been great incentive to investigate the effect of changing temperatures and water availability on tree functioning. For example, these climate change agents have been linked to changes in tree productivity (Boisvenue & Running 2006; Hember *et al*. 2012), mortality rates (Breshears *et al*. 2009; Allen *et al*. 2010; Anderegg *et al*. 2012), insect outbreak activity (Kurz *et al.* 2008; Johnson *et al*. 2010), disturbance dynamics (Bakkenes *et al*. 2002; Seidl *et al*. 2014), species distribution (Thuiller *et al*. 2008; Hanewinkel *et al*. 2013) and vegetative period (Peñuelas *et al*. 2009; Steltzer & Post 2009; Rigling *et al*. 2013).

More prominently, recent studies have focussed on annual tree-growth patterns occurring since the industrial revolution and described long-term positive or negative trends in stem growth, which have been described for both permanent sample plots (Pretzsch *et al.* 2014; Wu *et al.* 2014) and tree-ring studies (Villalba *et al*. 2012; Groenendijk *et al*. 2015; Girardin *et al.* 2016; Tei *et al.* 2017). Due to climate change a gradient from positive to negative effects would be expected

when moving from cold-humid to warm-dry growing conditions (e.g., Charney *et al.* 2016). Yet, no consensus exists on whether recent changes in climatic drivers will affect tree growth accordingly. This is highlighted by the fact that, despite warmer growing conditions and increased CO_2 concentrations, no clear patterns emerge from long-term trends in tree growth (e.g., large variability in detected trends in Figure 1.1). Additionally, mismatches between the climate sensitivity of forest productivity models and observed climate sensitivity derived from tree rings (e.g., Babst *et al.* 2013), stress that we still do not fully understand physiological mechanisms behind the climatic regulation of tree growth (Fatichi *et al.* 2014; Cuny & Rathgeber 2016).

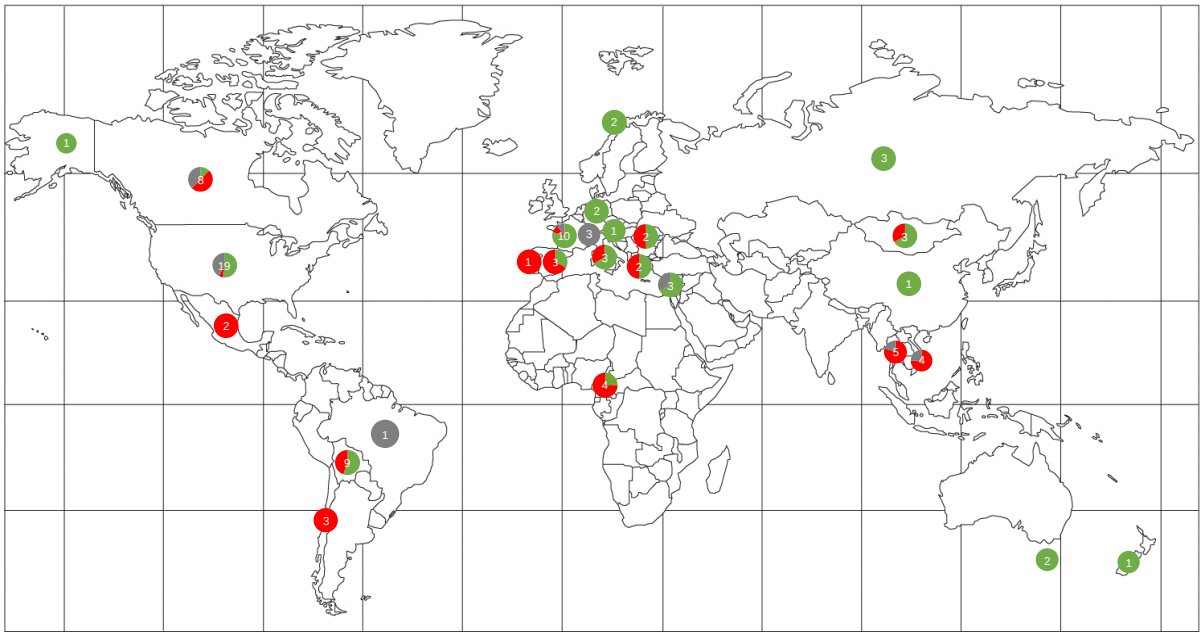

Figure 1.1 Review on detected long-term growth changes in tree species from tree-ring studies. The circle diagrams represent the number of species that have been investigated in a specific country. Red colour indicates a decreasing long-term growth trend, green an increase and grey no apparent change (adapted from Peters *et al.* 2015).

1.2 Drivers of cambial activity

When interested in carbon fixation performed by trees, we are concerned with the size and quantity of formed wood cells and eventually the longevity of the tree before the carbon respires back into the atmosphere due to decay (Körner 2017). Wood cell development stands at the physiological basis of tree diameter growth, where the structure of the cells dictate the carbon allocated in woody tissue. The cambium, the lateral meristematic tissue of a tree, is at the heart of xylem and phloem cell development (Kozlowski 1962; Rathgeber *et al.* 2016). The so-called

cambial zone can be defined as all cells capable of division (Wilson *et al*. 1966), including the phloem and xylem mother cells (Vaganov *et al*. 2006). While the phloem is a tissue mainly responsible for the transport of sugars produced by photosynthesis, ≈90% of the conifer wood volume consists of tracheid cells (Vaganov *et al*. 2006), which provide structural support and facilitate transport of water and nutrients (Kozlowski *et al*. 1997).

Due to their relatively simple anatomical structure, cambial activity studies have often focussed on conifers and the development of tracheids (e.g., Deslauriers & Morin 2005; Deslauriers *et al.* 2009; Rossi *et al*. 2012; Simard *et al.* 2013; Cuny *et al*. 2014; Cuny *et al*. 2015). Tracheid differentiation follows a sequence of cell division, enlargement, wall-thickening and programmed cell death or maturation (also referred to as xylogenesis; see Rathgeber *et al.* 2016). Enlargement is driven by water absorption in cellular vacuoles, where the resulting turgor pressure leads to cell expansion by stretching the thin primary cell walls (Lockhart *et al*. 1965; Abe *et al*. 1997). Subsequently, tracheids develop a more rigid secondary cell wall which are lignified for structural support. Maturation follows when autolysis of the nucleus and all cellular organelles occurs, so the cell can perform the function of water transport (Vaganov *et al.* 2006). Mature tracheids vary in their dimensions throughout the seasons, with relatively large radial diameters but thin cell walls in the beginning of the growing season (earlywood) and cells with small radial diameters and thicker cell walls at the end of the growing season (latewood; Schweingruber 1996).

How environmental drivers affect the cambial activity is still under debate, as two contrasting hypotheses exist, namely; source- or sink-limited growth regulation (White *et al*. 2016). Source-regulated growth assumes that glucose production via photosynthesis limits growth and its response to recent changes in CO_2 concentrations, increasing temperature and water availability dictates growth rates (Cramer *et al*. 2001; Anav *et al*. 2013; Friend *et al*. 2014). The prominent regulation of tree growth via changes in carbon source activity is however disputed by long-term free-air CO_2 enrichment experiments, tree-ring studies and modelling (Parent *et al*. 2010; Norby & Zak 2011; Peñuelas *et al*. 2011; van der Sleen *et al*. 2014). Some studies show that temperature-limited plants tend to reduce growth but increase carbon storage (Körner 2003; Woodruff & Meinzer 2011; Sala *et al*. 2012). This finding is supported by the minimum cambial activity threshold, which appears to be 5-6 °C, above the photosynthetic minimum of 0 °C (Saxe *et al*. 2001; Körner 2008). Such findings provide evidence that the direct control of carbon investment into tree tissue (or carbon sink) is under limitation

at lower temperatures (see Körner 2012), but also during droughts (see Fatichi *et al.* 2014). In other words, increasing carbon availability from changing photosynthetic activity does not necessarily translate into 1:1 increased growth, as the dynamics of growth show a different sensitivity to environmental conditions (Figure 1.2). In this case, temperature can directly influence metabolic processes, or affect hydraulic pressure needed for cell enlargement, determining the potential growth rate of woody tissue (Fatichi *et al.* 2014). This evidence supports the need for investigating the direct interaction between environment and cambial activity for understanding and modelling tree growth (Fonti & Jansen 2012; Fatichi *et al.* 2014; Hayat *et al.* 2017).

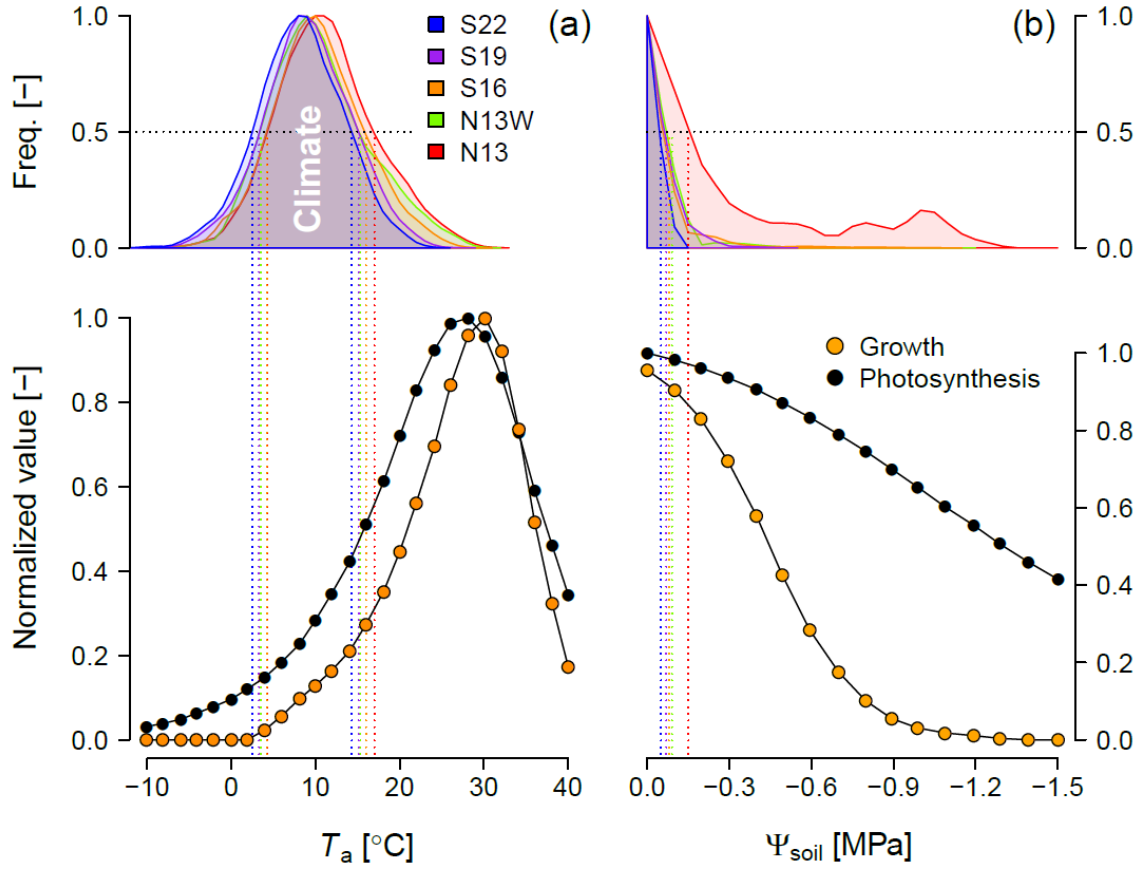

Figure 1.2 Growth vs. photosynthesis dynamics against increasing air temperature (T_a; a) and drought or soil water potential (ψ_{soil}; b). The lower panels show normalized growth and photosynthesis responses derived from Fatichi *et al.* (2014), who hypothesised these responses based on apical meristem growth. The offset between photosynthesis is especially apparent at lower T_a and more negative ψ_{soil}. As a reference, the upper panels provide the frequency of occurring environmental conditions in the Lötschental high-elevation sample plots (King *et al.* 2013a), derived from hourly measurements from 2008-2015 (see section 1.7). Especially the highest elevation site (S22; south-facing slope at 2200 m above sea level), appears to fall in the range where there is a large difference between photosynthetic activity and growth. Also, the dry site at the valley bottom (N13; north-facing slope at 1300 m a.s.l.) in contrast to a wet site (N13W) shows drought conditions where growth is impaired, while photosynthesis appears less affected.

1.3 Turgidity and tree hydraulics

A tree does not transport water from root to leaf solely as a resource for sugar production. They tightly regulate the internal water transport to perform multiple tasks, which include regulating turgidity (or pressure exerted on the cell walls of plant cells). The regulation of turgor within the cambial zone is particularly important for the initiation of cell enlargement and thus plays a central role as a regulating mechanism of sink-limited growth processes (as discussed by Fatichi *et al*. 2014).

The process of wood cell enlargement is best described by the Lockhart (1965) model, presuming the initiation and enlargement rate are largely regulated by turgor pressure (i.e., a positive water pressure potential). Within this model, the irreversible deformation of the cell wall and expansion of the cell compartment requires turgor above a threshold value. The turgor pressure dynamics are regulated by the daily occurring mismatch between atmospheric demand for water at the leaf surface and the supply of water from the roots, forcing woody plants to use and refill water-storage compartments in the bark (e.g., Zweifel & Häsler 2001; Zweifel *et al*. 2001). This causes typical diel cycles of bark and xylem shrinking during the day and swelling during the night (e.g., Steppe *et al*. 2005; King *et al*. 2013a). Based on this paradigm, the work by Gérard *et al*. (2001) was among the first to simulate the importance of stem and root diameter variation in woody plants and offers a basis for integrating water-storage dynamics and diameter growth.

Both turgor regulation and production of carbohydrates are tightly linked to the way a tree regulates the flow of water through the soil-plant-atmosphere continuum. As higher fluxes of water molecules exit the leaf during gas exchange compared to the fixation of carbon molecules (Nobel 2009), strong selective pressure has caused trees to develop specialized ways to regulate their internal hydraulics (Brodribb *et al*. 2014; Anderegg *et al*. 2016). Besides anatomical adjustments (Bouche *et al*. 2014; Anderegg 2014), stomatal regulation has been identified as a key mechanism for controlling water losses under changing environmental conditions (Hetherington & Woodward 2003; Buckley 2005; Lin *et al*. 2015). When considering the importance of turgidity in initiating cell enlargement, elucidating stomatal conductance dynamics is thus crucial for our mechanistic understanding of tree growth.

Regulation of stomatal conductance has been of central interest for explaining transpiration from the single leaf, to the tree- and forest-stand level (e.g., Jarvis 1976; Tuzet *et al*. 2003; Damour *et al*. 2010; Buckley & Mott 2013; Verhoef & Egea 2014; Klein 2014). Due to the size of a tree, stomatal conductance is often derived from sap flow measurements, as it is difficult to measure conductance on a leaf level and properly upscale this to the entire canopy (Arneth *et al*. 1996; Granier *et al*. 1996; Ewers & Oren 2000; Chang *et al*. 2014; Wieser *et al*. 2014). Sap flow is mainly measured with heat-based sap flow methods applied at the tree-stem level, which have provided estimates on whole-tree water use behaviour across a wide range of spatio-temporal scales (e.g., Swanson 1994; Smith & Allen 1996; Wullschleger *et al*. 1998; Lu *et al*. 2004; Kallarackal *et al*. 2013, Van de Wal *et al*. 2015). Yet, many challenges persist with the application of sap flow methods, especially in terms of translating the temperature signal, measured with thermal dissipation probes, into sap flux density or amount of transpired water (Köstner *et al*. 1998; Lu *et al*. 2004). Nonetheless, when carefully applied, these methods can provide crucial information for explaining stomatal behaviour and inferring mechanisms of wood formation patterns at high temporal resolutions (Steppe *et al*. 2015).

1.4 Tree growth modelling paradigms

Due to the complex nature of tree physiological processes, models are necessary to link complex hydraulic processes to wood formation. Since the 1950s it is clear that plant models are useful tools to better understand the complex nature of plant growth (e.g., De Wit 1959; Tardieu 2010). Various classes of models have shown to be crucial in describing and predicting the interaction between the environment, variability in tree growth, forest productivity and other tree-atmosphere interactions. Yet, the inability of these efforts to unravel long-term growth trends detected in tree-ring data and discrepancies between model results and empirical data (Cramer *et al*. 2001; Friedlingstein *et al*. 2006; Frank *et al*. 2010; Beer *et al*. 2010; Babst *et al*. 2013), indicates that significant progress is still needed to improve our modelling performance.

One class of models, the dynamic global vegetation models (DGVMs), can simulate fundamental mechanisms of photosynthesis (i.e., source-driven growth), water fluxes, nutrient allocation, competition and energy transport at the plant functional type level (Cramer *et al.* 2001). DGVMs can operate on large spatial scales, although being among the coarser growth models. This is reflected in their use of simple allocation rules for a limited number of vegetation types, instead of

including mechanistic formulations of sink-limited growth response (i.e., cambial activity) to environmental change (Fatichi *et al*. 2014).

A more detailed class of models includes the cambial growth models (CGMs), which simulate the process of cellular division, enlargement and maturation driven by the cambium (Shashkin & Vaganov 1993; Fritts *et al*. 1999; Downes *et al*. 2010). CGMs have been mainly validated for annual growth rates (i.e., ring-width time series) in Russia, North America and Australia (Anchukaitis *et al*. 2006; Evans *et al*. 2006; Drew *et al*. 2010), however the mechanistic connections to photosynthesis, water flow and other biological regulations are rarely considered. Additionally, the anatomical structure generated with these models still has to be validated against xylogenesis observations (Shishov *et al.* 2015).

The third class of models simulates the mechanistic dynamics of water fluxes and radial growth for individual trees, hence referred to as mechanistic whole-tree models (MWMs; see Steppe *et al*. 2005; Zweifel *et al*. 2006). MWMs link two main processes; (1) dynamic water transport within the tree and (2) stem diameter variations. The transport of water is modelled by using a simple van der Honert principle of flow, forces and resistance (van den Honert 1948). Stem diameter variation is determined by two processes; expansion/shrinkage and growth (irreversible expansion). Growth is assessed by using a model of cell wall expansion (Lockhart's 1965; Hsiao *et al.* 1976; Proseus & Boyer 2006), relating the expansion rate to cell turgor pressure (see Steppe *et al*. 2005). MWMs are promising tools for understanding sink-limited growth patterns, with the possibility to include source-driven mechanisms (or photosynthetic activity; see De Schepper & Steppe 2010). Although MWMs have been mainly applied on cultivated or juvenile trees under highly controlled conditions, or on low replicated mature trees without long-term monitoring (e.g., Verbeeck *et al.* 2007a; De Pauw *et al.* 2008; Steppe *et al*. 2008; De Swaef *et al.* 2012), their application should be extended to mature trees growing under natural conditions.

1.5 Bridging gaps with mechanistic modelling

MWMs are among the more advanced growth models, which at the most basic level use sap flow and dendrometer measurements to predict wood formation dynamics (Steppe *et al*. 2005). They thus show great potential in trying to answer how the environmental conditions dictate radial growth rates, independently from photosynthesis (see Figure 1.2). Additionally, these models are able to bridge temporal gaps between growth measurements (e.g., annual tree rings vs. weekly

xylogenesis observations) and link different tree physiological measurements (e.g., dendrometer and sap flow measurements). The large range of tree physiological measurements collected across the globe (see Figure 1.3) should thus stimulate the use of MWMs in the future. Below I provide examples on how MWMs could bridge gaps between different types of tree physiological measurements presented in Figure 1.3:

(a) MWMs can use tree hydraulics to simulate and mechanistically explain annual tree-ring patterns. Tree rings provide the longest records on annual tree growth (e.g., The International Tree-Ring Data Bank; Babst *et al*. 2017), in some cases stretching over millennia.
(b) High-resolution flux tower measurements record the H_2O and CO_2 exchange between the atmosphere and forest canopies for over 20 years now (e.g., FLUXNET; Chu *et al*. 2017). With MWMs both water fluxes and photosynthetic activity can be linked to address how these processes interact to form tree-ring structures.
(c) Dendrometers are used to measure a combination of a hydraulic and a growth signal on the individual tree level and have been applied over large temporal and spatial scales (e.g., DendroGlobal database; King *et al*. 2013a). Yet, disentangling these two signals is not easy (see Zweifel *et al*. 2016). MWMs are able to disentangle the signals and provide additional physiological parameters, like the hydraulic resistance, capacitance or stem water potential (Steppe *et al*. 2005).
(d) Wood anatomical measurements provide intra-annual resolution measurements of growth and can be used to define the start and end of the growing season and disentangle both cell enlargement and wall thickening processes (e.g., XCELL database; Rossi *et al*. 2008; Cuny *et al*. 2015). However, the collection of these measurements and data handling can be challenging and limits their application (see von Arx *et al*. 2016). Modelling these intra-annual growth patterns with measured sap flow data in MWMs is thus of great interest, as sap flow measurements have been widely collected (e.g., SAPFLUXNET; Poyatos *et al*. 2016).

If we can correctly replicate annual and intra-annual growth patterns by applying the sink-limited growth mechanisms included in MWMs, then we provide an incentive to include these mechanisms into the current global models (i.e., DGVMs) dealing with climate change-growth interactions. Notwithstanding, the application of these models is especially interesting at sites where there are

large discrepancies between photosynthetic activity and growth (either at temperature limited sites or sites with episodes of drought; see section 1.2). Applying MWMs on mountainous ecosystems (a temperature limited ecosystem; Körner 2012), where a large quantity of tree physiological measurements are present is thus of great interest to advance our knowledge on sink-limited growth processes.

1.6 Main objective of this study

Tree growth requires turgidity to exert the pressure necessary for cell expansion, assimilates to lengthen and thicken cell walls, warmth to allow the metabolic reactions to take place, and time for these processes to be completed. The general objective of this thesis is to supply a better mechanistic understanding on how these physiological and environmental factors interact in regulating wood formation and shaping tree rings in high-elevation conifer trees. We put specific focus on the coupling between stem hydrological cycles and structural carbon dynamics in the context of increasing temperature and water scarcity.

In this thesis I combine multi-annual records of both intra-annual wood formation data and high-resolution hydraulic measurements within MWMs to mechanistically explain inter- and intra-annual growth patterns. To simulate the impact of recent climate change on these mechanisms, we applied a space-for-time experimental setting (see section 1.7) within the Swiss Alps where we collected data along an elevation/thermal gradient and contrasting wet and dry sites. Additionally, I critically evaluate existing methodologies for measuring sap flow and handling large datasets of wood anatomical properties.

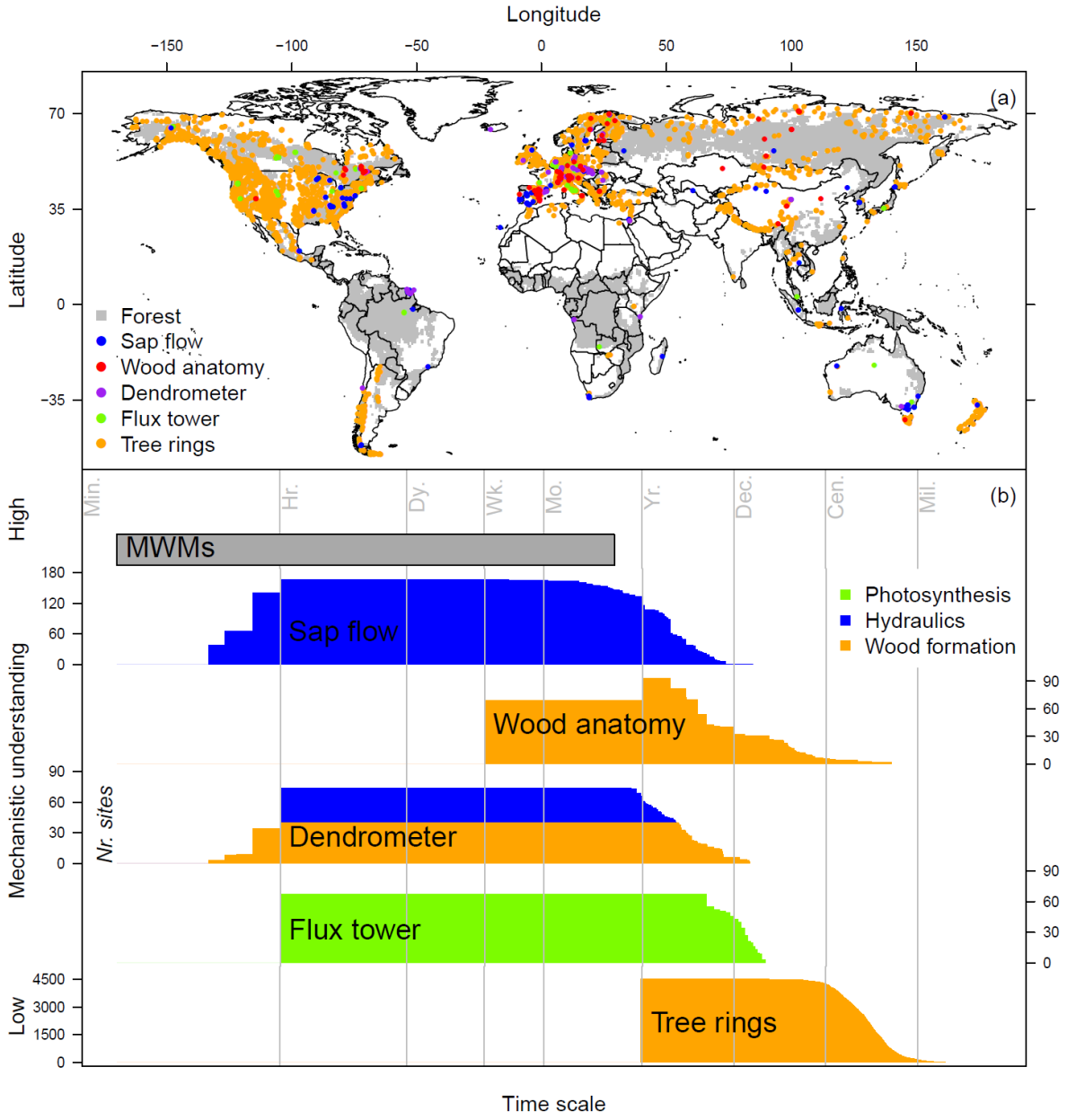

Figure 1.3 (a) Global distribution of sites where relevant tree physiological measurements were collected, including sap flow (SAPFLUXNET; Poyatos *et al.* 2016), wood anatomy (XCELL and GLOBOXYLO database), dendrometer (DendroGlobal database), flux tower (FLUXNET; Chu *et al.* 2017) and tree-ring width measurements (The International Tree-Ring Data Bank; Babst *et al.* 2017). The forest data has been extracted from the MODIS land cover data products (Forest= fractional forest cover >60%; Friedl *et al.* 2010). (b) The temporal extend of the datasets presented spatially in (a). Histograms on the availability of sites with the specific tree physiological measurements against a log-transformed time scale is provide in (b). The tree physiological measurements are grouped with colours into measurements addressing photosynthesis, tree hydraulics and wood formation. The grey lines indicate the time scale steps, including minutes, hours, days, weeks, months, years, decades, centuries and millennia. The histograms are horizontally ordered according to the general mechanistic understanding on the measured process.

1.7 Space-for-time experimental setting

When considering the climatic interaction with tree hydraulics and wood formation, environmental gradients in mountainous regions are of great scientific value. Environmental gradients provide a unique space-for-time experimental setting (see Moser *et al*. 2010), where changes in growth due to temperature and water availability (= time) are substituted by changes along the elevation transect and contrasting sites in soil moisture (= space; Körner *et al*. 2007).

The experimental setting is located within the Lötschental valley in the Swiss Alps (46°23′40″N, 7°45′35″E; Figure 1.4a). The valley is characterised by steep slopes (>60%) and mainly covered with a mixed forest of evergreen *Picea abies* (L.) Karst. and deciduous *Larix decidua* Mill. The valley is oriented along a northeast-southwest direction and connects to the Rhône Valley. The mean annual temperature in the valley is approximately 5 °C and mean annual precipitation exceeds 800 mm (Figure 1.4b), where the growing season temperature from 1975-2009 showed a significant positive trend of 0.6 °C per decade (data from MeteoSwiss surface observation network; see King *et al*. 2013b).

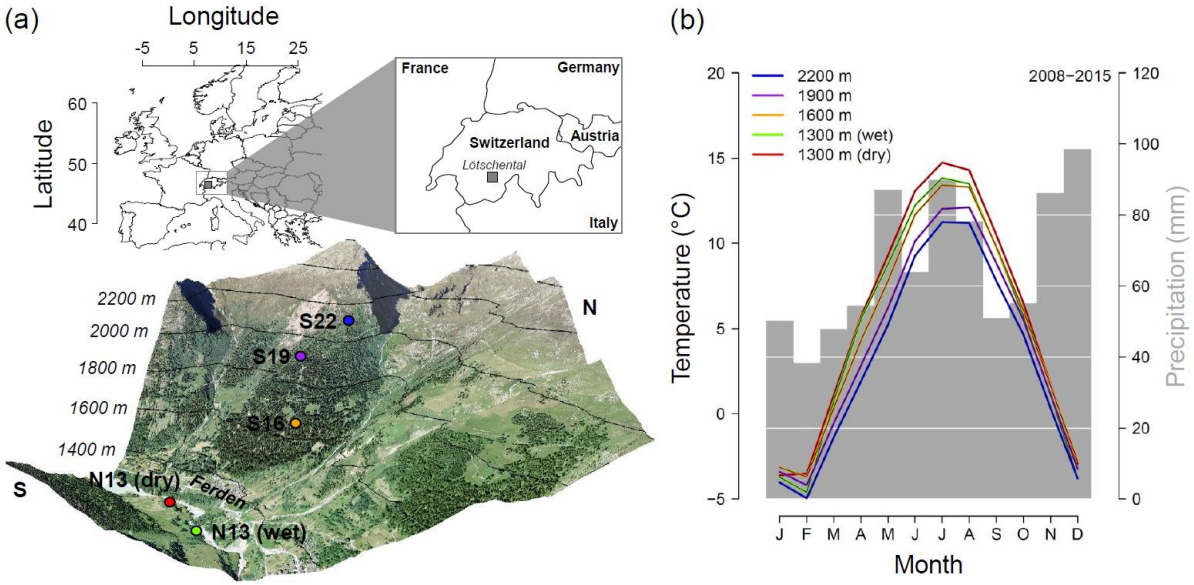

Figure 1.4 (a) Location and the space-over-time experimental setup within the Swiss Lötschental. At every 300 m a.s.l. a site was established (e.g., 2200 m a.s.l.= 22) on either the north- (= N) or south-facing (= S) slope. (b) Climate diagram providing the mean monthly air temperature measured at the sites (in °C) and the monthly precipitation obtained from the nine nearest climate stations for the period 2008-2015 (ranging from 6 to 43 km; Federal Office of Meteorology and Climatology MeteoSwiss). Mean daily precipitation data obtained from the stations were weighted according to the distance to the setup.

We continuously monitored five sites across a thermal and moisture gradient from April 2012 until October 2015, with a minimal temporal resolution of 15 minutes (see Figure 1.5 for examples of performed measurements). Four of these sites are situated along an elevational gradient on a south-facing slope with a 300 m interval from the valley bottom at 1300 m above sea level until the treeline at 2200 m a.s.l. (Figure 1.4a). At the treeline (S22), and close to the distribution limit of *L. decidua*, the mean annual growing season temperature is 8.3 °C (mean microclimatic measurement from 2012-2015, including May-October). At 1900 m a.s.l. (S19), a site close to the distribution limit of *P. abies*, has slight warmer conditions with mean annual growing season temperature of 9.2 °C. The two lower sites at 1600 (S16) and 1300 m a.s.l. (N13) experience both drier and warmer conditions, with a mean annual growing season temperature of 10.4 and 11.5 °C, respectively. Finally, a contrasting wet site was established at the valley bottom close to the Lonza river (N13W), with slightly cooler mean growing season conditions of 10.4 °C. The growing season temperature difference between the highest and lowest elevation site (of 3.2 °C) is of comparable magnitude to the expected warming in Switzerland by the end of the century (e.g., CH2011 2011), making this research highly relevant in the context of climate change.

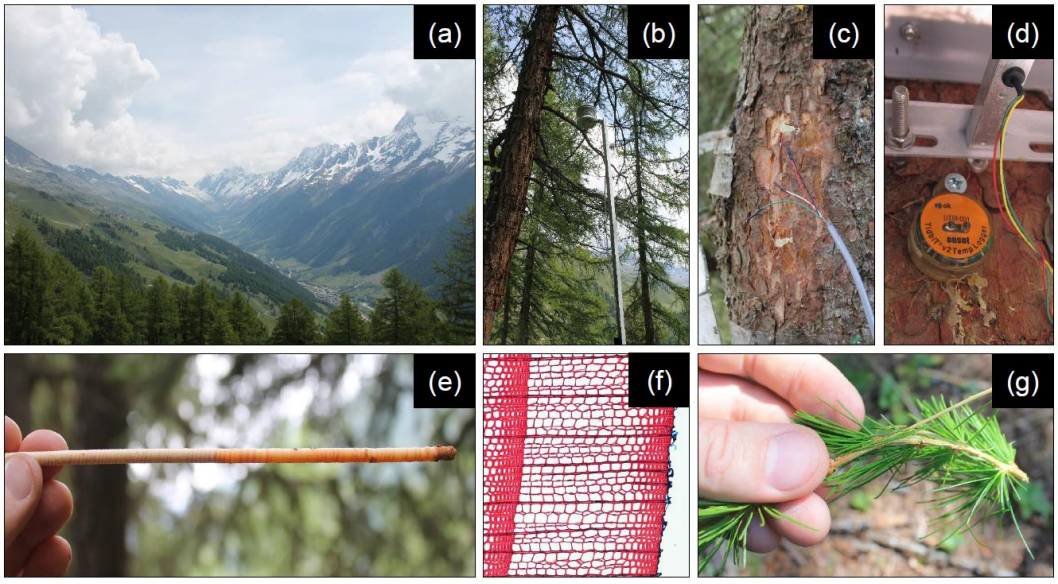

Figure 1.5 (a) Picture of the Lötschental valley, facing the Langgletscher. (b) Environmental conditions like air temperature and relative humidity were monitored at each site. (c) Thermal dissipation sap flow probes were installed on multiple trees per site to measure the water transport through the stem. (d) Point dendrometers recorded high-resolution stem radial changes on the same trees where sap flow probes were installed. (e) Wood increment cores were collected for measuring ring width. (f) Thin sections were produced from wood increment cores for applying quantitative wood anatomy, determining lumen size and cell wall thickness. (g) Twigs were collected on a weekly basis for measuring leaf water potential.

1.8 Thesis outline

Within this thesis I assess growth dynamics and tree hydraulics independently and integrate them into a mechanistic modelling framework. The first step when analysing tree-growth dynamics, is to assess how long-term growth variability within the Lötschental is affected by different climatic and non-climatic drivers. Using tree-ring width measurements, CHAPTER 2 of this thesis is dedicated to address climatic-growth relationships of the surveyed species compared to other drivers, such as insect outbreaks. For both species wood cores were sampled along the elevational gradient, and plots of a fixed size were sampled to upscale our measurements to forest biomass increment.

After collecting growth information on an inter-annual scale, large amounts of wood anatomical data had to be processed for the analysis on intra-annual growth patterns. CHAPTER 3 describes algorithms that aid in the processing of image based wood anatomical measurements. The algorithms are tested on a multitude of different conifer species and able to automatically produce positional information, needed for generating tracheidograms which are valuable for linking anatomical measurements to xylogensis observations.

Within CHAPTER 4 wood anatomical data is combined with xylogenesis observations collected along a ≈2000 m elevational gradient in Europe (including the Lötschental), to analyse cell enlargement and cell wall thickening processes against climatic conditions. This analysis includes 7 years of weekly cellular-based monitoring of wood formation for *L. decidua* and *P. abies* coniferous species across an 8 °C thermal gradient.

Besides analysing growth patterns, I critically evaluate the thermal dissipation method, which is used to measure sap flow, in CHAPTER 5. I quantify uncertainties generated by data-processing decisions on both sap flow data collected from the Lötschental and on datasets from across the Northern Hemisphere. Additionally, I perform a laboratory controlled calibration experiment to ensure the accuracy of our measurements.

In CHAPTER 6, I use thermal dissipation probe measurements to inspect hydraulic functioning of *L. decidua* and *P. abies* along the elevational gradient. More specifically, I examine the within- and between-species responses of sap flow derived stomatal conductance to micrometeorological changes. By analysing the stomatal response to environmental conditions, I am able to simulate sap flow and detect differences in stomatal behaviour between species.

CHAPTER 7 combines the inter- and intra-annual growth data (from tree rings and xylogenesis oberservations) and the hydraulic data (from sap flow measurements) within an MWM. Per individual, time-series of over 50,000 measurements are used to simulate hourly resolved growth dynamics (driven by turgor). First, we calibrate the model with weekly leaf water potential measurements to obtain hydraulic parameters and constrain the model. Second, I compare simulated turgor-driven growth to radial growth observations and assess models performance. The simulations are then used to analyse environmental conditions which are limiting turgor-driven growth.

Finally, CHAPTER 8 provides a synthesis of the thesis. In this chapter I connect the main findings of each chapter and discuss their implications. Additionally, I provide an overview of critical development points and potential future research avenues.

Acknowledgements

The author would like to thank Flurin Babst, Jesper Björklund, Patrick Fonti, Stefan Klesse, Ana Stritih and Anne Uilhoorn for providing valuable comments on earlier versions of this chapter.

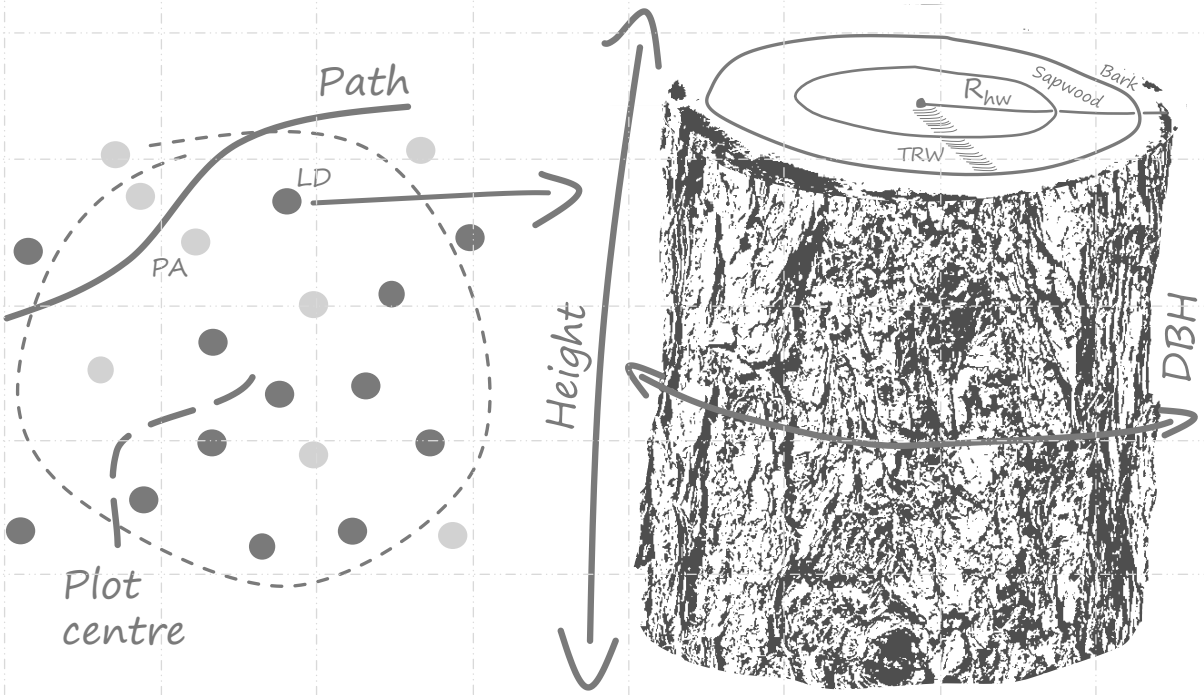
Path
LD
PA
Plot
centre
Height
Sapwood
Bark
R_{hw}
TRW
DBH

Chapter 2

Contribution of climate vs. larch budmoth outbreaks in regulating biomass accumulation in high-elevation forests

Richard L. Peters, Stefan Klesse, Patrick Fonti, David C. Frank
Published in Forest Ecology and Management

Abstract

Forest growth and biomass response to environmental change depends upon climatic, but also upon interactions with biotic drivers, such as insect outbreak activity. In this study we use tree-rings along a temperature gradient to assess the relative importance of climate versus altered larch budmoth (*Zeiraphera diniana*) outbreak cycles for forest biomass accumulation at high elevations. We established climate-growth relationships and performed outbreak-growth response analysis for >500 individuals from host (*Larix decidua*) and non-host trees (*Picea abies*) at different elevations (from 1300 to 2200 m a.s.l.) in the Swiss Alps. We quantified outbreak-induced reductions of absolute biomass increment and modelled effects of the recent absence of outbreaks. Our results reveal that average outbreaks reduced biomass accumulation by 1130 kg ha^{-1} y^{-1} during the four years after the event, having an equal or even greater impact on carbon sequestration than climate. Recent growth increases previously observed at the study sites are largely attributable to the outbreaks absence since 1981, suggesting that regular outbreaks have hampered host-trees from realising their growth potential for centuries. The presented impact analysis quantifies the importance of non-lethal insect activity on forest biomass dynamics, revealing the relevance of including such biotic drivers and their interactions with climate in models assessing the future productivity and carbon sink capacity of forests.

2.1 Introduction

Forest ecosystems are essential in regulating earth-atmosphere fluxes. By capturing on average ≈30% of anthropogenic CO_2 emissions within woody biomass, forests play a key role in dampening global warming (Friedlingstein *et al.* 2010; Pan *et al.* 2011). Hence, it is of great interest to know how climate change will affect the distribution, composition, and productivity of forest ecosystems and consequently their carbon storage capacity (Frank *et al.* 2010; Kirtman *et al.* 2013; Reitalu *et al.* 2013).

Forest inventory data, satellite imaging, and model simulations often show non-consistent patterns of forest net primary productivity and biomass responses to climate change (Fang *et al.* 2001; Nemani *et al.* 2003; Etzold *et al.* 2014; Wu *et al.* 2014). Some of this uncertainty is caused by challenges in adequately incorporating various drivers affecting forest productivity, including: management practises, forest age and structure (Lindner *et al.* 2010; Nabuurs *et al.* 2013; Pretzsch *et al.* 2014), nutrient and CO_2 fertilization (Hyvönen *et al.*

2007), wind throws and wildfires (Seidl *et al.* 2011; Trotsiuk *et al.* 2016), and insect activity (Hicke *et al.* 2012; Klapwijk *et al.* 2013). This array of physiological, ecological, biogeographical, and environmental controls on tree growth generates uncertainty in predicting the future role of European forests as a carbon sink (Ciais *et al.* 2008; Nabuurs *et al.* 2013).

Tree-ring investigations in European forests at high elevations have shown an increase in tree growth in the recent decades (Rolland *et al.* 1998; Büntgen *et al.* 2008). As tree growth at these locations is mainly limited by temperature (Büntgen *et al.* 2007; Babst *et al.* 2013), growth increases have usually been attributed to more favourable growing conditions due to the recent warming. Yet, detailed observations performed on high-elevation forests indicate that growth of *Larix decidua* trees has increased more than other species such as *Picea abies* (King *et al.* 2013a, b), questioning whether climate alone is responsible.

The larch budmoth (*Zeiraphera diniana* Guénée) outbreaks play an important role in reducing growth of the host *L. decidua* across the European Alps (Baltensweiler *et al.* 2008; Konter *et al.* 2015). This insect has an annual life cycle, with its larvae hatching in spring and feeding on the new flushes of needles as well as producing masses of webbing, causing severe defoliation of its host up to 3 years after an outbreak (Baltensweiler & Rubli 1999; Baltensweiler *et al.* 2008). The outbreaks occurred in more or less regular 9-year cycles over the past millennium, although they have not been observed after the 1980s (Esper *et al.* 2007; Büntgen *et al.* 2009). This change in outbreak regime has been attributed to changes in forest structure and species composition (Battipaglia *et al.* 2014), changes in nitrogen, water, starch and sugar content of foliage (Turchin *et al.* 2003; Asshoff & Hättenschwiler 2006), but also to increasing winter temperature (Kress *et al.* 2009; Johnson *et al.* 2010; Iyengar *et al.* 2016). This raises the question whether changing insect activity competes with the direct physiological effects of warming as a possible explanatory factor for the recent growth increase of *L. decidua*.

To assess future productivity of high-elevation forests, we analyse; i) the relative contribution of climatic and biotic drivers on tree growth and ii) the absolute impact of larch budmoth outbreaks on aboveground biomass accumulation. To understand the interaction between climatic and biotic drivers, we take advantage of the well documented outbreak history (see Esper *et al.* 2007) and the potential for reconstructing aboveground biomass dynamics with tree rings (see Babst *et al.* 2014a). We sampled co-occurring populations of budmoth hosts (*L. decidua*) and non-hosts (*Picea abies*) species along a steep elevational

gradient, which show different climate sensitivities (Moser *et al.* 2010; King *et al.* 2013b). This dataset allows us to disentangle growth responses caused by insect outbreaks and climate variation. We assessed climate-growth relationships and performed outbreak-growth response analysis to model their impact and importance. The quantification of the relative contribution of climate and insect activity on biomass accumulation offers a unique opportunity to improve our understanding on the future fate of high-elevation forest productivity.

2.2 Materials and methods

Study area and sampling design

Our study was conducted in the central Swiss Alps (Lötschental, 46°23′40″N 7°45′35″E; Figure 2.1a), where the occurrence of budmoth outbreaks (≈9-year cycles; as explained by Turchin *et al.* 2003) has been documented over the past millennium until 1981 (Esper *et al.* 2007; Büntgen *et al.* 2009). The valley is characterised by steep slopes (>60%) and covered by coniferous forests comprised of *Larix decidua* Mill. (the host species) and *Picea abies* (L.) Karst (hence referred to as *Larix* and *Picea*). The mean annual temperature in the valley bottom is approximately 5 °C and mean annual precipitation exceeds 800 mm, where the growing season temperature from 1975-2009 showed a significant positive trend of 0.6 °C per decade (data from MeteoSwiss surface observation network; see King *et al.* 2013b). The mean annual temperature difference between the tree line and valley bottom is ≈2.5 °C (measured at ≈1300 and 2200 a.s.l. from 2008 until 2015).

The study uses tree-ring measurements to construct a model of growth responses to both climate and larch budmoth outbreaks, and assess the development of biomass increment over time. For growth-response modelling, trees were randomly sampled at four elevations from the valley bottom to the upper tree line along both the north- and south-facing slopes near the town of Ferden (Figure 2.1a; at ≈1300 m, 1600 m, 1900 m, and 2200 m a.s.l.). In addition, we established three circular fixed plots (17 m radius) positioned at comparable elevations to address aboveground biomass increment (ABI), on the south- (Figure 2.1a; near Blatten, representative for the conditions at S22) and north-facing slope (near N19 and N13).

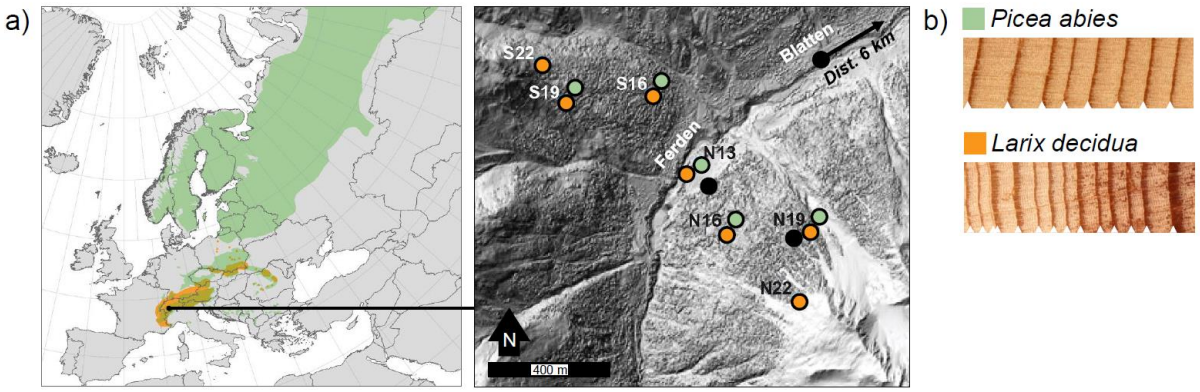

Figure 2.1 (a) Map indicating the centre of the Lötschental sampling area and the distribution range of the studied species (source: EUFORGEN). The north- and south-facing slope are presented with an N and S, while the elevation is specified with the numbers (e.g., 22 indicated the site at ≈2200 m in elevation). Fixed plots are indicated with black dots, where the direction to the Blatten plot on the south-facing slope at 2200 m is provided. (b) Examples of the wood structure for both species.

Tree sampling and ring-width measurements

Between 2007 and 2014, we sampled 973 wood cores from 285 *Larix* and 228 *Picea* trees (Table 2.1; Figure 2.1b). Along the two transects, trees larger than 10 cm diameter at breast height (DBH, 1.3 m) were pseudo-randomly sampled (i.e., irrespective of size and social status). For each site, trees were selected along the same elevation and within a horizontal distance of approximately 500 m from the research sites described in King *et al.* (2013a). For the fixed plots, all trees with a DBH greater than 5.6 cm, including dead trees and stumps, were measured in order to capture the population characteristics (Babst *et al.* 2014a; Nehrbass-Ahles *et al.* 2014). For 57% of the sampled trees we measured DBH and height (using a Vertex, Haglöf Sweden), while maximum bark thickness at breast height on two opposing sides of the stem was measured on 24% of the trees.

We used increment borers (Haglöf Sweden) to collect approximately two radial cores per tree stem at breast height and perpendicular to the slope to avoid reaction wood. Standard dendrochronological techniques were used to prepare, measure (see Schweingruber 1996; using either TSAP Rinntech Inc. or WinDENDRO Regent Instruments) and visually and statistically cross-date tree-ring width series collected from the transects and fixed plots (see Figure S2.1; COFECHA Holmes 1983).

Table 2.1 Main characteristics of the species and elevation specific tree-ring chronologies. *Mean inter-series correlation and mean sensitivity as produced by the program COFECHA (Holmes 1983). **Expressed population signal calculated for the CD standardized individual series by the R package dplR (Bunn *et al*. 2008).

Elevation	2200	1900		1600		1300	
Species	*Larix decidua*	*Picea abies*	*Larix decidua*	*Picea abies*	*Larix decidua*	*Picea abies*	*Larix decidua*
Individuals (radii)	101 (204)	118 (224)	72 (133)	67 (121)	77 (144)	43 (82)	35 (65)
Time span	1515 - 2014	1683 - 2014	1693 - 2014	1657 - 2014	1629 - 2014	1825 - 2013	1795 - 2012
Mean series length (min/max)	225 (25/497)	127 (19/331)	185 (23/322)	137 (25/358)	128 (19/379)	123 (22/187)	130 (55/213)
Mean DBH (min/max)	43.34 (13.4/76.7)	37.68 (5.8/74.0)	50.72 (8.4/80.4)	42.25 (16.4/79.5)	45.81 (11.5/85.4)	47.24 (14.0/92.0)	48.81 (17.6/76.6)
Mean age (min/max)	257 (26/551)	144 (20/331)	213 (24/326)	168 (31/461)	149 (24/379)	140 (22/187)	142 (68/213)
Mean inter-series correlation*	0.60	0.59	0.66	0.49	0.61	0.54	0.54
Mean sensitivity*	0.35	0.18	0.30	0.17	0.25	0.19	0.27
Mean EPS (1850-2011)**	0.98	0.96	0.99	0.92	0.98	0.90	0.91

Aboveground biomass assessment

The annual ABI was calculated for the fixed plots by using species and region specific volume and mass allometric relationships, as applied by the Swiss national forest inventory (NFI data; Brassel & Lischke 2001) and DBH-height and -bark thickness relationships established per elevation with measured data (Figure S2.2). Aboveground wood volume was calculated according to allometric equations (Etzold *et al.* 2014) that were simplified based on Kaufmann (2001) to require only DBH and height as input variables (instead of the additional diameter at 7 m height) by summing stem (V_{stem}), branches (V_{branch}) and twigs (V_{twig}) volume:

Larix

$$V_{stem} = 0.042 + 0.372 \cdot height \cdot DBH^2 - 0.027 \cdot height \cdot DBH^3 \quad \text{(Eq. 1)}$$

$$V_{branch} = V_{stem} \cdot e^{(-1.934 - 0.017 \cdot DBH)} / (1 + e^{(-1.934 - 0.017 \cdot DBH)}) \quad \text{(Eq. 2)}$$

$$V_{twig} = V_{stem} \cdot e^{(-4.940 + 0.062 \cdot DBH)} / (1 + e^{(-4.940 + 0.062 \cdot DBH)}) \quad \text{(Eq. 3)}$$

Picea

$$V_{stem} = 0.017 + 0.417 \cdot height \cdot DBH^2 - 0.083 \cdot height \cdot DBH^3 \quad \text{(Eq. 4)}$$

$$V_{twig} = V_{stem} \cdot e^{(-1.206 - 0.019 \cdot DBH)} / 1 + e^{(-1.206 - 0.019 \cdot DBH)} \quad \text{(Eq. 5)}$$

Picea does not have an equation for branch volume, as the definition requires branches to be >7 cm in diameter, otherwise they are classified as twigs. DBH was reconstructed using the cumulative radial tree-ring increment following Bakker (2005), including pith-offset estimates using the curvature of the last ring

(the concentric circles method, as described in Pirie *et al.* 2015). If the curvature was not visible, DBH excluding bark was used to estimate the missing distance. We used wood density values of 500 g/cm^3 for larch and 390 g/cm^3 for spruce to convert wood volume to biomass (Brändli 2010). Plot level ABI was derived from the sum of tree-growth increment of all individuals in the fixed plot and scaled up to kg ha^{-1}. For the analysis of the stand biomass accumulation and stand density developments we only considered the last ≈50 years of the reconstructed ABI, as we confirm no human intervention during this period. To address the absolute effect of outbreak absence we compared the mean ABI for the fixed plots over the periods 1961-1980 with outbreaks and 1990-2009 without outbreaks. We chose the 1990-2009 period to reduce the effect of the last budmoth outbreak of 1981 on growth and compared it to a period of equal length.

Growth-response modelling

We constructed elevation specific chronologies combining the north- and south-facing slope to perform growth-response modelling and disentangle the importance of climatic variables and budmoth outbreaks. We applied multiple detrending methods, including; regional curve standardization (RCS), basal area correction (BAC) and conservative detrending (CD), to verify that biases related to age/size removal were not artificially altering the tree-ring indices (Briffa & Melvin 2011; Bowman *et al.* 2013; Peters *et al.* 2015; Groenendijk *et al.* 2015). Detrending was performed using the dplR package in R (Bunn 2008; R software, version 3.2.00, R development core team 2013).

Due to prominent rapid increases in growth indices in RCS and BAC chronologies at 1300 and 1600 m, which might be caused by replication changes of fast and slow-growing trees (Figure S2.3), we decided to use the more conservative tree-specific detrending with linear or negative exponential curves (CD) to account for tree age/size effects and also correct for differences in growth level. A bi-weight robust mean chronology was constructed, including the stabilization of variance to minimize artefacts from changes in sample replication (Osborn *et al.* 1997; Frank *et al.* 2007). To further minimize the effect of possibly retained release effects and canopy dynamics on trends in tree-growth that might affect the climate-growth relationship in the CD time-series, we isolated the high-frequency signal of these chronologies by detrending the series with a cubic smoothing spline, with a 50% frequency cut-off at 10 years (henceforth spline-detrended; see Cook & Peters 1981).

We constructed tree-ring chronologies with an average of 73 individuals per elevation and species (total of 513). Sample replication ranged from 35 to 118 individual trees and was greater at higher elevations (Table 2.1). We found strong common signals between individuals from the same species and elevation, with a mean inter-series correlation ranging from 0.49 to 0.67. The final chronologies had at least 10 trees covering a period from 1850 till 2011 (Figure S2.1).

Climate-growth response analysis

Climatic datasets were obtained by interpolating daily values of MeteoSwiss weather stations from 1930 to 2011 down to a resolution of 100 m and then aggregating them into monthly mean time-series (Thornton *et al.* 1997). To extend the downscaled MeteoSwiss data back to 1850, we adjusted the mean and variance of an additional climate dataset (HISTALP; Auer *et al.* 2007) to the elevation specific time-series. For temperature, anomalies were calculated by subtracting the long-term (1930-2008) monthly means from the entire HISTALP time-series, while relative anomalies were calculated for precipitation (1930-2003, observed precipitation divided by monthly means). These anomalies were added to (or multiplied with, in the case of precipitation) the MeteoSwiss baseline climatology.

To test the short-term inter-annual climate signal of the spline-detrended chronologies we also spline-detrended the climate time-series, to ensure similarity in their frequency domains. Pearson correlations were performed over the 1850-2011 period after confirming normality of the residuals. We included seasonal climate aggregates from 1 to 12 months (from January prior to the growth year to current October). The climate correlation analysis for *Larix* was performed by excluding the years influenced by the budmoth, i.e., the outbreak years and the two subsequent years (≈1/3 of the data, leaving ≈110 years for the analysis). As outbreak events, we used the years reported in Esper *et al.* (2007), who reconstructed the outbreak history for the Lötschental based on ring width, wood anatomical and density observations from tree rings. The outbreak years were visually validated on our sampled material by observing narrow ring widths and thin latewood.

Subsequently, the three-month aggregation of climate (as it supplied the strongest and most consistent correlations) was used within a stepwise multiple regression using forward/backward elimination to identify the most important climatic drivers (see Venables and Ripley 2002). This selection process starts by including the predictor (i.e., the three month climate aggregate) with the highest goodness of fit and adds predictors, at each step considering whether the criterion (based on goodness of fit and model complexity) improves by removing a

previously added variable or keeping both previously selected and added variables. For the multiple regression analysis, we used the spline-detrended ring-width chronologies and 10-year spline-detrended climate data. We accounted for outbreaks by including an average growth response curve after an outbreak (see next paragraph) or excluding outbreak years and the two years after outbreak. Multiple regressions were performed using the R Commander package (Rcmdr; Hutcheson 2012). The final model variables were chosen based on Bayesian Information Criterion (BIC), as it appeared to be more conservative in selecting independent variables (Burnham & Anderson 2003). We addressed multicollinearity by excluding models with variance inflation factors larger than 10 (see Graham 2003; Chatterjee *et al*. 2012). With the individual seasonal climate correlations and the multiple regression analysis, we established a common set of climate variables relevant across the gradient.

Outbreak-growth response analysis

To model and verify the impact of the budmoth outbreaks on *Larix* tree growth, we performed an outbreak-growth response analysis. We aligned the CD individual specific tree-ring series to year since outbreak and divided the post-outbreak annual ring-width indices by the growth level of the 5 years prior to the outbreak, to reduce overlap with the effect from the previous outbreak cycle (occurring every ≈9 years). We calculated median outbreak-growth responses per site and years since outbreak and applied a smoothing (cubic smoothing spline with a 50% frequency cut-off at 10 years) to reduce climatically induced inter-annual variability in the response curves. We chose the cut-off at 10 years, as this spline rigidity resulted in a good fit of the raw median curve. For the final response curves, the original first four values after outbreak were used, after which we added the smoothed values until 13 years after outbreak (with values thereafter replaced by the value of year 13, due to data scarcity and the possible confounding climate effect of the post 1980 period). Within this analysis, we included 13 events (see Baltensweiler and Rubli 1999; Esper *et al.* 2007): 1856, 1864, 1880, 1888, 1908, 1915, 1923, 1937, 1945, 1954, 1963, 1972 and 1981 with an exception at 1300 m elevation, where our tree-ring data did not show signs of outbreaks prior to 1930.

Quantifying growth benefit of outbreak absence

Additive linear models (see Chambers 1992) were constructed in R to quantify the importance of climatic variables and budmoth activity on tree-growth variance within the chronologies. These growth-response models allowed for the

simulation of the impact of only climate, only outbreaks, and of both the components as determined from the previous climate and outbreak response assessments. In addition to using climatic parameters, we also simulated *Larix* growth as a function of the *Picea* growth (i.e., the non-host tree) with our budmoth response curves (see Table S2.1).

When including the outbreak components for the *Larix* data, we tested multiple response curves (Table S2.2) and finally used the elevation specific response curves. After fitting the model on the 1850-1981 period, a simulation was run until 2011, with and without continued outbreaks every 9 years. This simulation was used to quantify the growth "benefit" due to the absence of outbreaks as the mean percentage differences of the values obtained for the period 1990-2011 between the continued outbreak and the original model. Similarly, the unexplained growth change was quantified as the average percentage difference between the observed chronology and the fitted model.

2.3 Results

Aboveground biomass increment

We assessed long-term changes in aboveground biomass increment (ABI) for the fixed plots (Table 2.2). The plot at 1300 m was younger than the other plots and reached an average tree age of 150 at the year 2000. Stand density at this plot, as reconstructed from the live trees per year from the ring-width measurements (Figure 2.2), decreased between the early 20th century and 2011 from 550 to 420 trees ha^{-1}. However, we observed constantly increasing ABI from 1901 (decadal mean: 2716±279 kg ha^{-1} y^{-1}) to 1980 and a levelling off afterwards (mean: 6205±820 kg ha^{-1} y^{-1}). After the last reported outbreak in 1981, the plots at 1900 m and 2200 m showed a strong increase in mean ABI (Figure 2.3a), predominantly caused by increased growth of *Larix* (Figure 2.3b). Between 1950 and 1980 the ABI rates were relatively stable at high elevations, with 2291±476 kg ha^{-1} y^{-1} at 1900 m; and 1632±518 kg ha^{-1} y^{-1} at 2200 m (Figure 2.2). Until 1960, stand density was stable at both sites with mean tree ages above 150 years, after which a strong *Picea* recruitment occurred at 1900 m, causing an increase in stand density (Figure 2.2).

The three budmoth outbreaks in 1954, 1963, and 1972 had a dramatic impact on ABI for all three plots (Figure 2.2). Taking into account the standard deviations (sd) of the five years prior to the outbreak as a measure of regular inter-annual variability, the 1972 outbreak caused a >2 sd growth decrease in the 4 following years at 1300 m (where the stand basal area consists of 50% spruce and

50% larch), reducing ABI to 4347-4908 kg ha^{-1} (compared to the pre-outbreak mean of 6491 kg ha$^{-1)}$. In 1963, growth reduction exceeded the 2 sd threshold during the first three years after the outbreak (1100-2000 kg ha^{-1}), whereas in 1954 a strong negative impact (2.5 sd or 980 kg ha^{-1}) was restricted to the first year after the outbreak. Negative impacts on ABI could be observed at 1900 m, where in 1972 and 1963 growth was reduced by 1100 kg ha^{-1} (mean sd= 485 kg ha^{-1}) in the 3 years following the outbreak. The budmoth outbreak of 1963 caused a 3.5 sd departure at 2200 m, reducing the ABI from 2613 kg ha^{-1} to 1018 kg ha^{-1}. The other two outbreaks also reduced growth in the year of outbreak until at least the second year following the outbreak by 1000-1600 kg ha^{-1}, which is equivalent to 2-3.5 sd (mean sd= 476 kg ha^{-1}).

Table 2.2 Characteristics of the fixed plots.

Site code	Coordinates °N	Coordinates °E	Plot radius (m)	Plot size (m^2)	Basal area (m^2 ha^{-1})	Stem density (trees ha^{-1})	Dominant species # 1 (%)	Dominant species # 2 (%)
N13	46.39022	7.76325	17.0	907.92	76.70	420	*Larix decidua* (52)	*Picea abies* (48)
N19	46.38631	7.77371	17.0	907.92	47.27	540	*Larix decidua* (66)	*Picea abies* (34)
BLA	46.428609	7.823441	16.5	855.30	56.74	420	*Larix decidua* (87)	*Picea abies* (13)

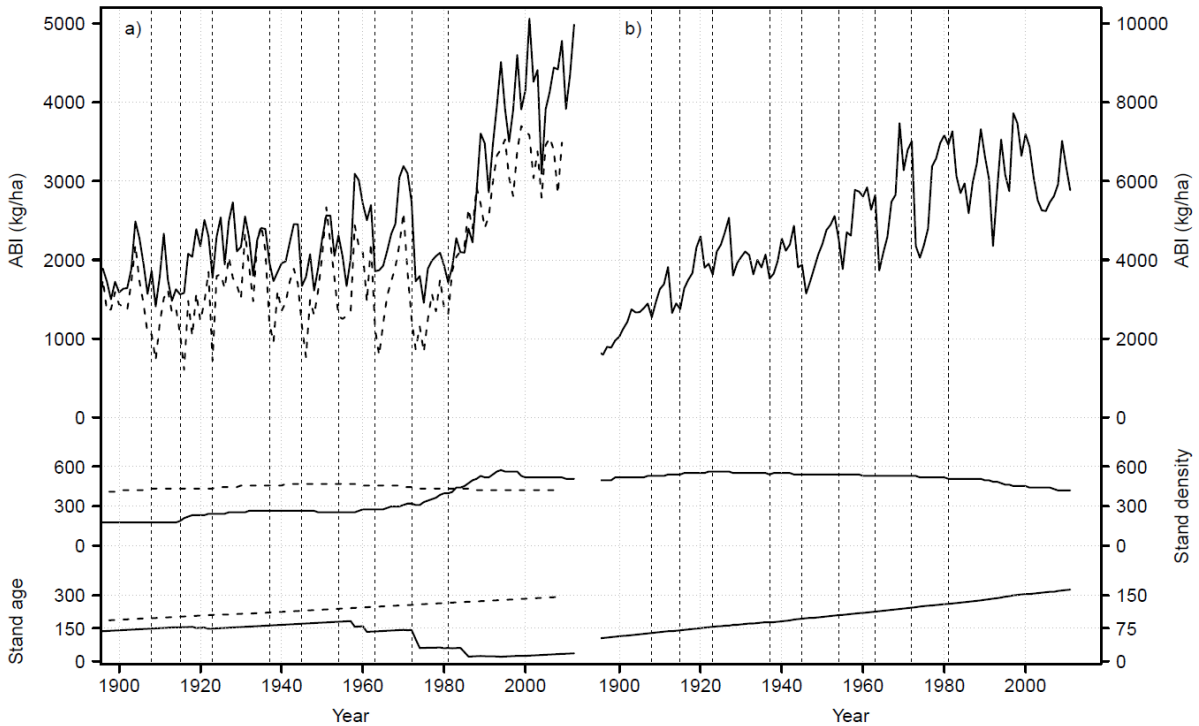

Figure 2.2 Stand level aboveground biomass increment for (a) the two high elevation plots at N19 (full lines) and Blatten (dashed lines) and (b) the low elevation plot N13. The panels below represent reconstructed stand density (mid panel) and stand age (lower panel). Stand age is defined as the mean age of all trees at a given year. Note the different y-axes in (a) and (b). The vertical dashed lines denote the reported budmoth outbreaks from the literature.

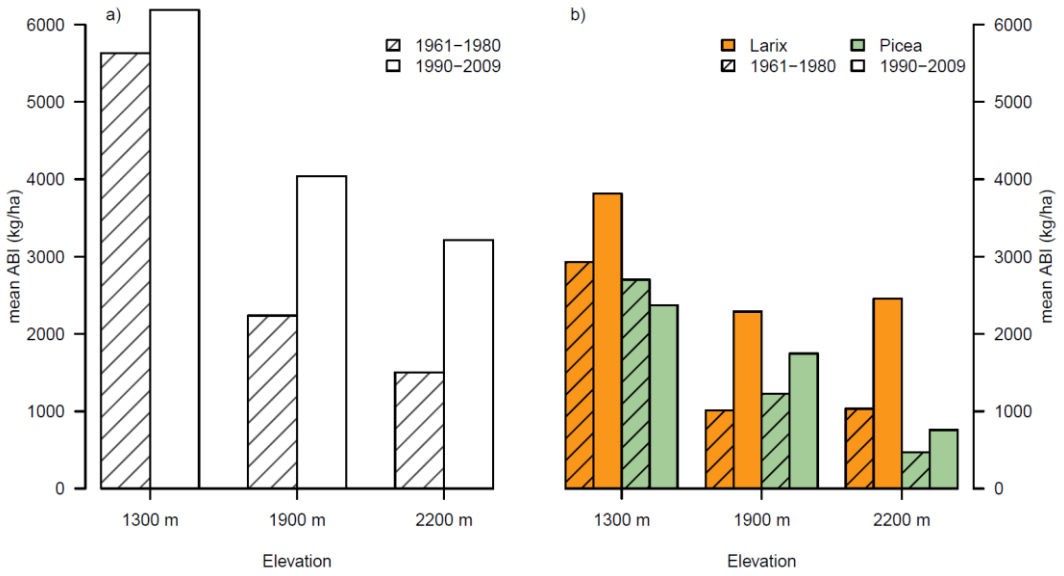

Figure 2.3 Mean aboveground biomass increments (ABI) for the fixed plots over the periods 1961-1980 with outbreak and 1990-2009 without outbreaks for both species together and b) separated.

Climate-growth response

Correlations between growth and temperature were stronger than precipitation (strongest r= -0.582, p <0.001 for previous year July-September temperature; and 0.441, p <0.001 for previous year July-September precipitation; Figure 2.4). High-elevation *Larix* growth was positively correlated with current year June-August temperature (2200 m: r= 0.413, p <0.001; 1900 m: r= 0.290, p <0.001). Towards the lower elevations, summer temperature correlations decreased notably and even became negative. Additionally, *Larix* showed to be responsive to previous year September-November temperature (mean r= 0.227, p <0.05). For *Picea* we found strong negative correlations with previous year July-September temperature (average across elevations r= -0.486, p <0.001). We also observed a strong positive relationship with previous year July-September precipitation across elevations (mean r= 0.306, p <0.01), although this variable is negatively collinear with temperature of the same period.

Climate variables selected according to the BIC (Table 2.3) within the multiple regression analysis were similar to the strongest correlations described above (Figure 2.4). Considering the common response across elevations, we selected for *Larix* current year June-August and previous year September-November temperature, and current year June-August precipitation. For *Picea,* previous year July-September and current year May-July temperature, and previous year October-December and current year May-July precipitation were selected. However, discrepancies are observed for *Picea* where previous year October-December precipitation was selected instead of previous year July-

September (Figure 2.4), which is likely due to co-linearity with temperature. Additionally, temperature of current year May-July was selected instead of current year June-August.

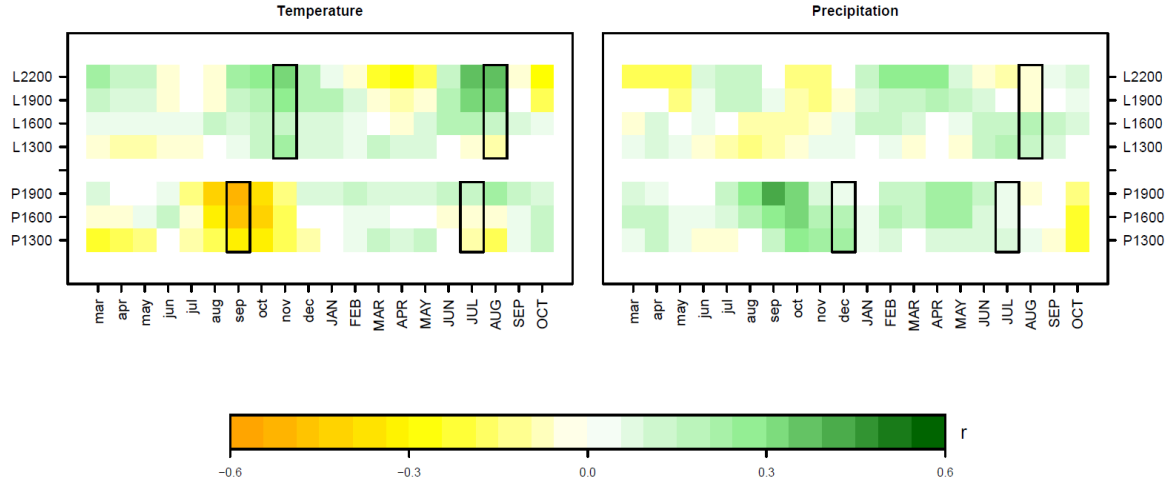

Figure 2.4 Pearson correlation coefficients (r) of chronologies along different elevations of *Picea* (P) and *Larix* (L) with temperature and precipitation. A three-month moving window was used, with monthly labels indicating the last month of the window. Lowercase month abbreviations represent previous year correlations with climate, while uppercase represents the current year. Black boxes indicate the windows selected as common climatic drivers along the elevational gradient, according to the multiple regression analysis.

Table 2.3 Selected climatic variables based on the forward/backward multiple regression analysis. Three-month average climate data was correlated with the elevation-specific chronologies of *Picea* and *Larix*. Outbreaks were included into the analysis by either removing the outbreak year and subsequent two years after outbreak or using an average negative growth response curve after an outbreak. For the three-month average, the last month is presented. Commonly occurring climatic variables where selected. *Selected climate variables and #highly overlapping with selected month in the final model.

Species	Outbreak	Elev. (m)	Selected variable (slope)							
Picea abies	None	1300	Int. (0.92)	Tsep (-0.04)*	Pdec (0.05)*	PJUL (0.09)*	Tmar (-0.01)	TJAN (0.02)	POCT (-0.05)	
		1600	Int. (0.88)	Tsep (-0.04)*	Pdec (0.05)*	TJAN (0.01)	TJUL (0.02)*	PJUL (0.08)*	POCT (-0.04)	PAPR (0.04)
		1900	Int. (0.81)	Tsep (-0.05)*	TJUL (0.04)*	Tdec (0.02)	PMAY (0.04)	Poct (0.06)	PJUL (0.06)*	PFEB (0.03)
Larix decidua	Removing up to two years after outbreak	1300	Int. (0.91)	Tnov (0.03)*	PJUL (0.11)#					
		1600	Int. (1.12)	Tnov (0.03)*	TSEP (0.04)	Psep (-0.09)				
		1900	Int. (1.05)	TAUG (0.07)*	Tnov (0.04)*	TAPR (-0.02)				
		2200	Int. (0.95)	TAUG (0.10)*	Tnov (0.04)*	TAPR (-0.03)	PMAR (0.078)	TNOV (-0.03)		
	Including negative outbreak response curves	1300	Int. (0.71)	Outbreak (0.24)	PAUG (0.13)*	Toct (0.03)#				
		1600	Int. (0.43)	Outbreak (0.63)	Toct (0.04)#					
		1900	Int. (0.28)	Outbreak (0.79)	Tnov (0.05)*	Tmar (0.03)				
		2200	Int. (0.54)	TAUG (0.13)*	Tnov (0.05)*	Outbreak (0.43)	TAPR (-0.03)	TSEP (-0.05)	PFEB (0.07)	

Budmoth impact analysis

Larix growth decreased on average by 19% for eight years following a budmoth event compared to ring-width index (RWI) of the five years prior to outbreak (Figure 2.5). When considering the biomass growth of a 150-year old *Larix* tree within the valley, this would result in an annual reduction of 1.6 kg ABI. We observed the strongest growth reductions in the first year after an outbreak followed by the second and third year (42%, 29% and 22% in RWI, respectively). Typically, it took eight years for the RWI to return to the pre-outbreak levels.

Site-specific impacts of budmoth outbreaks revealed strongest growth reductions at 1900 m (57% relative growth change in the first year following the outbreak), followed by trees at 1600 m. Outbreak events in 1854 and 1964 caused *Larix* trees at 1900 to experience the biggest decrease in growth. Outbreaks at 2200 m usually reduced growth less than at other sites, although often causing significant impacts at year 0 (23%; Figure 2.5). At 1300 m, growth recovery in the second year after outbreak was highly dampened compared to other sites, with similar growth levels as for the year following the outbreak.

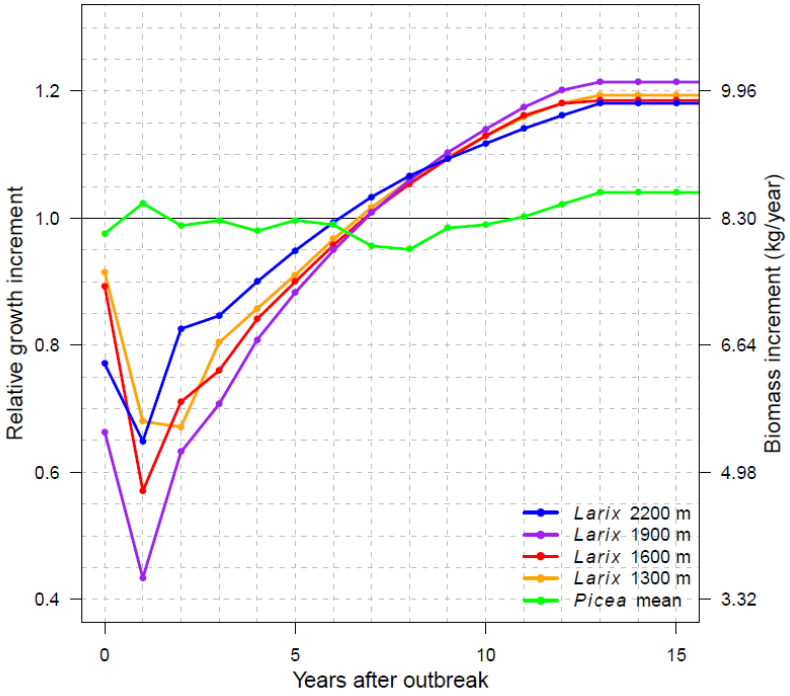

Figure 2.5 Mean impact of budmoth outbreaks occurring between 1850 and 1980 on annual growth of *Larix* and *Picea* derived from ring-width indices. Relative growth increment is defined as the current growth divided by the mean growth of 5 years prior to the outbreak. To provide an indication on the reduction magnitude, the relative growth changed was multiplied with the mean biomass increment of a 150 year old *Larix* tree from the fixed plots (as *Picea* does not show a response).

Modelling growth responses

When considering only climatic variables, the best model fits were found for *Picea* at 1900 m and *Larix* at 2200 m (R^2= 0.21 and 0.25, respectively; see Table 2.4 for slopes and residual standard errors). The explained variance in the models strongly decreased towards lower elevations (R^2= 0.03 obtained for *Larix* at 1300 m; Table 2.4). In the most recent years (>1990), the model underestimated *Picea* growth at 1600 and 1900 m on average by 7%, when comparing the difference between the model including only climatic parameters and tree-ring chronologies (Figure 2.6). At 1900 m, the underestimation of *Larix* growth was even larger and reached 24% (Table 2.4).

Table 2.4 Model fits for *Picea* and *Larix* chronologies along different elevations. Three month average climate variables for precipitation (P) and temperature (T) from previous and current year (capital letters) are presented (last month is shown). Three different types of scenarios are included; climatic variables alone, climate in combination with outbreak response curves and outbreak response curves alone. Budmoth absence growth change describes the average annual percentage of modelled ring width index gained compared to the model where outbreaks would have continued with a 9-year frequency from 1990 onwards. Unexplained growth change is the average annual percentage growth increase of observed ring width indices over the modelled *Larix* series without outbreaks. For *Picea* this value reflects the average annual percentage difference between observation and climate model. Significance codes: p >0.001= **, 0.001< p >0.05= *, 0.05< p >0.1= ·.

Species	Scenario	Elevation (m)	Variables (slope)					Residual standard error	Adjusted R^2	Budmoth absence growth change (%)	Unexplained growth change (%)
			Intercept	Tsep	Pdec	TJUL	PJUL				
Picea abies	Climate	1300	1.30**	-0.0344*	0.0002	-0.0060	0.0005*	0.134	0.11**	-	-2.45
		1600	0.89**	-0.0378**	0.0002*	0.0299*	0.0005**	0.115	0.18**	-	7.63
		1900	1.07**	-0.0515**	-2.48E-06	0.0441**	0.0002	0.101	0.21**	-	6.40
			Intercept	TAUG	Tnov	PAUG	Outbreak				
Larix decidua	Climate	1300	0.59*	0.0099	0.0196	0.0005*	-	0.158	0.03·	-	0.27
		1600	-0.48	0.1122**	0.0278	0.0003	-	0.247	0.14**	-	15.16
		1900	-0.88*	0.1664**	0.0501*	0.0004	-	0.283	0.24**	-	23.67
		2200	-0.22	0.1311**	0.0364*	0.0002	-	0.221	0.25**	-	9.16
	Climate + Outbreak	1300	0.42·	-0.0041	0.0187	0.0005*	0.3761**	0.151	0.11**	19.32	-14.29
		1600	-0.51*	0.0512*	0.0168	0.0002	0.8534**	0.190	0.49**	23.44	6.60
		1900	-0.81**	0.0841**	0.0314*	0.0003	0.9087**	0.187	0.67**	28.91	19.49
		2200	-0.56*	0.0835**	0.0246·	0.0002	0.8191**	0.180	0.50**	18.83	0.43
	Outbreak	1300	0.62**	-	-	-	0.3623**	0.154	0.08**	18.17	-9.76
		1600	0.14·	-	-	-	0.9349**	0.194	0.47**	25.13	11.40
		1900	0.08	-	-	-	1.0248**	0.202	0.61**	31.19	25.43
		2200	0.06	-	-	-	0.9921**	0.195	0.41**	22.49	10.44

Accounting for outbreaks greatly increased the explained variance of the model fit for *Larix* (Table 2.4). Average R^2 improved from 0.17 to 0.44 when comparing the climate and outbreaks scenarios versus climate alone. The smallest model improvement was observed at 1300 m (Table 2.4), while at 1900 m the best fit was found for the scenario that included outbreaks and climate (R^2= 0.67).

Including budmoth outbreaks in the models also increased the ability to explain the growth increase in the most recent decades (1990 to 2011; see Table 2.4 and Figure 2.3b). When simulating continued budmoth outbreaks across elevations, 23% of the recent growth increase could be explained (Figure 2.6). We observed the strongest growth benefit from the absence of outbreak at 1900 m, where the continued outbreaks are modelled to reduce growth by 29% (Table 2.4). For 2200 m, unexplained growth was reduced from 9.2% to 0.4% when including estimates for the recent outbreak absence, although this model started to overestimate growth at lowest elevations (overestimation of growth increase by 14%; Table 2.4).

2.4 Discussion

Importance of climate vs. outbreaks and its variation along elevation

In this study we analysed the relative importance of climate and non-lethal insect outbreaks on tree growth and their impact on forest biomass accumulation. To the best of our knowledge, no other study has provided empirical data on the above-ground biomass reduction caused by budmoth outbreaks during the past century, the relative importance of climatic versus biotic drivers, and the possible beneficial effects due to the absence of outbreaks in recent decades.

Our tree-growth model, which includes climate and outbreak responses, was able to explain up to 67% of the observed inter-annual growth patterns of high elevation *Larix decidua*. The model performed best at 1900 m elevation, while showing weak performance at the lowest elevation (1300 m; Table 2.4). Climatic drivers in the growth model alone at best explained 21% and 25% of growth variability for *Picea abies* at 1900 m and *Larix* at 2200 m respectively. The strong positive responses to summer temperature at higher elevations match previous observations for these species (Frank & Esper 2005; King *et al.* 2013b; Hartl-Meier *et al.* 2014), and agree with findings showing the sensitivity of high-elevation trees growing at mesic sites to increasing temperatures (Jacoby *et al.* 1996; Körner and Paulsen 2004; Bunn *et al.* 2005; Salzer *et al.* 2009, Babst *et al.* 2013). At the same time, negative correlations with summer temperature at 1300 m (Figure 2.4) support findings of greater drought sensitivity for forests at sites with higher mean annual temperatures (Barber *et al.* 2000; Gómez-Guerrero *et al.* 2013; Galván *et al.* 2015; Qi *et al.* 2015), although the magnitude will depend upon species-specific responses (Babst *et al.* 2013).

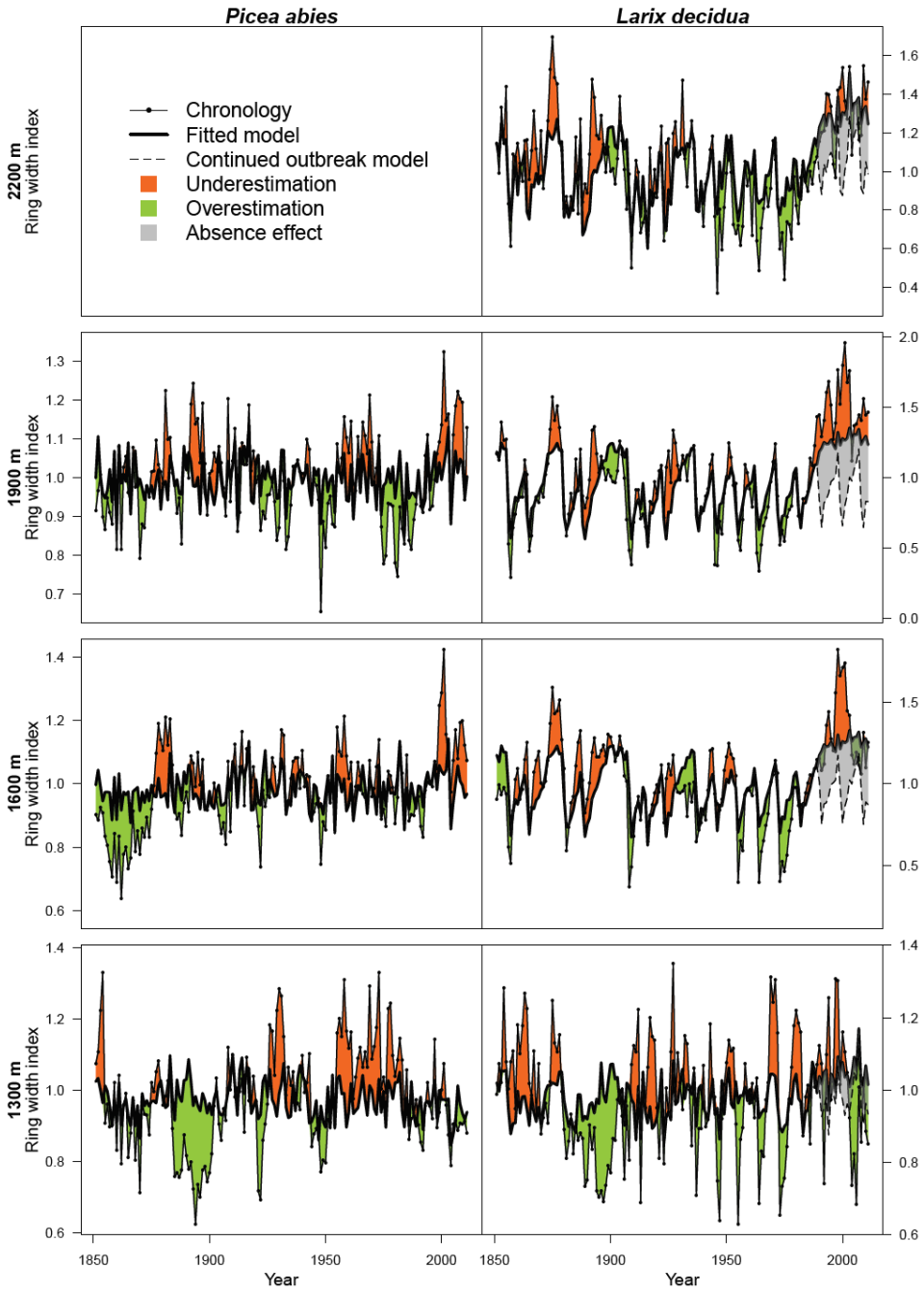

Figure 2.6 Modelled ring width index compared to the chronologies from *Picea* and *Larix* along the elevational gradient. For *Picea* only climatic drivers are included, while for *Larix* the outbreaks are added and simulated to continue after 1981 (see Table 2.4 for more model fitting statistics).

Growth response to the reported budmoth outbreak years (see Esper *et al.* 2007) explained 39% of the observed *Larix* growth variability across elevations (Table 2.4), which is twice the variance explained by climate. *Larix* at 1300 m did not show evidence of outbreaks prior to 1930 and displayed a delayed response to outbreaks (Figure 2.5). This absence could be explained by the more intense land-use at lower elevations during this period, which reduced host abundance,

connectivity between forest stands, and subsequently the outbreak intensity (Johnson *et al.* 2004; Battipaglia *et al*. 2014; Hartl-Meier *et al.* 2017). We hypothesize that the delay in response may be a result from the fact that a large part of the ring had already been formed before the outbreak, or that the insect activity and outbreak intensity can be different at lower elevations. *Larix* at 2200 m appeared to be least impacted by the outbreaks and recovered relatively quickly (Figure 2.5), while trees at 1900 m suffered most from the impact. Our observations for strongest outbreak effects at 1900 m and the decreasing impact towards both upper and lower elevations confirm previous reports indicating that the optimal outbreak conditions are present at an elevation of 1700-2000 m (Baltensweiler & Rubli 1999).

Consequences due to the absence of outbreaks

Both *Larix* and *Picea* showed increased growth rates at higher elevations (>1600 m) in recent times. Yet, recent growth increase of *Larix* since 1981 cannot be explained solely by climatic variables (Table 2.4), but rather, can be largely attributed to the absence of budmoth outbreaks (Figure 2.6). Additionally, our outbreak-growth response analysis showed that periods of outbreak absence longer than eight years result in higher growth compared to the years prior to outbreak (Figure 2.5). Thus, model simulations suggest that the growth of *Larix* might even over-proportionally benefit from the recent absence of insect outbreaks, as past absence periods could not explain the recent increase. When simulating continued outbreaks after 1980 we found strongest benefits from budmoth absence especially at 1900 m (Table 2.4).

When comparing tree-ring width indices from 1990-2011 to the modelled indices including outbreaks, it becomes evident that at intermediate elevations simulations underestimated the growth release that occurred in absence of budmoth outbreaks (Table 2.4). This is most prominent for *Larix* at 1900 m, where the model underestimates growth on average by 23.67% per year, compared to only 6.4% annual offset for *Picea*. We obtained similar underestimations when modelling *Larix* growth based on a non-host species (*Picea*) and outbreaks (Table S2.1 and S2.2), which does not require the selection of climatic variables (possibly prone to uncertainties and overfitting). However, considering the amount of the models' unexplained deviations throughout the past ≈150 years, the observed underestimation of recent increased *Larix* growth is not exceptional (Figure 2.6).

We cannot exclude that other drivers might be responsible for the unexplained deviances, such as management activities, successional processes (e.g., natural thinning and mortality events) or non-linear climate responses. Yet,

at 1900 m and 2200 m there was little evidence for management in the recent decades, which could have positively influenced remaining trees. Furthermore, the outermost years of dead trees could be dated back to the 1930s, which would speak against missed successional processes at these two sites. However, effects from increasing nitrogen deposition or higher CO_2 concentrations cannot be easily excluded (Paulsen *et al.* 2000; Huang *et al.* 2007; Camarero *et al*. 2015) or invoked to explain the growth increase (Girardin *et al.* 2008). Alternatively, our outbreak response curve might still not capture the true magnitude of increase growth responses. The fact that the response curves were established with site-specific chronologies renders this variable not fully independent (Table 2.4). Furthermore, the absence of outbreak events in three decades represents an unprecedented state for the past millennium (Esper *et al*. 2007), which is not included in our empirical outbreak response estimates.

A defoliation experiment performed on *Larix* in the Central Alps showed the impact of defoliation on non-structural carbon storage and its carbon limitation (Handa *et al.* 2005), pointing to the mechanistic explanation that carbon available for radial growth was limited. Although more attention should be given to this mechanistic explanation, our results clearly show that the regular 9-year outbreak cycle prevented *Larix* from fully realizing its growth potential.

Implications for forest biomass accumulation

Our quantifications of the aboveground biomass increment (ABI) show that either the presence or absence of budmoth outbreaks has large consequences for forest biomass accumulation and carbon storage potential (Figure 2.3). On average, budmoth outbreaks reduce tree individual ABI in the year subsequent to the outbreak by 58% in comparison to the 5-year average growth prior to outbreak. Most severe growth reductions could be as high as 80%, found for outbreaks at 1600 m in 1908 and 1954.

In terms of aboveground biomass, the three outbreak events occurring between 1950 and 1980 induced an average reduction in ABI of ≈770 and ≈1130 kg ha^{-1} y^{-1} in year 0-4 after the outbreak at 1900 and 2200 m and ≈300 kg ha^{-1} y^{-1} at 1300 m. Of the strong post-1980 increase at 1900 m, we can attribute a maximum of 770 kg ha^{-1} y^{-1} to the absence of outbreaks (from a total increase of 1800 kg ha^{-1} y^{-1}; Figure 2.2a). Here we assume that the absence of outbreaks explains roughly 60% of the observed increase of *Larix* growth (Table 2.4). Similarly, we observed a twofold ABI increase at 2200 m (from 1500 to 3210 kg ha^{-1} y^{-1}; Figure 2.3a) that is largely caused by *Larix* and the absence of outbreaks (1420 of 1710 kg; Figure 2.3b).

It is remarkable that despite large differences in age structure, stand density and recruitment, we observed nearly identical long-term trends in ABI over the last century at 1900 and 2200 m. However, one should be cautious when attributing the increase in plot level ABI to climate drivers or budmoth outbreak dynamics, as we are aware that stand development and management cause a constant loss of signal back in time (i.e., the "fading-record" problem; see Swetnam *et al.* 1999; Foster *et al.* 2014). We want to stress that within the context of forest biomass increment, changes in forest structure, stand dynamics, distribution, and tree growth should not be overlooked when analysing long-term biomass changes (Etzold *et al.* 2014; Pretzsch *et al.* 2014; Hansen *et al.* 2015). Therefore, especially for forests at 1300 m, we refrain from attributing the long-term increase in plot level ABI to climate drivers or budmoth outbreak dynamics.

Interestingly, plot level ABI at 1300 m shows a quick recovery following the outbreaks to pre-outbreak level, which could either be due to high carbohydrate reserves or due to a larger fraction of spruce (≈50% of the standing biomass in 2011; see Table 2.2) and favourable growing conditions in the years after the outbreaks. In the light of weak negative tree growth-summer temperature relationships, recent warmer temperatures might have partially counteracted the growth benefits expected due to lack of recent budmoth outbreaks. However, it becomes obvious from Figure 2.3b that *Larix* growth still increased in the 1990-2009 period, thus counterbalancing the slower growth of *Picea*.

In this study we analysed the impact of a reduced outbreak frequency, however globally many phytophagous insects show increased activity associated with shifts in distribution range (Battisti 2008; Axelson *et al.* 2015), improved breeding and growing conditions (Battisti *et al.* 2000; Pasztor *et al.* 2014), and increased frequencies and magnitude of outbreaks (Creeden *et al.* 2014). Although there is a lack of similar tree-ring data or biomass quantification to directly compare our values, multiple studies support the relevance of insect outbreaks for tree growth and forest productivity (Kurz *et al.* 2008; Medvigy *et al.* 2012; Moore *et al.* 2013). Aerial images for North-America provide evidence for large areas being affected by major forest insect species (Hicke *et al.* 2012). Also, eddy covariance flux tower on multiple forest sites in New Jersey (USA) revealed strong reductions in net annual CO_2 exchange changes due to gypsy moth (*Lymantria dispar* L.) defoliation, although wood increment only decreased slightly (Clark *et al.* 2010). Although our study focusses on the Lötschental, *Larix* is an abundant species in high-elevation forests across the European Alps

(EUFORGEN), indicating that these forests might increase their carbon sink relevance with persistent absence of budmoth outbreaks.

Tree rings have a huge potential in both reconstructing ABI (Babst *et al.* 2014b; Klesse *et al.* 2016) as well as assessing the absolute impact of insect outbreaks on ABI. As non-lethal disturbances, such as the larch budmoth outbreaks, are rather under-represented in current ecological models (Seidl *et al.* 2011), our study provides valuable input for modelling budmoth induced growth reductions. Further tree-ring investigations, from other sites and species that contain necessary structural data (stand density, tree size and height), will contribute to better understanding the importance of insect outbreaks and their absence on the carbon source or sink function of forests in the future (e.g., Bale *et al.* 2002; McMahon *et al.* 2010; Medvigi *et al.* 2012).

Conclusion

Our study provides data on the relative importance of insect outbreaks compared to climate variation on *Larix* growth. Both *Picea* and *Larix* at high elevations show positive growth responses to increasing temperature. However, our simulations show that the recent absence of budmoth outbreaks is crucial to explain the strong growth increase for *Larix* at higher elevations, far beyond what can be explained by climate alone. Additionally, the different magnitude of growth responses to insect outbreaks as a function of elevation suggests that budmoth activity and its impact are likely temperature dependent. From the biomass reconstructions it is clear that *Larix* productivity was severely dampened by regular outbreaks at higher elevations, preventing these trees from fully realizing their growth potential.

Acknowledgements

We thank Stefan Bechet, Daniele Castagneri, Katarzyna Czober, Gregory King, Roger Köchli, Lenka Mateju, Daniel Nievergelt, Elisabeth Graf Pannatier, Angela Luisa Prendin, Kerstin Treydte and Anne Verstege for their aid in the extensive field- and labwork performed throughout the past years at the Lötschental transect. We also would like to thank Georg von Arx, Flurin Babst, Daniel Balanzategui, Jesper Björklund, Ana Stritih and Volodymyr Trotsiuk for discussion. This work was funded by two Swiss National Science Foundation projects, LOTFOR (no. 150205) and iTREE sinergia project (no. 136295).

Supporting information Chapter 2

After cross-dating sites on both north and south slopes, sites on the same elevation where combined per species. Diameter increment data was calculated by multiplying the mean ring-width data for the individual by two, which was used for chronology building and biomass calculations (Figure S2.1). A minimum of ten individuals was used for the chronology building and biomass calculations.

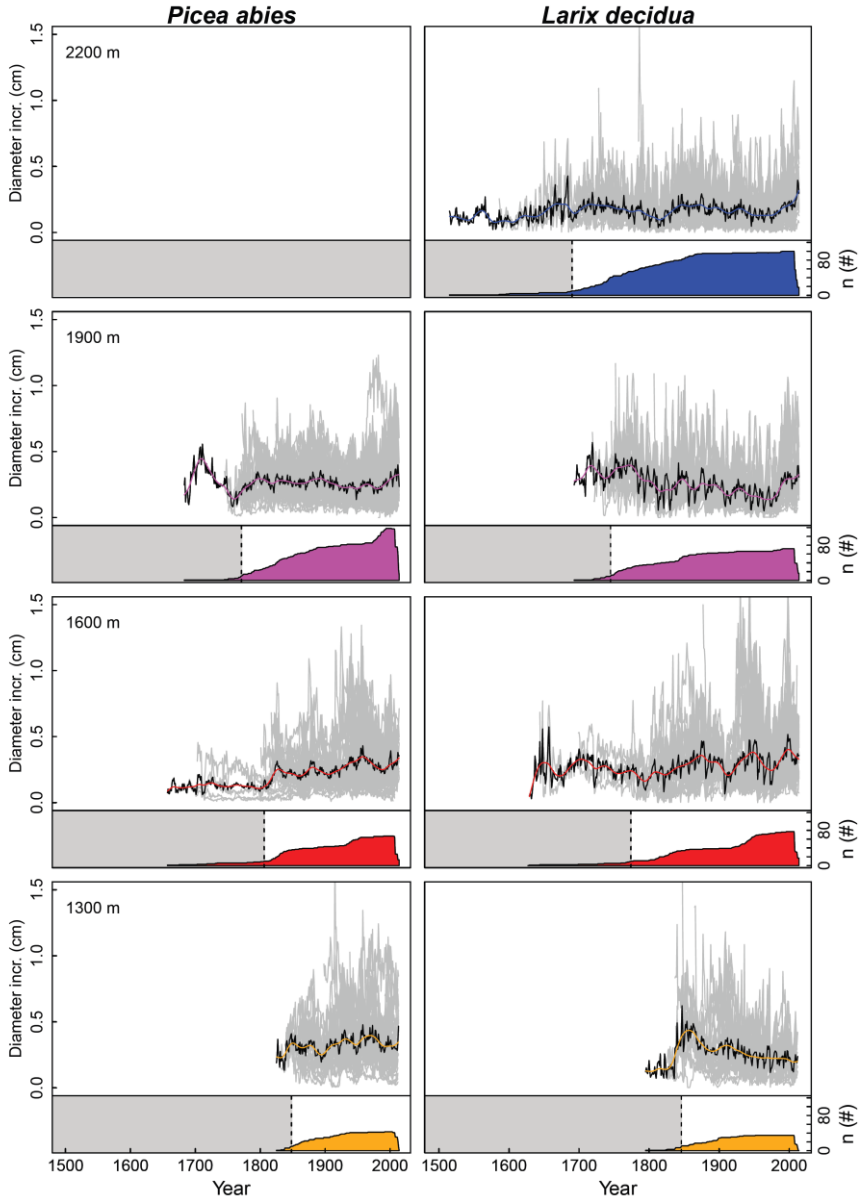

Figure S2.1 Development of diameter increment over time for all elevations and species. Grey lines indicate individual series, black lines indicate the mean and the coloured lines a 30 year spline of the mean diameter increment data. Sample size is indicated with the smaller plots, where the grey area indicates years where the sample size is below 10 individuals.

Figure S2.2 presents the functions that have been used for reconstructing height and bark thickness of individual trees in relation to DBH. All function fits were significant ($p < 0.05$) with an $R^2 \geq 0.7$. At 2200 m only sparsely *Picea abies* is found, therefore it was excluded from further analysis.

Spurious trends can be introduced due to the detrending procedure applied, which accounts for the age/size related signal within tree-ring series. According to Peters *et al.* (2015) we applied multiple detrending methods and verified whether the signal preserved within the regional curve standardization (RCS) chronology, is similar to the once attained by conservative detrending (CD) and basal area correction (BAC; Figure S2.3).

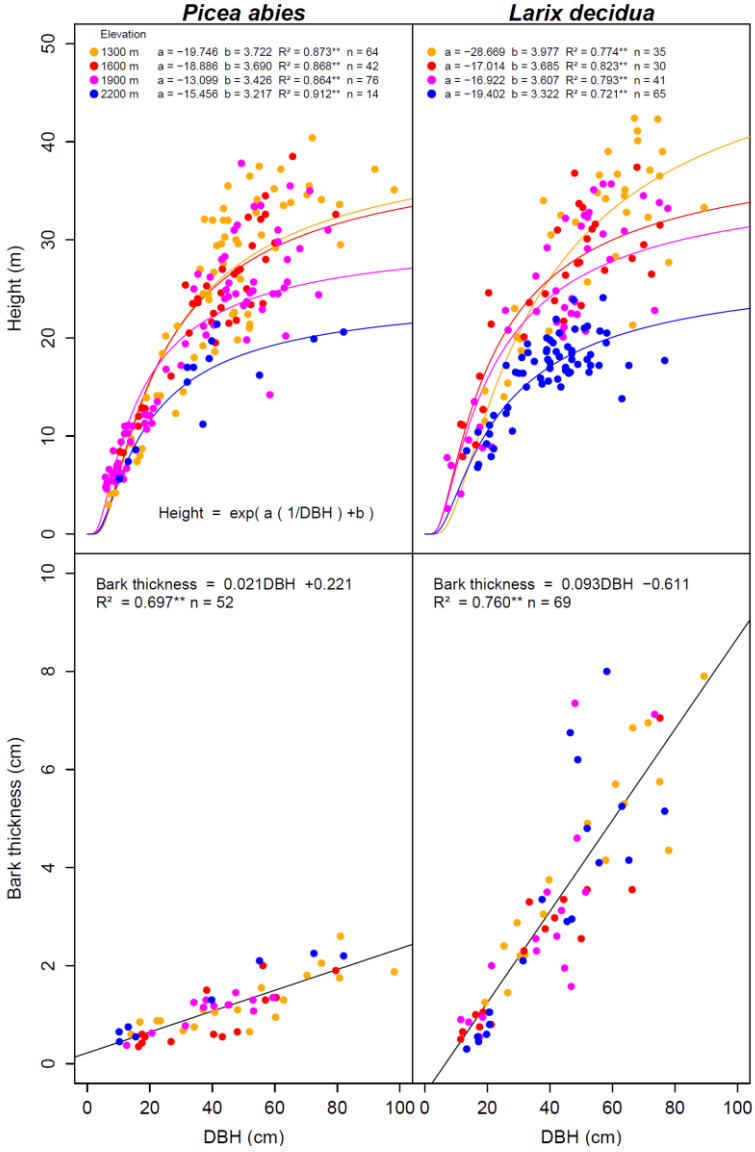

Figure S2.2 Allometric functions of height and bark thickness in relation to diameter at breast height (DBH). Top plots show functions per elevation and species, while the bottom plots show functions for all elevation combined. Goodness of fit is provided in addition to the significance level (*= p <0.05, **= p <0.001).

Multiple outbreak and climate scenarios were simulated with the additive linear model to quantify the growth benefit due to the absence of outbreak on growth over the recent outbreak-free period (i.e., after 1981). We analysed model performance by including: 1) Climate alone, 2) Climate + Outbreak, and 3) Outbreak alone. For climate alone we used the raw climatic variables, selected from the multiple regression analysis. For *P. abies* two alternative sets of climatic variables were selected (Climate and Climate alt.; Table S2.1). When including the outbreak components for the *Larix decidua* data, we used three types of outbreak

response curves depending on three types of possible long-term post outbreak growth responses. These scenarios include i) the original response curve (referred to as the "Beneficial" type), ii) the "Threshold" type, where no benefit from longer absence of the budmoth is assumed and all response values greater than one were reset to one, and iii) the "Linear Increase" type, where all values from year eleven onward were extrapolated from the linear slope between years two and ten (Table S2.1).

Model fittings for *P. abies* and *L. decidua* chronologies along different elevations are shown in Table S2.2. Three month average climate variables are presented (last months is shown). For the *L. decidua* model fit statistics are provided for different scenarios when including all years as when excluding years with budmoth absence. Additionally, for the beneficial scenario, climatic variables have been excluded to illustrate the strength of the outbreak variable. The "budmoth absence growth change" describes the average annual percentage of modelled ring-width index gained compared to the model where outbreaks would have continued with a 9-year frequency from 1990 onwards. The "unexplained growth change" is the average annual percentage growth increase of observed ring width indices over the modelled *L. decidua* series without outbreaks. For *P. abies* this value reflects the average annual percentage difference between observation and Climate model. The alternative climate scenario for *P. abies* did not improve model performance. Additionally, both threshold and the linear increase scenario did not improve model fit nor better explained the recent growth increase.

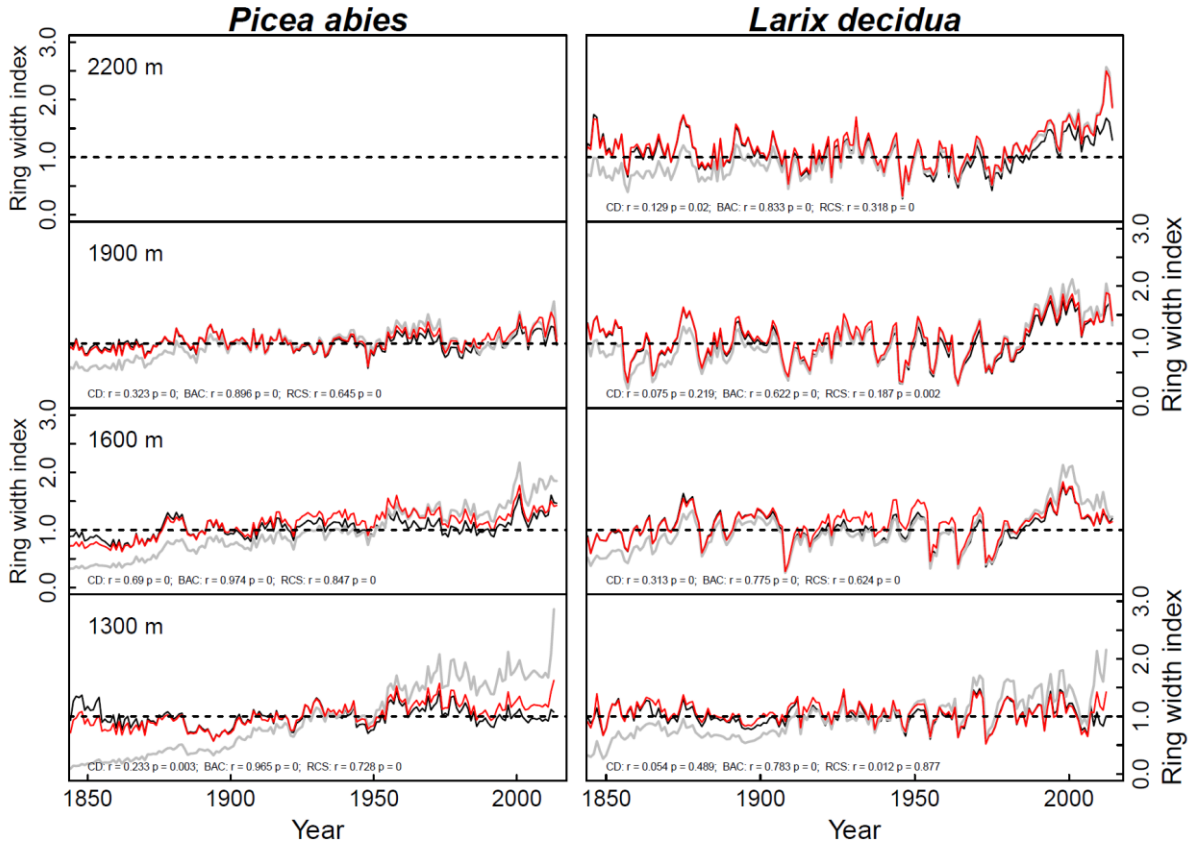

Figure S2.3 Impact of method selection on trend detection. Lines indicate chronologies produced by conservative detrending (CD; in black), basal area correction (BAC; in grey) and regional curve standardization (RCS; in red) for the different species and elevations. For every method Spearman rho (r) and significance values (*p*) are presented.

Table S2.1 Scenarios for growth modelling. Climatic drivers of temperature (T) and precipitation (P) are included for current (capital letters) and previous year.

Species	Scenario	Climatic drivers	Threshold outbreak	Beneficial outbreak	Linear increase outbreak	Formula; Growth =	Description
Picea abies	Climate	X				Tsep + Pdec + TJUL + PJUL	Climatic drivers selected by multiple regression
	Climate alt.	X				Tsep + Psep + TAUG + PJUL	Climatic drivers adjusted for individual climate growth correlations
Larix decidua	Isolated Climate	X				TAUG + Tnov + PAUG	Climatic drivers selected by multiple regression
	Threshold	X	X			TAUG + Tnov + PAUG + Thres	Addition of outbreak response which only affects growth negatively (no positive effect of absence)
	Beneficial	X		X		TAUG + Tnov + PAUG + Ben	Addition of outbreak response where negative and positive effects of outbreak absence are included
	Linear increase	X			X	TAUG + Tdec + PAUG + Lin	Addition of outbreak response where linear positive growth effects are simulated after reaching original growth levels
	Isolated outbreak		X	X		Thres	Solely threshold outbreak response
						Ben	Solely beneficial outbreak response
					X	Lin	Solely linear increase outbreak response
	Outbreak *Picea*	*Picea abies* replacing climate	X	X		Picea + Thres	*Picea* chronology and threshold outbreak
						Picea + Ben	*Picea* chronology and beneficial outbreak
					X	Picea + Lin	*Picea* chronology and linear increase outbreak

In addition to modelling the growth variation using the multiple regression of climate parameters, we modelled *L. decidua* growth as a function of the spruce growth (i.e., the non-host tree) plus our budmoth response curves (Table S2.1). This approach is more similar to classical dendroecological methods that use a reference chronology from a non-disturbed population in order to identity disturbances such as insects. We did not note an improvement in the explained variance of growth, but note that this approach does not require the selection of climate variables (possibly prone to uncertainties or overfitting).

Table S2.2 Model fits for *Picea abies* and *Larix decidua* chronologies grouped by elevations. Three month average climate variables for precipitation (P) and temperature (T) from previous and current year (capital letters) are presented (last months is shown). For *L. decidua* model fit statistics are provided by including all years (for adjusted R^2, intercept and slopes) or by excluding years with budmoth absence (adjusted R^2; ≤1980). Four different types of outbreaks are included; no outbreak (None), outbreaks with only negative impact (Threshold), original outbreak fits (Beneficial) and outbreaks where linear increase is assumed after obtaining the mean 5 year growth values prior to outbreak (Linear increase). Additionally, for the beneficial simulation, climatic variables have been excluded and *P. abies* has been in combination with the outbreaks to illustrate the strength of the outbreak variable. Budmoth absence growth change describes the average annual percentage of modelled ring-width index gained compared to the model where outbreaks would have continued with a 9-year frequency from 1990 onwards. Unexplained growth change is the average annual percentage growth increase of observed ring-width indices over the modelled L. decidua series without outbreaks. For *P. abies* this value reflects the average annual percentage difference between observation and Climate model. Significance: p >0.001= **, 0.001< p >0.05= *, 0.05< p >0.1= ·.

Species	Scenario	Elevation (m)	Variables (slope)					Adjusted R^2 (all years)	Budmoth absence growth change (%)	Unexplained growth change (%)	Adjusted R^2 (≤1980)
			Intercept	Tsep	Pdec	TJUL	PJUL				
Picea abies	Climate	1300	1.30**	-0.0344*	0.0002	-0.0060	0.0005*	0.11**		-2.45	
		1600	0.89**	-0.0378**	0.0002*	0.0299*	0.0005**	0.18**		7.63	
		1900	1.07**	-0.0515**	-2.48E-06	0.0441**	0.0002	0.21**		6.40	
			Intercept	Tsep	Psep	TAUG	PJUL				
	Climate alternative	1300	1.22**	-0.0297*	0.0002	-0.0048	0.0005*	0.10**		-2.19	
		1600	0.70**	-0.0280*	0.0002·	0.0314*	0.0005**	0.15**		8.22	
		1900	0.89**	-0.0399**	0.0002·	0.0380**	0.0001	0.21**		6.52	
			Intercept	TAUG	Tnov	PAUG	Outbreak				
Larix decidua	Isolated climate	1300	0.59*	0.0099	0.0196	0.0005*		0.03·		0.27	
		1600	-0.48	0.1122**	0.0278	0.0003		0.14**		15.16	
		1900	-0.88*	0.1664**	0.0501*	0.0004		0.24**		23.67	
		2200	-0.22	0.1311**	0.0364*	0.0002		0.25**		9.16	
	Threshold	1300	0.13	0.0096	0.0244·	0.0005*	0.4538**	0.13**	11.45	-5.30	0.21**
		1600	-1.06**	0.0743**	0.0113	0.0004·	1.1956**	0.47**	19.18	12.24	0.41*
		1900	-1.27**	0.1104**	0.0245	0.0005*	1.1862**	0.63**	25.20	27.21	0.54**
		2200	-1.02**	0.1061**	0.0203	0.0003	1.1178**	0.46**	14.85	8.44	0.36**
	Beneficial	1300	0.42	-0.0041	0.0187	0.0005*	0.3761**	0.11**	19.32	-14.29	0.24**
		1600	-0.51*	0.0512*	0.0168	0.0002	0.8534**	0.49**	23.44	6.60	0.40**
		1900	-0.81**	0.0841**	0.0314*	0.0003	0.9087**	0.67**	28.91	19.49	0.54**
		2200	-0.56*	0.0835**	0.0246·	0.0002	0.8191**	0.50**	18.83	0.43	0.39**
	Isolated outbreak: Beneficial	1300	0.62**				0.3623**	0.08**	18.17	-9.76	0.16**
		1600	0.14·				0.9349**	0.47**	25.13	11.40	0.40**
		1900	0.08				1.0248**	0.61**	31.19	25.43	0.53**
		2200	0.06				0.9921**	0.41**	22.49	10.44	0.32**
	Linear increase	1300	0.63*	0.0049	0.0185	0.0004*	0.0371	0.03·	33.33	-29.54	0.22**
		1600	-0.08	0.0543*	0.0207	8.8913E-05	0.3367**	0.33**	24.41	1.99	0.24**
		1900	-0.39·	0.0723**	0.0348*	0.0001	0.5667**	0.61**	33.43	9.66	0.47**
		2200	-0.16	0.0761**	0.0271·	5.0321E-05	0.4717**	0.46**	23.00	-5.80	0.35**
			Intercept	*Picea*			Outbreak				
	Beneficial *Picea*	1300	0.37**	0.4368**			0.1910*	0.17**	21.02	-9.64	0.33**
		1600	0.02	0.1283			0.9278**	0.47**	25.30	13.35	0.40**
		1900	-0.40*	0.5031**			1.0050**	0.64**	30.97	22.32	0.54**

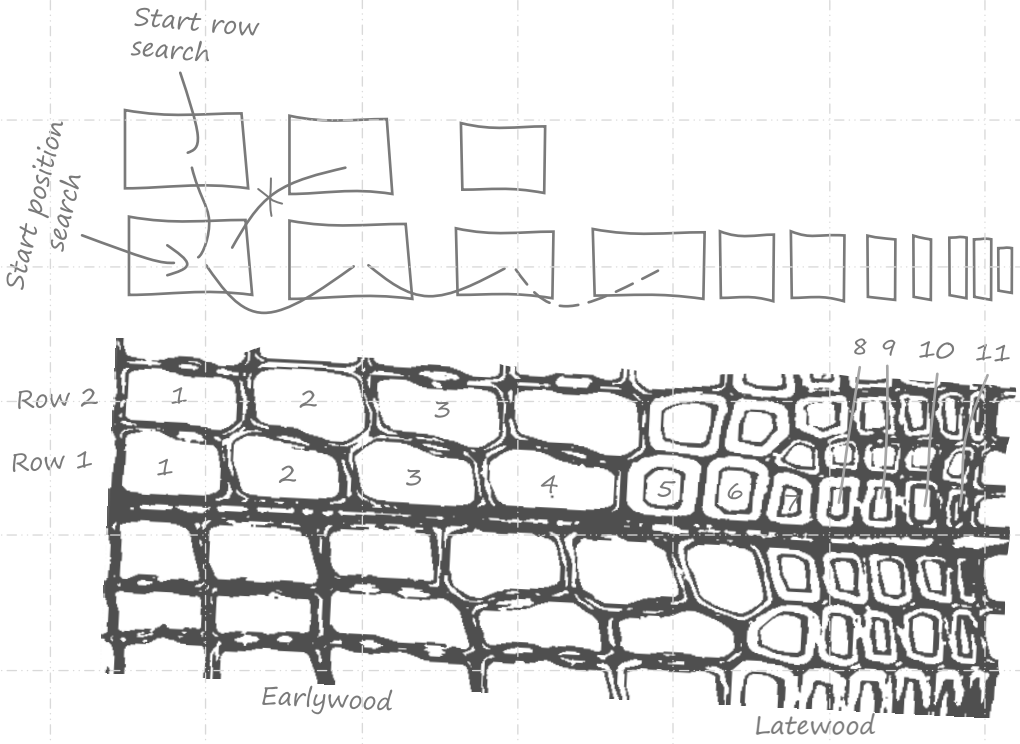
Start row search
Start position search
Row 2
Row 1
1
2
3
1
2
3
4
5
6
7
8
9
10
11
Earlywood
Latewood

Chapter 3

RAPTOR: Row and position tracheid organizer in R

Richard L. Peters, Daniel Balanzategui, Alexander G. Hurley, Georg von Arx, Angela Luisa Prendin, Henri E. Cuny, Jesper Björklund, David C. Frank, Patrick Fonti

Published in Dendrochronologia

Abstract

Mechanistic understanding of tree-ring formation and its modelling requires a cellular-based and spatially organized characterization of a tree ring, moving from whole rings, to intra-annual growth zones and individual cells. A tracheidogram is a radial profile of conifer anatomical features, such as lumen area and cell wall thickness, of sequentially- and positionally-ranked tracheids. However, its construction is tedious and time-consuming since image-analysis-based measurements do not recognize the position of cells within a radial file, and present-day tracheidograms must be constructed manually. Here we present the R-program library RAPTOR that complements tracheid anatomical data obtained from quantitative wood anatomy software (e.g., ROXAS, WinCELL, ImageJ), with the specific positional information necessary for the automatic construction of tracheidograms. The package includes functions to read and visualize tracheid anatomical data, and uses local search algorithms to ascribe a ranked position to each tracheid in identified radial files. The package also provides functions to ensure that tracheids are adequately aligned for identifying the first tracheid in each radial file, and obtaining the correct ranking of tracheids along each radial file. Additional functions allow automating the analyses for multiple samples and rings (batch mode) and exporting data and plots for quality control. RAPTOR allows tracheidogram users to take advantage of the latest generation of cell anatomical measuring systems. With this R-package we aim at facilitating the construction of more robust and versatile tracheidograms for the benefit of the research community.

3.1 Introduction

Quantitative wood anatomy is a rapidly expanding discipline that uses measurements of tree-ring anatomical features to provide highly resolved information on plant functioning, growth and environment (von Arx *et al.* 2016). Indeed, depending on the plant status and weather conditions occurring at the time of growth, the tree-ring structure varies among differing years, sites or provenances. Thus, the variation in anatomical structure of tree-rings from both gymnosperms and angiosperms species can retrospectively be used to infer climatic signals (e.g., Martin-Benito *et al.* 2012; Fonti and Babushkina 2016; Castagneri *et al.* 2017; Soute-Herrero *et al.* 2017), dynamics of growth and biomass allocation (e.g., Cuny *et al.* 2015; Carrer *et al.* 2017), and modifications

of important xylem functional traits (e.g., Petrucco *et al.* 2017; Marin-Benito *et al.* 2017; Olano *et al.* 2017).

The structure of gymnosperm wood is relatively simple, as it is mainly composed of tracheid cells. Notably, tracheids are aligned along radial files due to their sequential formation from parent cambial cells. By tracking the order of tracheids along the radial axis it is thus possible to link the cell position to its timing of formation. Tracheidograms - i.e., cell-based radial profiles of anatomical features such as lumen diameter, lumen area, or cell wall thickness of positionally ranked tracheids - have been commonly used to analyse how tracheid sequences vary along the radial axis of the tree-ring during the growing season (Vysotskaya & Vaganov 1989; Vaganov 1990; Vaganov *et al.* 2006). After determining tracheid position, it is common practise to normalize the varying number of cells between radial files to a fixed value, facilitating intra-annual comparison (DeSoto *et al*. 2011). Since their development, tracheidograms have been crucial in timing cell formation and investigating the influence of intra-annual weather fluctuations on wood structure (Kirdyanov *et al.* 2003; Cuny and Rathgeber 2016) and its derived functional and mechanical properties (Park *et al*. 1998; Darikova *et al.* 2013). This representation of a tree-ring unit (i.e., through a typical radial file, from the first to the last cell produced during the growing season) is thus crucial for mechanistically understanding tree-ring structure and functioning from a cellular perspective.

Since the construction of tracheidograms requires tracheid positional information within the radial files, the anatomical data (obtained from magnified images of wood cross-sections) are often generated with laborious and time-consuming manual measurements along a selection of at least 5 to 10 radial files (Seo *et al.* 2014), preserving the positional sequence in the data (DeSoto *et al.* 2011; Campelo *et al.* 2016). Over the last decade, the techniques for quantitative wood anatomy have significantly improved, particularly with the development of specific software such as WinCELL (see Larocque & Smith 2005 as an example of use), ImageJ (see Schuldt *et al.* 2013 as an example of use) and ROXAS (von Arx & Carrer 2014). Progress in micro-slide preparation (Gartner & Schweingruber, 2013; Arx *et al.* 2016) and wood surface imaging (Liang *et al.* 2013), combined with powerful image-analysis software (von Arx & Dietz 2005; Prendin *et al.* 2017), are now facilitating the measurements of large quantities of cells (e.g., Castagneri *et al.* 2017; Carrer *et al.* 2017), which can easily be processed and analysed in versatile data-science platforms such as R (Crawley 2007). Although providing a spatial position of the cell within the image (e.g., x-

and y-coordinates of the centroid of each cell), these programs are not designed to identify individual radial files and thus do not provide the positional data required to build tracheidograms (Figure 3.1). To overcome this limitation, we present a new package called RAPTOR (Row And Position Tracheid Organizer in R) to assign the cell position within a radial file to each measured tracheid.

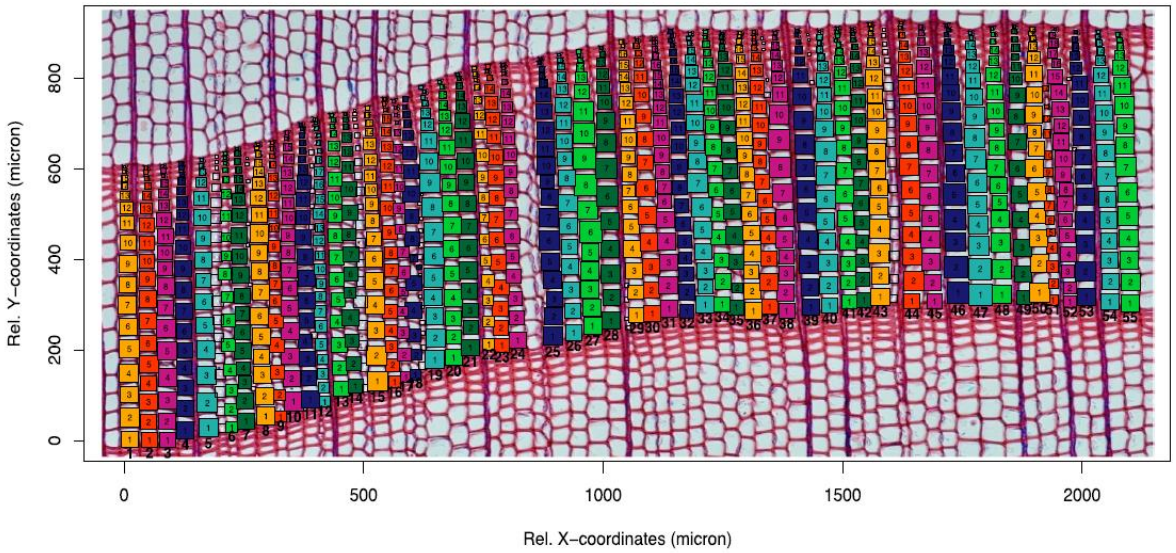

Figure 3.1 Visualisation of a RAPTOR output overlaid on the original cross-section image of the ring 2007 from the example data LOT_PICEA (*example.data (species="LOT_PICEA")*) used for the tracheid measurements. In the example RAPTOR assigns a position number to each tracheid within the 55 identified radial files in vertically aligned squares of the same colour.

3.2 Package functionalities

RAPTOR is an R add-on package freely accessible via the CRAN repository (CRAN: http://cran.r-project.org, version 3.3.3; see Supporting information), which contains functions to: i) verify the required data format (*is.raptor*), ii) plot the spatial distribution of tracheids within a specified tree-ring for visual verification (*graph.cells*), iii) rotate data along the radial axis to properly align the cells for the searching algorithm (*align*), iv) identify the first tracheid of the radial files (*first.cell*), v) assign each tracheid to a position within the radial file (*pos.det*), and vi) save data and produced plots (*write.output*). These functions should be used sequentially as each procedure uses data output provided from previous functions, and can be serially automated for large datasets to be processed in batches (*batch.mode*). To assist the user in understanding the operation and the functionalities of the RAPTOR package, there are several example datasets to be studied (*anatomy.data*, *example.data*).

3.3 Data format and image requirements

To provide positional output, RAPTOR requires input data to be formatted into an R data-frame object with a designated row for each tracheid, as typically obtained from measurements performed on images of thin cross-sections of wood increment cores (see Figure 3.1). RAPTOR uses a local-search algorithm based on tracheid size and position within the ring, which is less precise if the ring shape is highly irregular or if only a modest number of cells are measured (e.g., along small radial strips or incomplete rows). Furthermore, the images used for measurements should be oriented so that incremental growth occurs parallel to the y-axis (i.e., with the earlywood facing the image bottom). The appropriate image orientation can be obtained by using the function *align()*.

The input data-frame must include six specific columns; an identifier column for the wood sample (e.g., ID), an identifier for the tracheid (e.g., CID), the year of the dated tree ring (e.g., YEAR), the cell lumen area (e.g., CA), and the x- and y-coordinates of the centroid of the tracheid lumen (e.g., XCAL and YCAL). Commonly used software's provide the information on CID, CA, XCAL and YCAL, while the ID and YEAR can be added afterwards. These column names must either match the names mentioned above or columns have to be ordered according to the order presented here. Additional non-compulsory columns with other anatomical metrics or other types of information may be included. Table 3.1 provides an example of an anatomical dataset from Norway spruce (*Picea abies* Karst.) as generated by ROXAS that can be called using the function *example.data (species="LOT_PICEA")*. The package also provides examples from several other conifer species.

The user can verify if a data-frame fits the requirements for RAPTOR data format by using the function *is.raptor()*. The input data can be visualized with the *graph.cells()* function, which produces an interactive plot allowing the user to cycle through the years to see the position, lumen size, and the identifier of the tracheids in each ring (Figure 3.2).

3.3 Main RAPTOR functionalities

The *align()* function provides an interactive procedure to rotate the coordinate system (Figure 3.3a). The argument *interact* allows the user to select if the rotation is performed automatically or determined by the user. In the default case (*interact*= FALSE), the rotation is optimized automatically using a simple linear regression through all tracheid located along the horizontal axis. In the case of a

user-guided rotation (*interact*= TRUE), the function produces a plot for each ring with a superimposed crosshair and rotational slopes to guide the alignment. The user is then asked to provide the rotational slope corresponding to the line that parallels the annual ring border and to visually check the rotation result.

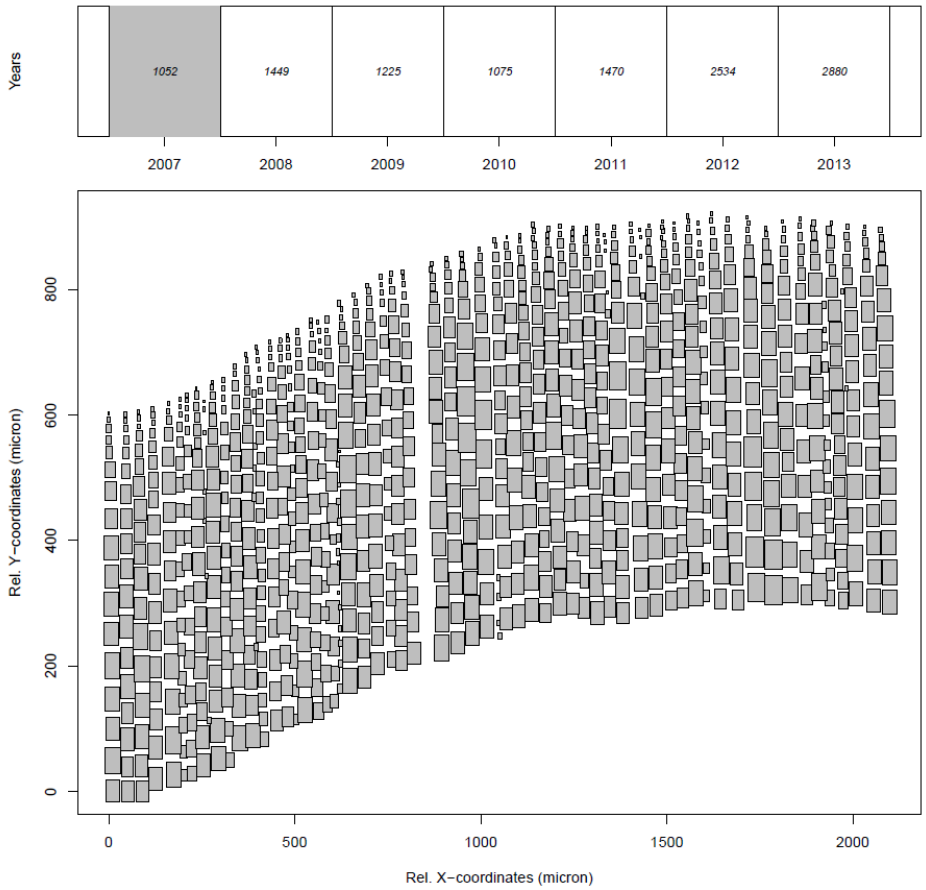

Figure 3.2 Graphical representation of anatomical data presented with the function *graph.cells()* for the ring 2007 from the LOT_PICEA example (*example.data (species="LOT_PICEA")*). The upper panel indicates the calendar year for each ring and its total number of cells. The lower panel provides the positional data and the lumen area of each tracheid (size of the square) for the grey coloured annual ring shown in the upper panel. When plotting in R the number within the square provide the cell identifier.

Once the ring is optimally aligned, the process of radial file identification can start. Starting from the bottom left corner of the ring, the function *first.cell()* searches to the right for the lower most adjacent cell using a local search algorithm that moves from the first recognized cell tracheid to the next (Figure 3.3b and 3.4a). The argument *frac.small* (default= 0.5) defines the threshold lumen area (expressed as a percentage of the average tracheid lumen area of the ring) that filters out tracheids that are too small to be considered as the first earlywood cell within a radial file. As a result, a column "ROW" is added to the input data-frame that assigns a row number to each recognized first cell (see Table 3.1).

Table 3.1 Example of RAPTOR data format of the ring 2007 from the LOT_PICEA example (*example.data (species="LOT_PICEA")*). Bold column names indicate mandatory columns. Bold grey columns indicate RAPTOR outputs.

ID	**CID**	**YEAR**	**CA**	**XCAL**	**YCAL**	CWTALL	…	**ROW**	**POSITION**	**MARKER**
LOT_PICEA	31	2007	1252	-1481	108980	3.01	…	1	1	NA
LOT_PICEA	32	2007	1136	-1440	108979	2.76	…	2	1	NA
LOT_PICEA	34	2007	1139	-1402	108979	2.04	…	3	1	NA
LOT_PICEA	40	2007	1320	-1365	109000	2.69	…	4	1	NA
LOT_PICEA	45	2007	1688	-1317	109006	2.36	…	5	1	NA
LOT_PICEA	50	2007	340	-1288	109005	2.21	…	NA	NA	NA
LOT_PICEA	53	2007	553	-1268	109007	2.47	…	6	1	NA
LOT_PICEA	56	2007	1321	-1238	109021	2.51	…	7	1	NA
LOT_PICEA	57	2007	1300	-1404	109020	2.59	…	3	2	NA
…	…	…	…	…	…	…	…	…	…	…

ID= sample identifier; CID= tracheid identifier; YEAR= year of formation of the annual ring; CA= tracheid lumen area; XCAL= X-value of cell centroid; YCAL= Y-value of cell centroid; CWTALL= Mean thickness of all cell walls; ROW= number of the radial file the tracheid is belonging to; POSITION= position of the tracheid within the radial file; MARKER= tracker of RAPTOR decision (see text).

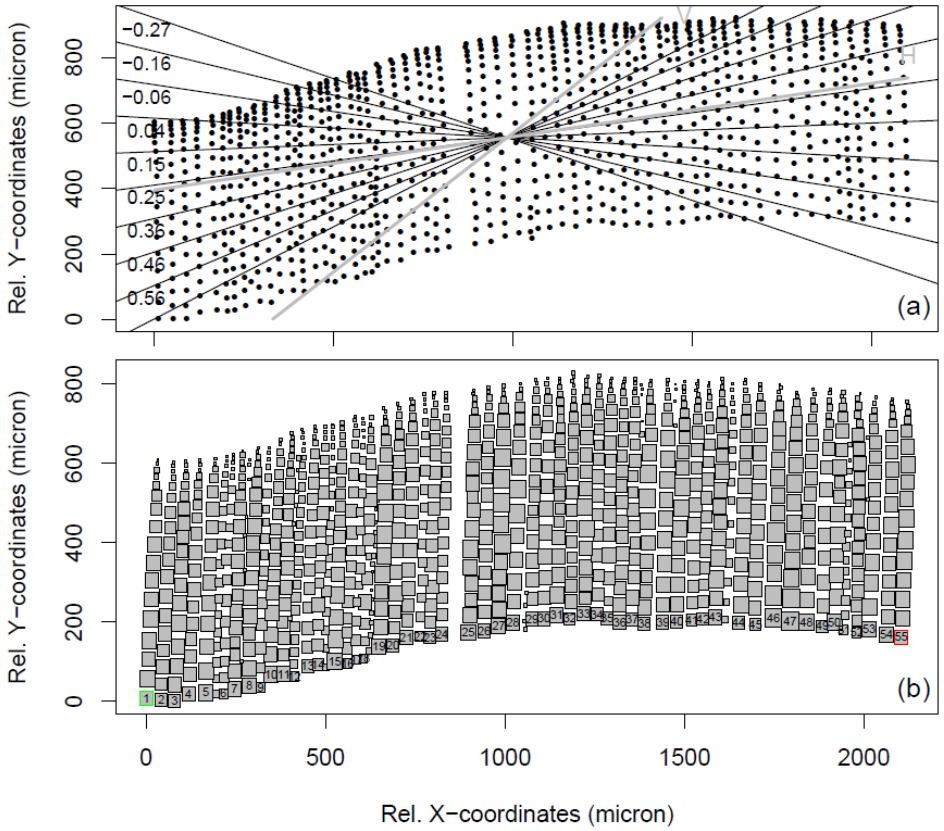

Figure 3.3 Tree-ring alignment and first cells detection for the ring 2007 from the LOT_PICEA example (*example.data (species="LOT_PICEA")*). (a) Plot obtained from the *align()* function where a crosshair is provided to assess the rotational angle (expressed as the slope of a linear regression) required for optimizing the alignment of the radial growth axis of the ring to the image y-axis. (b) Plot of the tree ring after the rotation and identification of the first cells (as a result of the *first.cell()* function). The first and last identified cells are marked in green and red respectively.

The recognition of continuous radial files - i.e., radial files which display an uninterrupted sequence of cells from the start to the end of the ring - and the assignment of a tracheid cell's position within each radial file, is obtained using the function *pos.det()* (Figure 3.4b). By looping through each identified first-row cell, this function uses another algorithm to identify the next sequential tracheid in the radial file. The algorithm is instructed by user-defined "earlywood" and "latewood" variables, dependent on the anatomical characteristics of the wood sample (see package description). The algorithm moves from one target cell (*n*), to the next (*n*+1) using a rectangular search grid. The width and the length of the grid are defined as the proportion of a target cell's lumen diameter (where $L_n = CA_n^{1/2}$) multiplied by *sle* (*sl*= search length) and *swe* (*sw*= search width) for larger earlywood cells (*e*) and *sll* and *swl* for smaller latewood cells (*l*; see Figure 3.4b).

If more than one tracheid falls within the rectangular search grid, the closest tracheid will be selected. Specified size ratio variables between consecutive tracheid (i.e., *ec*= earlywood cut off, and *lc*= latewood cut off) are used to stop the algorithm search when unrealistically small cells are detected. A flexible spline moving along each established radial file with a search width determined by the average radial file width is used to detect cells that should have been assigned to a radial file. Finally, the arguments *prof.co* (i.e., a threshold ratio of distance to the previous [between n and n-1] and the consecutive tracheid [n and n+1]), and *max.cell* (expressed as a proportion of the annual maximum number of radial file cells) can be used to filter out incomplete radial files. The output file contains the "ROW" and "POSITION" column, with *NA*'s assigned to tracheids that do not belong to continuous radial files, and a column "MARKER" that track RAPTOR decisions in each radial file. Specifically, values are assigned to the last detected "earlywood" cell (value= 1), the last detected "latewood" cell (value= 2), the last detected cell (value= 3), and radial files removed due to gaps (value= 4) or too few cells (value= 5).

These three main functions of the package also offer graphical visualization of results (with the argument *make.plot= TRUE*). The function *write.output()* allows the user to export results in numerical (as **.txt*) and graphical (as **.pdf*) formats to a repository or folder selected by the user. The *batch.mode()* function allows the user to automatically run the above functions from a target folder populated by previously prepared files with defined settings.

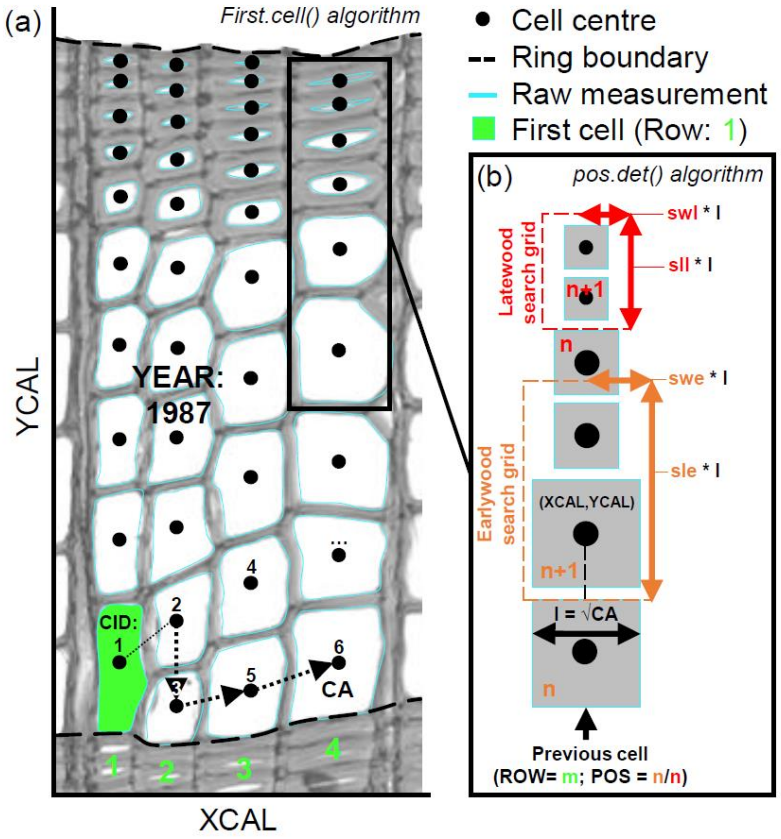

Figure 3.4 Visual representation explaining the local search algorithms used in RAPTOR. (a) Image of the wood anatomical section from an annual ring. Cell lumen of the identified tracheids are outlined in cyan. The *first.cell()* algorithm starts from the first cell at the bottom left of the image (green filled cell lumen) and searches to its right for adjacent cells. The cell closest to the target cell is selected and a check is performed to select the lowest cell (according to YCAL), where the selected cell is subsequently used for the next search (cells 1, 3, 5 and 6 are selected). Identified first cells of the radial files are labelled with a green number. (b) Visual representation of the *pos.det()* algorithm. The *pos.det()* search grid above the target cell (*n*) is defined as a rectangle whose sides are a proportion of L_n and defined by the user through the function arguments *sle*, *swe* for the large cells (mainly the earlywood, see orange dashed grid) and *sll* and *swl* for the small cells (mainly the latewood, see red dashed grid). If more than one cell falls in the rectangle, the cell closer to the target is selected. The algorithm moves sequentially from cell to cell until it reaches the end of the radial file, i.e., when no neighbouring cell can be found within the search grid.

3.4 Prospects from radial file positional data

RAPTOR is designed to complement the latest generation of software tools that measure cell parameters in conifer wood. The implementation of RAPTOR into wood anatomical research enhances the possibility to investigate and model tree-ring growth and functioning from a cellular perspective. The provided positionally-ranked tracheid information within identified radial files facilitates rapid construction of tracheidograms from wood anatomical measurements (e.g.,

de la Cruz & DeSoto 2015; Campelo *et al.* 2016). With these functionalities, RAPTOR allows tracheidogram-users to access and exploit the recently improved efficiency in term of measured number of cells (e.g., Castagneri *et al.* 2017) and parameters (e.g., von Arx *et al.* 2016, Prendin *et al.* 2017) offered by the latest quantitative wood anatomical measuring systems.

We offer access to the characterisation of a significantly increased number of radial files, aiding in the development of more robust and versatile intra-annual anatomical parameters. Also, these measurements provide a better appreciation of the large variability of anatomical parameters among radial files, annual rings, and species (Figure 3.5; see Supporting information for installation and coding examples). The increased robustness will benefit a multitude of studies that require representative cell-based anatomical tree-ring profiles for gymnosperm species, as is often the case when modelling tree-ring formation, structure and functioning (Vaganov *et al.* 1990; Fritts *et al.* 1991; Vaganov *et al.* 2006).

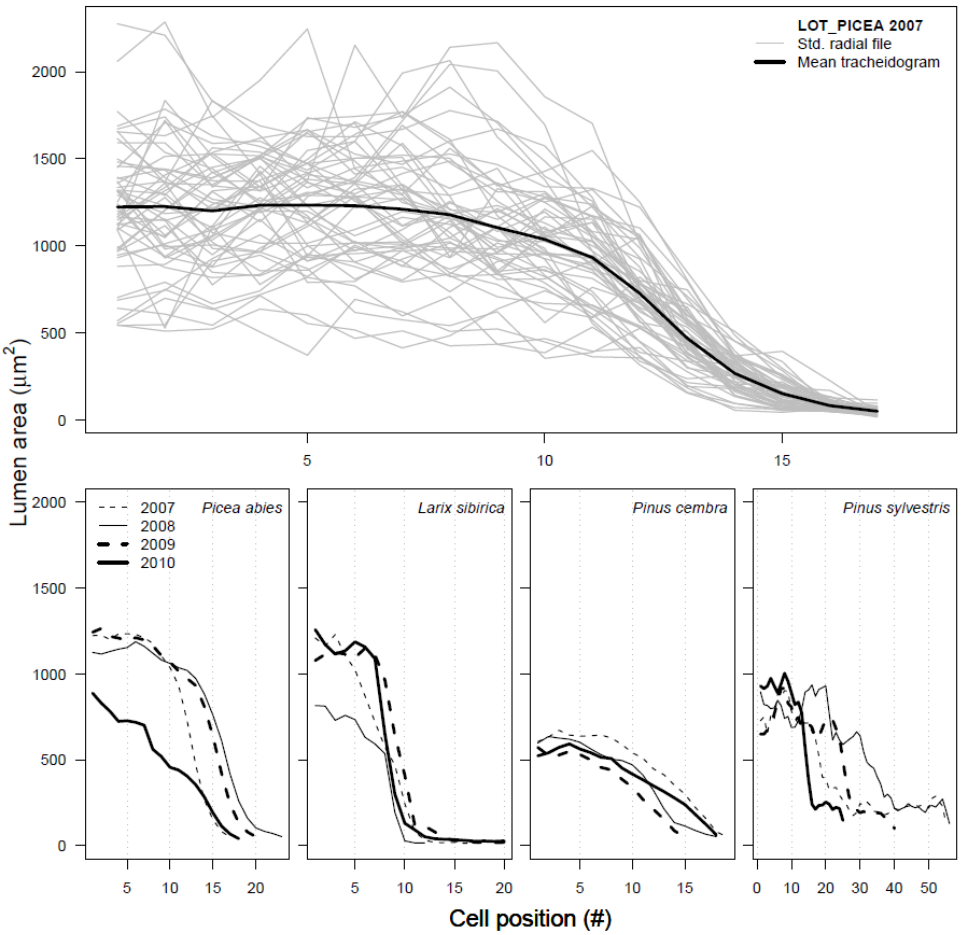

Figure 3.4 Comparison of individual tracheidograms within a single annual ring (upper graph) and mean tracheidogram among years and species (lower graph) as obtained with RAPTOR using the example data (including *Picea abies, Larix siberica, Pinus cembra* and *Pinus sylvestris*; see *example.data ()*).

Acknowledgements

We thank Stefan Klesse and Ana Stritih for discussion on the algorithm development. This work was funded by the Swiss National Science Foundation (Project LOTFOR no. 150205). DB used infra-structure of the Terrestrial Environmental Observatory (TERENO) ofthe Helmholtz Association and was supported by the DeutscheForschungsgemeinschaft, DFG, project number HE 7220/1-1.

Supporting information Chapter 3

Supplementary data associated with this chapter can be found, in the online version of the article, at http://dx.doi.org/10.1016/j.dendro.2017.10.00.

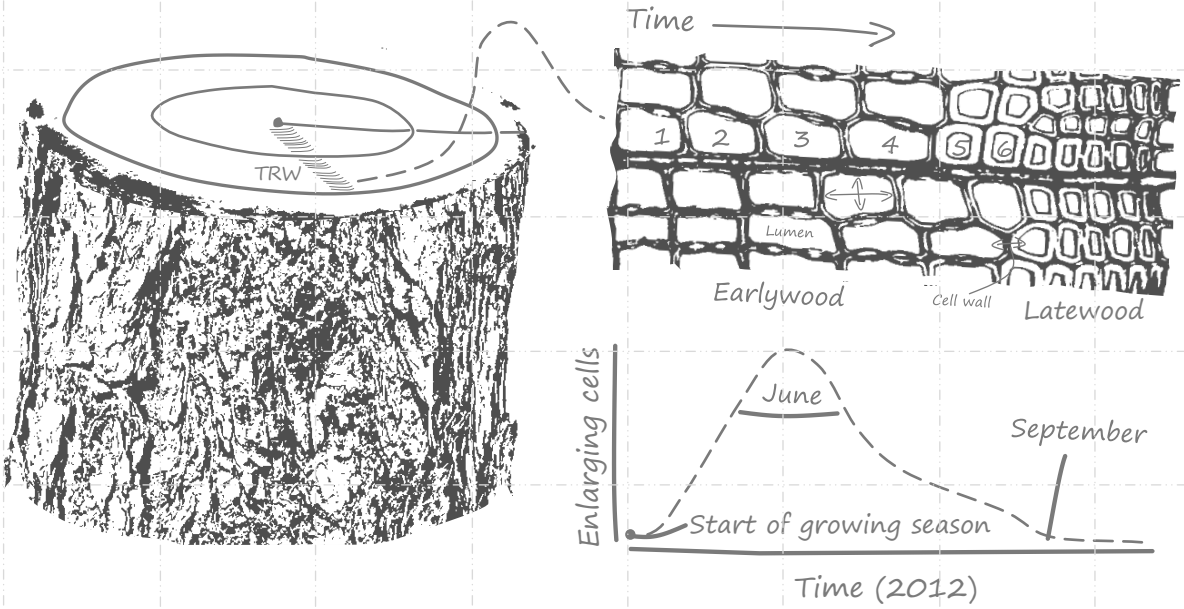
Time
TRW
1
2
3
4
5
6
Lumen
Earlywood
Cell wall
Latewood
Enlarging cells
June
September
Start of growing season
Time (2012)

Chapter 4

Couplings in cell development kinetics mitigate temperature influence on conifer wood anatomy

Henri E. Cuny, Patrick Fonti, Cyrille B.K. Rathgeber, Georg von Arx,
Richard L. Peters, David C. Frank
Under review in Plant, Cell & Environment

Abstract

Conifer trees possess similar anatomical tree-ring structures from tropical to boreal forests. However, little is known on how these characteristic structures, which play a crucial role in tree functioning by ensuring sap ascent and mechanical support, are maintained stable across contrasting environmental conditions. In this study we performed several years of weekly cellular-based monitoring of wood formation in two temperate coniferous species across an 8 °C thermal gradient to investigate the impact of temperature on wood cell formation. Results indicated that when moving towards colder sites, differentiating wood cells compensate to a decreased enlarging and wall-thickening rate with an increased duration, except for the wall-thickening latewood cells. This compensation allows conifer trees to mitigate the influence of temperature on the final tree-ring structure, with important implications for the functioning of the xylem. The lack of compensation for the thickening latewood might explain the superior climatic sensitivity usually found in maximum latewood density. Coupling duration with rate appears as a fundamental feature to increase resilience in xylogenesis.

4.1 Introduction

Conifers display an extraordinary biogeography with more than 600 species widely distributed across the globe: from the latitudinal limits of tree growth in the Northern and Southern Hemispheres to the Equator; from lowland savannas to near the perpetual snow line of the highest mountains; and from the wet forests of Alaska to the central Sahara (Farjon & Filer 2013). Despite growing in highly contrasted environments, conifers generally develop similar tree-ring structures (Schoch *et al.* 2004). Tracheids - the cells which provide both water transport and mechanical support and in conifers represent about 90% of wood tissue (i.e., xylem) - are characterized by a progressive transition in their dimensions. In wood tissue produced during the early part of the growing season, the earlywood, tracheids are large with thin cell walls. Whereas tissue produced at the end of the growing season (the latewood), is characterized by narrow, thick-walled cells. In short, a continuous transition in cell size and wall thickness is characteristic of conifers (Cuny *et al.* 2014, Schoch *et al.* 2004). This typical tree-ring structure reflects structural and physiological trade-offs that are important for tree functioning and performance. Wider tracheids are more efficient in transporting water but more prone to cavitation, while narrower thick-walled tracheids provide

most of the mechanical support, yet are less efficient in transporting water (Chave *et al.* 2009).

To date, most studies dealing with the influence of environment on wood formation (i.e., xylogenesis) have focused on the phenology (i.e., beginning, end, and duration of cambial activity and wood formation season; Deslauriers *et al.* 2008, Rossi *et al.* 2007, Rossi *et al.* 2008, Rossi *et al.* 2016). Such studies have revealed the strong plasticity of this aspect in response to temperature variations: e.g., towards colder environments growing season is shorter because wood formation starts later and ends earlier. But much less is known on how tree-ring structure is shaped during xylogenesis beyond the dependence upon kinetics of xylem cell differentiation processes: namely, the duration and rate of cell enlargement determine the final size of a xylem cell, while the duration and rate of wall thickening govern its final weight. The contribution of each kinetic parameter in shaping the typical tree-ring structure has been recently quantified for temperate coniferous species (Cuny *et al.* 2014, Rathgeber *et al.* 2016). Yet, it remains unknown how these kinetic parameters may or may not vary across changing environments to maintain characteristic anatomical structures.

Here, we investigate how xylogenesis shapes conifer tree-ring structure across contrasting thermal environments. For this purpose, we gathered up to seven years (depending on site) of quantifications of wood formation dynamics and tree-ring structure for 2 coniferous species - Norway spruce (*Picea abies* L.) and European Larch (*Larix decidua* Mill.) - along a ≈2000 m elevational gradient in western Europe (see Figure S4.1). The elevational gradient exhibits an amplitude of 8 °C in mean annual temperature (Table 4.1). We used a novel modelling approach to associate cell differentiation kinetics and final cell dimensions with the corresponding thermal conditions (Cuny & Rathgeber, 2016; see Figure S4.2). We establish the following three hypotheses: H1) lower site temperature is associated with a later start, earlier ending and shorter duration of xylem tissue formation; H2) due to these adjustments in phenology, xylem cells experience similar thermal conditions during their differentiation along the thermal gradient; H3) consequently, the kinetics (rates and durations) of the cell differentiation processes (cell enlargement and wall thickening) which determine the final dimensions of xylem cells, and thus shape the tree-ring structure, is similar in all thermal environments.

4.2 Materials and methods

Study area

The research was conducted at two main locations: one in the Lötschental valley (LTAL), in the Swiss inner Alps (46°23'N, 7°45'E), and one in the Donon (DNN), in the Vosges Mountains in northeast France (48°35'N, 7°08'E; see Figure S4.1). In total, the research design includes 12 sites (nine at the LTAL and three at the DNN) covering a wide range of temperature, with a difference of about 8 °C between the mean annual temperatures of the coldest (2.2 °C) and the warmest sites (10.3 °C; Table 4.1). The nine sites of the LTAL were selected along a 1400 m elevational transect (from 800 to 2200 meters above sea level; MASL) including both north and south aspects (see Figure S4.1). At 1300 MASL two sites were chosen on the same north aspect, with one site presenting particularly wet conditions (N13W). At each site of the LTAL, Norway spruce (*Picea abies* (L.) Karst.) and European Larch (*Larix decidua* Mill.) are growing in inter-mixed stands, with the exception of the highest sites (N22 and S22) where only Larch is present. In the DNN, the three sites were selected along a 300 m elevational gradient (from about 350 to 650 MASL; see Figure S4.1). At each of these sites, Norway spruce is growing in mixed coniferous stands.

Table 4.1 Main characteristics of sites and trees monitored. The table describes the sites (elevation, orientation, mean temperature and number of freezing days over the monitoring period), the trees (age, diameter at breast height [DBH] and height [H]), and the monitoring characteristics (number of years and period of monitoring, species studied, number of sampled trees) for the DNN (Donon, Vosges Mountains, France) and LTAL (Lötschental, Alps, Switzerland) locations. For age, DBH and H, the mean ± the standard deviation are given. For species PA and LD indicated *Picea abies* and *Larix decidua*, respectively.

Location	Site	Elevation (m a.s.l.)	Orientation	Mean T (°C)	Nb of freezing days	Nb of years	Period of monitoring	Species	Nb of trees per year	Age (year)	DBH (cm)	H (m)
DNN	WAL	370	South-West	10.3	27	3	2007-2009	PA	5	89±8	53±4	32±2
	ABR	430	West	9.1	36	3	2007-2009	PA	5	85±15	41±5	32±1
	GRA	650	South-West	8.6	39	3	2007-2009	PA	5	74±7	55±9	33±3
LTAL	N08	800	North	9.2	64	3	2008-2010	LD	4	167±21	49±5	22±3
								PA	4	154±12	43±9	27±3
	N13	1300	North	5.7	107	7	2007-2013	LD	4	151±18	53±16	31±7
								PA	4	134±40	46±6	27±5
	N13W	1300	North	4.2	123	2	2012-2013	LD	3	153±26	55±14	28±6
								PA	3	111±24	53±16	28±8
	N16	1600	North	4.9	117	4	2007-2010	LD	4	214±33	55±8	33±3
								PA	4	223±64	55±6	34±3
	S16	1600	South	5	113	7	2007-2013	LD	4	152±128	54±12	27±3
								PA	4	221±139	43±9	24±3
	N19	1900	North	3.1	132	4	2007-2010	LD	4	264±20	52±3	32±2
								PA	4	200±25	52±9	30±4
	S19	1900	South	3.9	115	7	2007-2013	LD	4	206±66	43±6	22±2
								PA	4	186±72	50±9	24±3
	N22	2200	North	2.2	152	4	2007-2010	LD	4	251±96	42±9	18±4
	S22	2200	South	3.2	129	7	2007-2013	LD	4	246±39	41±8	18±2

Sampling, preparation, and microscopic observations of xylem development

Xylogenesis was monitored during three years in DNN (2007-2009) and up to seven years in the LTAL (2007-2013), depending on the site (Table 4.1). On each site, three to four (in LTAL) or five (in DNN) mature and dominant trees per species (Norway spruce at DNN; Norway spruce and European larch at LTAL) were monitored each year. In the LTAL, because of the long-term monitoring performed, the monitored trees were changed after the 2007, 2009 and 2011 growing seasons in order to reduce impact of sampling-related wound reaction. In the DNN, the same five trees were monitored during the three years.

To monitor xylogenesis, microcores were collected weekly at breast height on the stem of the selected trees from April to November, using a Trephor tool (Rossi *et al.* 2006a). Successive microcores were then taken at least 1 cm apart from each other and following a slightly ascending spiral pattern to avoid wound reaction. Microcores were then prepared in the laboratory, and 5-15 µm-thick transverse sections were cut with a microtome. Sections were stained (with cresyl violet acetate at DNN, safranin and astrablue at LTAL) and permanently mounted on glass slides (Rossi *et al.* 2006b). Xylogenesis observations were performed on the sections using an optical microscope under visible and polarized light at ×100-400 magnification to distinguish the different phases of development among the cells. Thin-walled enlarging cells were discriminated from cambial cells by their larger size. Cells in the thickening zone developed secondary walls that can be detected under polarized light because of the orientation of cellulose microfibrils (Abe *et al.* 1997). Staining was used to follow the advancement of lignification (Rossi *et al.* 2006b). Thickening cells exhibited two-colored walls indicating that lignification was in progress, whereas mature tracheids presented entirely lignified and thus monochromatic walls.

Count data of cells in different xylogenesis phases were standardized by the total number of cells of the previous ring (Rossi *et al.* 2003) using the R package CAVIAR (Rathgeber *et al*. 2011a). This standardization process reduces the noise in the data, thus increasing the signal-to-noise ratio by about 50% (Cuny *et al.* 2014).

Quantitative wood anatomy

For each tree, anatomical sections from microcores (DNN) or from standard 5 mm cores (LTAL) taken after the end of the growing season were used to characterize the structure of the tree rings produced during the monitoring period. Digital images of the tree rings were analyzed using image analysis software specifically developed for wood cell analysis in order to measure the dimensions of tracheids

along radial files. The WinCell software (Regent instruments, Canada) was used for trees at DNN to measure cell dimensions along an average of five radial files per tree; and ROXAS (von Arx & Carrer 2014; von Arx *et al.* 2016) was used for trees at LTAL to measure cell dimensions along an average of 30 radial files. Both software measures the radial and tangential lumen diameter, the lumen area and the wall thickness of each tracheid from transversal cuts. However, while WinCell measures only the tangential wall thickness, ROXAS measures both the tangential and the radial wall thicknesses. ROXAS measurements revealed that for both species the radial and tangential wall thicknesses are similar in earlywood, whereas in latewood the radial wall thickness is about 1.3 times larger. We used these values to estimate the radial wall thickness at DNN. From these anatomical variables, the cell and wall cross-sectional areas (CCA and WCA) were then calculated and considered as the final results of the differentiation phases of cell enlargement and wall deposition, respectively (Figure 4.1; Cuny *et al.* 2014).
To show variations in tracheid dimensions along a ring, individual cell morphological measurements were grouped by radial file in profiles called tracheidograms (Vaganov 1990). Because the number of cells varied between radial files within and between trees, tracheidograms were standardized according to Vaganov's method (Vaganov 1990) using a dedicated function of the R package CAVIAR (Rathgeber 2012). This standardization allows adjusting the length of the profiles (cell numbers) without changing their shape (cell dimensions (Vaganov 1990). We checked visually that this standardization didn't alter the shape of the anatomical profiles. The standardized tracheidograms were then averaged by site, year and species.

Mature tracheids were classified into three different types of wood: earlywood, transition wood and latewood; according to Mork's criterion (*MC*) (Denne 1988), which is computed as the ratio between four times the tangential wall thickness divided by the radial lumen diameter. Tracheids were classified as follows: $MC \leq 0.5$, earlywood; $0.5 < MC < 1$, transition wood (not further used in the analysis); $MC \geq 1$, latewood (Figure 4.1; Park & Spiecker 2005).

Quantification of wood formation dynamics quantification
In order to characterize accurately wood formation dynamics, generalized additive models (GAMs) were fitted on the standardized numbers of cells for each phase of xylem development, each year, and each individual tree (Cuny *et al.* 2013), using the R package mgcv (R development core team, 2015; Wood 2006). The predictions of the fitted models were then averaged in order to characterize the mean behavior of each species, during each year, and at each site.

Moreover, for each species, we used the average cell numbers predicted by GAMs to calculate the date of entrance of each cell in each differentiation zone (enlargement, wall thickening and mature) of xylem formation along the developing tree ring, following the method described in (Cuny *et al.* 2013; see Figure S4.2). From these dates, the duration of stay of each cell i in the enlargement ($d_{E,i}$) and wall thickening ($d_{W,i}$) zones were computed. For each cell i, we then estimated the rate of enlargement ($r_{E,i}$) and wall thickening ($r_{W,i}$) by dividing its final dimensions (CCA_i and WCA_i) by the duration ($d_{E,i}$ and $d_{W,i}$) it spent in the corresponding phase (enlargement and wall thickening; Cuny *et al.* 2014).

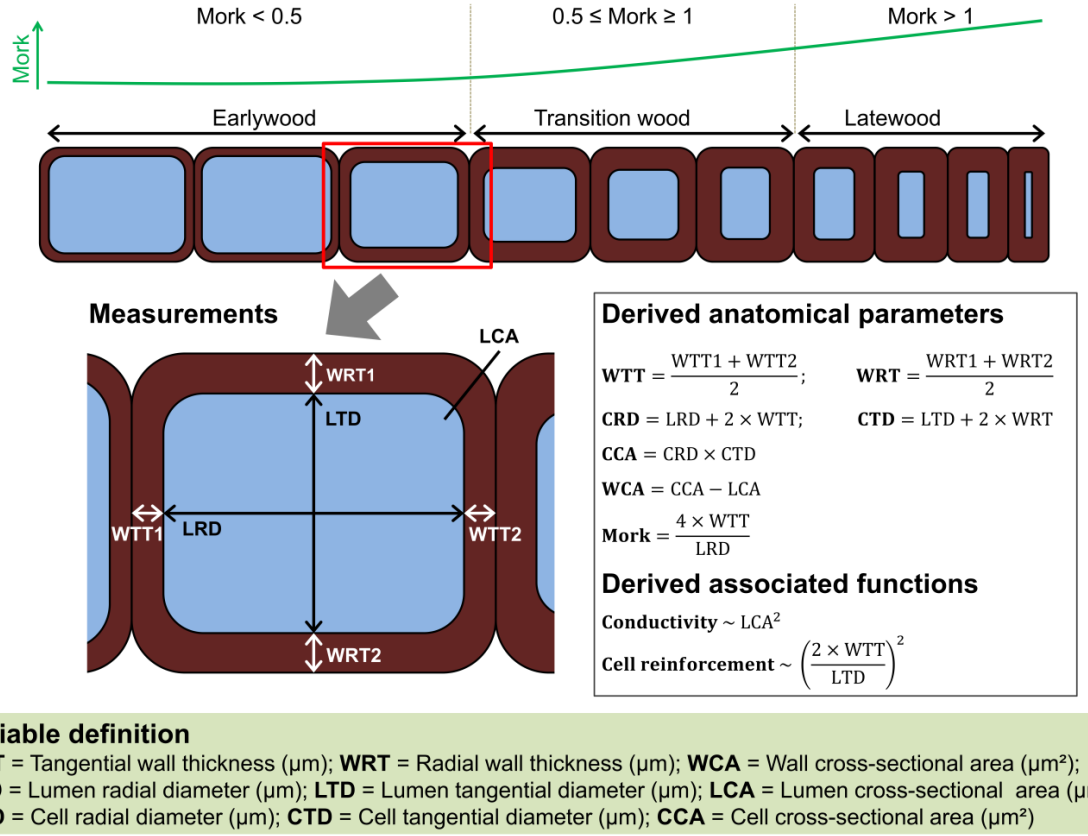

Variable definition
WTT = Tangential wall thickness (µm); **WRT** = Radial wall thickness (µm); **WCA** = Wall cross-sectional area (µm²); **LRD** = Lumen radial diameter (µm); **LTD** = Lumen tangential diameter (µm); **LCA** = Lumen cross-sectional area (µm²); **CRD** = Cell radial diameter (µm); **CTD** = Cell tangential diameter (µm); **CCA** = Cell cross-sectional area (µm²)

Figure 4.1 Illustration of the cell anatomical measurements performed. For every cell along a radial file, we measured the lumen radial and tangential diameter and the cross-sectional area of the lumen, as well as the radial and tangential wall thicknesses. From these measurements, we could then calculate the diameters and area of the cells, and the area of the wall. These dimensions were used to derive some indexes related to cell functional performances, specifically the conductivity and the cell reinforcement.

Meteorological data

In the LTAL, climatic conditions (air temperature, air relative humidity, soil moisture) were measured in-situ at each site beneath the canopy during the monitoring period with a 15-min interval. At the DNN, daily meteorological data

(temperature, precipitation, cumulative global radiation, wind speed, and air relative humidity) of the monitoring period were gathered from three meteorological stations spread in the studied area, following the disposition of the selected sites. For every site, the soil relative extractable water (REW) was calculated. For the LTAL, the REW was directly calculated using the measurements of soil moisture and the soil depth. For the DNN, the REW was assessed with the model Biljou©, which takes as input the measured meteorological parameters along with several soil (e.g., number and depth of layers as well as proportion of fine roots per layer) and stand (forest type and maximum leaf area index) parameters, and gives as output the REW at a daily scale (https://appgeodb.nancy.inra.fr/biljou/; Granier *et al.* 1999).

Temperature influence on wood formation dynamics and tree-ring structure
In order to study accurately the mechanisms by which xylogenesis and tree-ring structure respond to air temperature, the kinetics of tracheid differentiation and the resulting dimensions of xylem cells were associated with the exact thermal conditions prevailing during the process (see Figure S4.2). For example, the kinetics of enlargement and the final cross-sectional area of a cell were related to the mean temperature experienced during the enlargement of this cell. Similarly, the kinetics of wall thickening and the final wall cross-sectional area of a given cell were related to the mean temperature it experienced during its wall thickening. Finally, the lumen area and wall thickness, which integrate both cell size and wall amount, were related to the mean temperature experienced during the whole period of cell differentiation (i.e., enlargement plus wall thickening).

As we wanted to focus on the variations in kinetics and anatomy according to the different thermal environments (i.e., sites), data (cell development kinetics, cell dimensions and associated thermal conditions) were averaged per sites, species and also by separating earlywood and latewood cells in order to test the possibility of different sensitivities between these two tree-ring compartments. Transition wood was discarded to only focus on clearly defined wood structures. Then, relationships between averages of thermal conditions, kinetics parameters (rate and duration of cell enlargement and wall thickening), and anatomical variables (cell area, lumen area, wall area, wall thickness) were assessed using linear models. In particular, covariance analyses were performed to evaluate the effects of species (European larch and Norway spruce), wood types (earlywood and latewood), tree age and dimensions (height and diameter) on the relationships. Significant variables and interactions were identified by backward elimination using the R function drop1 (R development core team 2015), which allows

selecting the best model based on the Akaike information criterion (AIC). Finally, as the assessed kinetics and anatomical parameters are on different scales and have different absolute values between them and between early- and late-wood, relationships were also assessed on normalized data in order to compare the slopes between the different variables and wood types. In order to test the effects of other potentially important climatic factors related to site hydric conditions, the same approach was conducted using the soil relative extractable water instead of temperature.

Implications of the xylogenesis response to thermal conditions for tree-ring structure and functions

To assess the implications of the xylogenesis response to thermal conditions in terms of tree-ring structure and associated functions, we used the relationships established to simulate the average kinetics and resulting dimensions of the cells produced at two theoretical sites representing a 5 °C gradient (≈3.5 °C and 8.5 °C in average temperature, respectively). For that, the relationships established between thermal conditions and kinetics parameters were used to simulate the rate and duration of differentiation processes for the two thermal modalities. The simulated kinetics were then used to calculate cell dimensions. For example, the cell cross-sectional area was calculated by multiplying the simulated rate and duration of cell enlargement, while the wall cross-sectional area was calculated by multiplying the simulated rate and duration of wall thickening. Other dimensions (lumen area, cell and lumen diameters, and wall thickness) could then be calculated from these two anatomical dimensions and used to build virtual cells assuming rectangular-shaped tracheids (Cuny *et al.* 2014). Finally, the calculated cell dimensions were used to infer some indices about the functions (conductivity) and mechanical properties (cell reinforcement) associated to the simulated tracheids (Figure 4.1). Conductivity was thus calculated as the power 2 of the lumen cross-sectional area according to Hagen-Poiseuille law (Sutera & Skalak 1993), while the cell reinforcement was calculated according to (Hacke *et al.* 2001):

$$Cell\ reinforcement = \left(\frac{2 \times WTT}{LTD}\right)^2 \quad \text{(Eq. 1)}$$

where *WTT* is the tangential wall thickness and *LTD* the lumen tangential diameter (Figure 4.1).

4.3 Results

Wood formation phenology partially adjusts to the thermal environment

Our observations only partially confirm our first hypothesis, namely the phenology of xylem tissue formation adjusts to thermal environment. We indeed find that along the gradient, the start of wood formation shows strong negative linear relationships with the mean annual temperature of the site (p <0.001, n= 19; Figure 4.2; see Table S4.1). For both species, the beginning of cell enlargement period is delayed by 4.7 days for a 1 °C decrease in temperature, whereas the beginnings of wall thickening and mature periods are delayed by 5.2 and 6.7 days, respectively (Figure 4.2). In contrast, the ending of wood formation phases does not show any statistical association with site temperature (Figure 4.2).

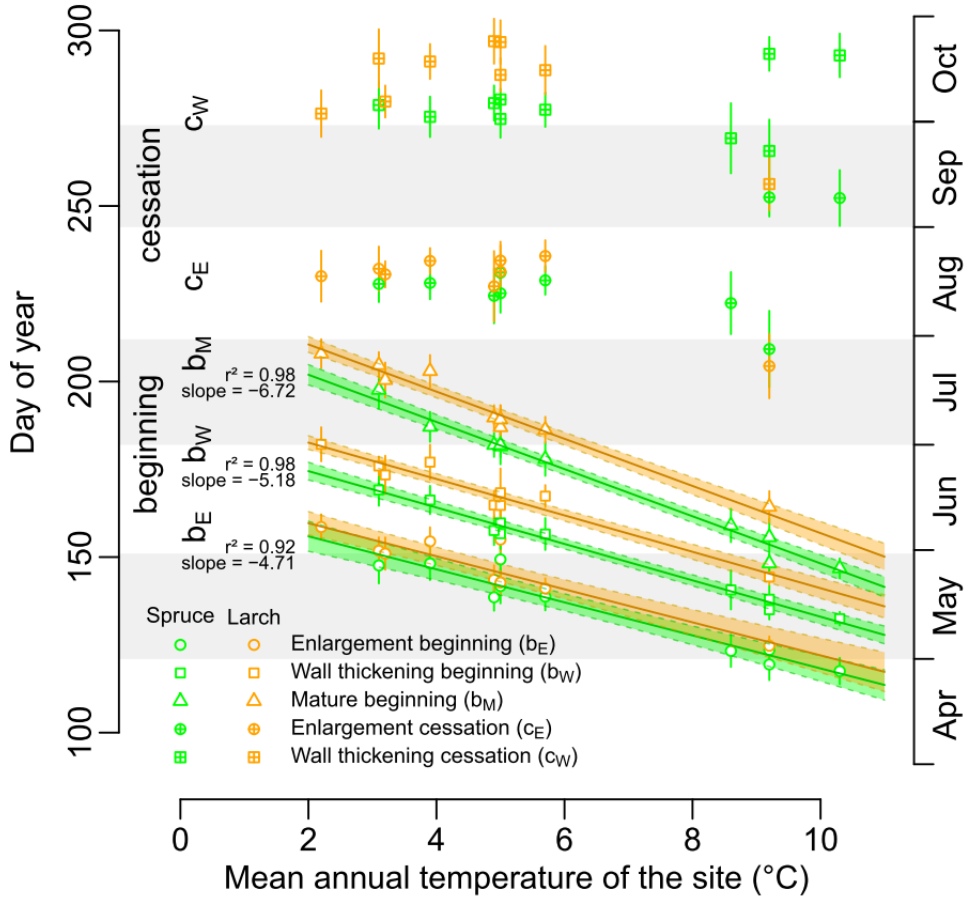

Figure 4.2 Phenology of wood formation. Timing of xylem tissue formation along the thermal gradient with the beginnings of cell enlargement (b_E), wall thickening (b_W) and mature (b_M) periods and the cessations of cell enlargement (c_E) and wall thickening (c_W) periods. Each point represents a site average for one species, while bar symbolizes the associated standard deviation. Orange and green lines represent the relationships between temperature and the different phenological dates for larch and spruce, respectively. Colored areas around lines represent the 95% confidence intervals.

Temperature during cell development largely varies between thermal environments

Contradicting the second hypothesis, despite the plasticity observed in phenology, xylem cell differentiation operates at different temperatures along the gradient (Figure 4.3). For example, the temperature during differentiation of the first cells varies by 5 °C across sites (Figure 4.3b). Similarly, a 6 °C range is observed for the temperature experienced by earlywood cells (Figure 4.3c). Whereas thermal differences exceed 8 °C for latewood cells and approach 10 °C for the last cells in a ring (Figure 4.3d, e). These observations of temperature differences, that generally increase when moving from early- to late-wood cells, indicate that the delayed phenological onset at cold sites only partially buffers the gradient observed in mean annual temperature.

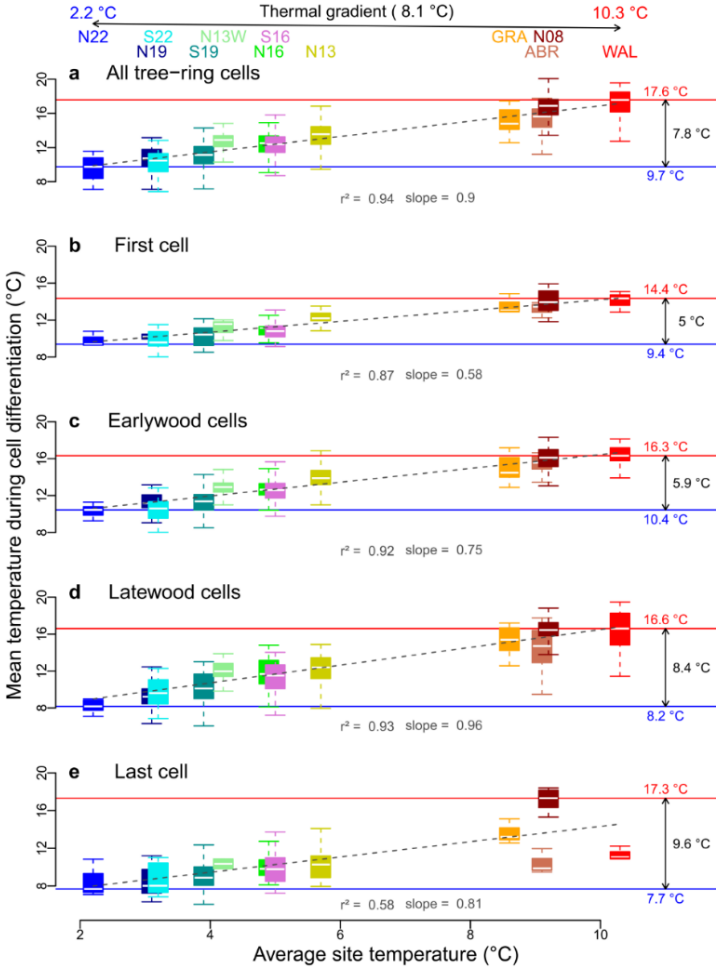

Figure 4.3 Temperature experienced during xylem cell differentiation. The figure shows the mean temperature experienced by xylem cells during their differentiation at the 12 sites along the thermal gradients considering all tree ring cells (a), the first cell of the tree-ring (b), earlywood cells (c), latewood cells (d) and the last cell of the tree-ring (e). Each boxplot represents the data included in one of the above-mentioned categories for the two species at one site over the monitoring period. The dashed lines represent the relationships between the mean temperature experienced during xylem cell differentiation and the average site temperature.

Temperature has strong influence on cell development kinetic

Figure 4.4 shows the implications thermal conditions have on xylogenesis processes, which exhibit different kinetics along the gradient, thereby disproving our third hypothesis. We find highly significant associations between temperature and the kinetics of cell differentiation processes (p <0.001, n= 38; see Table S4.2), whereas the hydric conditions have no effects (see Figure S4.3). For both species, we find strong, positive and linear relationships between the mean temperature experienced during process realization and the rates of this process (Figure 4.4a, b). However, we also observe strong, negative and linear relationships between temperature and the durations of processes (Figure 4.4c, d). In fact, it appears process rates and durations are tightly linked (Figure 4.4e, f). Towards colder sites, decreasing rates are associated with increasing durations. For cell enlargement, this coupling operates similarly in earlywood and latewood (Figure 4.4e). In contrast, for wall thickening, coupling breaks down in latewood (Figure 4.4f).

The plasticity observed in cell kinetics mitigate temperature influence on tree-ring structure

The observed compensation between rates and durations of xylogenesis processes mitigates temperature effects on tree-ring structure, which displays its characteristic pattern along the elevational gradient (see Figure S4.4). Yet, thermal conditions still have a significant influence on final cell dimensions (p <0.001, n= 38; Figure 4.5; see Table S4.3). Thus, we find consistent anatomical differences across the elevational gradient: tracheids have lower cell area (Figure 4.5a), wall area (Figure 4.5b), lumen area (Figure 4.5c) and wall thickness (Figure 4.5d) towards colder sites. Moreover, owing to the breakdown in rate-duration coupling for wall thickening, we observe a particularly high thermal sensitivity of wall area and wall thickness in latewood (Figure 4.5b, d).

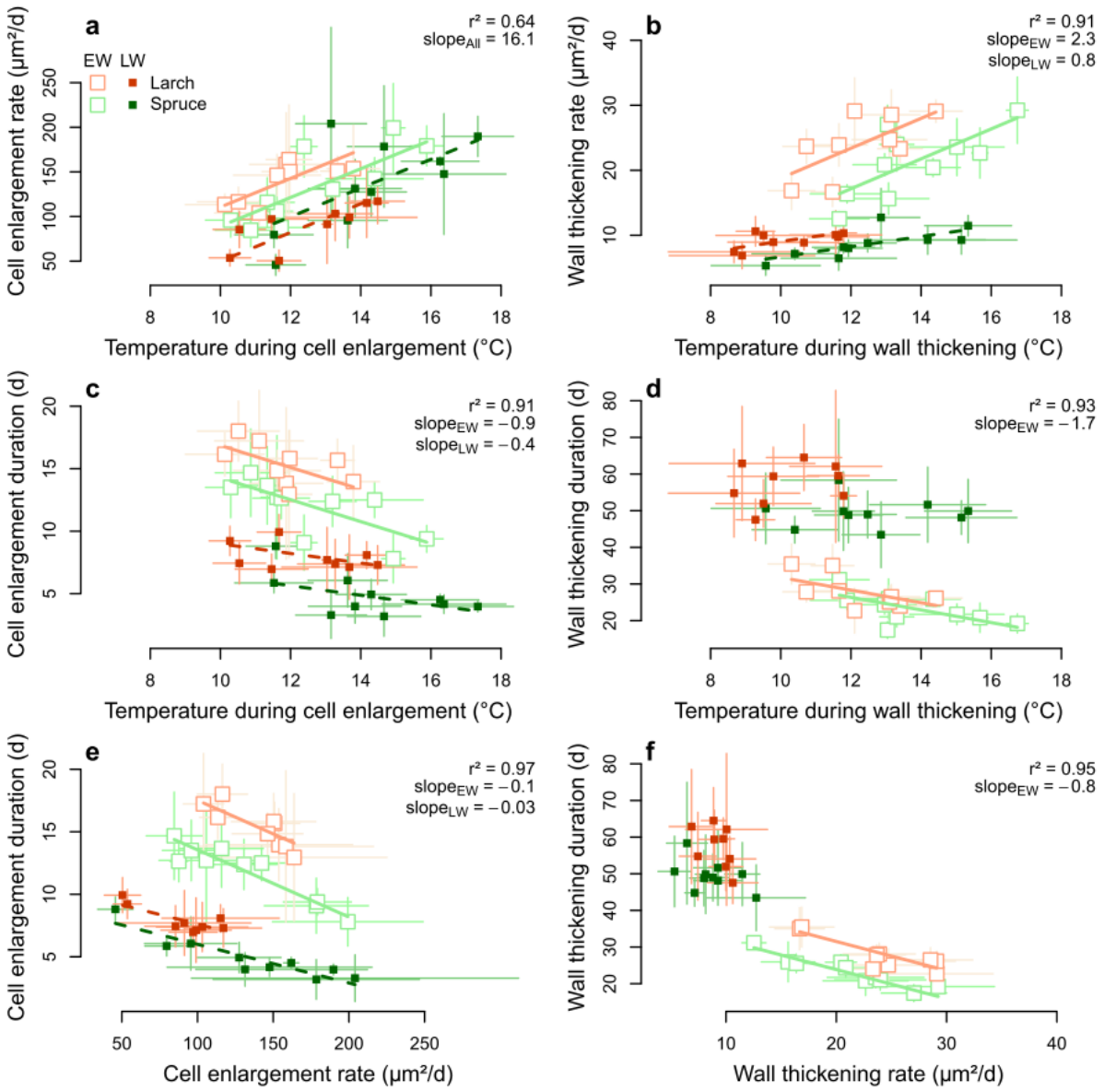

Figure 4.4 Influence of temperature on xylem cell kinetics. Relationships between the mean temperature experienced during process realization and process kinetics, including cell enlargement rate (a), wall thickening rate (b), cell enlargement duration (c) and wall thickening duration (d). Relationships between rate and duration of cell enlargement (e) and of wall thickening (f). Each point represents the site and species average for earlywood (*EW*) or latewood (*LW*) cells, with the corresponding 95% confidence interval. Lines represent the relationships for earlywood (solid light lines) and latewood (dashed dark lines). Slopes of relationships are given separately for earlywood ($slope_{EW}$) and latewood ($slope_{LW}$) when they are different; otherwise a single slope is given ($slope_{All}$). The provided r-squared values are for the whole model.

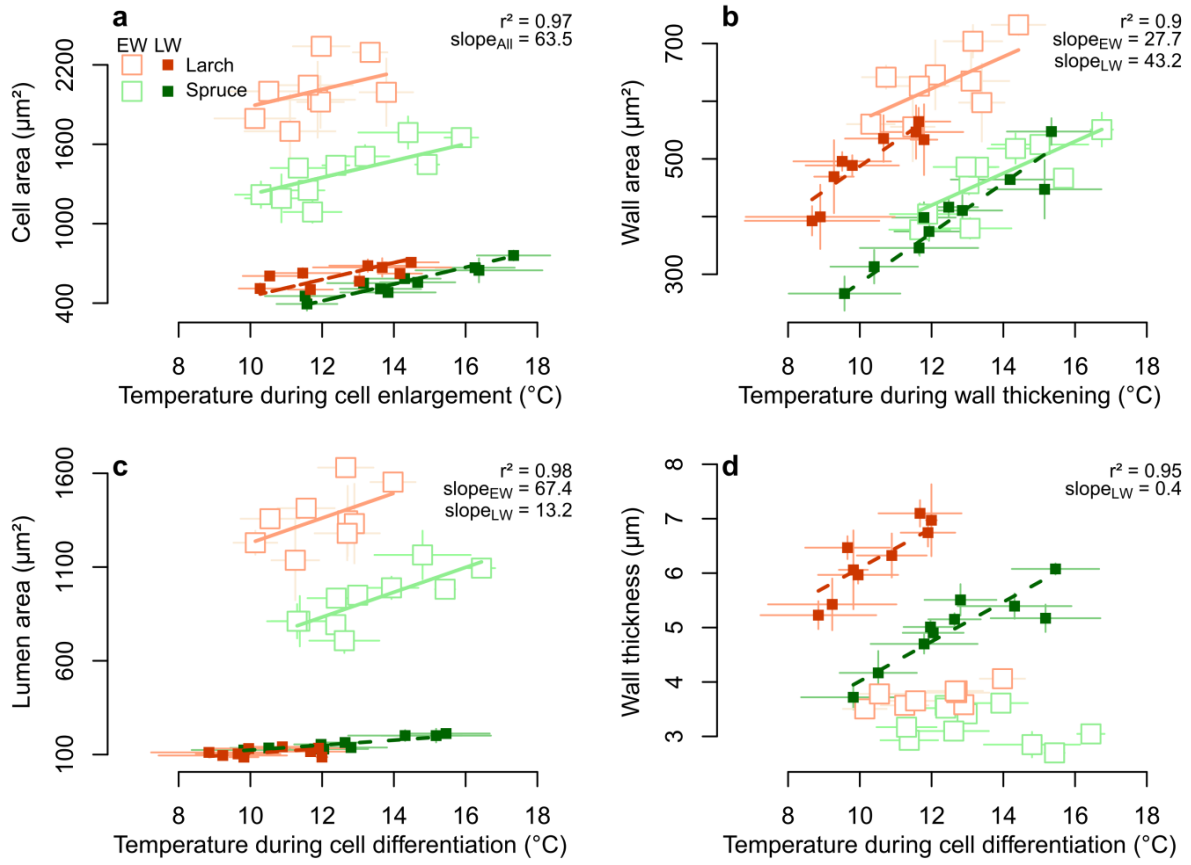

Figure 4.5 Influence of temperature on xylem cell dimensions. Relationships between the mean temperature experienced during process realization and the resulting cell dimension, with the cell cross-sectional area (a), the wall cross-sectional area (b), the lumen cross-sectional area (c) and the wall thickness (d). Each point represents the site and species average for earlywood (*EW*) or latewood (*LW*) cells, with the corresponding 95% confidence interval. Lines represent the relationships for earlywood (solid light lines) and latewood (dashed dark lines). Slopes of relationships are given separately for earlywood ($slope_{EW}$) and latewood ($slope_{LW}$) when they are different; otherwise a single slope is given ($slope_{All}$). The provided r-squared values are for the whole model.

4.4 Discussion

This study reveals the high plasticity and the complex interactions at play in the dynamic of wood formation in response to temperature. Our results emphasized a tight coupling between the rates and the durations of xylem cell development processes: towards colder environments, the rates of cell enlargement and wall thickening decreased, but in parallel their durations increased. Considering previous results from genetic studies performed along elevational gradients on the here-studied coniferous species are suggesting that the observed plasticity is rather a response to mean site climatology than a genetic adaptation of tree populations to local conditions (King *et al.* 2013b; Nardin *et al.* 2015).

The dependency of the start of xylem tissue formation to temperature we observed in our study sites matches well with previous reports for numerous other coniferous species in boreal (Rossi *et al.* 2016; Rossi *et al.* 2008), subalpine (Deslauriers *et al.* 2008; Rossi *et al.* 2007), temperate (Rossi *et al.* 2016), and Mediterranean (Camarero *et al.* 2010) forest biomes. In contrast, environmental factors controlling wood formation cessation remain unclear, even though temperature has also been recognized as an important driver across the Northern Hemisphere (Rossi *et al*. 2016). At more local geographical scales, the ending dates of wood formation have been related to the number of cells produced (Lupi, *et al.* 2010; Rossi *et al.* 2012), but here we observe no connection between the wood formation phenology and the annual increment, which is mostly related to the cell production rate (see Figure S4.5 and Table S4.4). Considering the stability of the ending dates across the thermal gradient, we speculate photoperiod (Mellerowicz *et al.* 1992) is an important factor controlling the end of xylem tissue formation in our sites.

Concerning the control of the kinetics of cell differentiation processes, the rate and the duration have usually been considered separately. On the one hand, the control of the rate has been associated with a direct influence of temperature on the metabolism (Balducci *et al.* 2016; Cuny & Rathgeber 2016; Cuny *et al.* 2015; Mellerowicz *et al.* 1992; Proseus *et al.* 1999; Proseus *et al.* 2000). Cell enlargement implies numerous enzyme reactions (e.g., cutting tethers to loosen the wall, synthesizing, transporting, delivering and inserting new wall polymers) with high activation energies, and thus likely being very sensitive to temperature (Proseus *et al.* 1999; Proseus *et al.* 2000), while the processes involved in wall thickening (e.g., cellulose and lignin biosynthesis, transport and deposition) are inhibited at temperatures still favorable for photosynthesis (Körner 1998; Körner 2003; Simard *et al.* 2013). On the other hand, the regulation of process duration has more commonly been associated with hormonal signaling (Schrader *et al.* 1997; Uggla *et al.* 1996). A morphogenetic gradient of auxin concentration would shape the zonation of the developing xylem and govern process durations by providing positional information to differentiating cells (Tuominen *et al.* 1997; Uggla *et al.* 1996).

By revealing a tight coupling between the rate and the duration of xylogenesis processes, our results plead in favor of a more integrated approach to understand xylogenesis and its control, with the necessity to consider together all components of the dynamics of the system and their interactions. Indeed, to date the mechanisms coordinating the durations and rates of cell differentiation

processes remain unknown. For wall thickening, a mechanism linking the rate of secondary wall deposition to the date of apoptosis may explain the observed coupling (Cuny & Rathgeber 2016; Groover & Jones 1999). But why and how this coupling is broken during latewood formation is unexplained (Cuny *et al.* 2014).

Thinking about the coupling, the question arises why do conifers put such efforts in maintaining their tree-ring structure instead of, for example, adjusting the number of cells. This strategy makes sense when viewed from a functioning standpoint, where a moderate change in cell dimension can trigger a dramatic change in functioning. For example, assuming tracheids behave as capillary tubes, the conductivity scales with the lumen diameter to the 4th power (Hagen-Poiseuille law; Sutera & Skalak 1993). Hence, a two-fold decrease in lumen diameter implies a 16-fold decrease in conductivity. In other words, 16 cells would be needed to achieve the conductivity of a single cell having a two times wider lumen.

We used the relationships presented in Figure 4.4 to simulate the average dimensions and associated properties of tracheids at two theoretical sites (cold and warm) representing a 5 °C gradient. To assess the implications of the observed kinetics regulation, we then performed this exercise for the cold site, but using durations of the warm site. We estimate that without adjustment in the durations of cell differentiation processes, trees growing at the cold site would produce earlywood tracheids with approximately two times smaller lumen areas than at warm site, implying nearly a four-fold reduction in conductivity (Figure 4.6). In reality, the duration adjustments allow producing cells with only 1.3 times smaller lumen areas and less than a two-fold reduction in conductivity. Simulations also reveal that duration adjustments allow increasing cell reinforcement and hydraulic safety of tracheids at the cold site (Figure 4.6). This makes sense with the necessity to increase resistance to frost-induced embolism by avoiding wall collapse under negative pressure (Charra-Vaskou *et al.* 2016).

Despite the compensatory mechanisms at play in the kinetics of cell development processes, anatomical differences were observed between the different thermal environments: trees growing at colder sites produced xylem cells having lower dimensions (cell area, wall area, wall thickness, and lumen area). Moreover, because of the breakdown of the coupling between rates and durations of wall thickening, latewood tracheids were particularly sensitive to temperature. Such result contribute to explain why the maximal wood density - a dendrochronological parameter tightly connected to the anatomy of latewood

tracheids - is particularly well related to temperature conditions and so useful as a proxy for paleoclimates (Briffa *et al.* 1998; Frank & Esper 2005; Hughes *et al.* 1984).

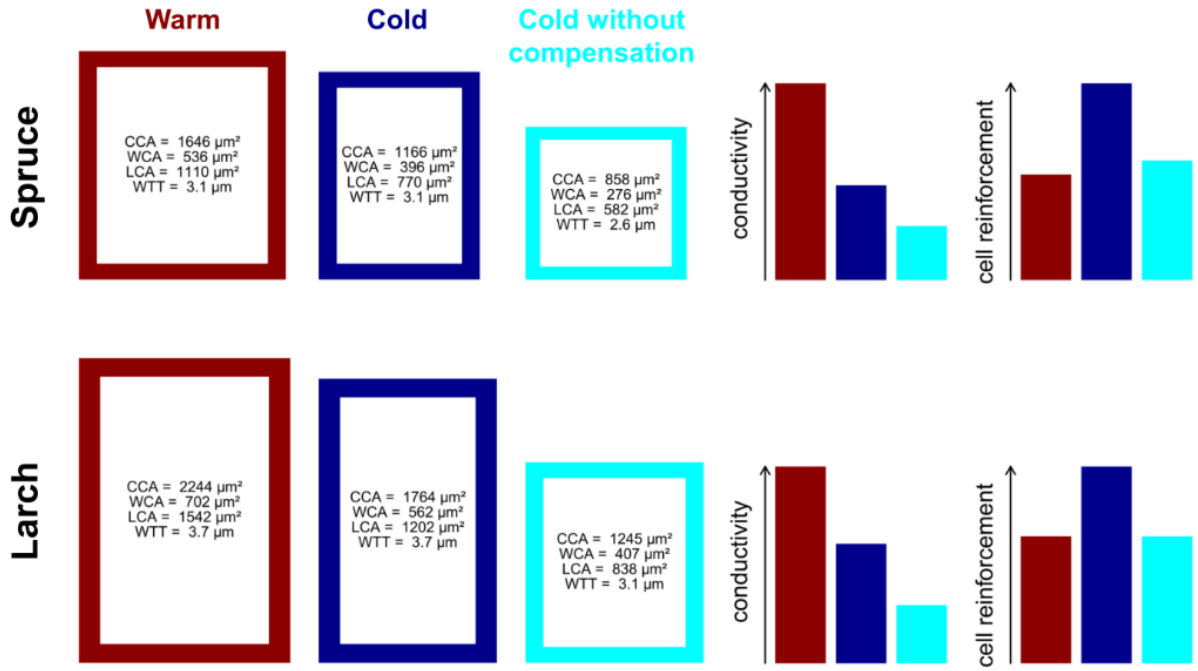

Figure 4.6 Morphology and associated derived cell functional performance of the earlywood xylem cells produced in European larch and Norway spruce simulated according to three scenarios (warm, cold and cold without compensation). Simulated tracheids were built using the relationships presented in Figure 4.4 and assuming a 5° C thermal gradient between the "warm" and "cold" scenarios. The "cold without compensation" scenario corresponds to the simulations performed for the theoretical cold site, but using the durations of the theoretical warm site in order to test the effect of the compensation played by the duration on the final cell dimensions and associated functions. The cell, wall and lumen cross-sectional areas (*CCA*, *WCA* and *LCA*), and the tangential wall thickness (*WTT*) of the simulated tracheids are given.

Our study reveals and quantifies the strong response of xylogenesis kinetics to the thermal environment. The compensation observed between rates and durations of tracheid differentiation notably appears as an essential mechanism that allows conifers to cope with environmental change. In addition to the role in dealing with seasonal climatic variations (Cuny & Rathgeber 2016) and mitigating the impacts of unusual extreme climatic events such as drought (Balducci *et al.* 2016), we show that this rate-duration compensation preserves the characteristic tree-ring structure optimized for mechanical stability and water transport across a wide range of thermal conditions. This study thus provides new fundamental insights into tree growth, as well as mechanistic understanding on response of trees to climate change.

Acknowledgments

We thank E. Cornu, E. Farré, J. Franzen, C. Freyburger, P. Gelhaye, Maryline Harroué, G. King, A. Mercanti, L. Moser, D. Nievergelt, L.Schneider, K. Treydte and A. Verstege for help in field- and lab-work; B. Longdoz, M. Nicolas and the association for the study and monitoring of air pollution in Alsace (ASPA) for supplying meteorological data. The authors acknowledge the Swiss National Science Foundation SNF (projects CLIMWOOD-160077 and LOTFOR-150205). GvA was supported by a grant from the Swiss State Secretariat for Education, Research and Innovation SERI (SBFI C14.0104). This research also benefited from the support of the FPS COST Action STReESS (FP1106).

Supporting information Chapter 4

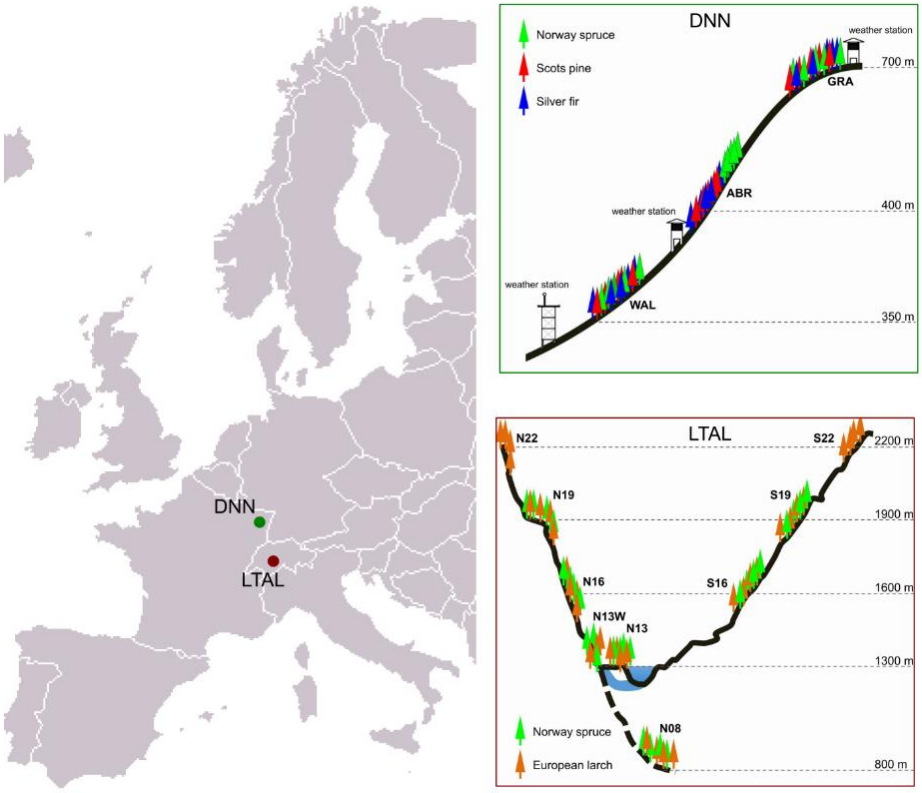

Figure S4.1 Location of the studied site. The DNN (Donon, Vosges Mountains, France) location includes three sites staged from 370 m to 650 m a.s.l., while the LTAL (Lötschental, Alps, Switzerland) location includes nine sites staged from 800 to 2200 m a.s.l. on both north (N) and south (S) aspects.

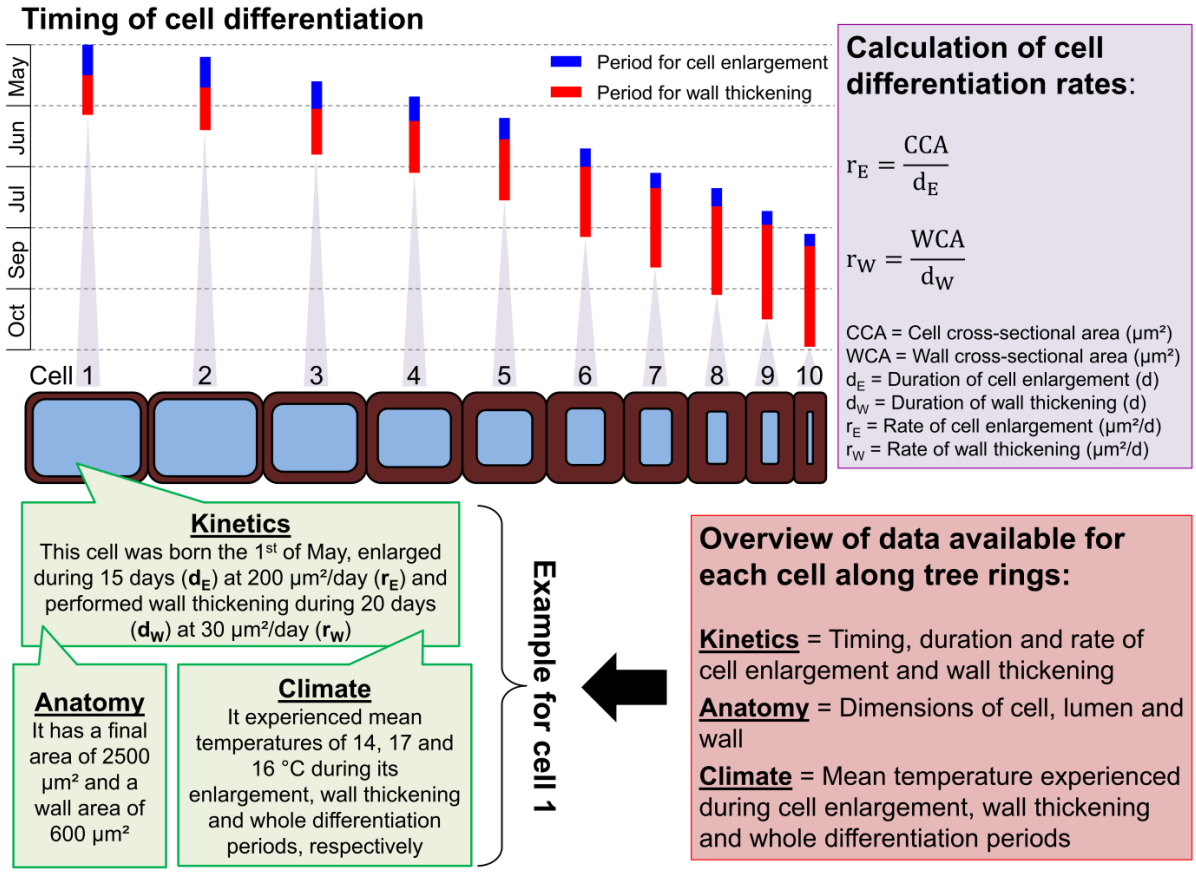

Figure S4.2 Overview of the information inferred by the approach applied along the thermal gradient for every site, year and species. For each xylem cell along a tree ring, the timing, duration, and rate of its enlargement and wall thickening are calculated. This allows linking cell anatomy with the co-occurring thermal conditions.

Table S4.1 Covariance analyses of the relationships between the site mean annual temperature (T_{site}) and the onset of wood formation between the two species. Points and asterisks highlight significant effects (˙ for p <0.1, * for p <0.05, ** for p <0.01 and *** for p <0.001).

Source	Df	Sum of squares	Mean Squares	F	p-value
Relationship between mean site temperature and beginning of cell enlargement period					
T_{site}	1	2699	2699	254.68	<0.001***
Tree species	1	56	56	5.32	<0.05*
Tree age	1	71	71	6.67	<0.05*
Residuals	15	159	11		
Relationship between mean site temperature and beginning of wall thickening period					
T_{site}	1	3666	3666	734.68	<0.001***
Tree species	1	268	268	53.78	<0.001***
Residuals	16	80	5		
Relationship between mean site temperature and beginning of mature period					
T_{site}	1	5913	5913	900.26	<0.001***
Tree species	1	303	303	46.12	<0.001***
Residuals	16	105	7		

Table S4.2 Covariance analyses of the relationships between temperature and cell kinetics for species and wood tissue (earlywood and latewood). T_E= cell enlargement; T_W= wall thickening); r_E and d_E= rate and duration of cell enlargement, r_W and d_W= rate and duration of wall thickening. Points and asterisks highlight significant effects (• for p <0.1, * for p <0.05, ** for p <0.01 and *** for p <0.001).

Relationships between T_E and r_E					
Source	Df	Sum of squares	Mean Squares	F	p-value
T_E	1	21844	21844	32.63	<0.001***
Wood tissue	1	14130	14130	21.12	<0.001***
Tree species	1	72	72	0.11	0.74
Wood tissue:Tree species	1	3541	3541	5.29	<0.05*
Residuals	33	22093	669		
Relationships between T_E and d_E					
T_E	1	251	251	134.52	<0.001***
Wood tissue	1	327	327	175.71	<0.001***
Tree species	1	52	52	27.84	<0.001***
T_E:Wood tissue	1	7	7	3.60	<0.1•
Residuals	33	61	2		
Relationships between T_W and r_W					
T_W	1	658	658	108.64	<0.001***
Wood tissue	1	1183	1183	195.37	<0.001***
Tree species	1	139	139	23.00	<0.001***
Tree height	1	51	51	8.48	<0.01**
T_W:Wood tissue	1	35	35	5.81	<0.05*
Wood tissue:Tree species	1	23	23	3.72	<0.1•
Residuals	31	188	6		
Relationships between T_W and d_W					
T_W	1	2493	2493	189.55	<0.001***
Wood tissue	1	5071	5071	385.54	<0.001***
Tree species	1	163	163	12.41	<0.01**
Tree height	1	169	169	12.84	<0.01**
T_W:Wood tissue	1	51	51	3.90	<0.1•
Wood tissue:Tree species	1	69	69	5.25	<0.05*
Residuals	31	408	13		

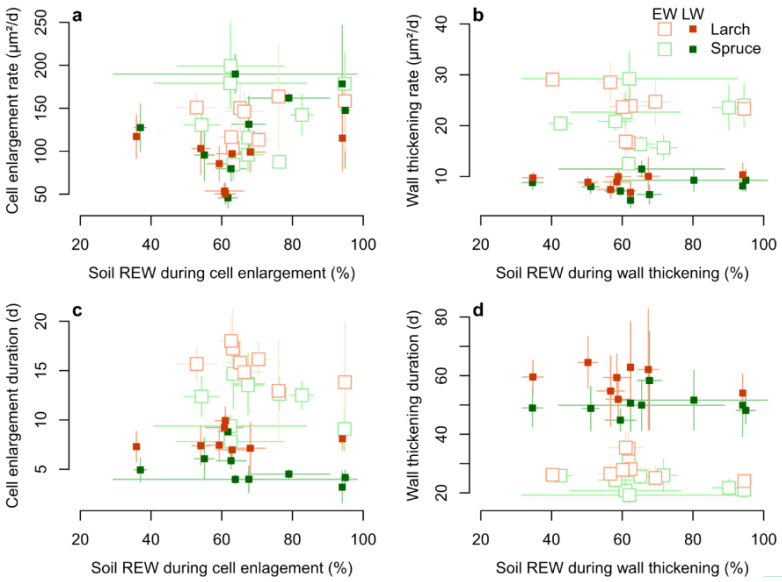

Figure S4.3 Kinetics of the processes of xylem cell development as a function of soil relative extractable water (REW). Each parameter of the kinetics of a process, including cell enlargement rate (a), wall thickening rate (b), duration of cell enlargement (c) and duration of wall thickening (d), is expressed as a function of the mean soil REW experienced during process realization. Each point represents the site and species average for earlywood (*EW*) or latewood (*LW*) cells.

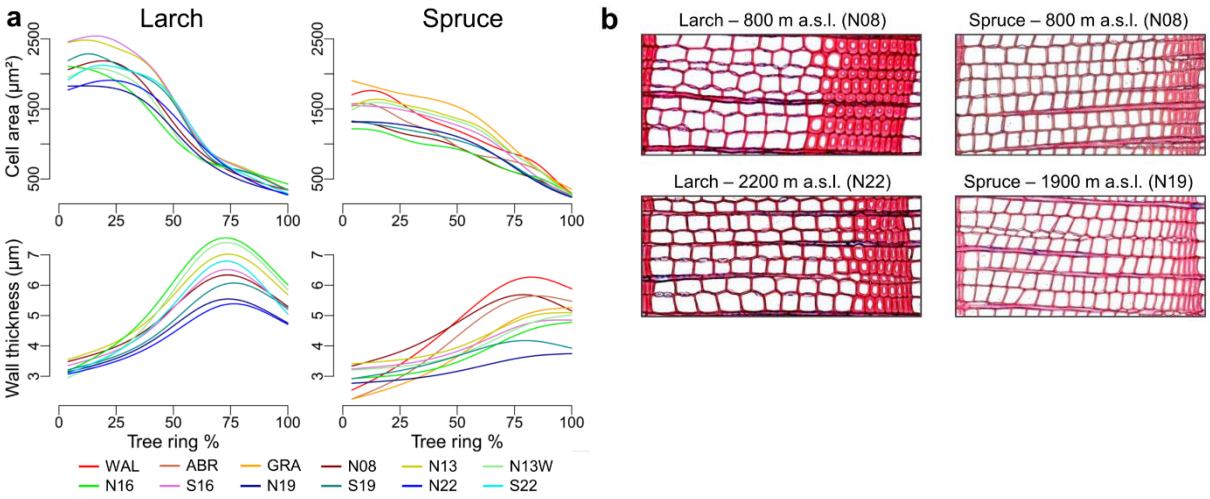

Figure S4.4 Tree-ring structure of the two coniferous species along the thermal gradient. (a) Average evolution of cell cross-sectional area and tangential wall thickness along the tree rings of the two species at each site of the gradient. (b) Pictures of tree rings of the two species at the bottom and too of the LTAL location.

Table S4.3 Covariance analyses of the relationships between temperature and cell dimensions for species and wood tissue (earlywood and latewood). T_E= cell enlargement; T_W= wall thickening); T_{Diff}= mean temperature during cell differentiation; *CCA*= cell cross-sectional area; *WCA*= wall cross-sectional area; *LCA*= lumen cross-sectional area; *WTT*= tangential wall thickness. Points and asterisks highlight significant effects (• for p <0.1, * for p <0.05, ** for p <0.01 and *** for p <0.001).

Relationships between T_E and *CCA*					
Source	Df	Sum of squares	Mean Squares	F	*p*-value
T_E	1	627839	627839	47.29	<0.001 ***
Wood tissue	1	10887122	10887122	820.07	<0.001 ***
Tree species	1	1492942	1492942	112.46	<0.001 ***
Tree height	1	69443	69443	5.23	<0.05 *
Wood tissue:Tree Species	1	560197	560197	42.20	<0.001 ***
Residuals	32	424828	13276		
Relationships between T_W and *WCA*					
T_W	1	37064	37064	37.00	<0.001 ***
Wood tissue	1	66447	66447	66.33	<0.001 ***
Tree species	1	271949	271949	271.49	<0.001 ***
Tree height	1	10660	10660	10.64	<0.01 **
T_W:Wood tissue	1	5186	5186	5.18	<0.05 *
Residuals	32	32054	1002		
Relationships between T_{diff} and *LCA*					
T_{diff}	1	1083523	1083523	183.31	<0.001 ***
Wood tissue	1	8345297	8345297	1411.83	<0.001 ***
Tree species	1	570048	570048	96.44	<0.001 ***
Tree height	1	41302	41302	6.99	<0.05 *
T_{diff}:Wood tissue	1	15647	15647	2.65	<0.1 •
Wood tissue:Tree species	1	499575	499575	84.52	<0.001 ***
Residuals	31	183241	5911		
Relationships between T_{diff} and *WTT*					
T_{diff}	1	4.94	4.94	53.58	<0.001 ***
Wood tissue	1	38.37	38.37	416.39	<0.001 ***
Tree species	1	9.94	9.94	107.90	<0.001 ***
T_{diff}:Wood tissue	1	0.64	0.64	6.91	<0.05 *
Wood tissue:Tree species	1	4.16	4.16	45.12	<0.001 ***
Residuals	32	2.95	0.09		

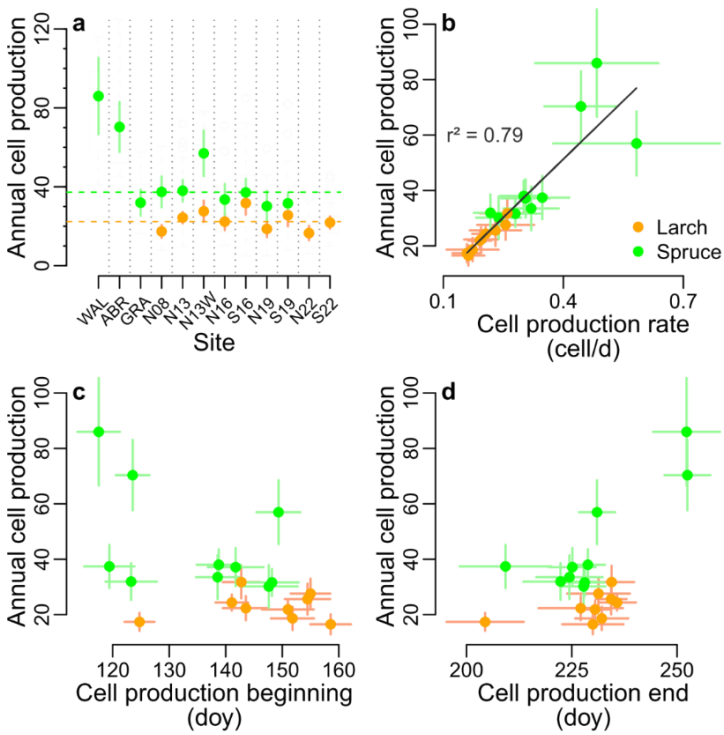

Figure S4.5 Cell production and wood formation phenology. (a) Number of xylem cells produced each year at the sites along the gradient (sites ordered by increasing altitude). (b) Relationship between the annual cell production and the daily rate of cell production. (c) Relationship between the annual cell production and the onset of wood formation. (d) Relationship between the annual cell production and the cessation of cell production. For each panel, every point represents the site and species average, while the bars symbolize the associated standard deviations.

Table S4.4 Covariance analysis of the relationship between the mean daily rate of cell production and the annual number of xylem cells between the two species. Points and asterisks highlight significant effects (˙ for p <0.1, * for p <0.05, ** for p <0.01 and *** for p <0.001).

Source	Df	Sum of squares	Mean Squares	F	*p*-value
Rate	1	4669	4669	72.80	<0.001 ***
Tree age	1	219	219	3.42	<0.1 ˙
Residuals	16	1026	64		

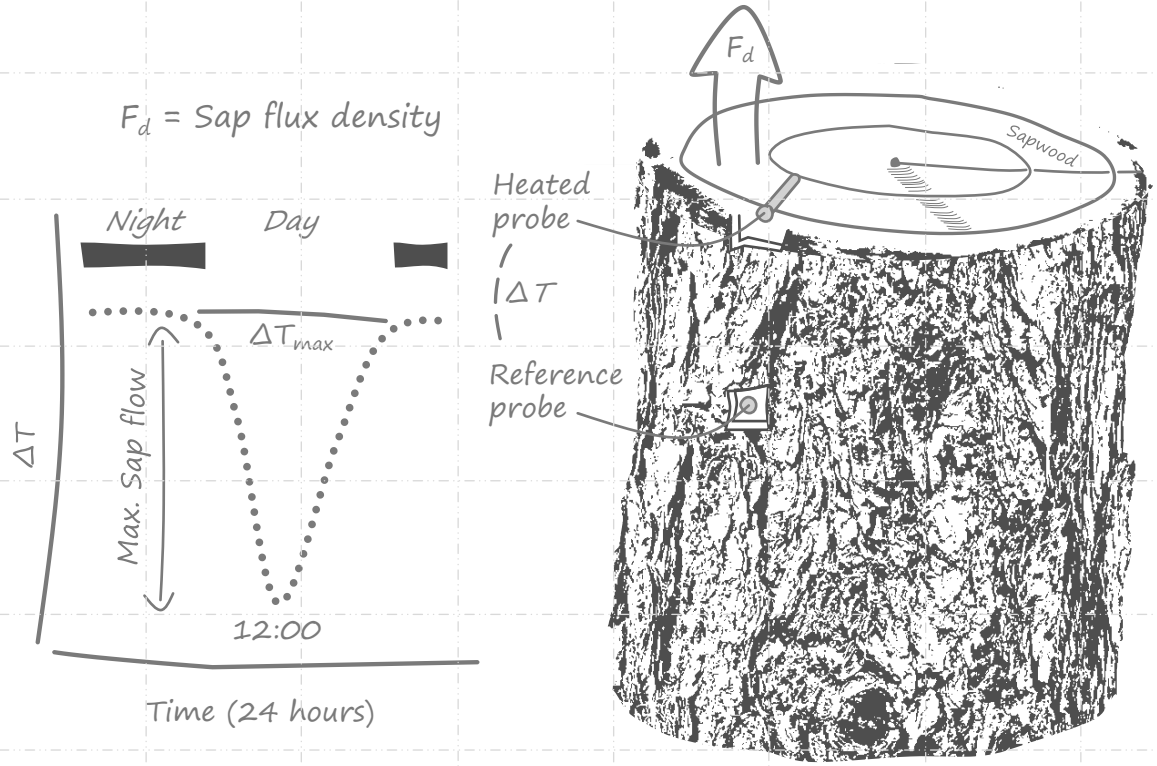
F_d = Sap flux density
Night
Day
ΔT_{max}
Max. Sap flow
ΔT
12:00
Time (24 hours)
F_d
Sapwood
Heated probe
ΔT
Reference probe

Chapter 5

Quantification of uncertainties in conifer sap flow measured with the thermal dissipation method

Richard L. Peters, Patrick Fonti, David C. Frank, Rafael Poyatos, Christoforos Pappas, Ansgar Kahmen, Vinicio Carraro, Angela Luisa Prendin, Loïc Schneider, Jennifer L. Baltzer, Greg A. Baron-Gafford, Lars Dietrich, Ingo Heinrich, Rebecca L. Minor, Oliver Sonnentag, Ashley M. Matheny, Maxwell G. Wightman, Kathy Steppe

Accepted in New Phytologist

Abstract

Trees play a key role in the global hydrological cycle and measurements performed with the thermal dissipation method (TDM) have been crucial in providing whole-tree water use estimates. Yet, different data processing to calculate whole-tree water use encapsulate uncertainties that have not been systematically assessed. We quantified uncertainties in conifer sap flux density (F_d) and stand water use caused by commonly applied methods for deriving zero-flow conditions, dampening and sensor calibration. Their contribution has been assessed using a stem segment calibration experiment and four years of TDM measurements in *Picea abies* (L.) Karst. and *Larix decidua* Mill., growing in contrasting environments. Uncertainties were then projected on TDM data from different conifers across the Northern Hemisphere. Commonly applied methods mostly underestimated absolute F_d. Lacking a site- and species-specific calibrations reduced our stand water use measurements by 37% and induced uncertainty in Northern Hemisphere F_d. Additionally, although the inter-daily variability was maintained, disregarding dampening and/or applying zero-flow conditions that ignored nighttime water use reduced the correlation between environment and F_d. The presented ensemble of calibration curves and proposed dampening correction, together with the systematic quantification of data-processing uncertainties, provide crucial steps in improving whole-tree water use estimates across spatial and temporal scales.

5.1 Introduction

Accurate measurements of whole-tree water use are important as terrestrial plant transpiration plays a key role in the global hydrological cycle (Holbrook & Zwieniecki 2003; Schlesinger & Jasechko 2014; Good *et al.* 2015; Fatichi & Pappas 2017). Furthermore, measurements of whole-tree transpiration show great value in validating regional water-balance simulations (Wilson *et al.* 2001; Ford *et al.* 2007; Reyes-Acosta & Lubczynski 2013), inter-specific comparison of stomatal conductance behaviour (Damour *et al*. 2010), modelling stable isotope enrichment (Song *et al.* 2013; Sutanto *et al.* 2014) and mechanistically explaining wood formation (De Schepper & Steppe 2010; Fatichi *et al.* 2014; Steppe *et al.* 2015). Whole-tree transpiration can be estimated by upscaling measurements of leaf-level transpiration or by partitioning eddy covariance flux tower data, which both require assumptions on crown and canopy architecture (Ansley *et al.* 1994; Hatton & Wu 1995; Lawrence *et al.* 2007; Matheny *et al.* 2014; Fatichi *et al.*

2016). The development of heat-based sap flow methods applied at the tree-stem level avoids these issues, and has provided whole-tree water use estimates across a wide range of spatiotemporal scales (Swanson 1994; Smith & Allen 1996; Kallarackal *et al.* 2013, Van de Wal *et al*. 2015).

Since 1985 over 1200 studies have collected heat-based sap flow measurements, to assess the effect of environment on transpiration and quantify forest stand water use (Figure 5.1a). Due to their low cost, ease of use, low energy requirement, and long-term measurement potential (Oliveras & Llorens 2001; Lu *et al.* 2004), sap flow data generated with the thermal dissipation method (TDM; Granier 1985, 1987) far exceed any other method (Poyatos *et al.* 2016), including heat pulse velocity (Green *et al.* 2003), stem heat balance (Langensiepen *et al.* 2014), heat field deformation (Čermák *et al.* 2004), heat ratio method (Burgess *et al.* 2001) and trunk segment heat balance (Smith & Allen 1996).

TDM measures sap flux density (F_d) by inserting two axially aligned probes into the sapwood and determining the temperature difference between a continuously heated probe and the non-heated reference (expressed as ΔT [°C]). F_d is typically estimated by first calculating the proportional difference between measured ΔT (denoted as the unitless K [-]) and zero sap flow conditions (denoted as ΔT_{max}; see Lu *et al.* 2004). Next, F_d is calculated from K, using a calibration curve (Ganier *et al.* 1985). Ignoring radial or circumferential profiles F_d can then be multiplied by the sapwood area to obtain whole-tree sap flow and potentially upscaled to stand water use (Granier 1987; Čermák *et al.* 1995; Matheny *et al.* 2014). Despite its simplicity, alternatives to process raw TDM measurements (see Figure 5.1b) generate a range of potential F_d values, and subsequently cause uncertainty in the quantification of whole-tree and stand water use. Typically, one set of TDM probes is installed per tree, assuming this local measurement represents sap flow in the entire stem. Yet, in some cases, strong radial and circumferential variations in sap flow require the installation of additional probes at different sapwood depths or circumferential positions (Lu *et al.* 2000; Nadezhdina *et al.* 2002; Fiora & Cescatti 2006; Saveyn *et al*. 2008), which is not always considered (54% of studies do not account for this variability; see rad./circ. variation in Figure 5.1b). Next, it is frequently assumed that the probes are inserted into the sapwood, although measured ΔT can be altered when partially inserted into non-conducting heartwood (Lu *et al*. 2004). In spite of available correction methods (see Clearwater *et al.* 1999), heartwood-sapwood boundaries can often not be precisely defined and may vary considerably within the stem (17% of studies apply a correction; see heartwood presence in Figure 5.1b;

Longuetaud *et al.* 2006; Paudel *et al.* 2013). Finally, natural variations in thermal conditions may alter ΔT (Köstner *et al.* 1998; Do & Rocheteau 2002; Vergeynst *et al.* 2014), which can be resolved, although this often requires more specialized, expensive and often energy demanding sap flow methods (e.g., Nourtier *et al.* 2011; Lubczynski *et al.* 2012; Vandegehuchte & Steppe 2012).

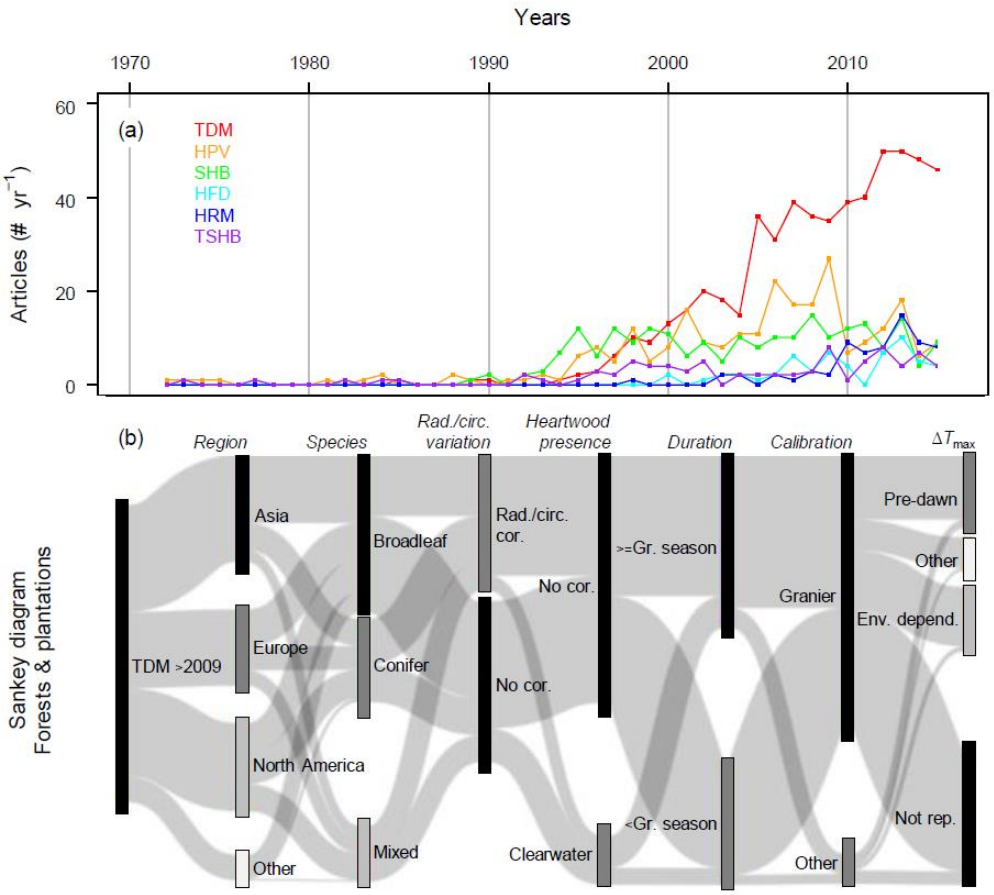

Figure 5.1 Literature review of heat-based sap flow methods. The search terms; "Stem", "Tree" and "Sap flow", were used in Scopus and Web of Science (www.webofknowledge.com and www.scopus.com; accessed on 01-12-2016). (a) Temporal development of the (major) applied methods from 1985-2015, including: Thermal Dissipation Method (TDM), Heat Pulse Velocity (HPV), Stem Heat Balance (SHB), Heat Field Deformation (HFD), Heat Ratio Method (HRM), and Trunk Segment Heat Balance (TSHB). (b) Sankey diagram revealing the proportion of studies from 2010-2016 within forests and plantations using TDM measurements, grouped according to region, species and different assumptions (175 studies). We noted; the study location, the study tree species, whether corrections were made for radial or circumferential variation (Rad./circ. cor.), whether corrections were applied for probes inserted into heartwood (see Clearwater *et al.* 1999), the temporal extent of the measurements (equal and longer or shorter than one growing season; Gr. Season), whether the original (Granier 1985) or a species-specific calibration was used to calculate sap flux density, and the assumptions for estimating zero-flow conditions (ΔT_{max}). For ΔT_{max} assumptions we noted the use of the predawn and environmental dependent (Env. depend.) method or whether the applied assumption was not reported (Not rep.). Black bars indicate the most widely applied options.

In addition to anatomical and morphological issues related to ΔT measurements, data-processing procedures to calculate F_d from ΔT present sources of uncertainty. First, zero-flow conditions (ΔT_{max}) have to be defined as a reference. The common practise is to assume that zero-flow conditions occur pre-dawn, neglecting nighttime activity (42% of the studies do not report the used zero-flow procedure; see ΔT_{max} in Figure 5.1b). Yet, previous findings demonstrate nighttime transpiration (Caird *et al*. 2007; Novick *et al.* 2009; Berkelhammer *et al.* 2013). Due to the way in which K and F_d are calculated, a small change in nighttime activity could result in large offsets in daily F_d (Rabbel *et al*. 2016). This argues for the application of environmentally or tree physiologically based criteria to define when zero flow occurs (Regalado & Ritter 2007; Oishi *et al.* 2008). Second, it is often assumed that installation of the probes into living xylem tissue causes only slight dampening of the signal due to probes burrowing deeper into the wood and wounding response that could alter K (Moore *et al.* 2010; Wullschleger *et al.* 2011; Wiedemann *et al.* 2016). Yet, most studies with a duration equal to or longer than one growing season (58% of studies; see duration in Figure 5.1b) do not account for these effects (Lu *et al.* 2004). Finally, most studies use the empirical calibration curve established by Granier (1985) to calculate F_d (90% of studies; see calibration in Figure 5.1b). Nonetheless, multiple studies contest its validity and propose species-specific calibrations (Bush *et al.* 2010; Steppe *et al.* 2010; Sun *et al.* 2012; Ma *et al*. 2017). Many different combinations of these data-processing procedures are applied in the literature (Figure 5.1b), which might jeopardize climate-response analyses (Poyatos *et al*. 2005), inter-species comparisons (Kunert *et al.* 2010; Brinkmann *et al.* 2016) or large-scale data collection initiatives (Poyatos *et al.* 2016). Although general reviews exist and individual data-processing procedures have been analysed, a systematic quantification on the impact of different combinations of data processing on TDM sap flow data is lacking.

In a systematic analysis, this study aims to quantify the impact of commonly applied data-processing procedures on sap flow estimates derived from single-point TDM measurements. In particular, in conifers, we (i) assess the effect of four commonly used methods to define zero-flow conditions on K, (ii) quantify the magnitude of K dampening and propose a correction, (iii) compare species-specific calibration curves to calculate F_d with previous studies, and (iv) quantify the uncertainty generated by combinations of these procedures on F_d, stand water use and inter-daily F_d variability compared to common practises. Four years of TDM sap flow measurements from *Picea abies* and *Larix decidua*, collected

under contrasting field conditions in the Lötschental (Switzerland), were used for the uncertainty analysis. Additionally, a laboratory controlled stem calibration experiment was performed to analyse the heat dissipation properties of the wood and the results were compared with existing calibration curves. Observed uncertainties were propagated to TDM datasets collected from conifers across the Northern Hemisphere to illustrate the importance of carefully selecting TDM data-processing methods when estimating F_d.

5.2 Materials and methods

Study design and site description

To analyse the uncertainty caused by (i) data-processing procedures to calculate zero-flow conditions, (ii) signal dampening and (iii) applied calibration curves on K, F_d and stand water use, we continuously monitored sap flow in 27 conifer trees in the Lötschental for four years. This inner Alpine valley in Switzerland (46°23′40″N, 7°45′35″E) is covered by a mixed forest of deciduous *Larix decidua* Mill. and evergreen *Picea abies* (L.) Karst. We collected measurements from contrasting thermal and soil moisture conditions, as consistent differences in environmental conditions might promote nighttime activity and the magnitude of the dampening response. A total of five sites were selected along an elevational gradient, with colder conditions at higher elevations and contrasting dry and wet conditions in the valley bottom (Table 5.1; King *et al*. 2013a).

A calibration curve was established for each tree species to calculate F_d using a laboratory calibration experiment on fresh cut-stem segments. The segments, collected from four trees per species, were harvested at the Centre for Studies on Alpine Environment of the University of Padova located in the Dolomite mountain region (Italy, San Vito di Cadore; Table 5.1), as harvesting stems in the Lötschental was logistically difficult. Although smaller in diameter, *P. abies* and *L. decidua* trees were selected with similar recent ring widths as observed in the Lötschental monitoring trees (Table 5.1).

The uncertainty introduced through data-processing methods for zero-flow conditions and sensor calibration was calculated for TDM datasets collected across the Northern Hemisphere for three conifer genera (Table 5.2). This analysis included datasets from Europe and North America. In total, 131 individual trees from 18 sites were included with climatic conditions ranging from 1.4-19.8 °C mean annual temperature and 428-1452 mm mean annual precipitation (Table 5.2)

Table 5.1 Overview of sites and monitored trees. Mean ring width was calculated for the last 2 cm of wood, covering the extent of the inserted thermal dissipation probes. The three *Larix decidua* and *Picea abies* trees at each Lötschental site were continuously monitored from 2012-2015. Four trees from San Vito di Cadore were used for the cut stem segment calibration. See Table 5.2 for site coordinates and climatic conditions. Site codes LOT= Lötschental and SVD= San Vito di Cadore, - = no data available, and DBH= diameter at breast height.

Site	Site code	Elevation [m a.s.l.]	Species	Age [years]	DBH [cm]	Height [m]	Sapwood thickness [cm]	Ring width [cm yr^{-1}]
Switzerland, Lötschental	N13W	1300 (Wet)	*L. decidua*	148 164 134	78 89 52	28 33 26	2.2 2.4 2.4	0.06
			P. abies	85 81 109	81 63 81	30 34 34	9.1 6.9 9.0	0.26
	N13	1300 (Dry)	*L. decidua*	131 128 131	30 32 31	20 19 19	1.5 1.8 1.6	0.06
			P. abies	90 93 87	31 37 48	15 20 19	2.5 5.3 5.1	0.13
	S16	1600	*L. decidua*	371 69 69	75 39 42	32 25 24	3.5 2.6 3.7	0.16
			P. abies	- 62 461	45 38 56	22 25 24	2.0 4.2 2.0	0.14
	S19	1900	*L. decidua*	200 326 170	48 49 36	24 22 26	3.2 1.8 2.6	0.08
			P. abies	137 229 245	34 48 37	25 25 21	1.7 5.5 3.6	0.06
	S22	2200	*L. decidua*	269 280 295	47 56 46	18 17 17	2.4 3.1 1.8	0.09
Italy, San Vito di Cadore		1000	*L. decidua*	28 91 30 62	15 17 16 18	17 19 15 20	2.9 1.7 1.6 1.1	0.12
			P. abies	50 35 73 28	16 16 20 12	18 16 14 9	3.1 5.0 3.3 2.8	0.13

Field measurements

At each Lötschental site, three mature dominant trees per species were selected for continuous sap flow monitoring from May 2012 until October 2015 (Table 5.1). New TDM probes were additionally installed with a horizontal distance of 10-15 cm away from the initial probes on four trees to assess dampening effects (one per species at S19 and N13 in June 2015). Environmental conditions were monitored at each site with a 15 to 60 minute interval (King *et al.* 2013b). A radiation-shield covered sensor was installed on a central tower (≈2.5 m above the ground) within the canopy to measure both air temperature (T [°C]) and relative humidity (RH [%]; Onset, USA, U23-002 Pro), used to calculate vapour pressure deficit (D [kPa]; see WMO 2008). Soil volumetric water content was measured hourly with five sensors at 10 and 70 cm depth in the centre of each site (θ [%]; Decagon, USA, EC-5). Solar irradiance (R_g [W m^{-2}]) was measured hourly in an open field at N13 using a micro-station (Onset, USA, H21-002 Micro Station) and pyranometer (Onset, USA, S-LIB-M003). Daily precipitation data was obtained from the nearest weather stations, where the distance to the site was used to calculate a weighted mean from the nine included stations (ranging from 6 to 43 km; Federal Office of Meteorology and Climatology MeteoSwiss).

For upscaling to whole-tree water use, sapwood thickness [cm] and ring width [mm] were measured from two increment wood cores taken perpendicular to the slope at breast height from the monitored trees (avoiding the slope-facing side with installed probes) and trees surrounding the site (see Peters *et al.* 2017).

Sapwood area was used for upscaling F_d to whole-tree water use, while ignoring radial and circumferential variability. For upscaling to stand water use, diameter at breast height (DBH) measurements were taken from all trees within 20 m (at S22), 15 m (at S19 and S16) and 10 m (at N13 and N13W) radius fixed plots, and used in combination with sapwood allometric relationships (Figure S5.1; see Čermák *et al.* 1995).

Thermal dissipation method

Sap flux density (F_d [$cm^3\ cm^{-2}\ h^{-1}$]) was measured using commercially available TDM probes (see Granier 1985; TeSAF, University of Padova, Italy). Two 20 mm long stainless steel probes, with a 2 mm diameter, were radially inserted into the xylem, with a vertical distance of 10 cm on the slope-facing side of the stem at ≈1.6 m height. The temperature difference between the continuously heated upper and unheated lower probe was measured (ΔT [°C]) and stored with a 15-minute resolution on a data logger (Campbell Scientific, USA, CR1000). The maximum ΔT (ΔT_{max} [°C]) was used to obtain K [-] according to Equation 1. K can be calibrated to obtain F_d using a power-type relationship with α [$cm^3\ cm^{-2}\ h^{-1}$]= 42.84 (0.0119 [$cm^3\ cm^{-2}\ s^{-1}$] × 3600) and β [-]= 1.231 (Granier 1985), according to Equation 2.

$$K = \frac{\Delta T_{max} - \Delta T}{\Delta T} \quad \text{(Eq. 1)}$$

$$F_d = \alpha \cdot K^{\beta} \quad \text{(Eq. 2)}$$

ΔT was corrected (denoted as ΔT_{sw} [°C]) for the proportion of the probe that was inserted in the sapwood (γ [$cm\ cm^{-1}$]) versus the proportion in the inactive heartwood and used instead of ΔT in Equation 1 (Clearwater *et al.* 1999):

$$\Delta T_{sw} = \frac{(\Delta T - (1-\gamma) \cdot \Delta T_{max})}{\gamma} \quad \text{(Eq. 3)}$$

Because our sensors were measuring over four years and the probes could progressively burrow deeper into the heartwood, γ was annually corrected for the ring width occurring after the installation year. For this correction we assumed sapwood thickness remained constant.

Zero-flow conditions

Four methods to calculate zero-flow conditions (ΔT_{max}) were used, including the daily pre-dawn (PD; Lu *et al.* 2004), maximum moving window (MW; Rabbel *et al.* 2016), double regression (DR; Lu *et al.* 2004) and environmental dependent method (ED; Oishi *et al.* 2016). The PD method was applied by selecting daily maximum ΔT values occurring between 00:00 and 08:00 hours (GMT) when R_g was below 100 W m^{-2}. For the MW method, maximum ΔT_{max} was calculated during an 11-day window from the pre-dawn ΔT_{max} values. The DR method was applied by calculating the mean over pre-dawn ΔT_{max} with a moving-window of 11-days, removing all values below the mean, and calculating a second 11-day moving window which was used as ΔT_{max}. The ED method was applied according to Oishi *et al.* (2016), where pre-dawn ΔT_{max} values were selected when T was <1 °C or D was <0.1-0.05 kPa for a period of two hours (D threshold depending on elevation). In addition, the coefficient of variation of pre-dawn ΔT within this period should be below 0.5% to ensure selection of nights with stable zero-flow conditions. All ΔT_{max} values were visually checked for drifts or outliers cause by low θ or low T.

Signal dampening detection and correction

First, data from long-term and newly installed probes were compared with linear regressions to demonstrate absolute offsets and daily maximum K variability. Second, the long-term data collected since 2012 was used to assess dampening for each monitored tree. Daily maximum K was used as the dependent variable within a Generalized Least Squares model (GLS in the "nlme" package for R software version 3.2.00, R development core team 2013; Pinheiro *et al.* 2017), to account for high first-order temporal auto-correlation (see Zuur *et al.* 2010). As independent variables, we selected daily maximum D, T, daily mean θ and day of year (DOY; to account for changes in leaf-phenological stages). Days with a daily maximum K <0.05 and precipitation >1 mm d^{-1} were excluded from the analysis, as these obstructed detection of the environmental relationships. The polynomial structure of the model was established using the Akaike Information Criterion (AIC), while accounting for interactions between variables (e.g., high D coincides with low θ). Equation 4 was used to fit a function and calculate the residual K (K_{res} [-]; observed minus fitted values; see Table S5.1)

$$K_{\mathrm{res}} = \mathrm{resid}\,(\,Intercept + \varepsilon_1 \cdot D^{-1} + \varepsilon_2 \cdot T + \varepsilon_3 \cdot T^2 + \varepsilon_4 \cdot \theta^{-1} + \varepsilon_5 \cdot \mathrm{DOY} + \varepsilon_6 \cdot \mathrm{DOY}^2\,) \qquad \text{(Eq. 4)}$$

Monthly averages of K_{res} were calculated (to reduce first-order auto-correlation) and fitted to the mean time since installation (t [days]) with a third-order polynomial model to determine significant reductions in response to t.

For the study trees with a significant reduction in K (p <0.05), a tree-specific function was fitted to generate a correction curve. To avoid overfitting with environmental variables, used in subsequent analyses, we only included seasonality (DOY) and the time since installation (t) as independent variables for the correction curve. A nonlinear model was fitted to the daily maximum K, excluding rainy days and low values to generate the correction curve (K_{cor}; see Table S5.2):

$$K_{\mathrm{cor}} = \frac{(a + b \cdot t)}{(1 + c \cdot t + d \cdot t^2)} + e \cdot \mathrm{DOY} + f \cdot \mathrm{DOY}^2 \quad \text{(Eq. 5)}$$

The fitted parameters for t (with a, b, c and d) were used to correct K and scale it to the maximum value within the first year of installation (see Figure S5.2 and S5.3).

Stem segment calibration

Calibration curves to calculate F_d were established by comparing gravimetrically induced flows through a stem segment against K measured with TDM probes. The stem segments, harvested in San Vito di Cadore, with a length of ≈1 m (≈50 cm above and below DBH), were transported to the laboratory in wet black plastic bags to prevent dehydration. Directly after harvesting, the stems were recut under water to ≈25 cm in length and trimmed with razor blades to reopen closed tracheids. The stem segments were used for calibration within a Mariotte-based verification system (Steppe *et al.* 2010). In short, a water-filled flask was connected to a plastic cylinder via flexible tubing, functioning as a siphon. The horizontal height of the flask was adjusted to deliver a specific water flow to a cylinder attached to the top of the stem segment with installed TDM probes, producing a constant pressure head.

Within a temperature-controlled environment, no water flow was applied during a 10 hour period to generate zero-flow conditions. Next, the stem segment was flushed with water for 2 hours until the readings stabilized. The water level was increased and then decreased in 2, 5, 10, 15, 25 and 30 cm (±0.5 cm) increments and kept constant at every level for 45 min (resulting in sap flux densities ranging from ≈2-45 $cm^3\ cm^{-2}\ h^{-1}$). Finally, no flow was generated for 4

hours, after which post- and pre-zero flow conditions were used to determine ΔT_{max} with the TDM probes.

A calibration curve was established by fitting a quadratic function between K and the gravimetric F_d (providing a better relationship compared to a power function; see Table S5.3 and S5.4). Mixed-effect modelling was applied to test for species-specific differences in the calibration parameters using the "lme4" R package (Bates *et al.* 2015), with the individual as a random factor. A literature review was performed on existing species-specific calibration curves in order to compare sampling locations, species, wood types, size of stem segments, sapwood properties, goodness-of-fit for the calibration curve and the calibration parameters.

Uncertainty analysis and upscaling

Uncertainty induced by different data-processing procedures on daily F_d and stand water use estimates was analysed by applying all available data-processing combinations on the Lötschental trees, including: (i) ΔT_{max} calculation with PD, MW, DR or ED method, (ii) dampening or no dampening correction, and (iii) Granier's original calibration or tree species-specific calibration. Absolute effects of all possible combinations on mean daily F_d (mean annual F_d in $cm^3\ cm^{-2}\ d^{-1}$, averaged over all years of observation) and stand water use were calculated and compared to the commonly applied procedure (measuring for one growing season, using PD, no dampening correction and Granier's calibration; Figure 5.1b). Mean annual stand water use was calculated by averaging the 15-minute F_d measurements per site and species and multiplying them by the species-specific total sapwood area per site. For addressing inter-daily variability and the environmental response of F_d, daily F_d averaged per species and elevation was correlated against mean daily D (see Oren *et al.* 1999a; Moore *et al.* 2010) with a third-order polynomial to obtain the changes in goodness-of-fit (expressed in R^2). Northern Hemisphere TDM measurements (Table 5.2) were used to illustrate the relevance of selected data-processing procedures. As most datasets had a short monitoring period, no dampening correction was applied and measurements from first year after sensor installation were used (except for VAL and TIL due to data gaps; see Table 5.2). The 99^{th} quantile was determined for the maximum daily F_d calculated for all individuals from K within a site (generated with the reported ΔT_{max} method; see Table 5.2), when using the different calibration curves available for softwood species, to avoid the effect of spurious outliers (excluding the steepest curves proposed by Lundblad *et al.* 2001). Additionally, for sites where ΔT values were provided, various daily F_d time-series were calculated by

using PD, MW or DR ΔT_{max} and the softwood calibration curves (Table 5.2). The ED ΔT_{max} method could not be applied due to the lack of high-quality environmental data. Uncertainty was quantified by calculating the mean daily F_d, after which the difference from the most commonly applied data-processing procedure was determined.

5.3 Results

Zero-flow conditions and the effect on K

Offsets in ΔT_{max} were observed between pre-dawn and other methods (PD in Figure 5.2a), with the largest differences found in *L. decidua*. The criteria needed for the environmental dependent method to determine zero-flow conditions (including low nighttime *D* or *T*; ED in Figure 5.2a) were in some cases not met for a period longer than 10 days. In these cases, the pre-dawn method resulted in a strong reduction in daily maximum *K* (squares in Figure 5.2b), as it does not allow for nighttime water use (circles in Figure 5.2b). The moving-window method showed the highest daily maximum *K* (MW in Figure 5.2b).

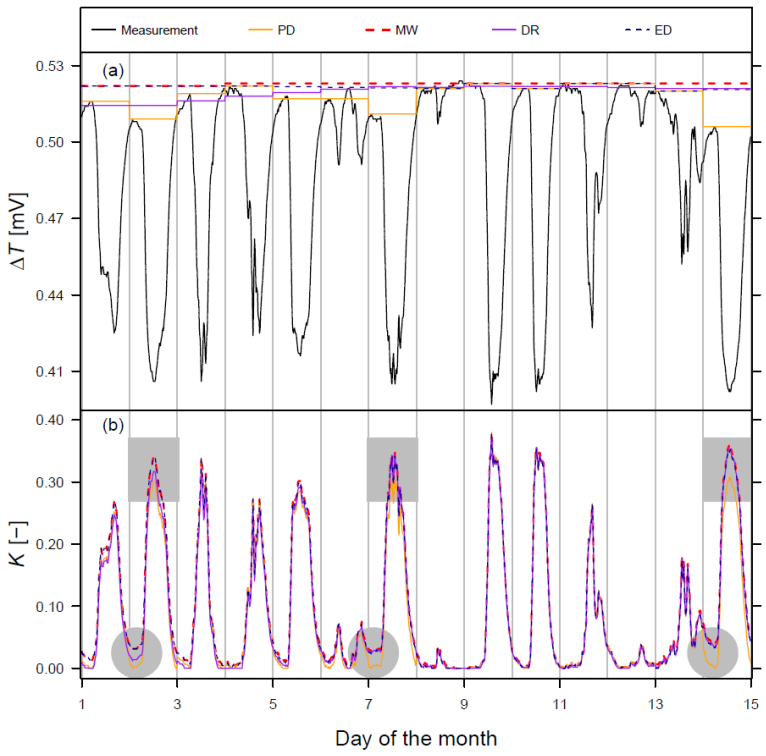

Figure 5.2 Widely applied zero-flow condition procedures and their implications on *K* for a *Larix decidua* tree at the S19 in the first week of June 2012. (a) Raw ΔT measurements (expressed in mV instead of °C; see Lu *et al.* 2004) and ΔT_{max} determined by using the pre-dawn maximum (PD), an 11-day moving window (MW), the double regression method (DR) and the environmental dependent method (ED). (b) Implications of the different ΔT_{max} methods on the resulting *K* (using Equation 1). Grey circles reveal times when nighttime sap flow activity could be expected and the implication on daily maximum *K* (grey squares).

Table 5.2 Overview of Northern Hemisphere sap flow measurements for the genera *Picea*, *Larix* and *Pinus* used for the uncertainty analysis. Latitude and longitude are provided in decimal degrees. Only dominant and co-dominant individuals are included within the analysis. Methods include: MW= moving window, DR= double regression and ED= environmental depended. The selected years, average DBH and number of individual trees are provided. Site conditions are described with elevation, mean annual temperature and total annual precipitation. No raw ΔT values were obtained for sites indicated with a * symbol.

Site	Country	Lat.	Long.	Species	Method	Year	DBH [cm]	Trees [#]	Elev. [m a.s.l.]	Temp. [°C]	Prec. [mm]	Source
Picea												
SOBS	Canada	53.987	-105.118	*Picea mariana*	ED	2016	12	9	598	1.4	428	Pappas *et al.* (2018)
LOTS19	Switzerland	46.400	7.746	*Picea abies*	ED	2012	40	3	1900	3.9	872	King *et al.* (2013a)
LOTS16		46.397	7.755				47	3	1600	5	872	
LOTN13W		46.400	7.764				75	3	1300	5.5	872	
LOTN13		46.392	7.761				39	3	1300	5.7	872	
SVD*	Italy	46.450	12.214	*Picea abies*	MW	2008	-	2	1050	7	866	V. Carraro *et al.* unpublished
VISP	Switzerland	46.303	7.741	*Picea abies*	DR	2014	37	3	800	9.2	581	King *et al.* (2013a)
HOF	Switzerland	47.467	7.500	*Picea abies*	MW	2014	60	4	550	10.5	990	Pepin & Körner (2002)
Larix												
SOBS	Canada	53.987	-105.118	*Larix laricina*	ED	2016	18	9	598	1.4	428	Pappas *et al.* (2018)
LOTS22	Switzerland	46.400	7.743	*Larix decidua*	ED	2012	49	3	2200	3.2	872	King *et al.* (2013)
LOTS19		46.397	7.746				44	3	1900	3.9	872	
LOTS16		46.397	7.755				52	3	1600	5	872	
LOTN13W		46.394	7.764				73	3	1300	5.5	872	
LOTN13		46.392	7.761				31	3	1300	5.7	872	
SVD*	Italy	46.450	12.214	*Larix decidua*	MW	2008	-	2	1050	7	866	V. Carraro *et al.* unpublished
VISP	Switzerland	46.303	7.741	*Larix decidua*	DR	2014	47	3	800	9.2	581	King *et al.* (2013a)
HOF	Switzerland	47.467	7.500	*Larix decidua*	MW	2015	50	4	550	10.5	990	Pepin & Körner (2002)
Pinus												
SVD	Italy	46.450	12.214	*Pinus sylvestris*	MW	2008	-	2	1050	7	866	V. Carraro *et al.* unpublished
VAL	Spain	42.196	1.814	*Pinus sylvestris*	MW	2004	19	10	1257	7.3	924	Poyatos *et al.* (2005)
HIN	Germany	53.332	13.192	*Pinus sylvestris*	ED	2012	58	8	95	8	572	Ford *et al.* (2004)
HOF	Switzerland	47.467	7.500	*Pinus sylvestris*	MW	2014	39	4	550	10.5	990	Pepin & Körner (2002)
MTL	USA	32.417	-110.725	*Pinus strobiformis*	DR	2014	-	3	2573	11	800	Brown-Mitic *et al.* (2007)
MTL	USA	32.417	-110.725	*Pinus ponderosa*	DR	2014	29	3	2573	11	800	
TIM	Spain	41.333	1.014	*Pinus sylvestris*	ED	2010	42	10	1018	11.3	664	Poyatos *et al.* (2013)
TIL	Spain	41.328	1.007	*Pinus sylvestris*	ED	2010	38	9	1065	11.3	664	Aguadé *et al.* (2015)
CAN	Spain	41.431	2.074	*Pinus halepensis*	ED	2011	34	3	270	15.2	608	Sánchez-Costa *et al.* (2015)
UMBS*	USA	45.600	-84.700	*Pinus strobus*	MW	2015	22	4	236	5.9	796	Matheny *et al.* (2014)
PER*	USA	30.200	-89.300	*Pinus taeda*	MW	2013	15	12	14	19.8	1452	Wightman *et al.* (2016)

Dampening effect on absolute value and inter-daily variability of K

Comparison of new and long-term installed TDM probes at S19 and N13 (Figure 5.3a), revealed that all *L. decidua* trees showed steeper slopes than the 1:1 line, indicating dampening of mean daily *K* although the slope was tree-specific (N13= 1.42 in Figure 5.3b and S19= 3.41). For *P. abies*, one tree showed dampening (N13= 3.13, see Figure 5.3b), while another individual presented a shallower slope (S19= 0.61), showing little reduction in mean daily *K*. However, similar variability of mean daily *K* was observed even after four years (average $R^2 \approx 0.8$, $p < 0.05$).

Dampening of mean daily *K* was found in trees from both species monitored since 2012, after removing the influence of environmental factors (including *D, T, θ*, and DOY; Figure S5.2 and S5.3). The residual standard error (RSE) revealed that appropriate fits with environmental factors were achieved for all trees (mean RSE of 0.074; see Table S5.1). Only 6 out of 27 trees did not show a significant reduction in monthly mean K_{res} (Table 5.3). Although the goodness of fit varied among trees showing dampening (R^2 ranges from 0.17 to 0.95), on average a 31% reduction was found when comparing maximum daily *K* from 2013 with 2012 ($K_{\%2013\text{-}12}$ in Table 5.3). Within the first year of installation both *L. decidua* and *P. abies* showed a significant reduction ranging from approximately -0.0003 to -0.0015 mean monthly K_{res} per days since installation (*t*; Table 5.3). By applying a non-linear function including *t* and DOY (seasonal term), the 15-minute *K*-values could be corrected for trees showing a significant reduction (see Table S5.2).

Species-specific calibration and literature review

The cut-segment experiment revealed a steeper calibration curve than proposed by Granier (1985; Figure 5.4). A quadratic polynomial function showed the best fit where $\alpha = 26.236$ and $\beta = 56.495$ ($R^2 = 0.96$, $p < 0.001$). Despite *P. abies* showing a steeper relationship than *L. decidua*, no significant species-specific effect was found (see Table S5.4). Large variability in published calibration curves was apparent (Figure 5.4) and on average a maximum *K* of 1.1 was generated (see Table S5.5). Ring-porous calibration curves were the steepest, followed by diffuse-porous and softwood species (Figure 5.4).

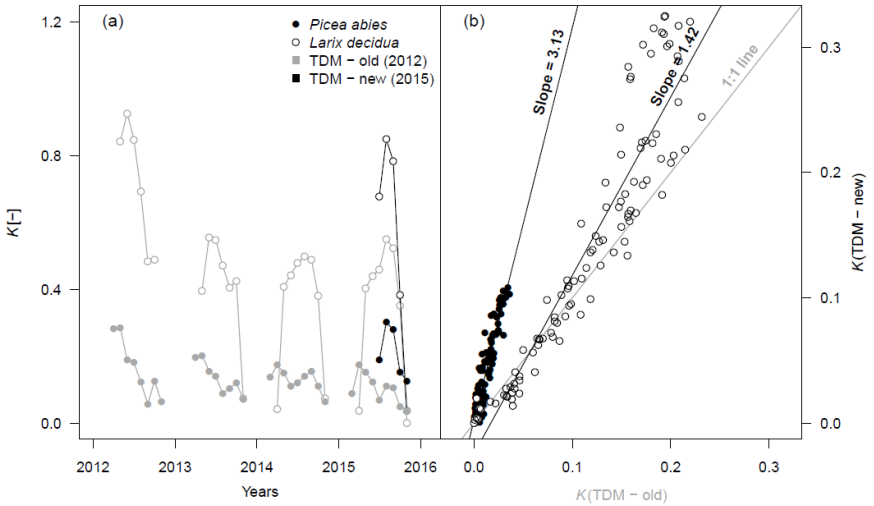

Figure 5.3 Example of *K* (Equation 1) in function of time since installation (*t* [days]) for two trees at the site N13. (a) Mean monthly *K* for thermal dissipation method (TDM) probes installed at different times on the same tree. Open or closed circles indicate *Larix decidua* and *Picea abies*, while black and grey indicates the new and old sensor, respectively. (b) Linear correlation between daily mean *K* for the overlapping period between old and new TDM probes (installed in May 2012 and June 2015, respectively). Open and closed circles indicate the species as provided in (a).

Table 5.3 Descriptive statistics of linear regressions (K_{res}= Int. + $\eta_1 t + \eta_2 t^2 + \eta_3 t^3$), where monthly mean K_{res} (see Equation 4) for individual trees were fitted against time since installation (*t* [days]), when applying pre-dawn ΔT_{max}. The slope indicates the reduction in mean monthly K_{res} for 2012 when fitting a linear function against *t*. Change in mean monthly *K* [%] from the first (2012) to the second (2013) year after installation, in addition to the second last (2014) and last year (2015) of monitoring. The - symbols indicates no data was available. Significant parameters (p <0.05) are identified with the * symbol.

Site	Species	Tree	Int.	η_1	η_2	η_3	df	R^2	p	K_{res} Slope$_{2012}$	K %$_{2013-12}$	K %$_{2015-14}$
N13	*P. abies*	1	0.0633*	-0.0003*	4.0E-07*	-1.7E-10	29	0.41	0.000	-0.00043	-31	0
		2	0.0867*	-0.0007*	1.2E-06*	-6.7E-10*	25	0.40	0.001	-0.00046	-23	-26
		3	0.0481*	-0.0002	2.0E-07	-8.7E-11	29	0.17	0.039	-0.00034	-17	-12
	L. decidua	1	0.2729*	-0.0012*	1.3E-06*	-4.3E-10	22	0.69	0.000	-0.00150	-38	10
		2	0.0797*	-0.0004*	6.9E-07	-3.3E-10	20	0.24	0.035	-0.00068	-12	-10
		3	0.0809	-0.0009*	1.5E-06	-6.7E-10	28	0.06	0.186	-0.00029	-17	-23
N13W	*P. abies*	1	0.0596*	0.0002	-7.3E-07*	3.7E-10*	30	0.73	0.000	-0.00007	-7	-33
		2	-0.0208	0.0001	-2.1E-07	9.0E-11	30	0.07	0.843	0.00009	15	-1
		3	0.0512*	0.0001	-3.8E-07*	2.2E-10*	30	0.70	0.000	-0.00017	-26	-26
	L. decidua	1	0.1134*	-0.0004	3.0E-07	-9.2E-11	20	0.47	0.001	0.00003	-22	-6
		2	0.1980*	-0.0003	-4.8E-08	1.0E-10	21	0.72	0.000	0.00026	-32	-14
		3	0.1697*	-0.0005	4.2E-07	-1.2E-10	20	0.66	0.000	-0.00027	-34	-10
S16	*P. abies*	1	0.0795*	-0.0002	4.9E-08	-4.7E-12	18	0.74	0.000	-0.00023	-	0
		2	0.0343	-0.0002	2.2E-07	-9.5E-11	29	0.03	0.276	-0.00005	-5	1
		3	0.1491*	-0.0008*	1.3E-06*	-6.9E-10*	23	0.75	0.000	-0.00089	-50	-42
	L. decidua	1	0.1232*	-0.0008*	1.2E-06*	-4.8E-10	15	0.68	0.000	-0.00052	-	-2
		2	0.1687*	-0.0008*	1.1E-06	-4.5E-10*	23	0.78	0.000	-0.00051	-49	-11
		3	0.2455*	-0.0007*	1.2E-06*	-7.1E-10	12	0.95	0.000	-0.00051	-	-65
S19	*P. abies*	1	0.0143	-0.0001	9.2E-08	-7.4E-11	19	0.00	0.422	-0.00090	-19	-15
		2	-0.0054	0.0001	-2.7E-07	1.6E-10	28	0.07	0.838	-0.00025	-10	3
		3	0.0347*	-0.0001	1.2E-07	-3.9E-11	27	0.42	0.000	-0.00028	-33	3
	L. decidua	1	0.1202*	-0.0006*	5.9E-07	-1.7E-10	14	0.79	0.000	-0.00110	-55	-20
		2	0.0191	-0.0001	-6.9E-08	8.8E-11	21	0.02	0.333	0.00028	-9	1
		3	0.1317*	-0.0007*	1.1E-06*	-5.0E-10	14	0.76	0.000	-0.00090	-52	-21
S22	*L. decidua*	1	0.0239	0.0001	-2.4E-07	1.2E-10	17	0.39	0.010	0.00007	-8	-9
		2	0.1698*	-0.0008*	7.9E-07*	-2.4E-10	18	0.77	0.000	-0.00057	-48	6
		3	0.0916*	-0.0005*	6.5E-07	-2.5E-10	17	0.45	0.004	-0.00028	-27	9

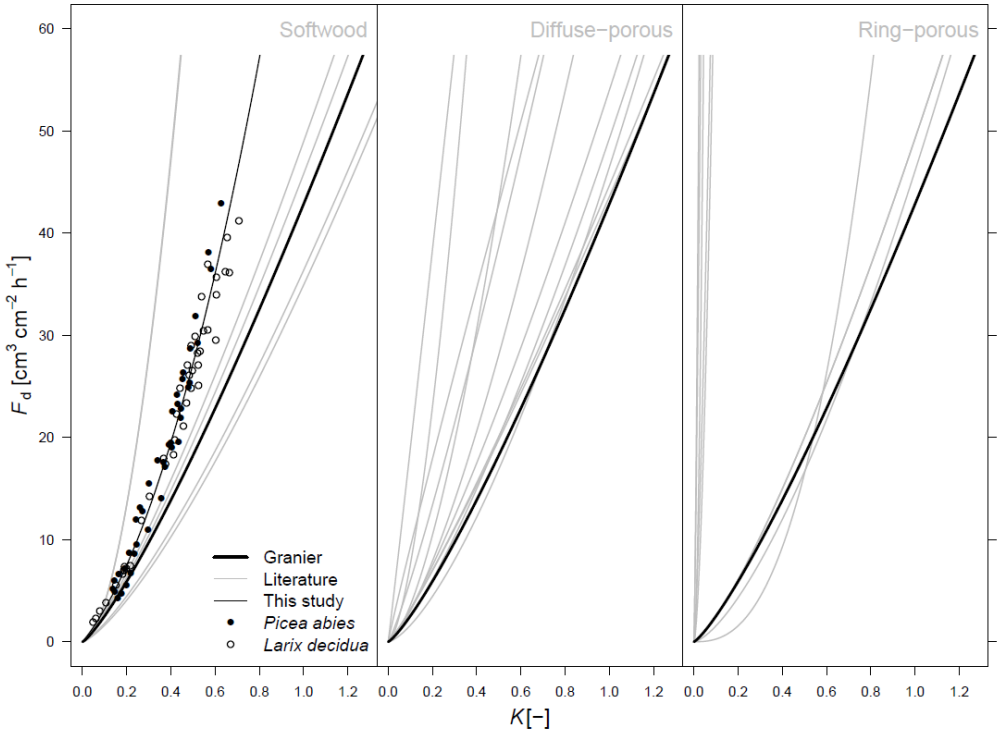

Figure 5.4 Calibration curves obtained from a cut-stem segment experiment and literature separated by wood type, including; softwood, diffuse-porous and ring-porous (see Table S5.5). A quadratic polynomial function best explained the calibration curve constructed in this study for both *Picea abies* and *Larix decidua*, where F_d= 26.236K +56.495K^2 (R^2= 0.96, p <0.001). The Granier (1985) calibration curve is highlighted, as it is the most commonly applied calibration (see Figure 5.1).

Uncertainty analysis for Lötschental F_d and stand water use

Large offsets in mean daily F_d throughout the year (growing season) were attributed to the used calibration method. During the four years of monitoring, Granier's calibration on average reduced mean daily F_d by 39 cm^3 cm^{-2} d^{-1} for *L. decidua* and 14 cm^3 cm^{-2} d^{-1} for *P. abies* in comparison to our species-specific calibration (Figure 5.5a). Lower mean daily F_d was found when using the PD zero-flow condition, while MW produced the highest values (Figure 5.5a; change of 39 cm^3 cm^{-2} d^{-1} for *L. decidua* and 13 cm^3 cm^{-2} d^{-1} for *P. abies*), when using a species-specific calibration. Applying a dampening correction increased F_d by 61 cm^3 cm^{-2} d^{-1} for *L. decidua* and 14 cm^3 cm^{-2} d^{-1} for *P. abies* (when using a species-specific calibration). When considering the species-specific calibration, the ED method and dampening correction, on average 50, 53, 26, 34% and 14% of the total annual precipitation is transpired at N13, N13W, S16, S19 and S22, respectively. From all commonly applied TDM procedures (Figure 5.1b) using a species-specific calibration generated the largest offset in mean annual stand water use, when considering only the first year of measurement (Figure 5.6a; reduction from 286 mm to 207 mm). Additionally, PD ΔT_{max} showed consistently

lower mean annual stand water use, which is mainly caused by the in- or exclusion of nighttime water use (Figure 5.6b; reduction of 54 mm when considering MW). The effect of dampening is however not pronounced when considering the absolute values in the first year (Figure 5.6a; reduction of 10 mm).

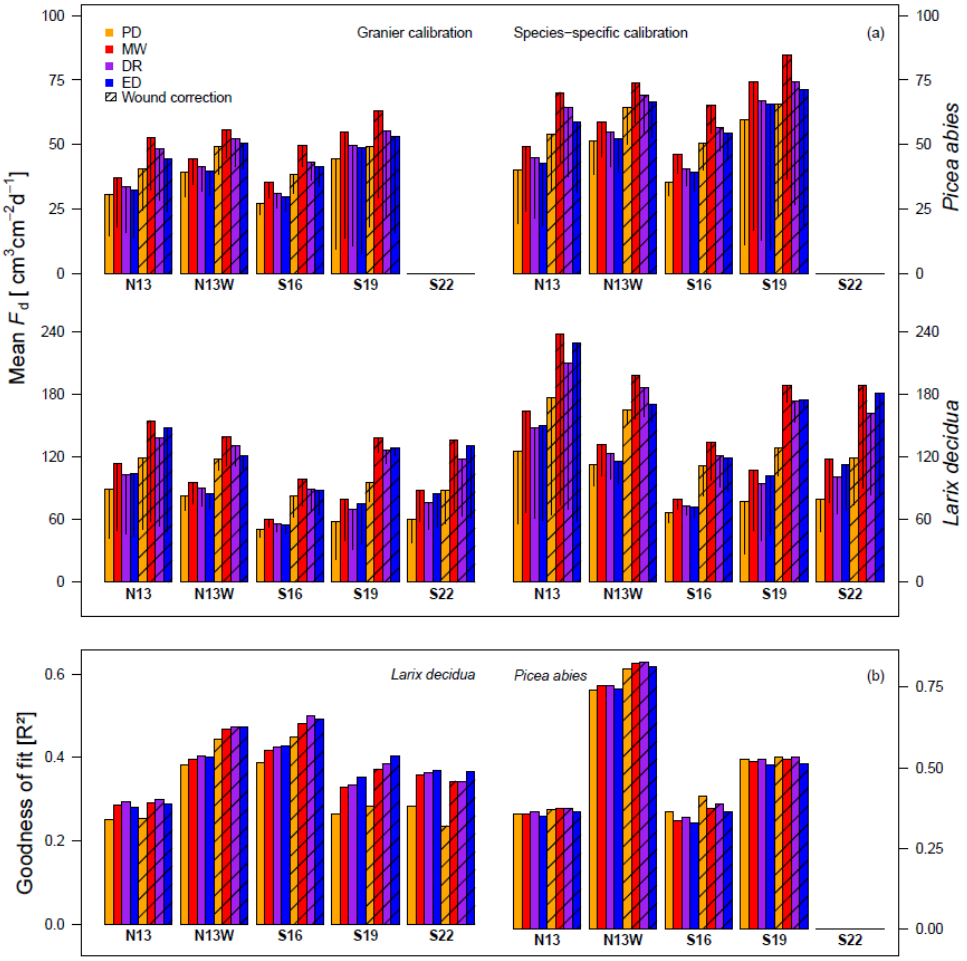

Figure 5.5 Uncertainty analysis of data-processing procedures on mean daily F_d [cm^3 cm^{-2} d^{-1}] and inter-daily sap flux density variability (R^2) arranged per species and Lötschental monitoring site. (a) The effect of zero-flow condition (ΔT_{max}), dampening correction and calibration curve selection on mean daily F_d. Zero-flow condition methods include: PD= pre-dawn, MW= moving window, DR= double regression and ED= environmental dependent. Standard deviation induced by the individual trees is provided with the vertical lines in the boxes. (b) Goodness of fit (R^2) for a third-order polynomial describing the relationship between *D* (daily mean [kPa]) and daily F_d when considering the Granier (1985) calibration.

Species-specific responses were observed in the relationship between mean *D* [kPa] and daily F_d (Figure 5.5b). A third-order polynomial could explain up to 74% (p <0.001) of the variance for *P. abies* at N13W, when using PD, no dampening correction and Granier's calibration, while for *L. decidua* this was only 36% (p <0.001). No distinct change in goodness of fit with *D* was observed when using Granier's or species-specific calibration. Slight improvements in

correlation strength were found when correcting for dampening (Figure 5.5b; from 0.39 to 0.42 across species). The applied zero-flow conditions had little effect on *P. abies*, in contrast to *L. decidua*. Site-specific effects were found for *P. abies* where correlations with *D* were highest at N13W, followed by S19, S16 and N13. For *L. decidua* pre-dawn ΔT_{max} showed the weakest correlation to *D* compared to the other methods (Figure 5.5b). Additionally, when correlating nighttime *D* with nighttime F_d, only strong correlations were found for ED when considering *L. decidua* (R^2= 0.30), DR (0.21) and MW (0.22).

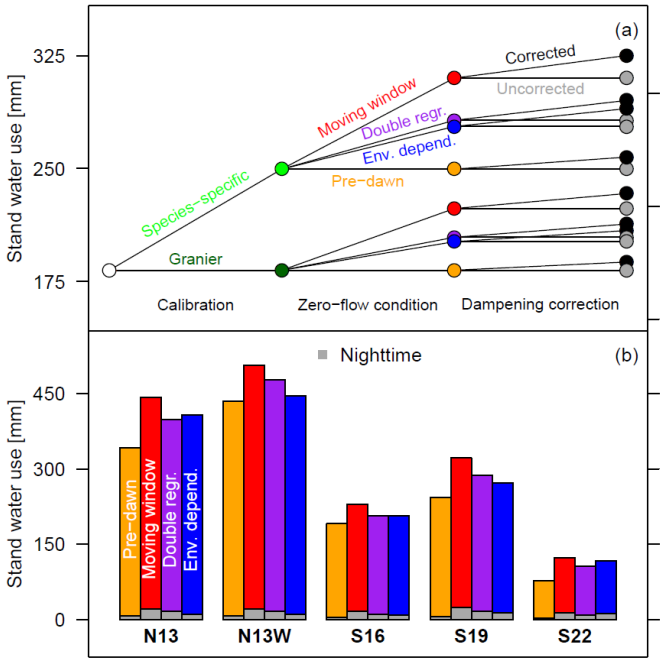

Figure 5.6 Effects of method combinations on average Lötschental stand water use [mm] for the first year of monitoring (2012). (a) Impact of data-processing assumptions compared to the most commonly applied method: pre-dawn zero-flow conditions (ΔT_{max}), no dampening correction and applying the Granier calibration. Data-processing procedures include; the application of a Species-specific or the Granier calibration, zero-flow conditions defined with the Moving window, Double regression (Double regr.), Environmental dependent (Env. depend.) or Pre-dawn method, and the absence (Uncorrected) or application (Corrected) of a dampening correction. (b) Contribution of nighttime sap flow for the different zero-flow condition methods to stand water use, when considering a species-specific calibration and dampening correction. The values correspond to the filled dots for the species-specific calibration when applying the dampening correction presented in (a), separated by site.

Uncertainty in sap flux density on Northern Hemisphere conifers

Including uncertainty due to calibration (Figure 5.4 softwood; excluding the steepest curve from Lundblad *et al.* 2001) had a strong effect on absolute F_d on the Northern Hemisphere dataset (Figure 5.7a, b). The genus *Pinus* showed the lowest maximum F_d, ranging from 11 to 239 $cm^3\ cm^{-2}\ d^{-1}$ (Figure 5.7b), with highest uncertainty ranges at the PER and UMBS sites (Table 5.2). For the genus

Picea, maximum F_d ranged from 35 to 294 $cm^3\ cm^{-2}\ d^{-1}$, with the greatest range at the SOBS and LOTS19 sites (Table 5.2). The genus *Larix*, the only deciduous conifer species in our study, showed the highest maximum F_d ranging from 56 to 967 $cm^3\ cm^{-2}\ d^{-1}$.

When comparing mean daily F_d to the most commonly applied data processing, the different softwood calibration curves introduced an average uncertainty of 31 $cm^3\ cm^{-2}\ d^{-1}$, across species (Figure 5.7c). *L. decidua* showed the strongest offset of 51 $cm^3\ cm^{-2}\ d^{-1}$, which increased to 75 $cm^3\ cm^{-2}\ d^{-1}$ when including the uncertainty induced by ΔT_{max} methods (including PD, MW and DR). The ΔT_{max} method alone (using a Granier calibration) induced an average uncertainty of 10 $cm^3\ cm^{-2}\ d^{-1}$ across species. When considering the uncertainty generated by both the calibration curves and the ΔT_{max} methods (with a mean uncertainty of Δ 45 $cm^3\ cm^{-2}\ d^{-1}$), it becomes apparent that sites with generally higher *K* values also have larger difference between individuals (Figure 5.7c).

5.4 Discussion

We quantified uncertainties introduced by different data-processing procedures when calculating sap flux density (F_d) with the thermal dissipation method (TDM; Figure 5.1a). Our results show that commonly applied data processing (using pre-dawn zero-flow conditions, absence of dampening correction and Granier's calibration; Figure 5.1b) likely underestimates F_d. Additionally, incorrect handling of zero-flow conditions and dampening of the signal may introduce inaccuracies in inter-daily variability of whole-tree transpiration rates, although the temporal dynamics and relative inter-specific variability of F_d is well captured.

Differences in F_d caused by zero-flow condition assumptions

Determination of ΔT_{max} requires informed assumptions on when zero-flow conditions occur (see Figure 5.2). The effect of applying different methods for estimating ΔT_{max} on mean daily F_d is most pronounced when comparing pre-dawn (PD) ΔT_{max}, which produced the lowest values, to other zero-flow condition procedures (Figure 5.2a). The moving-window (MW) method provides the highest absolute values in mean daily F_d. However, the MW method can be significantly affected by thermal drifts and changes in stem water content (Vergeynst *et al.* 2014), increasing ΔT_{max} for an extensive temporal period and thus adding uncertainty (Rabbel *et al.* 2016). Also, for *L. decidua* the correlation with vapour pressure deficit (*D*) consistently decreased when using the PD method (e.g., from 0.40 to 0.28 R^2 for S19 when applying a dampening correction;

Figure 5.5b) in contrast to *P. abies*. Although the mechanism behind this species-specific difference is unclear, one explanation could be the larger water storage capacity of *L. decidua* which requires longer refilling during the night (Zweifel & Häsler 2001; Meinzer *et al*. 2009; Zheng *et al*. 2014). These results are in agreement with findings of Kavanagh *et al*. (2007) for *L. occidentalis*, showing the occurrence of nighttime transpiration which impacted ΔT_{max}.

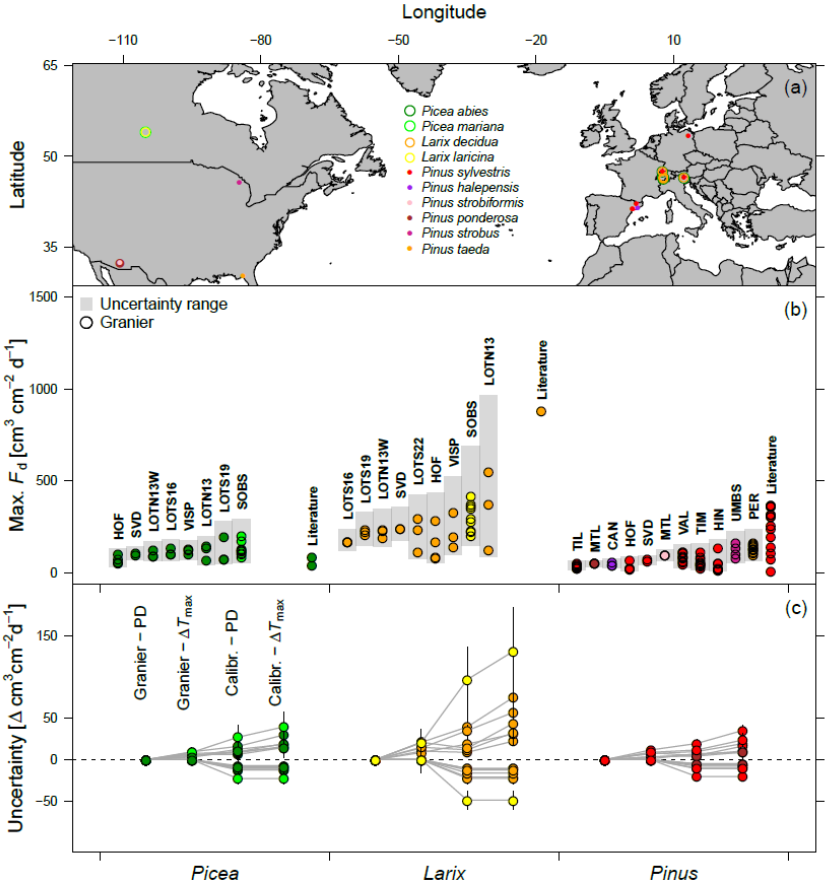

Figure 5.7 Uncertainty analysis on the Northern Hemisphere sap flow data. (a) Map indicating the included research sites and species. (b) Maximum of daily sap flux density (99th quantile of F_d [cm^3 cm^{-2} d^{-1}]) and the uncertainty generated by calibration curves (see softwood in Figure 5.4) for three conifer genera; *Picea*, *Larix* and *Pinus*. The dots indicate Granier's calibration for every individual tree, while the grey area is the maximum range generated by the different softwood calibration curves for all trees within the site (used zero-flow conditions are presented in Table 5.2). Additionally, reported literature values are described in Wullschleger *et al.* (1998) and Kallarackal *et al.* (2013). (c) Uncertainty of the mean daily F_d, when comparing commonly applied data processing (Granier calibration and pre-dawn ΔT_{max}) against other softwood calibrations (see Figure 5.4) and ΔT_{max} methods (PD, MW or DR; see Figure 5.2). Positive uncertainty is determined when using the Granier calibration and different ΔT_{max} methods (Granier - ΔT_{max}), using different softwood calibrations with PD (Calibr. - PD) and when both are variable (Calibr. - ΔT_{max}). Negative uncertainty is determined for Calibr. - PD, as the data was standardized to PD which provides the lowest values. Each dot connected by grey lines represents a site, in which the standard deviation induced by the individual trees is presented with horizontal black lines. A detailed descriptions of the sites is presented in Table 5.2.

Although it is difficult to differentiate between refilling of the storage tissue and actual nighttime transpiration (De Schepper and Steppe 2010), the improvement in correlation between daily F_d and D when not using the PD method suggests nighttime activity (Figure 5.5b). Evidence for nighttime activity provided by flux tower data supports our findings (see Novick *et al.* 2009). Although in conifers the nighttime to daytime transpiration fraction is relatively small (≈5% of total stand water use), its inclusion has a profound effect on the annual stand water use (Δ67 mm when comparing PD to MW in Figure 5.6b). When environmental measurements are available, it is advised to apply the environmental dependent (ED) method (Oishi *et al*. 2016), as it provides independent evidence for selecting periods with zero-flow conditions. If not available, the double regression (DR) method appears to perform well, as both daily F_d values and its intra-daily variability lies closest to the ED method (Figure 5.5), although being dependent upon the subjective selection of a window size.

On the causes of apparent signal dampening

We found a significant dampening in TDM-measured K, which reduces climate-F_d relationships (Figure 5.5b), although inter-daily K variation appeared to be preserved (Figure 5.3b; Oliveras & Llorens 2001). K decreased up to 55% after the first year of measurement (Table 5.3) and stabilized afterwards (e.g., Figure 5.3a). Also, ΔT consistently increased, indicating a reduced heat dissipation from the upper probe to the surrounding sapwood. The signal dampening and increase in ΔT can be explained by either the sensor being burrowed deeper into wood with lower water conductance (Phillips *et al.* 1996; Beauchamp *et al.* 2013; Berdanier *et al.* 2016), or due to a wound reaction (Wiedemann *et al.* 2016). Although our probes are progressively grown deeper into the xylem, we find this alone unlikely to explain the strong dampening patterns observed only in the first year after installation. Additionally, the slow growth rates of the monitored trees (≈1 mm $year^{-1}$ while the probes are 20 mm in length; see Table 5.1) are not expected to cause burrowing rates which can explain a K reduction of >50%. Although visual confirmation of wound tissue formation or resin build-up is needed (see Marañón-Jiménez *et al.* 2017), we hypothesize that wound reaction occurring in these coniferous species play a major role in altering the thermal properties and reduces the overall water conductance (Moore *et al.* 2010; Wullschleger *et al.* 2011).

It is difficult to establish generally applicable corrections, as wound reactions are likely tree-specific and influenced by abiotic factors and phenology, among others (Wiedemann *et al.* 2016; Marañón-Jiménez *et al*. 2017). To avoid the effect of wound reaction a common practise is to reinstall the probes every

year (Köstner *et al.* 1998; Moore *et al.* 2010). This however may cause issues due to circumferential variability (Oliveras & Llorens 2001). We thus propose using our statistical correction procedure (Equation 5) which helped to isolate the dampening signal, when longer-term measurements are conducted, and only reinstalling sensors if circumferential variability is low. However, caution is required for long-term installation with fast-growing species, as the probes will likely grow deeper into the heartwood, and for diffuse- or ring-porous species, as these may exert stronger radial variation in F_d (Beauchamp *et al.* 2013; Berdanier *et al.* 2016). Further studies should experimentally test the validity of our proposed correction to corroborate that it can be appropriately applied in monitoring studies, better revealing long-term effects (i.e., climatic) on plant water transport.

Calibration curve comparison

Our species-specific calibration curve demonstrates that Granier's calibration (Granier 1985) produces lower F_d for a given K (Figure 5.4). This causes a change in the exponent of the TDM calibration curve (Equation 2; we used $F_d = 26.236K + 56.495K^2$) with implications for the magnitude of fluxes. In some cases, an underestimation of 50% was reported (Paudel *et al.* 2013), while we found a 37% underestimation (Figure 5.5a; difference in stand water use of 71 mm yr^{-1}). In softwood species, the steepest calibration curve was found by Lundblad *et al.* (2001), but caution should be taken as this calibration curve was established by comparing TDM and the trunk segment heat balance (TSHB), assuming that the latter has no methodological issues (Poyatos *et al.* 2005; González-Altozano *et al.* 2008; Renninger & Schäfer 2012). Cut-stem segment experiments also do not fully portrait natural conditions occurring in the stem, as there might be differences between applying suction or gravimetric pressure to generate flow (Fuchs *et al.* 2017), which should be investigated.

No species-specific difference between *P. abies* and *L. decidua* was found in the calibration curves (Figure 5.4). However, our literature review reveals steeper calibration curves for denser wood types, with the steepest curves found for ring-porous species (Figure 5.4). The efficiency by which heat is conducted at different F_d is likely affected by wood anatomical properties (Wullschleger *et al.* 2011; Fan *et al*. 2018). Despite *P. abies* showing a smaller earlywood lumen area than *L. decidua* (Cuny *et al*. 2014; Carrer *et al.* 2017), thus a smaller proportion of water-filled tracheid to carry heat through conductive woody tissue, we did not find a significantly steeper curve. Also, when including species-specific wood density, no clear patterns were found for the steepness of the reviewed curves

(results not shown). We hypothesise that the anticipated relationship between wood density and steepness of the calibration curve is distorted by variability in local wood properties (e.g., smaller or wider rings that have specific anatomical features), which are affected by site conditions (Anfodillo *et al.* 2013; Greenwood *et al.* 2017). Nevertheless, the most accurate estimation of absolute F_d is likely obtained when applying a site- and species-specific calibration curve.

Implications of uncertainty for sap flow measurements

When interested in the response of canopy conductance derived from sap flow measurements to environmental change (see Poyatos *et al.* 2013), the choice of zero-flow conditions to determine ΔT_{max} is important as it affects the inter-daily variability in F_d. As PD ΔT_{max} showed consistently weaker correlations with D when considering diurnal F_d variability in the Lötschental (Figure 5.5b), studies that apply methods which allow for nighttime sap flow activity are presumed to obtain more appropriate climate-transpiration response patterns, although species dependent. Additionally, dampening occurring within the first year after installation could affect F_d-climate correlations, as they induced a consistent reduction in F_d which could be co-linear with other environmental variables.

Whole-tree water use measured with TDM is commonly collected during one growing season and estimated by using PD ΔT_{max}, no dampening correction and Granier's calibration (Figure 5.1b). When comparing this standard to other data-processing procedures for the Lötschental measurements, employing species-specific calibration curves caused the largest deviation in mean daily F_d and annual stand water use (Δ27 $cm^3\,cm^{-2}\,d^{-1}$ in Figure 5.5a and Δ79 mm in Figure 5.6a). This uncertainty will most likely increase further when considering circumferential variation in F_d (Lu *et al*. 2000) and when upscaling from tree to stand water use (Čermák *et al*. 2004). Dampening appeared less relevant for stand water use when considering one growing season (Figure 5.7a). Current studies applying PD ΔT_{max} most likely underestimate annual stand water use compared to other methods, while causing only minute differences in nighttime transpiration (Figure 5.6b; see Rabbel *et al*. 2016).

The uncertainty generated by the calibration curve depends upon the range of K values measured within the individual, as the deviation between the curves increases with K (Figure 5.4). Additionally, the uncertainty generated by ΔT_{max} depends upon species-specific responses and site-specific environmental conditions which allow zero-flow conditions. However, when considering the 131 Northern Hemisphere conifers, the uncertainty in maximum F_d caused by the selected calibration curve remains substantial (Figure 5.7b; using the reported

ΔT_{max} and ignoring dampening). Due to the power function shape of most softwood calibration curves (Figure 5.4), large uncertainties are generated for species with high *K* such as the genus *Larix* which can be explained by many factors, including a deeper rooting system, greater access to soil resources, or its deciduous strategy (Anfodillo *et al.* 1998). Additionally, a link has been proposed between xylem structure in conifers and F_d, as wood with larger tracheids and lower density will be able to facilitate higher flow rates (Roderick & Berry 2001; Barbour & Whitehead 2003).

When comparing the combined uncertainty generated by calibration and ΔT_{max} methods against commonly applied data processing (one growing season, Granier calibration and pre-dawn ΔT_{max}), again the calibration curve appears to generate the largest uncertainty (on average 31 cm^3 cm^{-2} d^{-1}; Calibr.-PD in Figure 5.7c). Yet, ΔT_{max} methods contribute to an even larger uncertainty of 75 cm^3 cm^{-2} d^{-1} (Calibr.-ΔT_{max} in Figure 5.7c). Besides large variations among trees, site conditions likely affected the F_d range, although this requires site-specific environmental measurements. When interested in absolute conifer-stand water use or inter-specific stomatal conductance response, TDM users should thus be critical about decisions regarding the calibration curve and detection of nighttime sap flow activity for conifers. Yet, as the calibration curve might be dependent on wood density, F_d estimates from trees with greater wood density and higher flow rates, like ring- and diffuse-porous species (Wullschleger *et al.* 1998), will likely show greater uncertainty.

Conclusion and outlook

TDM will likely remain widely applied and thus a blueprint on data processing and reporting should be established to avoid irreconcilable biases in F_d measurements. Here, we show that Granier's generalized calibration, compared to site- and species-specific calibrations, might cause an underestimation of F_d. This in turn affects stand-level water use estimates and comparisons of site- and species-specific transpiration behaviour. Development of calibration curves is thus important for obtaining more accurate absolute F_d estimates. Also, allowing nighttime sap flow activity (avoiding the use of pre-dawn ΔT_{max}) improved F_d-climate responses, although being species-specific and less severe compared to absolute effects on F_d. Finally, applying a dampening correction is important for conserving F_d inter-daily variability, although the timeframe for the application of dampening corrections is still uncertain (Wiedemann *et al.* 2016). Indeed, independent whole-tree water use measurements are needed to further quantify all sources of uncertainty in TDM measurements (see Oishi *et al.* 2008). Besides data

processing, variable sapwood thickness, radial and circumferential variability, changes in stem water content, and natural temperature gradients most likely increase uncertainty and should be systematically assessed in the future. However, recent progress on the development of free software tools for TDM data processing (Oishi *et al.* 2016; Ward *et al.* 2017) and upscaling (Berdanier *et al.* 2016) will lead to more harmonized, transparent, and reproducible sap flow data, better quantifying the associated uncertainties. This generalisation would then allow for the incorporation of uncertainty quantifications in the global pattern analyses of whole-tree water use.

Acknowledgments

R.L.P. acknowledges funding from the Swiss National Science Foundation project (SNSF), LOTFOR (no. 150205). R.P. acknowledges funding from the grant CGL-2014-5583-JIN awarded by the Spanish MINECO. C.P. acknowledges support from the Stavros Niarchos Foundation, the ETH Zurich Foundation, and the SNSF (Grants P2EZP2_162293, P300P2 174477). I.H. acknowledges support from the Deutsche Forschungsgemeinschaft (DFG project number He7220/1-1) and the Terrestrial Environmental Observatory (TERENO) of the Helmholtz Association. G.A.B.G. acknowledges funding from the United States National Science Foundation (EAR 1417101, EAR 1331906). O.S. acknowledges funding from the Canada Research Chairs, Canada Foundation for Innovation Leaders Opportunity Fund and Natural Sciences and Engineering Research Council Discovery Grant programs.

Supporting information Chapter 5

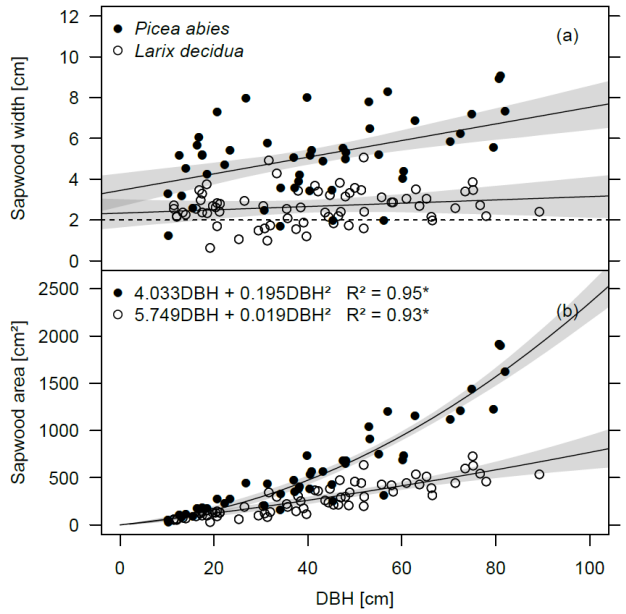

Figure S5.1 Allometric relationships between diameter at breast height for *Picea abies* and *Larix decidua* (DBH), (a) sapwood width and (b) sapwood area. No significant fit was found for DBH versus sapwood width. Grey areas presents the Bayesian credible interval of the fitted function (see Gelman & Hill 2007).

Table S5.1 General statistics for generalized least squares models, correcting for first order auto-correlation (using corAR1 correlation), when explaining K (pre-dawn ΔT_{max}) with vapour pressure deficit (D [hPa]), temperature (T [°C]), soil moisture (θ [%]) and seasonality (DOY, day of year). For every tree the intercept (Int.) and slopes (ε) of the model are provided, in addition to the residual standard error (RSE), degrees of freedom (df) and temporal auto-correlation coefficient (Φ).

Site	Species	Tree	Generalized Least Squares – Linear model									
			Int.	ε_1	ε_2	ε_3	ε_4	ε_5	ε_6	RSE	df	Φ
N13W	*P. abies*	1	-0.04	-0.0004*	-5.71	0.0019	-4.7E-06	-0.03*	0.020*	0.07	532	0.95
		2	0.27*	-0.0004*	-15.93*	0.0002	2.8E-09	-0.04*	0.023*	0.05	540	0.81
		3	0.09	-0.0002*	-6.08	0.0011	-2.6E-06	-0.02*	0.010*	0.05	530	0.95
	L. decidua	1	-1.70*	-0.0004*	-27.99*	0.0234*	-5.4E-05*	-0.02*	0.014*	0.08	402	0.94
		2	-2.58*	-0.0005*	0.02*	0.0175*	-4.1E-05*	-0.01*	0.021*	0.13	374	0.98
		3	-1.95*	-0.0006*	0.00*	0.0169*	-3.9E-05*	0.03*	0.024*	0.10	412	0.98
N13	*P. abies*	1	0.06	-0.0003*	-1.79*	0.0003	-7.7E-07	-0.04*	0.013*	0.03	374	0.90
		2	0.09	-0.0006*	-3.23*	0.0013	-3.4E-06	-0.06*	0.020*	0.06	414	0.91
		3	-0.06	-0.0006*	-4.12*	0.0035*	-8.1E-06*	-0.05*	0.022*	0.06	486	0.88
	L. decidua	1	-1.80*	-0.0008*	-5.97*	0.0220*	-5.1E-05*	-0.02*	0.028*	0.15	435	0.94
		2	-0.76*	-0.0001*	-2.70*	0.0100*	-2.3E-05*	-0.03*	0.006*	0.06	384	0.97
		3	-1.96*	-0.0012*	-8.78*	0.0237*	-5.2E-05*	-0.02*	0.041*	0.13	437	0.88
S16	*P. abies*	1	-0.02	-0.0004*	-1.96*	0.0014	-3.8E-06	-0.02*	0.017*	0.07	298	0.95
		2	0.04	-0.0005*	-3.35*	0.0019*	-4.5E-06*	-0.02*	0.017*	0.04	518	0.85
		3	-0.09	-0.0003*	0.20	0.0015	-3.8E-06	-0.01*	0.012*	0.07	410	0.97
	L. decidua	1	-1.08*	-0.0004*	0.08	0.0112*	-2.6E-05*	0.00	0.017*	0.07	281	0.96
		2	-0.75*	-0.0001*	1.40*	0.0077*	-1.8E-05*	0.00	0.006*	0.08	422	0.97
		3	-1.44	-0.0002*	0.57	0.0135*	-3.0E-05*	-0.01	0.010*	25.23	218	1.00
S19	*P. abies*	1	-0.20*	-0.0007*	-3.36*	0.0036*	-8.3E-06*	-0.02*	0.027*	0.04	328	0.81
		2	-0.36*	-0.0012*	-0.88	0.0044*	-1.1E-05*	-0.02*	0.047*	0.08	477	0.79
		3	0.03	-0.0003*	-1.42*	0.0012*	-2.8E-06*	-0.03*	0.011*	0.03	443	0.80
	L. decidua	1	-0.73	-0.0002	-1.37	0.0084*	-1.9E-05*	0.00	0.005	0.08	248	0.92
		2	-2.03*	-0.0003*	-0.32	0.0217*	-4.9E-05*	-0.01*	0.012*	0.06	381	0.77
		3	-1.27*	-0.0003*	0.06	0.0131*	-3.0E-05*	-0.01*	0.010*	0.08	268	0.96
S22	*L. decidua*	1	-1.47*	-0.0005*	-2.61*	0.0155*	-3.5E-05*	-0.03*	0.016*	0.04	310	0.82
		2	-1.23*	-0.0004*	-4.71*	0.0137*	-3.1E-05*	-0.01	0.011	0.09	320	0.89
		3	-2.14*	-0.0006*	-0.46*	0.0223	-5.1E-05*	-0.03*	0.018*	0.07	305	0.76

$K = \text{Int.} + \varepsilon_1 D^1 + \varepsilon_2 T + \varepsilon_3 T^2 + \varepsilon_4 \theta^1 + \varepsilon_5 \text{DOY} + \varepsilon_6 \text{DOY}^2$

Table S5.2 General statistics for non-linear models when explaining the dampening effect K (pre-dawn ΔT_{max}) with time since installation (t [days]) and seasonality (DOY, day of year). For every tree values of the variable (a-f) are provided, in addition to the residual standard error (RSE) and degrees of freedom (df).

Site	Species	Tree	Non-linear model							
			a	b	c	d	e	f	RSE	df
N13W	*P. abies*	1	0.14*	0.000*	-0.001*	1.2E-06	2.1E-03	-5.46E-06*	0.038	527
		2	-0.33	0.001	1.137	4.2E-04	3.0E-03	-7.55E-06*	0.053	541
		3	0.14*	0.000	0.001	1.8E-06	1.1E-03*	-3.16E-06*	0.028	437
	L. decidua	1	-1.39*	-0.004	0.002	4.0E-08*	1.8E-02*	-4.13E-05*	0.043	403
		2	-0.59*	-0.001	0.001	7.6E-08	1.1E-02*	-2.44E-05*	0.046	375
		3	-0.70*	-0.002*	0.002*	6.0E-08	1.2E-02*	-2.72E-05*	0.042	413
N13	*P. abies*	1	0.28*	0.005*	0.039*	2.4E-06	2.6E-05	-7.39E-07*	0.023	375
		2	0.28*	0.002	0.011	-1.7E-06	3.9E-04	-2.07E-06*	0.058	415
		3	0.23*	0.003	0.020	1.8E-06	1.5E-03*	-4.76E-06*	0.061	480
	L. decidua	1	-0.19*	-0.005*	0.007*	1.1E-06*	9.7E-03*	-2.35E-05*	0.094	436
		2	-0.31*	-0.002	0.004	-3.6E-07	6.2E-03*	-1.57E-05*	0.051	337
		3	-0.58*	-0.005	0.006	8.9E-07	1.2E-02*	-2.67E-05*	0.133	438
S16	*P. abies*	1	0.17*	0.000*	0.000	-6.6E-07	1.1E-03*	-3.27E-06*	0.031	277
		2	0.21*	0.001	0.007	-7.8E-07	0.6E-03*	-2.29E-06*	0.040	519
		3	0.31*	0.000	0.006*	-3.6E-06	0.6E-03*	-2.30E-06*	0.024	324
	L. decidua	1	-0.64*	-0.002	0.002	2.2E-07	9.7E-03*	-2.24E-05*	0.036	282
		2	-0.11*	-0.003*	0.005*	8.2E-07	5.6E-03*	-1.30E-05*	0.023	407
		3	-1.01*	0.000*	0.000	0.0E-07	12.9E-03*	-2.92E-05*	0.034	171
S19	*P. abies*	1	0.28*	0.008	0.069*	-5.4E-06	6.7E-04	-1.85E-06*	0.041	329
		2	-0.03	0.000	0.002	2.6E-06	5.0E-03*	-1.23E-05*	0.062	478
		3	0.15*	0.000	0.011*	-2.2E-06*	7.8E-04*	-2.12E-06*	0.019	434
	L. decidua	1	0.02	-0.003*	0.010*	1.9E-06*	2.9E-03*	-6.84E-06*	0.017	249
		2	-1.78*	-0.003	0.001	5.2E-08*	2.1E-02*	-4.64E-05*	0.043	382
		3	-0.39*	-0.012*	0.018*	-5.5E-07*	7.5E-03*	-1.71E-05*	0.019	269
S22	*L. decidua*	1	-1.12*	-0.028	0.025	-1.2E-06	13.1E-03*	-2.98E-05*	0.030	311
		2	-0.26*	-0.002*	0.002*	8.3E-07*	6.0E-03*	-1.32E-05*	0.032	321
		3	-1.71*	-0.007*	0.003*	2.9E-07*	20.1E-03*	-4.60E-05*	0.037	306

$K = (a + b\,t) / (1 + c\,t + d\,t^2) + e\,\mathrm{DOY} + f\,\mathrm{DOY}^2$

Table S5.3 Raw data of the cut-segment calibration experiment. Mean F_d [cm^3 cm^{-2} h^{-1}] against K measured at a specific water column height (level in cm, increasing or decreasing) with thermal dissipation method (TDM) for four stems from *Larix decidua* and *Picea abies* trees.

Species	Tree	Level	K mean	K Stdev.	SFD mean	SFD Stdev.	Species	Tree	Level	K mean	K Stdev.	SFD mean	SFD Stdev.
Larix decidua	1	L2	0.217	0.009	7.430	0.219	*Picea abies*	1	L2	0.146	0.005	4.892	0.078
		L5	0.198	0.007	7.119	0.275			L5	0.137	0.001	5.173	0.063
		L10	0.189	0.005	6.998	0.329			L10	0.143	0.002	5.932	0.073
		L15	0.182	0.005	6.603	0.338			L15	0.164	0.004	6.642	0.067
		L25	0.187	0.003	6.984	0.240			L25	0.211	0.009	8.711	0.118
		L33	0.190	0.003	7.293	0.151			L33	0.271	0.007	12.771	0.279
		L-25	0.150	0.010	5.542	0.285			L-25	0.244	0.003	9.529	0.141
		L-15	0.106	0.008	3.765	0.132			L-15	0.218	0.006	6.702	0.128
		L-10	0.078	0.005	2.950	0.100			L-10	0.199	0.004	5.550	0.086
		L-5	0.060	0.004	2.304	0.081			L-5	0.176	0.005	4.682	0.067
		L-2	0.048	0.003	1.928	0.077			L-2	0.159	0.003	4.211	0.056
	2	L5	0.441	0.012	24.795	0.370		2	L10	0.372	0.003	17.085	0.118
		L10	0.474	0.006	27.047	0.409			L15	0.403	0.003	19.025	0.137
		L15	0.491	0.003	28.997	0.458			L25	0.446	0.004	22.818	0.294
		L25	0.538	0.003	33.718	0.450			L33	0.479	0.005	24.846	0.421
		L33	0.567	0.003	36.908	0.558			L-25	0.434	0.008	19.548	0.643
		L-25	0.510	0.009	29.828	0.716			L-15	0.355	0.005	13.995	0.417
		L-15	0.425	0.009	22.217	0.608			L-10	0.296	0.011	10.989	0.363
		L-10	0.367	0.010	17.911	0.440			L-5	0.235	0.011	8.575	0.259
		L-5	0.303	0.008	14.182	0.355			L-2	0.190	0.010	7.146	0.223
		L-2	0.267	0.006	11.878	0.285							
	3	L5	0.496	0.003	26.549	0.455		3	L2	0.427	0.007	24.179	0.190
		L10	0.531	0.005	28.417	0.518			L5	0.453	0.004	25.682	0.217
		L15	0.567	0.003	30.460	0.463			L10	0.486	0.006	28.725	0.213
		L25	0.646	0.007	36.186	0.296			L15	0.511	0.002	31.866	0.215
		L33	0.707	0.006	41.185	0.312			L25	0.570	0.003	38.080	0.335
		L-25	0.664	0.009	36.071	0.497			L33	0.626	0.009	42.873	0.285
		L-15	0.603	0.010	29.521	0.542			L-25	0.580	0.010	36.444	0.484
		L-10	0.525	0.009	25.067	0.437			L-15	0.521	0.008	29.225	0.258
		L-5	0.457	0.005	21.055	0.354			L-10	0.484	0.003	25.309	0.306
		L-2	0.412	0.005	18.298	0.311			L-5	0.444	0.004	21.935	0.306
									L-2	0.399	0.005	19.433	0.321
	4	L2	0.492	0.015	24.818	0.334		4	L10	0.366	0.006	17.515	0.176
		L5	0.483	0.003	26.029	0.346			L15	0.390	0.005	19.294	0.171
		L10	0.521	0.002	28.201	0.353			L25	0.430	0.004	23.298	0.230
		L15	0.547	0.005	30.427	0.320			L33	0.455	0.003	26.330	0.244
		L25	0.606	0.005	35.682	0.341			L-25	0.406	0.002	22.496	0.209
		L33	0.654	0.004	39.537	0.454			L-15	0.340	0.005	17.781	0.210
		L-25	0.606	0.007	33.910	0.476			L-10	0.300	0.005	15.506	0.190
		L-15	0.523	0.009	27.026	0.326			L-5	0.260	0.006	13.138	0.131
		L-10	0.470	0.007	23.309	0.343			L-2	0.242	0.004	11.920	0.199
		L-5	0.417	0.007	19.722	0.293							
		L-2	0.376	0.010	17.396	0.244							

Table S5.4 General statistics of linear mixed-effect modelling for the thermal dissipation calibration curves (K [-] against Fd [cm^3 cm^{-2} h^{-1}]). Effects of species was tested on the calibration curve while using the individual stems as a random factor (model 1) or excluding the species effect (model 2). Additionally, the power-type function proposed by Granier (1985) is presented (model 3). The slope (Estimate), standard error of the slope (Std. error), frequentist statistics (t-value, p), goodness of fit [R^2] and the Akaike Information Criterion (AIC) is provided.

Model	Formula (in R)	Random effects	Coefficients	Estimate	Std. error	t-value	p	R^2	AIC
1	lmer(SFD ~ 0 + K * species + I(K^2) * species + (K | tree))	Tree: Int. var.= 7.3 K var.= 75.7	K	25.82	10.59	6.08	0.050	0.96	267.8
			speciesLarix	0.47	2.53	3.89	0.862		
			speciesPicea	3.95	2.67	5.83	0.190		
			I(K^2)	52.34	11.85	7.60	0.003		
			kn:speciesPicea	-24.33	17.24	8.53	0.194		
			speciesPicea:I(K^2)	44.48	21.79	10.88	0.066		
2	lmer(SFD ~ 0 + K + I(K^2) + (K | tree))	Tree: Int. var.= 1.3 K var.= 46.4	K	26.24	1.56	16.85	<0.001	0.96	283.9
			I(K^2)	56.50	4.51	12.53	<0.001		
3	nls(SFD ~ α * K ^ β)	None	α	69.97	2.09196	33.45	<0.001	0.96	356.9
			β	1.364	0.04101	33.25	<0.001		

Table S5.5 Literature review on calibration curves. We distinguish: DB= Deciduous Broad-leaved, EB= Evergreen Broad-leaved, EC= Evergreen Coniferous, DC= Deciduous Coniferous. Wood anatomical properties include, DP= Diffuse-porous, RP= Ring-porous, SW= Softwood, DRP= Diffuse- to semi-ring-porous. For some of the measurements the standard error of the mean (SE) is provided. The symbol * indicates that the calibration curves is $\alpha K + \beta K^2$ instead of αK^{β}. All α values were recalculated to provide F_d in $cm^3\ cm^{-2}\ h^{-1}$.

Site	Coordinates	Species	Leaf type	Wood type	n	Diameter (cm) [SE]	Sapwood area (cm^2) [SE]	Sapwood depth (mm) [SE]	K range	R^2	α	β	Source
USA; Gibbs Farm	83°35'W | 31°26'N	*Liriodendron tulipifera*	DB	DP							53.978	1.231	Bosch *et al.* (2014)
		Pinus elliottii	EC	SW							48.966	1.231	
		Pinus palustris	EC	SW							45.796	1.231	
USA; Salt Lake Valley	111°55'W | 40°66'N	*Populus fremontii*	DB	DP	6	5.08 [0.15]	16.02 [1.01]	12.8 [1.46]	0-6		42.84	1.23	Bush *et al.* (2010)
		Tilia cordata	DB	DP	5	4.83 [0.15]	13.08 [0.75]	15.2 [0.80]	0-3		42.84	1.23	
		Elaeagnus angustifolia	DB	RP	7	4.36 [0.30]	1.70 [0.18]	1.63 [0.23]	0-0.7	0.86	3348	1.65	
		Gleditsia triacanthos	DB	RP	6	5.06 [0.26]	0.73 [0.09]	0.98 [0.09]	0-0.8	0.8	11052	1.4	
		Quercus gambelii	DB	RP	6	4.37 [0.08]	0.35 [0.06]	0.88 [0.04]	0-0.5	0.85	20916	1.88	
		Sophora japonica	DB	RP	6	4.47 [0.22]	0.51 [0.12]	1.08 [0.14]	0-0.55	0.84	4284	1.24	
France; Montfavet		*Malus pumila*	DB	DP	4				0-1	0.97	49.248	1.300	Cabibel & Co (1991)
		Quercus palustris	DB	RP	4				0-1	0.97	49.248	1.300	
		Castanea sativa	DB	RP	4				0-1	0.97	49.248	1.300	
		Quercus pedunculata	DB	RP					0-0.8		42.84	1.231	Granier (1985)
		Pinus nigra	EC	SW					0-1		42.84	1.231	
		Pseudotsuga menziesii	EC	SW					0-1.1		42.84	1.231	
UK; Swindon	1°42'W | 51°36'N	*Acer campestre*	DB	DP	3	6-23			0-1.1	0.98	46.44	1.46	Herbst *et al.* (2007)
		Crataegus monogyna	DB	DP	5	6-23			0-0.8	0.88	73.44	1.387	
UK; Wytham Woods	1°20'W | 51°47'N	*Fraxinus excelsior*	DB	RP	5					0.96	728.28	0.428	Herbst *et al.* (2008)*
Brasil; Piracicaba	46°38′W | 23°33′S	*Eucalyptus grandis x urophylla*	DB	DP	4				0-0.8	0.95	304.46	1.606	Hubbard *et al.* (2010)
USA; Utah's Entrada Field Station	-109°12'E | 38°47' N	*Tamarisk ramossisima Ledeb. × chinensis*	DB	DP	11	4.15 [0.2]	4.45 [0.77]	5.8 [0.6]	0-1	0.98	86.4	1.16	Hultine *et al.* (2010)
Australia; Darwin	130°52'E | 12°25'S	*Mangifera indica*	EB	DP	1						42.84	1.231	Lu & Chacko (1998)
Sweden; Norunda forest	17°29'E | 60°5'N	*Picea abies*	EC	SW	2	22.1 [2.7]	290.5 [35.5]	78 [13]	0-0.20	0.95	248.832	1.816	Lundblad *et al.* (2011)
		Pinus sylvestris	EC	SW	3	21.2 [2.4]	214 [61.4]	57 [1.3]	0-0.30	0.95	252.828	1.822	
New Zealand; Huapai	174°30'E | 36°48'S	*Agathis australis*	EC	SW	1	19				0.57	42.84	1.231	Macinnis-Ng *et al.* (2016)
Panama; Santa Cruz	79°W | 9°N	*Pseudobombax septenatum*	DB	DP	3	6.4 [0.12]	18.1 [0.69]				42.84	1.231	McCulloh *et al.* (2007)
		Calophyllum longifolium	EB	DP	3	6.0 [0.17]	21.3 [1.62]				42.84	1.231	
Germany; Grossfahner	10°49'E | 51°30'N	*Populus nigra × P. maximowiczii*	DB	DRP	5	10.30 [0.48]			0-0.8	0.93	126.756	1.552	Schmidt-Walter *et al.* (2014)
USA; Whitehall forest	83°21'W | 33°54'N	*Fagus grandifolia*	DB	DP	2	18 [3]				0.70	82.8	0.952	Steppe *et al.* (2010)
USA; Whitehall Forest	83°21'W | 33°54'N	*Liquidambar styraciflua*	DB	DP	5	7.5 [0.4]	29.3 [3.1]	26 [1]	0-1.2	0.89	44.64	1.151	Sun *et al.* (2012)
		Populus deltoides	DB	DP	5	7.5 [0.4]	29.3 [3.1]	27 [1]	0-0.7	0.94	43.56	1.141	
		Quercus alba	DB	RP	5	7.5 [0.4]	29.3 [3.1]	28 [1]	0-0.4	0.87	46.08	1.47	
		Ulmus americana	DB	RP	5	7.5 [0.4]	29.3 [3.1]	29 [1]	0-0.8	0.95	97.92	2.572	
		Pinus echinata	EC	SW	5	7.5 [0.4]	29.3 [3.1]	30 [1]	0-0.9	0.91	36.36	1.303	
		Pinus taeda	EC	SW	5	7.5 [0.4]	29.3 [3.1]	31 [1]	0-1.2	0.88	34.92	1.336	
USA; Red Butte Canyon	111°47'W | 47°48'N	*Acer grandidentatum*	DB	DP	1	5-6					198	1.02	Taneda & Sperry (2008)
		Quercus gambelii	DB	RP	1	5-6					2084.4	1.38	
Italy; San Vito di Cadore		*Larix decidua*	EC	SW	4	16.5 [0.6]	71.9 [6.7]	18.4 [3.9]	0-0.72	0.96	26.236	56.495	This study*
		Picea abies	EC	SW	4	15.9 [1.5]	121.2 [15.5]	35.8 [4.9]	0-0.65				

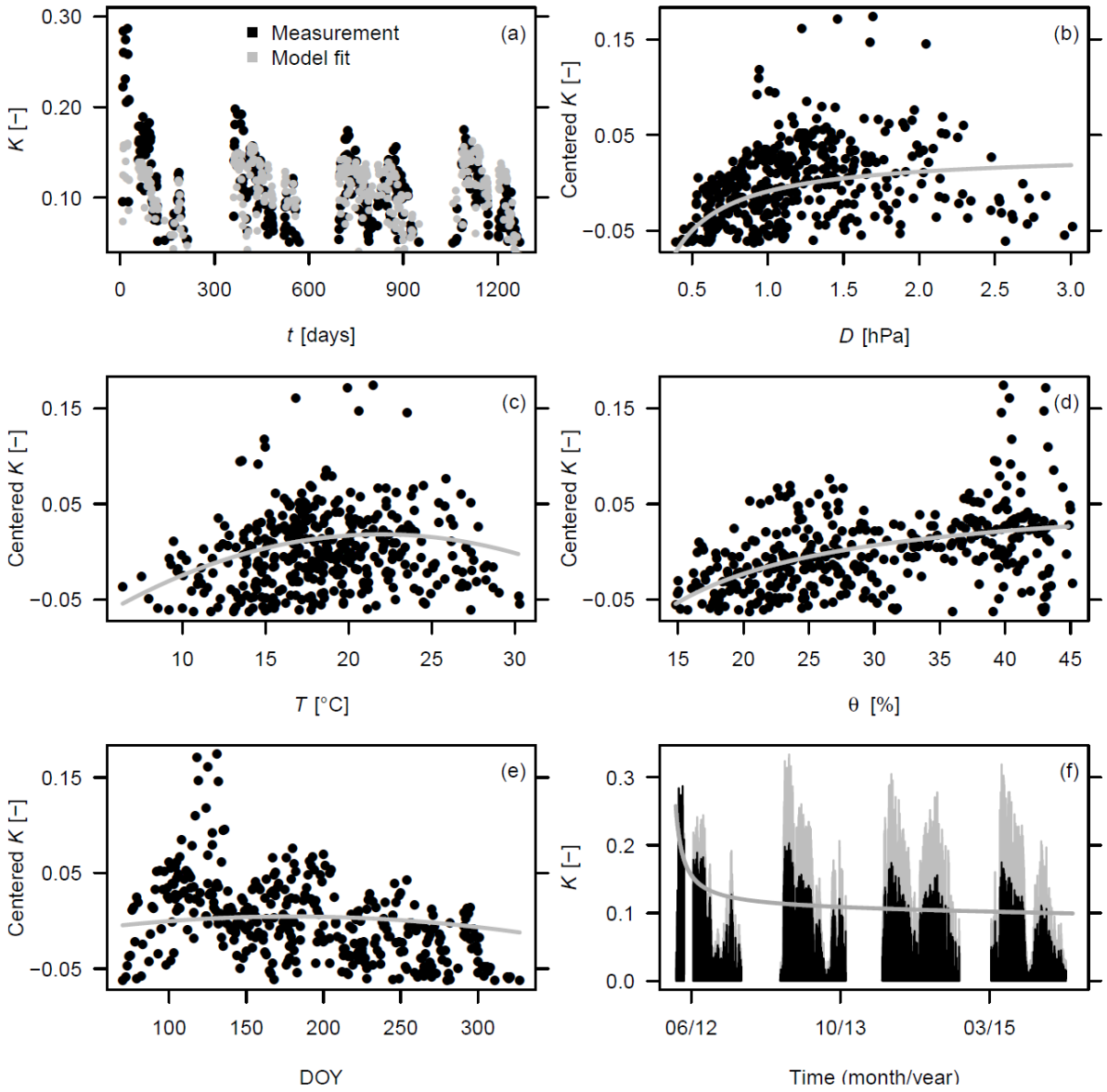

Figure S5.2 Example of the procedure to isolate the dampening effect for *K* (pre-dawn ΔT_{max}) measured for a *Picea abies* tree at N13. (a) Residuals are calculated by subtracting the measurements from the model values constructed with environmental factors and seasonality. This model, explained in Table S5.2, uses daily maximum vapour pressure deficit (b), daily mean temperature (c), daily mean soil moisture (d) and a seasonality term (e) to explain the daily maximum *K* pattern. Then the residuals containing the dampening are explained with a non-linear model (f), after which this model is used on the raw values (black lines) and transformed to corrected values (grey lines).

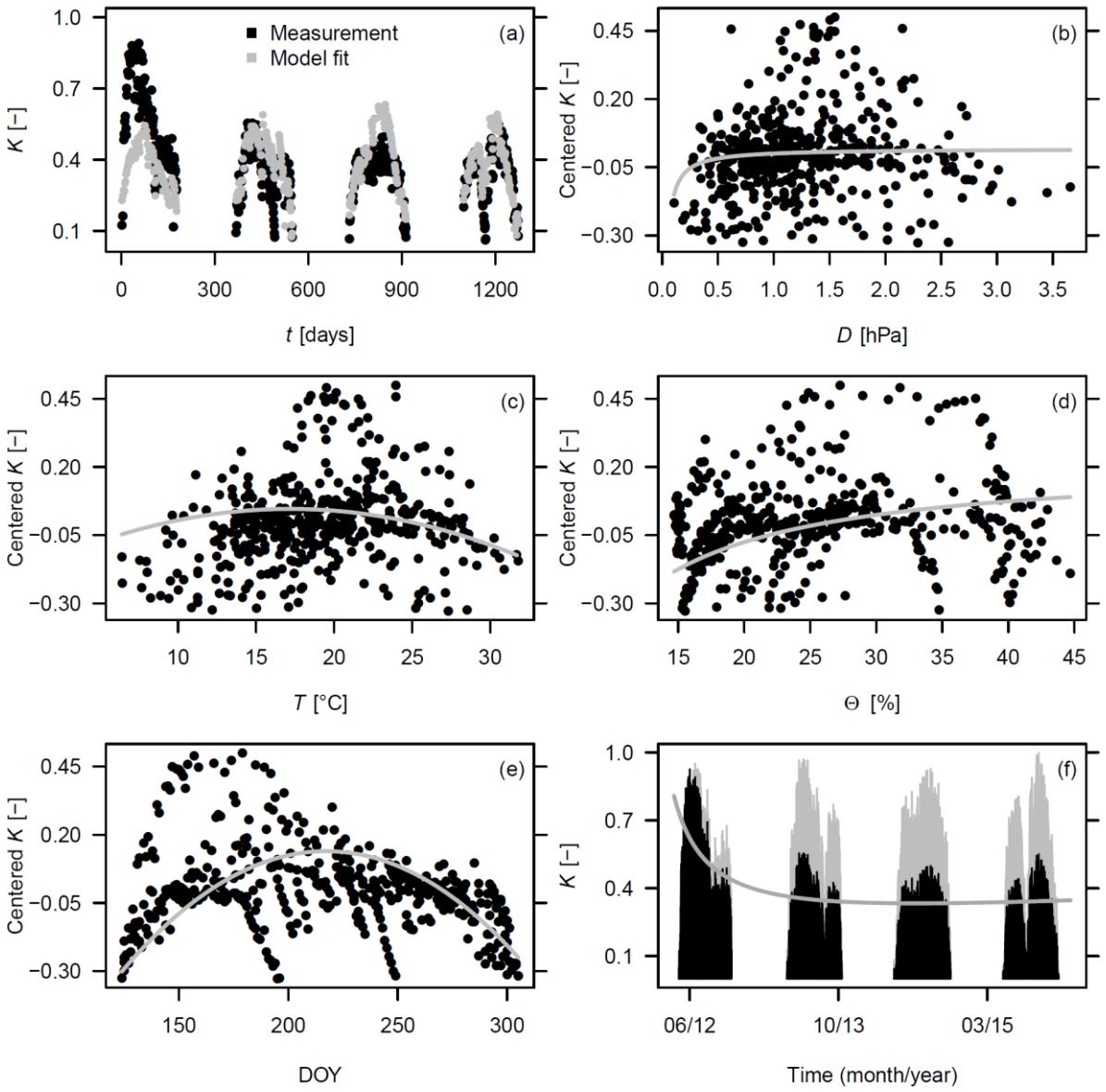

Figure S5.3 Example of the procedure to isolate the dampening effect for *K* (pre-dawn ΔT_{max}) measured for a *Larix decidua* tree at N13. (a) Residuals are calculated by subtracting the measurements from the model values constructed with environmental factors and seasonality. This model, explained in Table S5.2, uses daily maximum vapour pressure deficit (b), daily mean temperature (c), daily mean soil moisture (d) and a seasonality term (e) to explain the daily maximum *K* pattern. Then the residuals containing the dampening are explained with a non-linear model (f), after which this model is used on the raw values (black lines) and transformed to corrected values (grey lines).

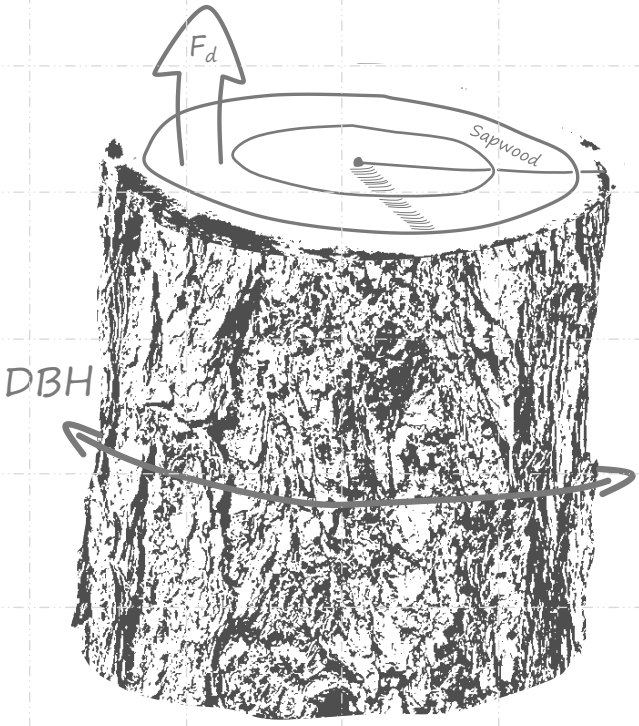

Transpiration

$$\lambda E = \frac{\Delta R_n + \rho_a \times c_p \times VPD \times r_a^{-1}}{\Delta + \gamma \times (1 + r_s / r_a)}$$

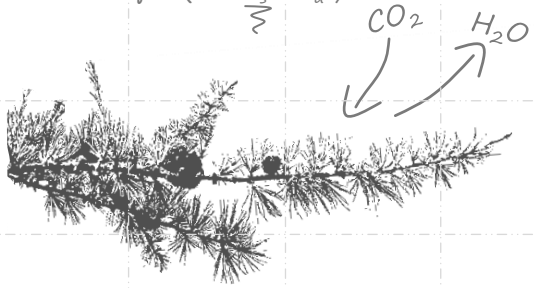

Chapter 6

Contrasting plasticity of stomatal conductance to temperature and drought in high-elevation *Larix decidua* and *Picea abies*

Richard L. Peters, Matthias Speich, Christoforos Pappas, Ansgar Kahmen, Georg von Arx, Elisabeth Graf Pannatier, Kathy Steppe, Kestin Treydte, Ana Stritih, Patrick Fonti

In preparation for Plant, Cell & Environment

Abstract

Conifers growing at high elevations optimize stomatal conductance (g_s) for minimizing winter water loss and maximizing photosynthetic yield under temperature-limited conditions. Yet, the ability of high-elevation conifers to adjust their g_s response to environmental drivers remains largely unexplored. We quantified in *Larix decidua* Mill. and *Picea abies* (L.) Karst. intra- and inter-specific variability in g_s along an elevational gradient and contrasting dry and wet sites based on four years of sap flow measurements. Site- and species-specific g_s response to main environmental drivers were examined, including; vapour pressure deficit, air temperature, solar irradiance and soil water potential. Our results indicate that the g_s of *L. decidua* is higher, shows a more plastic response to temperature, and downregulates stronger during drought compared to *P. abies*. These differences allow *L. decidua* to better exploit water under favourable conditions, adjust to site-specific thermal conditions, and reduce water loss during drought episodes. The stronger plasticity of g_s response to temperature and higher conductance of *L. decidua* compared to *P. abies* provides new insights into contrasting species-specific water-use strategies, which impact future species' performance and should be considered when predicting terrestrial water dynamics under climatic change.

6.1 Introduction

The biogeographic distribution of coniferous trees extends across a wide range of contrasting environmental conditions, from the Arctic Circle to the equator and Southern Hemisphere (Farjon & Filer 2013). Conifers often dominate at high elevations where temperatures severely limit tree growth and survival (Bannister & Neuner 2001; Körner 2012). For example, it is very common to find conifers at the upper tree line with growing season temperatures as low as 5.5-7.5 °C (Körner & Paulsen 2004). Under such temperature-limiting conditions, growth is known to be highly sensitive to ongoing climate change (see Beniston 2003; Soja *et al.* 2007; Thuiller *et al.* 2008; IPCC 2013). Recent studies indicate that warmer and drier conditions in temperature-limited ecosystems (at high elevations and latitudes) are altering the forest composition and the timing and duration of both primary and secondary growth (e.g., Esper & Schweingruber 2004; Steltzer & Post 2009; Allen *et al.* 2010; Meier *et al.* 2012; Rigling *et al.* 2013; Peters *et al.* 2017). Subsequently, these changes have consequences for the ability of forests

to regulate terrestrial biogeochemical processes and the global climate system (Myneni *et al.* 2001; Bonan *et al.* 2008).

When growing under a wide range of climatic conditions, trees need to optimize carbon assimilation and its use, i.e., the formation and maintenance of (woody and non-woody) tissues (see Maseyk *et al.* 2008; Rossi *et al.* 2008; Körner 2012; Fatichi *et al.* 2014). Both the processes of producing carbohydrates (via photosynthesis; Nobel 2009) and the generation of turgidity within the cambium required for growth (Lockhart 1965), depend on the way a tree regulates the flow of water through the soil-plant-atmosphere continuum (Mencuccini 2003; Tuzet *et al.* 2003; Damour *et al.* 2010; De Schepper & Steppe 2010). Conifers thus underwent strong selective pressure to develop specialized ways for regulating their internal hydraulics (Brodribb *et al.* 2014; Klein 2014; Anderegg *et al.* 2016). Main mechanisms for controlling tree water use usually include anatomical adjustments of the water conducting xylem (e.g., Mayr *et al.* 2006; Bouche *et al.* 2014) and the optimization of stomatal conductance (g_s) to quickly respond to varying environmental conditions (Hetherington & Woodward 2003; Lin *et al.* 2015). The regulation of g_s is crucial under temperature-limiting conditions, as transpiration has to be optimised for minimal winter water loss (Mayr 2007) and maximum photosynthetic yield during the short vegetative season (i.e., to produce ample sugars for frost damage protection; see Körner *et al.* 2016; Lintunen *et al.* 2016). This optimization is supported by observations of increasing maximum g_s with increasing elevation (Körner 2012) and deciduous conifers like *Larix decidua* Mill. (with a shorter vegetative season) showing an overall higher conductance than evergreen *Picea abies* (L.) Karst. and *Pinus cembra* L. (Anfodillo *et al.* 1998). However, although the species-specific difference in the response of g_s at temperature could be relevant for optimizing tree water use under temperature-limited conditions, most studies have focussed on stomatal responses to atmospheric and soil droughts (e.g., Lindroth 1985; Arneth *et al.* 1996; Day 2000; Leo *et al.* 2014; Wieser *et al.* 2014).

Under rapidly changing climatic conditions, the future occurrence of a species depends on its plasticity (Valladares *et al.* 2014), i.e., the ability to adjust physiological functioning under a wide range of growing conditions. This also holds for conifer water use, since species survival in persistent warmer and drier conditions largely depends upon the plastic adjustment of its hydraulic functioning (e.g., Körner *et al.* 1986; Cordell *et al.* 1998; Martínez-Vilalta *et al.* 2009; López *et al.* 2013). Thus, there has been interest in comparing intra-specific shifts in g_s response to vapour pressure deficit (D) at sites with contrasting

climatic conditions (e.g., Poyatos *et al.* 2007). For example, a study by Grossiord *et al.* (2017) on conifers growing in a semi-arid climate found a reduced stomatal sensibility to *D* when exposed to persistent warming. Although conifers growing at different thermal conditions (along elevational gradients) show a uniform g_s response to *D* (Mayr 2007), their ability to adjust their g_s response to air temperature (T_a) and solar radiance (R_g) might be crucial for optimizing tree water use (Livingston & Black 1987; Buckley & Mott 2013). For example - due to the shorter growing season, low temperatures and reduced partial pressure of CO_2 at higher elevations (Körner 2012) - a strategy to optimize carbon assimilation might allow higher g_s at low temperatures, despite thermal conditions being less favourable for photosynthetic activity (Wieser 2007; Damour *et al.* 2010). In addition, due to low water stress conditions (Körner 2012), high-elevation conifers could reduce g_s sensitivity to R_g, where incomplete stomatal closure during the night allows for a faster supply of water to the leaves at sunrise (e.g., Daley & Phillips 2006). Yet, the ability of high-elevation conifers to adjust their g_s response to these environmental drivers in the context of a warming atmosphere remains largely unexplored.

In this study, we investigated the stomatal regulation of *P. abies* and *L. decidua* and their plasticity along an elevational gradient in the Central Swiss Alps that stretches up to their upper distribution limits (Ellenberg & Leuschner 2010) and shows a genetically well-mixed population (King *et al*. 2013b). In addition to a thermal gradient, with a persistent difference in mean growing season temperature of up to 3.2 °C, trees at contrasting wet and dry conditions were also monitored. At five different sites, we installed thermal dissipation probes to obtain four years of continuous sap flow measurements, including a strong drought event in the summer of 2015. The sap flow measurements were used to calculate g_s and analyse its response to environmental conditions at each site. We hypothesize that drought sensitive *P. abies* (see Anfodillo *et al.* 1998; Ježík *et al.* 2015) will downregulate its stomatal conductance more than *L. decidua* in response to increasing *D* and increasing drought (by measuring soil water potential, ψ_{soil}). Additionally, we quantified the within species plasticity of g_s response functions to multiple environmental drivers (including *D*, ψ_{soil}, T_a and R_g) across the elevational gradient. As pioneer species are expected to show higher plasticity (Sultan 2000; Barigah *et al.* 2006), we presume that the pioneer *L. decidua* (Gower & Richards 1990) will show a more plastic adjustment of its g_s response to environmental drivers compared to the climax species *P. abies.* The analysis of the stomatal behaviour of high-elevation conifer species offers a unique

perspective on the plasticity of their hydraulic functioning and provides insight into their ability to optimize water use under future climatic change.

6.2 Materials and methods

Site description

The studied trees are located on several sites situated within the Lötschental valley in the Swiss Alps (46°23′40″N, 7°45′35″E; Figure 6.1a). The valley is characterised by steep slopes (>60%) and covered with a mixed forest of evergreen *P. abies* and deciduous *L. decidua*. Average forest stand density at the sites is 401±144 trees ha^{-1}, with an average tree age of 173±45 years, diameter at breast height (DBH) of 45±4 cm and canopy height of 22±4 m (Peters *et al.* 2017). Soils are formed from calcareous-free substrate, including moraines and crystalline bedrock (gneiss and granite) from the Aar massif. This contributes to acidic soil characterized by coarse stones and low amounts of clay. Several different soil types were classified on the valley slope, including Leptosol, Cambisol to Podzol. Soil texture consists of 10±4% clay, 56±10% sand and 35±8% silt content and with fine soil bulk density of 0.77±0.42 g cm^{-3}. At the valley bottom with wetter soil conditions, organic soils (Histosol) with low bulk density (0.19±0.07 g cm^{-3}) occur. Long-term mean annual total precipitation and mean annual temperature in the valley exceeds 800 mm and approximates 5.7 °C, respectively (data from MeteoSwiss surface observation network; King *et al.* 2013b).

Sap flow and environmental conditions were continuously monitored from April 2012 to October 2015 at five sites distributed across a thermal and moisture gradient. Four of these sites are situated along an elevational gradient on a south-facing slope with a 300 m interval from the valley bottom (1300 m a.s.l.) to the treeline (≈2200 m a.s.l.). The site at the treeline, close to the distribution limit of *L. decidua* (hereafter referred as S22, where S indicates the south-facing slopes), showed a mean growing season (May-October) temperature of 8.3 °C (covering 2012-2015). At 1900 m a.s.l. (S19), corresponding to the distribution limit of *P. abies*, showed slightly warmer conditions with a mean annual growing season temperature of 9.2 °C. The two sites at 1600 (S16) and 1300 m a.s.l. (N13, where N indicates the north-facing slopes) experienced sequentially drier and warmer conditions, with a mean annual growing season temperature of 10.4 and 11.5 °C, respectively. A fifth contrasting wet site was established at the valley bottom close to the Lonza river, providing constant water saturation at 70 cm soil depth

(N13W), with slightly cooler mean growing season conditions of 10.4 °C. A detailed site description is provided in King *et al.* (2013a).

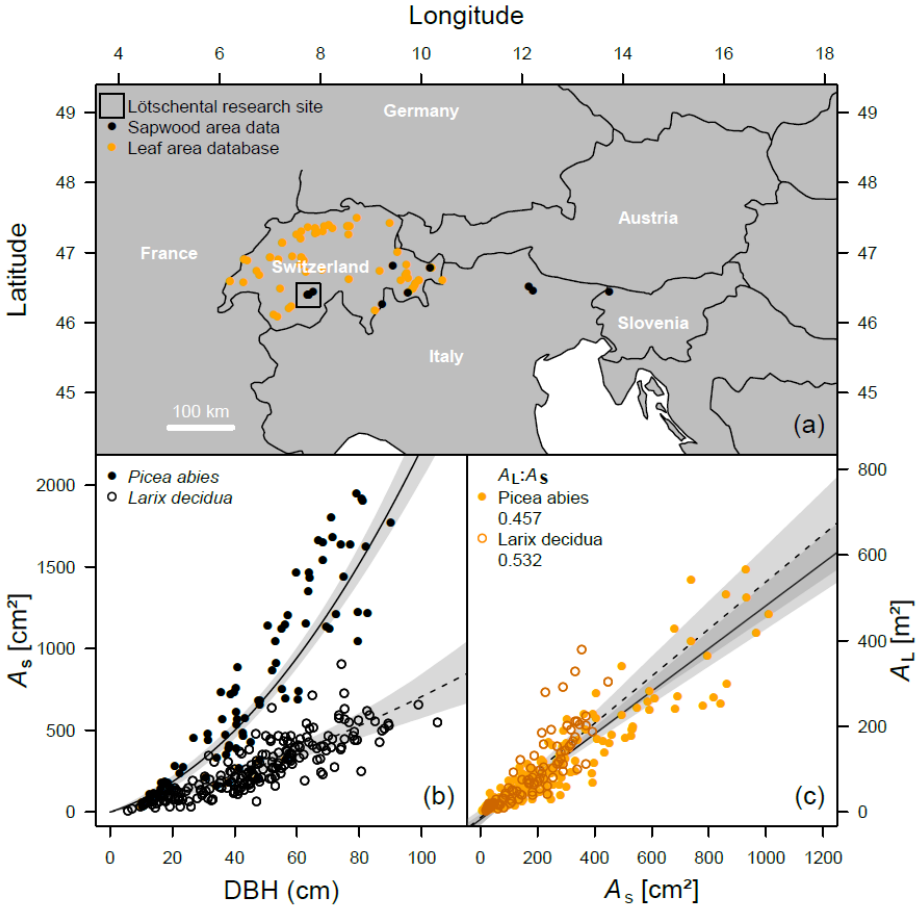

Figure 6.1 Research site, sampling locations (from sapwood area sites and leaf area database) and allometric relationships. (a) Location of the Lötschental research site, trees sampled in the leaf area database and trees of which the sapwood area was measured. (b) Allometric relationship between diameter at breast height (DBH) and sapwood area (A_S). (c) Relationship between projected leaf area (A_L) and modelled A_S (using DBH measurement with the function presented in b) and the respective A_L:A_S values are presented. The dotted and solid lines indicate the model fit for *Larix decidua* and *Picea abies*, respectively. Grey areas present the Bayesian credible interval of the fitted function (see Gelman & Hill 2007). For the statistics, see Table S6.2.

Micrometeorological measurements

Radiation-shield covered sensors were installed at each site on a central tower (≈2.5 m above the ground) within the canopy to measure air temperature (T_a [°C]) and relative humidity (*RH* [%]; Onset, USA, U23-002 Pro) with a 15-minute resolution. Vapour pressure deficit (*D* [kPa]) was calculated from T_a and *RH* (WMO 2008). Soil temperature (T_S [°C]) was recorded at each site with an hourly resolution at a depth of 10 cm (Onset, USA, TdbiT). At N13 solar irradiance (R_g [W m^{-2}]) was measured with 15-minute resolution using a micro-station (Onset,

USA, H21-002 Micro Station) and pyranometer (Onset, USA, S-LIB-M003) positioned in an open field. For the other sites, R_g measurements were adjusted for aspect and topographic shading after Schulla (2015). Calculations for topographic shading were based on the digital height model DHM25 (Swiss Federal Office of Topography Swisstopo).

Soil volumetric water content was measured hourly with five sensors at 10 and 70 cm depth at each site (θ [%]; Decagon, USA, EC-5). At the same depth, soil water potential was also measured (ψ_{soil} [MPa]; Decagon, USA, MPS-2) for the last year of monitoring. These measurements were used for establishing soil water retention curves using the van Genuchten model (van Genuchten 1980), where the saturated water content was established according to Teepe *et al.* (2003; see Table S6.1). This allowed retrospective determination of ψ_{soil} for the entire monitoring period. The water content at permanent wilting point and field capacity was visually determined to normalize θ to relative extractable water (in %; see Granier *et al*. 1999). The wettest conditions from both depths for θ and ψ_{soil} were used to represent the site conditions.

Daily precipitation was obtained from the nine nearest weather stations (6 to 43 km distance to the transect, including Adelboden, Blatten, Grächen, Montana, Jungfraujoch, Sion, Ulrichen, Visp, Zermatt; Federal Office of Meteorology and Climatology MeteoSwiss). The environmental measurements at each site were quality controlled and the few sporadic data-gaps were filled by linear interpolation or by using a regression approach with a stiff cubic spline on data from other sites and hourly averaged (using the mgcv package in R software version 3.2.00, R development core team 2013).

Sap flow measurements and transpiration calculations

At every site three mature trees per species (a total of 15 *L. decidua* and 12 *P. abies* trees; Table 6.1) were instrumented with commercially available thermal dissipation probes (Granier 1985; Tesaf, University of Padova, Italy), to estimate sap flux density (F_d [g H_2O cm^{-2} sapwood area h^{-1}]). Two 2 cm long probes were radially inserted into the xylem (below the cambium), with a vertical distance of 10 cm on the slope-facing side of the stem at ≈1.6 m height. The temperature difference between the continuously heated upper and unheated lower probe was measured (ΔT [°C]) and recorded with 15-minute resolution on a data logger (Campbell Scientific, USA, CR1000). The difference (denoted as unitless K [-]) between measured ΔT and zero sap flow conditions (ΔT_{max}; see Lu *et al.* 2004) was calculated. The method proposed by Oishi *et al.* (2016) was used to determine ΔT_{max}, where daily pre-dawn ΔT_{max} values were used when environmental

conditions favour zero-flow conditions (i.e., low nocturnal D). The measured ΔT was corrected for the proportion of the probe that was inserted into the sapwood versus the part in the heartwood according to Clearwater *et al.* (1999), using the sapwood thickness [cm]. Sapwood thickness was measured from two increment wood cores (using an increment borer; Haglöf, Sweden) taken perpendicular to the slope at breast height (≈1.3 m) from the monitored trees (based on discolouration for *L. decidua* and translucence for *P. abies*). Since K is known to progressively decrease over the years of monitoring (see Oliveras & Llorens 2001), we had to correct for this effect of signal dampening. Next, F_d was calculated from K (Granier 1985) using a species-specific calibration curve established with cut-stem calibration for the two species according to Steppe *et al.* (2010; $F_d = 26.236\ K + 56.495\ K^2$). See Note S6.1 and Peters *et al.* (In press.) for a detailed description on the ΔT_{max} determination and the cut-stem calibration experiment.

Table 6.1 Characteristics of trees instrumented with thermal dissipation probes. Age and sapwood area (A_S) were determined using increment core measurements.

Species	Site	Elevation [m a.s.l.]	Tree ID	Age [yr]	DBH [cm]	Height [m]	A_S [cm^2]
Larix decidua	N13	1300	N13Bd_L1	131	29.5	20.1	105
			N13Bd_L2	128	32.0	18.5	142
			N13Ad_L4	131	30.8	18.7	125
	N13W	1300	N13WAd_L1	148	78.0	27.7	464
			N13WBd_L2	164	89.3	33.3	541
			N13WBd_L3	134	52.0	25.7	304
	S16	1600	S16Bd_L1	371	75.2	31.5	629
			S16Ad_L1	69	38.5	24.5	251
			S16Ad_L4	69	41.5	23.8	369
	S19	1900	S19Ad_L1	200	48.0	23.7	300
			S19Ad_L3	170	35.5	26.3	224
			S19Bd_L1	326	48.7	22.4	208
	S22	2200	S22Ad_L1	269	47.0	17.8	292
			S22Ad_L2	280	55.7	17.2	434
			S22Ad_L3	295	45.5	16.6	218
Picea abies	N13	1300	N13Ad_S1	90	30.7	14.5	210
			N13Ad_S2	93	48.1	19.8	680
			N13Bd_S3	87	37.0	19.2	473
	N13W	1300	N13WAd_S1	85	81.0	29.5	1905
			N13WAd_S2	81	62.8	33.5	1155
			N13WBd_S3	109	80.7	33.6	1918
	S16	1600	S16Bd_S4	-	45.3	21.5	257
			S16Ad_S2	62	38.2	25.3	411
			S16Bd_S2	461	56.2	23.5	315
	S19	1900	S19Bd_S3	245	37.2	21.2	353
			S19Ad_S2	137	34.1	25.0	161
			S19Bd_S2	229	47.5	24.5	680

F_d was multiplied by the sapwood area (A_S [cm^2]) to obtain whole-tree water use [g H_2O h^{-1}]. Whole-tree water use was then used to estimate transpiration per unit of leaf area (i.e., E [g H_2O m^{-2} leaf area h^{-1}]) by using allometric relationships between A_S [cm^2] and total projected needle area (A_L [m^2]; Figure 6.1b, c). To generate a robust relationship between DBH and A_S, sapwood area and the associated DBH from over 450 trees was measured across the alpine range (Figure 6.1b). Species-specific allometric relationships of DBH-A_s where then used together with a leaf area database (constructed with the measurements from Burger 1953), recording A_L and DBH, to establish A_L:A_S values (Figure 6.1c; Tyree & Zimmermann 2002). To account for the delay between E and F_d, the mean difference between the time of sunrise and the onset of F_d (15-minute resolution) was calculated to shift back F_d to represent E. The timing of sunrise was defined every day as the time when R_g exceeds 10 W m^{-2}. The onset of F_d was determined when a persistent increase in F_d occurred after 3:00 am. Finally, we made use of weekly observations of phenological stages performed from 2008 till 2011, to remove periods where *L. decidua* did not have full foliage (Moser *et al*. 2010; see Figure S6.1).

Conductance calculations and response to environmental drivers

Both crown conductance (g_{sap} [g H_2O m^{-2} sapwood area s^{-1} kPa^{-1}]) and stomatal conductance (g_s [mm s^{-1}]) were calculated for all individuals. We complemented the g_s calculation with g_{sap}, as the latter is less dependent upon model assumptions. Crown conductance was determined by using D and F_d (adopted from Meinzer *et al.* 2013 and Pappas *et al.* 2018):

$$g_{sap} = \frac{(F_d * 10000/3600)}{D} \quad \text{(Eq. 1)}$$

Daily mean g_{sap} was considered as F_d usually lags behind the driving meteorological conditions on an intra-daily level, due to water storage in the stem (see Braun *et al.* 2010). Species-specific g_{sap} responses to atmospheric drought (using D) and soil drought (using ψ_{soil}) were analysed for periods where other factors are less limiting. For the response of g_{sap} to D, days were selected where T_a >12 °C, θ >60% and precipitation <10 mm, while for ψ_{soil} we selected days with D <1 kPa instead of θ. To explain responses in g_{sap} we fitted linear functions as $g_{sap.ref} - \delta * \ln D$ ($g_{sap.ref}$ is the reference conductance when D= 1 kPa; Oren *et al.* 1999b) and $g_{sap.ref} + \Lambda * \psi_{soil}$, respectively. Linear-mixed effect modelling was applied, where the individual is considered as the random effect and corrections are included to address first-order auto-correlation.

An inversed simplified Penman-Monteith equation was used to calculate g_s (Monteith 1965; Granier & Loustau 1994), assuming that conifer forests are aerodynamically well coupled to the atmosphere (Monteith & Unsworth 2013). Together with the hourly averaged T_a, D and E measurements, g_s was calculated according to the following equation (see Note S6.2):

$$g_s = \frac{\lambda E \gamma}{\rho C_p D} \quad \text{(Eq. 2)}$$

where λ is the latent heat of vaporization ([J g^{-1}]; as a function of air temperature), γ is referred to as the psychrometric constant [hPa K^{-1}] (as a function of air pressure, which is calculated from elevation and air temperature), ρ is the air density [kg m^{-3}] (as a function of air temperature and atmospheric pressure) and C_p is the heat capacity of air [J kg^{-1} K^{-1}] (taken as 1.01).

A Jarvis-type approach (Jarvis 1976) was used to analyse conductance (g_{sap} and g_s) response to D, T_a, θ, ψ_{soil}, and R_g. To account for individual variation in conductance, g_{sap} and g_s were standardized to the individual specific maximum conductance ($g_{sap.max}$ or $g_{s.max}$), defined as the 99th quantile of the data to avoid the effect of outliers. The resulting individual time-series were averaged per site and species. We excluded conductance values on rainy days (precipitation >1 mm d^{-1}) and with D <0.1 kPa as these conditions generate unreliable conductance values (e.g., Philips & Oren, 1998). For $g_s/g_{s.max}$ values a bootstrap resampled boundary-line analysis was performed to disentangle when the independent variable is limiting (Chambers *et al.* 1985; Shatar & McBratney 2004). Within this analysis a predefined upper quantile was selected when binning the independent variable (e.g., dividing the x-axis into classes of a specified size as described in Chambers *et al.* 1985; see Table 6.2). A bin width of 2% of the total range was used and overlapped by 1% with the previous bin to reduce the effect of uneven distribution of data. For the boundary-line analysis we excluded conditions where the selected independent variable could show collinearity with other meteorological variables (Table 6.2). Models were fitted through the upper quantiles to describe the relationship, referred to as response functions (see Table 6.3).

To show the effects of the variations in response function parameters, the species- and site-specific g_s curves were used to model transpiration patterns. We multiplied the site- and species-specific average $g_{s.max}$ with the response functions of D, T_a, ψ_{soil}, and R_g to obtain g_s, which was used together with T_a, D in equation 2. To highlight the effect of the different response function parameters on daily E dynamics, curves for T_a, D and R_g between high and low elevation sites were switched. For *L. decidua* effects of spring and autumn phenological development

on g_s were simulated with the models of Murray *et al.* (1989) and Delpierre *et al.* (2009), respectively. All analyses were performed with the R software (version 3.2.00, R development core team 2013).

Table 6.2 Model criteria for the boundary line analysis. Variable conditions are provided for every climatic factor to reduce collinearity. The boundary line is described with non-linear functions by dividing the dataset into bins (segments with a 2% size of the total independent variable range) and a specified quantile was selected per bin (see bin properties). Points where excluded where the bin included less than a specific minimum sample size (see Min. n). The quantiles and minimum sample size was increased for θ and ψ_{soil}, due to the larger and unequal spread of the data.

Independent variable	Variable conditions						Bin properties	
	D [kPa]	T_a [°C]	R_g [W m^{-2}]	Θ [-]	T_s [°C]	ψ_{soil} [MPa]	Quantile	Min. n
Vapour pressure deficit (D)	-	>10	>300	>0.5	-	-	0.95	5
Air temperature (T_a)	<1.5	<13	>300	>0.5	-	-	0.95	5
Solar irradiance (R_g)	<0.5	>10	<800	>0.5	-	-	0.95	5
Relative extractable water (θ)	<1.5	>10	>300	>0.8	-	-	0.98	15
Soil temperature (T_s)	<1.5	-	>300	>0.5	<11	-	0.95	5
Soil water potential (ψ_{soil})	<1.5	>10	>300	-	-	<-0.01	0.98	15

Table 6.3 Selected models used within the boundary-line analysis. Models were selected from literature or constructed to provide parameters which can be interpreted (as described for a and b). A general description of the model is provided in addition to the effect of the individual parameters. When relevant a source is provided.

Formula	Description	a	b
$g_{s\text{-}D} = a - bD^{-0.5}$	An exponential functions according to Roman *et al.* (2015).	Asymptote of g_s at high D values	Slope
$g_{s\text{-}Ta} = 1/(1+e^{-a(Ta-b)})$	Instead of applying parabolic shaped functions as proposed by Jarvis (1976), due to the collinearity with D, a Gompertz function that saturates to 1 g_s was used.	Slope of the inflection point (IP)	T_a of the inflection point (IP)
$g_{s\text{-}Rg} = 1-e^{-a(Rg-b)}$	An adaptation of the model proposed by Price & Black (1989) which allows for night-time activity.	Slope at the x-intercept (g_s= 0)	Shift in R_g for the x-intercept (g_s= 0)
$g_{s\text{-}\psi soil} = 1/(1+a\ e^{(-\psi soil\ b)})$	As most response functions are based on θ, a new functions was used to describe ψ_{soil} response which saturated at 1 g_s.	The point of the y-intercept (ψ_{soil}= 0), depending upon the slope	Slope of the inflection point (IP)

6.3 Results

Allometry, sap flow delay and temporal transpiration dynamics

Species-specific allometric relationships between A_S and DBH were established for *L. decidua* and *P. abies* (Figure 6.1b). The quadratic function showed a significantly steeper increase in A_S with increasing DBH for *P. abies* (p <0.001; A_S= 10.76 DBH + 0.18 DBH^2) than *L. decidua* (A_S= 4.78 DBH + 0.02 DBH^2). *P.*

abies showed more variable and thicker sapwood (5.6±2.2 cm) compared to *L. decidua* (2.3±0.8 cm), which translated into higher A_S for *P. abies* (Figure 6.1b). When applying these functions on the leaf area data (covering 59 sites across Switzerland), similar A_L:A_S values of 0.457 and 0.532 were found for *P. abies* and *L. decidua* respectively (p= 0.265 using a linear mixed-effect model; Figure 6.1c; see Table S6.2). The species-specific A_L:A_S values were used to determine E from F_d by using the tree specific A_S (Table 6.1), where *P. abies* has a mean A_S of 710 cm^2, with exceptionally high values for N13W, and *L. decidua* 307 cm^2.

A substantial delay between sunrise and start of F_d was revealed for both *P. abies* and *L. decidua* (see Figure S6.2). No significant difference in delay was found between sites (p >0.1; using a linear mixed-effect model, see Table S6.3), despite within species differences in height and DBH across the sites (Table 6.1). *P. abies* showed a significantly longer delay of 2 h and 45 min, while *L. decidua* showed an average delay of 1 h and 45 min (difference of ≈60 min, p <0.001; Table S6.3). Also, the spread of the delay and thus the uncertainty was higher for *P. abies*.

Over the four years of monitoring, E was consistently higher for *L. decidua* (Figure 6.2a) than *P. abies* (Figure 6.2b). Additionally, the seasonal pattern of E was more pronounced for *L. decidua* (showing a stronger parabolic shape) and showed stronger differences between sites than *P. abies* with the highest E at N13 (Figure 6.2a, b). In July 2015, a strong drought was recorded, resulting in a gradual decrease in E for *L. decidua* at N13 (Figure 6.2c), while *P. abies* showed an even stronger response and halted transpiration at N13 and S16 (Figure 6.2d). This drought caused an inverse pattern between N13 and N13W, where N13 showed lower E within July 2015 compared to N13W for both species.

Species-specific crown conductance response to environmental conditions

The analysis of *L. decidua* and *P. abies* crown conductance revealed that there is a species-specific difference in their maximum crown conductance ($g_{sap.max}$), while no significant effect of mean annual growing season temperature was found (p >0.5; Figure 6.3). *L. decidua* showed a significantly higher mean $g_{sap.max}$ of 132.06 g m^{-2} s^{-1} kPa^{-1} compared to *P. abies* (49.18 g m^{-2} s^{-1} kPa^{-1}; p <0.001; using a linear mixed-effect model). This difference was also found for maximum stomatal conductance ($g_{s.max}$), which was significantly higher for *L. decidua* (7.8 mm s^{-1}) compared to *P. abies* (with a value of 3.5 mm s^{-1}; p= 0.008). The calculated $g_{s.max}$ fell within the expected range for gymnosperms (Kelliher *et al.* 1993; Arneth *et al.* 1996).

Only the N13 site experienced a large enough variability in ψ_{soil} for addressing species-specific crown conductance response to soil drought (Figure 6.4). Daily $g_{sap}/g_{sap.max}$ showed a slightly more negative response to D for *L. decidua* (Figure 6.4a). Only small significant changes in the slope were obtained, when using a linear mixed effect model ($-\delta$ is increased by 0.042, p <0.001). For the response to ψ_{soil} *L. decidua* showed consistently higher $g_{sap}/g_{sap.max}$ values ($g_{sap.ref}$ *L. deicuda* > *P. abies*; Figure 6.4b; p= 0.164). The slopes of the linear relationship between $g_{sap}/g_{sap.max}$ and ψ_{soil} did not significantly differ between the two species (Λ in Figure 6.4b). Although less affected by assumptions on delay time and projected leaf area, daily g_{sap} cannot be used at the intra-daily time scale to uncover potential inter-specific variability of water conductance.

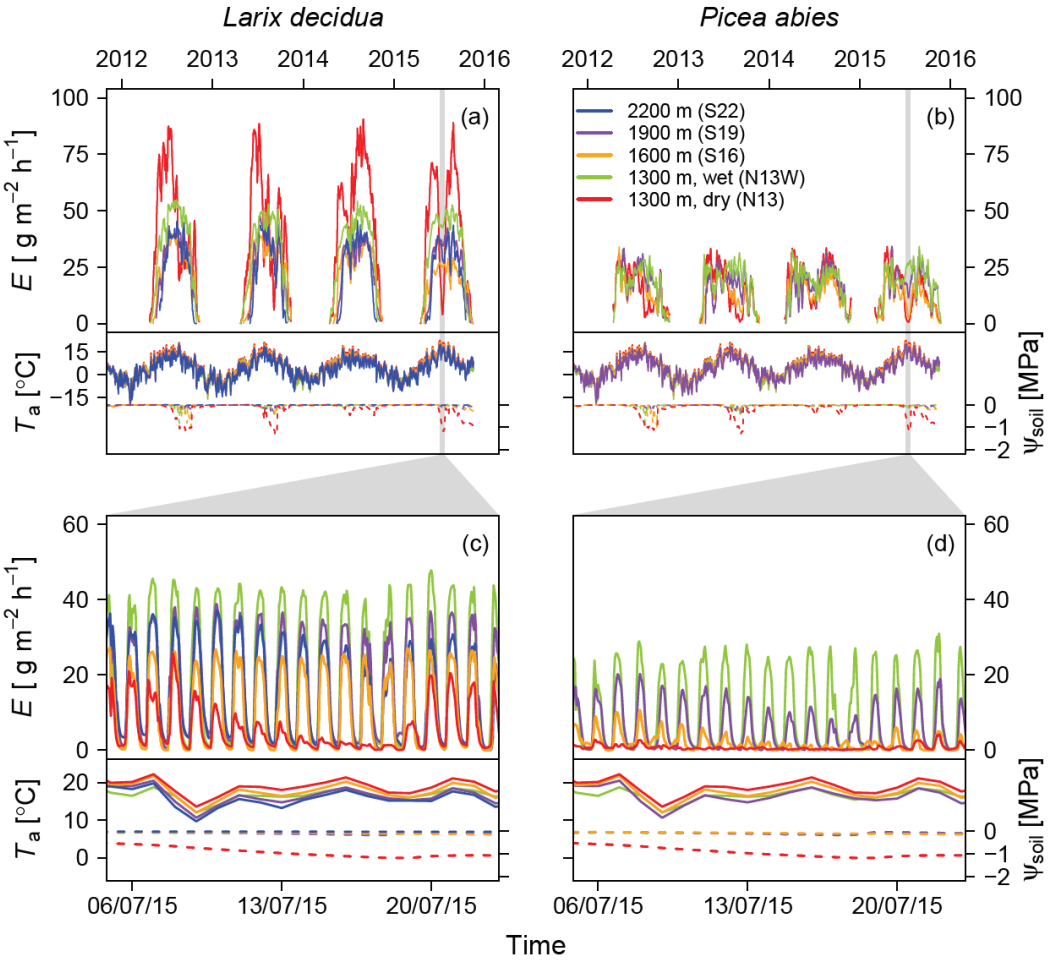

Figure 6.2 Seasonal and diurnal variations of transpiration (E) per site (indicated with elevation in m a.s.l. and specific dry or wet growing conditions) and species. The average E per site and species is presented (in g H_2O m^{-2} leaf area h^{-1}), accounting for the lag-time of F_d measurements. Weekly means of daily maximum E are shown for *Larix decidua* (a) and *Picea abies* (b) for the four years of monitoring. Additionally, for a drought period in 2015 a snap-shot of hourly E is provided for *L. decidua* (c) and *P. abies* (d). Note that *L.* decidua at the lowest dry site (N13) showed highest E under normal conditions (a), but lowest E during a drought period (c). For every panel the daily mean T_a and ψ_{soil} measurements are provided.

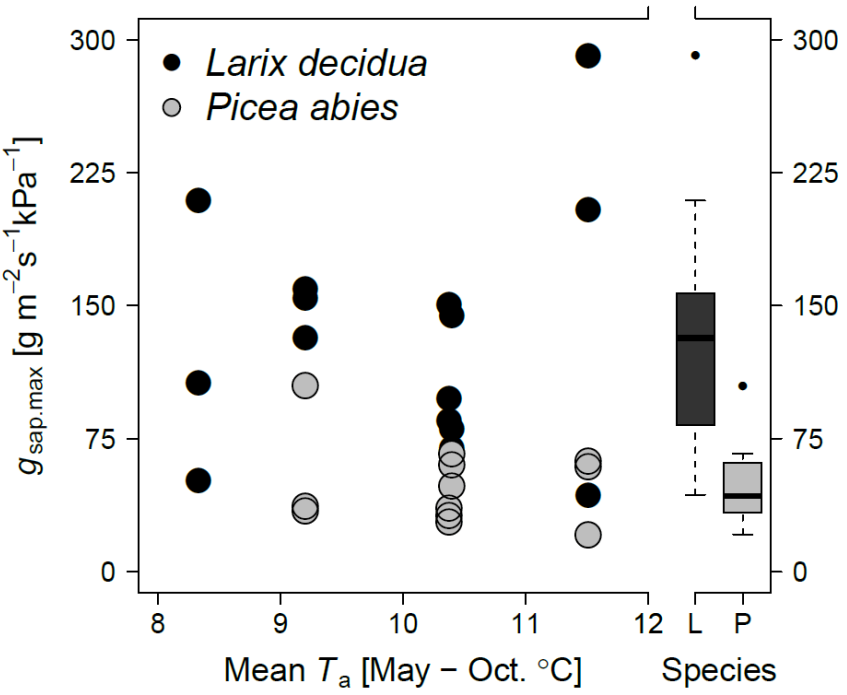

Figure 6.3 Dependency of maximum crown conductance (99th quantile $g_{sap.max}$) on mean annual growing season temperature (T_a from May to October), measured during the four years of monitoring, for all individuals (dots) and generalized for both species (L= *Larix decidua* and P= *Picea abies*). Days with precipitation >1 mm and mean daily D <0.1 kPa were excluded.

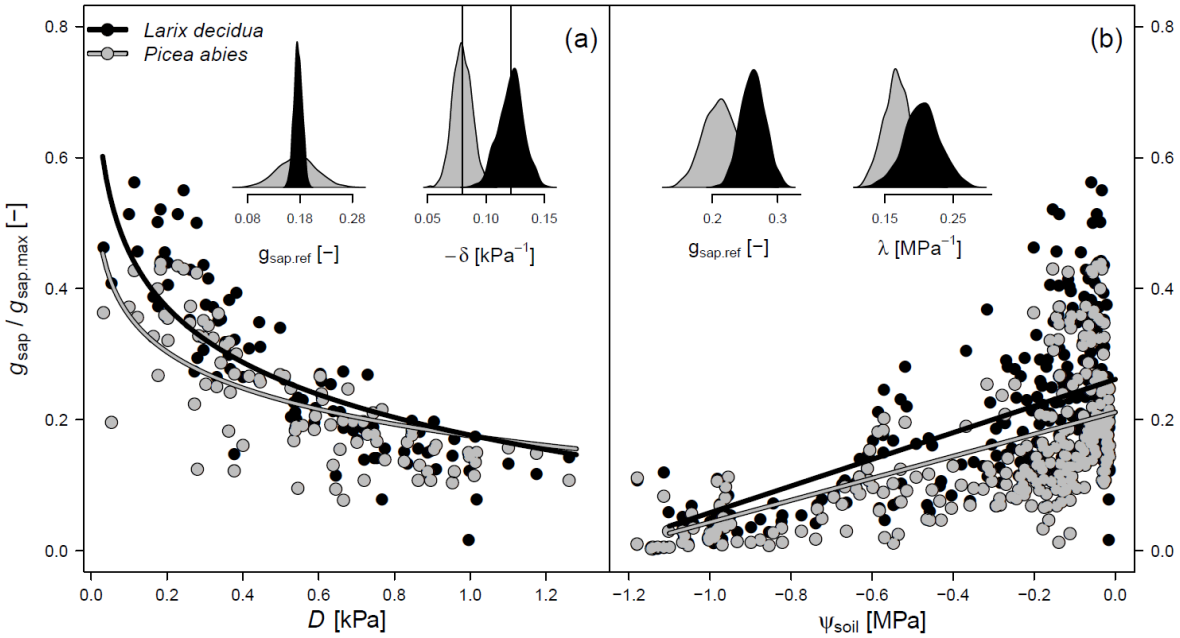

Figure 6.4 Daily mean standardized crown conductance (g_{sap} /$g_{sap.max}$) for *Larix decidua* and *Picea abies* against D and ψ_{soil} at N13, which was the driest site in the study. The species-specific conductance response to D (a) and ψ_{soil} (b) are provided. Additionally, we show the Gaussian distribution of the fitted parameters using μ (mean) and σ (standard deviation), derived from the linear mixed effect model (using the individual as a random factor), and indicate significant difference with lines (p <0.05; using a bootstrap resampling, with n= 1000).

Within-species differences in stomatal conductance response across sites

The response of standardized stomatal conductance ($g_s/g_{s.max}$) to D, T_a, R_g and ψ_{soil} revealed different responses between sites and species (Figure 6.5). The response to D showed a typical negative exponential behaviour in agreement with theoretical expectations to D (Roman *et al.* 2015; Figure 6.5a, b), with a stronger initial decrease for *L. decidua* than *P. abies* with increasing D (see Table 6.3 functions with a= -0.364±0.051 and b= -0.676±0.084 compared to -0.402±0.071 and -0.753±0.080, respectively). Yet, little within-species difference in *L. decidua* and *P. abies* response was found between the sites, except for the more gradual slope of the function for *L. decidua* trees at S22 (see Table 6.4 and Figure 6.5a).

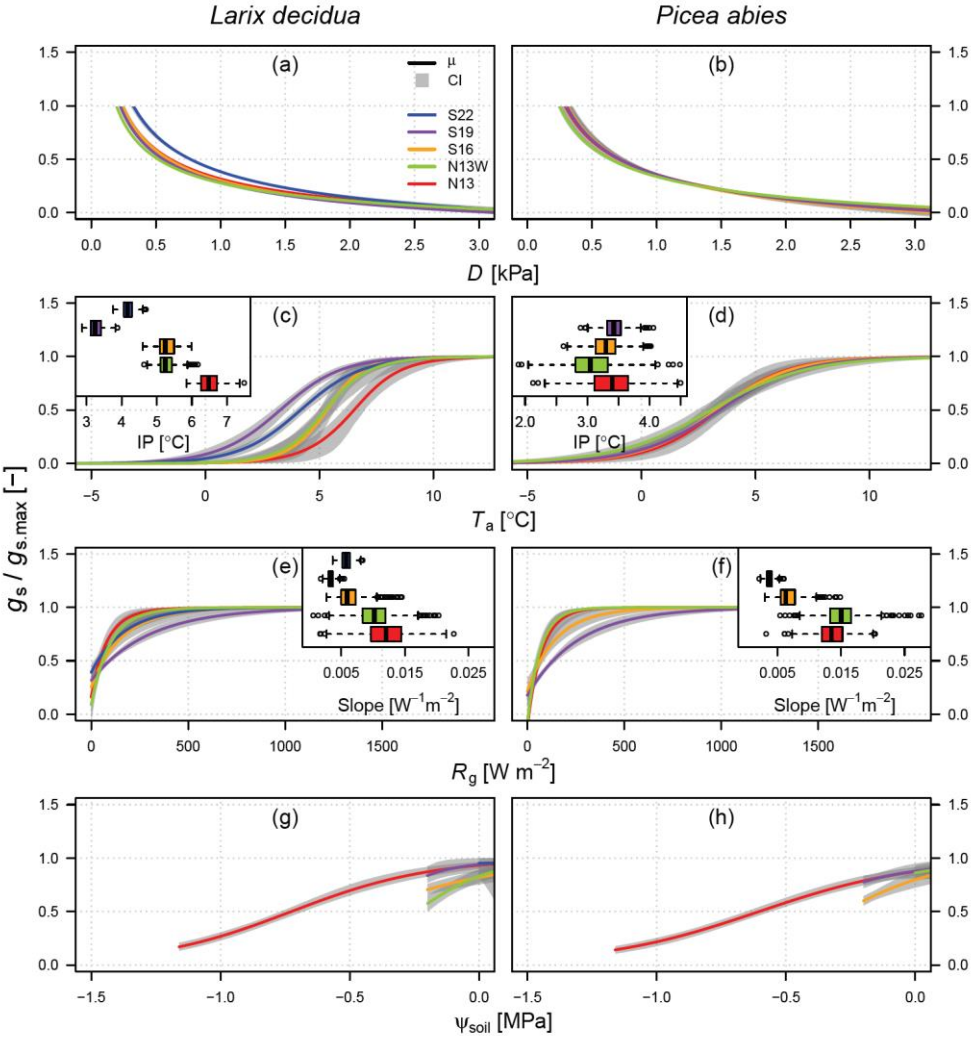

Figure 6.5 Response functions of the bootstrap boundary-line analysis for *Larix decidua* and *Picea abies* with standardized canopy conductance ($g_s/g_{s.max}$) fitted against (a, b) vapour pressure deficit (D), (c, d) air temperature (T_a), (e, f) solar irradiance (R_g) and (g, h) soil water potential (ψ_{soil}). For T_a (c,d) the inflection points (see the parameter b in Table 6.3) and for R_g (e, f) the slopes (see parameter a in Table 6.3) are presented in the inset boxplots, originating from the 1000 times bootstrap resampling. The mean (μ) curve and the 95% confidence interval (CI) are provided.

Table 6.4 Non-linear models used within the boundary-line analysis. For each site and species (LD= *Larix decidua* and PA= *Picea abies*) median and standard deviation of a and b parameters are provided, as obtained from the bootstrap resampling (n=1000).

Formula	Spec.	Var.	Site				
			N13	N13W	S16	S19	S22
$g_{s\text{-}D} = a - bD^{-0.5}$	LD	a	-0.347±0.02	-0.294±0.01	-0.385±0.02	-0.361±0.02	-0.443±0.03
		b	-0.663±0.02	-0.571±0.01	-0.685±0.03	-0.642±0.02	-0.827±0.03
	PA	a	-0.386±0.06	-0.320±0.02	-0.450±0.05	-0.408±0.05	-
		b	-0.743±0.07	-0.657±0.03	-0.805±0.06	-0.764±0.06	-
$g_{s\text{-}Ta} = 1/(1+e^{-a(Ta-b)})$	LD	a	0.916±0.29	1.012±0.38	1.195±0.32	0.733±0.10	0.729±0.09
		b	6.480±0.29	5.246±0.24	5.241±0.24	3.239±0.21	4.173±0.16
	PA	a	0.650±0.29	0.481±0.08	0.602±0.08	0.558±0.06	-
		b	3.399±0.40	3.051±0.38	3.301±0.25	3.426±0.17	-
$g_{s\text{-}Rg} = 1\text{-}e^{-a(Rg-b)}$	LD	a	0.012±0.00	0.010±0.00	0.006±0.00	0.003±0.00	0.006±0.00
		b	-12.18±58.68	-7.48±97.69	-50.64±35.99	-115.71±32.25	-85.76±25.93
	PA	a	0.014±0.00	0.015±0.00	0.006±0.00	0.004±0.00	-
		b	9.134±9.09	5.350±9.20	-38.56±25.65	-51.28±23.13	-
$g_{s\text{-}\psi soil} = 1/(1+a\ e^{(-\psi soil\ b)})$	LD	a	0.072±0.02	-	-	-	-
		b	3.654±0.39	-	-	-	-
	PA	a	0.142±0.03	-	-	-	-
		b	3.239±0.31	-	-	-	-

The stomatal conductance response to T_a showed distinct differences between the species (Figure 6.5c, d). The fitted Gompertz functions (Table 6.3), to describe the response of $g_s/g_{s.max}$ to T_a, revealed little difference in the inflection point (T_a where the slope of the function is steepest; b parameter in Table 6.4) between sites for *P. abies* (average of 3.3 °C; Figure 6.5d). On the other hand, *L. decidua* showed changing inflection point temperatures for higher elevation sites, decreasing from 6.5 to 3.2 °C (Figure 6.5c). The slope of the inflection point did not differ from the 95% confidence interval between the sites (parameter *a* in Table 6.4). Although the shift of the inflection points to lower T_a at sites with lower growing season temperature for *L. decidua* did not surpass the inflection point found for *P. abies*, an absolute offset between the species became apparent when considering the higher $g_{s.max}$ values for *L. decidua* (see Figure S6.3a). Similar differentiation between sites was found when considering T_s, although the 95% confidence interval was substantially larger (especially for *P. abies*; see Figure S6.3b).

The $g_s/g_{s.max}$ response to R_g (Table 6.3) showed for both species that above 1000 W m^{-2} global irradiance was no longer limiting for conductance (Figure 6.5e, f). Higher elevation sites appeared to respond more slowly to increasing R_g when considering the slope of the fitted function (parameter *a* in Table 6.4), where S19 showed the flattest slope with 0.003-0.004 W^{-1} m^{-2} (Figure 5e, f). Additionally, the response functions indicated that higher elevation sites allowed for higher conductance when R_g approached 0 W m^{-2} (parameter *b* in Table 6.4). Only the

N13 site showed sufficient spread in ψ_{soil} for response curve fitting, therefore intra-specific comparison of $g_s/g_{s.max}$ to ψ_{soil} was not possible. However, *P. abies* showed a stronger decrease in conductance with increasing ψ_{soil}, as was found for g_{sap} (Figure 5g, h).

Impact of plastic g_s response functions

Within-species differences in the stomatal conductance response functions to *D*, T_a and R_g was further highlighted by the calculated daily mean *E* for high- (S22 and S19) and low-elevation (N13) *L. decidua* (Figure 6.6a, d) and *P. abies* using the Penman-Monteith equation (Table 6.5). After considering the phenological development (Figure 6.6 c, f), S22 *L. decidua* would transpire up to 5.1±0.7 kg m^{-2} yr^{-1} less (4.6±0.7 for S19) if it had a similar T_a response as N13 *L. decidua*. The difference in *E* due to the altered T_a response is mainly caused by the additional transpiration at the end of the growing season (Figure 6.6b). For N13 an increase of 3.7±1.0 (added to 124.8±12.1 kg m^{-2} yr^{-1}) would be expected if *L. decidua* responded like the trees at S22. Here, the main difference is detected at the beginning of the growing season during colder conditions (Figure 6.6e). *P. abies* does not show a distinct change in *E* due to changing response functions (Table 6.4). Both the alteration in R_g and *D* response shows less consistent consequences for *E*, although N13 *L. decidua* would transpire up to 22.2±1.8 kg m^{-2} yr^{-1} more if it had the more gradual *D* response function of S22 *L. decidua* (Table 6.5).

Table 6.5 Modelled transpiration (*E*) considering alternative response functions for air temperature (T_a), global irradiance (R_g) and vapour pressure deficit (*D*), compared to site-specific response functions. As an example, if *Larix decidua* g_s-response to T_a for S22 (presented in Figure 6.5) would be similar to that of N13, then transpiration would have been reduced by 5.1 kg m^{-2} yr^{-1}. The annual mean and standard deviation of modelled transpiration are provided for the transpiration seasons of 2012-2015 for *L. decidua* and *Picea abies* growing under climatic conditions for S22, S19 and N13. The transpiration season is defined by the sap flow measurements (see Figure 6.2).

Species	Site	*E* [kg m^{-2} yr^{-1}]	Effect of alternative response function [kg m^{-2} yr^{-1}]		
Larix decidua	S22	63.7±4.8	$T_{a\,(N13)}$ -5.1±0.7	$R_{g\,(N13)}$ -7.3±0.9	$D_{(N13)}$ -9.6±1.3
	S19	59.7±5.4	$T_{a\,(N13)}$ -4.6±0.7	$R_{g\,(N13)}$ +0.6±0.5	$D_{(N13)}$ +4.7±1.0
	N13	124.8±12.1	$T_{a\,(S22)}$ +3.7±1.0	$R_{g\,(S22)}$ +10.6±0.9	$D_{(S22)}$ +22.2±1.8
			$T_{a\,(S19)}$ +4.8±1.3	$R_{g\,(S19)}$ -7.1±2.4	$D_{(S19)}$ -11.3±0.8
Picea abies	S19	46.0±4.0	$T_{a\,(N13)}$ +0.4±0.1	$R_{g\,(N13)}$ +0.3±0.4	$D_{(N13)}$ -0.2±0.1
	N13	46.6±6.4	$T_{a\,(S19)}$ -0.3±0.0	$R_{g\,(S19)}$ -2.6±0.6	$D_{(S19)}$ 0.0±0.1

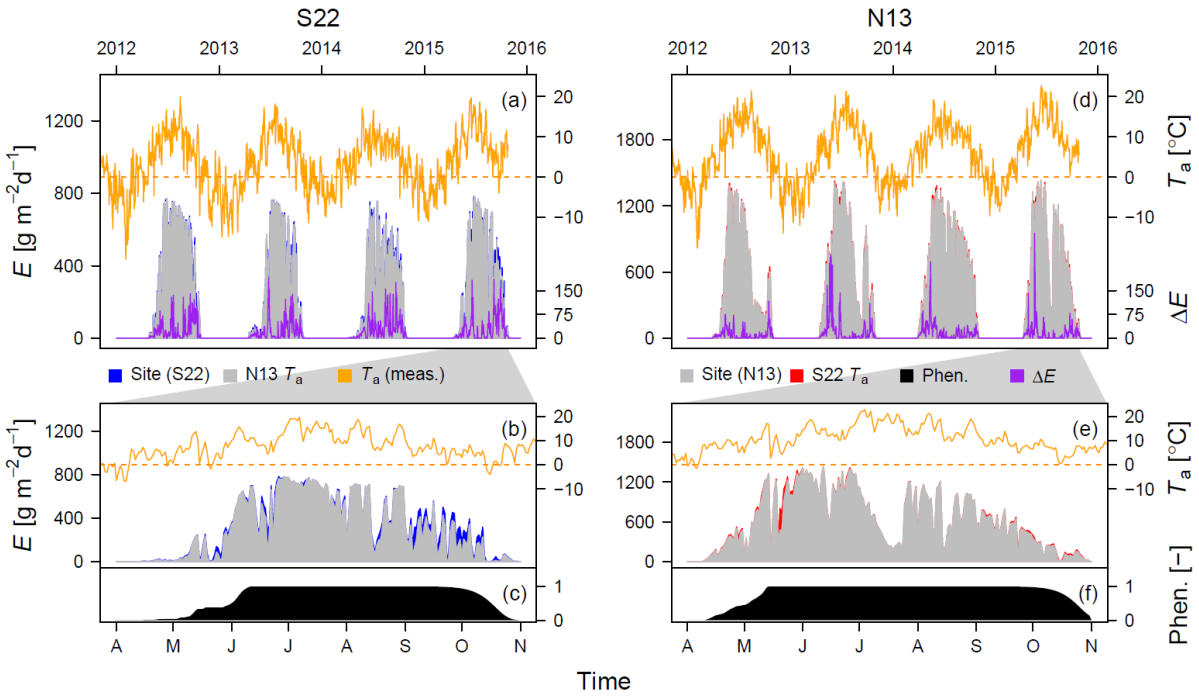

Figure 6.6 Modelled daily transpiration (*E*) patterns for *Larix decidua* under the climatic conditions of S22 (a-c) and N13 (d-f). Note the different scales of *E* for the S22 and N13 conditions. Response functions presented in Figure 6.5 are used to model the site response of *E*, where the T_a response was site-specific or exchanged with the response function of the site at the opposite end of the elevational transect. For example, for *L. decidua* growing at S22 the g_s-response to T_a would be replaced with the T_a response function observed at N13, resulting in a difference in modelled daily *E* (highlighted in blue in a and b). The difference in *E* induced by the replaced T_a response function is presented with ΔE (in g m^{-2} d^{-1}; purple lines in a and d). Additionally, mean daily T_a is provided (orange) with the dashed line indicating 0 °C. To highlight the differences, a snapshot is provided for the growing season of 2015 for S22 (b) and N13 (c). The modelled *E* was corrected for phenological development, where we corrected *E* for absence (0) to full crown development (1) using a phenological development model (c and f).

6.4 Discussion

Conifers growing at temperature-limiting conditions and exposed to shorter growing season optimize water transport to facilitate carbon assimilation and its use (Wieser 2007; Rossi *et al.* 2008; Körner 2012). Here, we showed that two conifer species commonly occurring at high elevations in Europe apply contrasting strategies in regulating their stomatal conductance (g_s), a key mechanism for controlling tree hydrodynamics and water use. The analysis of four years of sap flow measurements revealed that the pioneer species *L. decidua* facilitated higher water conductance while regulating water loss during droughts more tightly than a climax species like *P. abies.* Additionally, the within-species

ability to adjust their g_s response to environmental conditions differed between species, where *L. decidua* appeared more plastic.

Higher maximum crown and stomatal conductance for L. decidua

Our study revealed that the two conifer species differed in their efficiency to transport water, where *L. decidua* showed a >2 times higher maximum water conductance per unit leaf area (maximum stomatal conductance, $g_{s.max}$) and per unit sapwood area (maximum crown conductance, $g_{sap.max}$; Figure 6.3) than *P. abies* (despite *P. abies* showing an often higher water use due to the larger sapwood area; see Table 6.1). The species-specific difference in conductance is highlighted by the higher average transpiration (*E*) for *L. decidua* than *P. abies* over the four years of observations (Figure 6.2), although *P. abies* is able to reach higher transpiration levels at sites with warmer growing season temperatures than found in this study (e.g., Wullschleger *et al.* 1998). This species-specific difference in conductance at high elevations was also found by Anfodillo *et al.* (1998), with higher hydraulic conductance for deciduous *L. decidua* compared to evergreen *P. abies* or *Pinus cembra* L. Interestingly, none of our species showed a significant increase in maximum conductance at higher elevations (Figure 6.3), although this is commonly reported and attributed to wider tree spacing and more intense radiation (see Körner 2012). This absence of $g_{s.max}$ plasticity could be attributed to the uncertainty in A_S or A_L:A_S values. Yet, *P. abies* had consistently higher A_S values and variability compared to *L. decidua* in line with other studies (e.g., Longuetaud *et al.* 2006; Nawrot *et al.* 2008). Additionally, the A_L:A_S values fell in a range expected for these gymnosperms (see Tyree & Zimmermann 2002).

Adjusting xylem anatomical properties is an important mechanism for regulating $g_{s.max}$ and could explain species-specific differences in maximum conductance (Körner 2012; Locosselli & Ceccantini 2012; Klein 2014). The higher $g_{s.max}$ for *L. decidua* could be facilitated by a larger average tracheid lumen area compared to *P. abies*, reducing the resistance for water transport up to the crown (Tyree & Zimmermann 2002). According to Poisson's law (see Tyree & Zimmermann 2002), when assuming a lumen area difference of 700 and 1300 μm^2 for *P. abies* and *L. decidua*, respectively (e.g., Carrer *et al.* 2017), we find agreement, with a 3 times higher hydraulic conductance for *L. decidua* compared to *P. abies*. Although, these findings have to be confirmed with *in situ* anatomical measurements, they indicated that the xylem structure largely affects the maximum hydraulic conductance. Additionally, xylem density increases with elevation, where narrower tracheids and thicker cells walls help to avoid winter embolisms (Mayr 2007). This results in a decrease in lumen area and may prevent

high-elevation conifers from increasing $g_{s.max}$. Otherwise, leaf related explanations include osmotic adjustments within the stomata enabling this species to maintain high conductance during summer (Badalotti *et al.* 2000) or species-specific differences in leaf traits like stomatal size and density (Körner *et al.* 1986; Luomala *et al.* 2005; Locosselli & Ceccantini 2012).

Species-specific variations in water use strategies

The exceptional July 2015 drought, with low soil water potential (ψ_{soil}) and high air temperature (T_a), caused a transpiration stop in low elevation *P. abies* (N13; Figure 6.2d), while *L. decidua* showed a strong reduction (Figure 6.2b). Surprisingly, we found no evidence to support our hypothesis that more drought sensitive *P. abies* would apply a stronger water-saving strategy, by down regulating conductance to increasing vapour pressure deficit (*D*) faster than *L. decidua* (see Figure 6.4). The fact that the *P. abies* response function to *D* is not adjusted to drier growing conditions (e.g., no steeper decrease in g_s with increasing *D* at the drier site compared to the wet site; Figure 6.5b) could be explained by the low occurrence of severe droughts within this ecosystem. This is supported by Grossiord *et al.* (2017) who did found no adjustment of the g_s response to *D* after five years of precipitation reduction in a semi-arid region. On the contrary, *L. decidua* appeared to show a slightly stronger downregulation with increasing *D* compared to *P. abies* (Figure 6.4a), which matches with observations by Oren *et al.* (1999b) and Leo *et al.* (2014) for *Larix sp.* and *Picea abies*. When considering soil drought responses, *P. abies* exhibited consistently lower relative conductance with decreasing ψ_{soil} (or increasing drought; Figure 6.4b), as shown by Leo *et al.* (2014). Yet, the slopes of the response of $g_{sap}/g_{sap.max}$ to ψ_{soil} are similar, hinting to the fact that the shallower rooting strategy of *P. abies* versus *L. decidua* is potentially causing less water uptake and storage refilling (Oberhuber *et al.* 2015), instead of a stomatal specific response.

The stronger downregulation of g_s to *D* for *L. decidua* could be explained by its larger tracheids being disputably more prone to cavitation (Bouche *et al.* 2014). Another explanation could be that the thinner cuticula of the deciduous *L. decidua* dehydrates faster and thus initiates stomatal closure faster with higher *D* (Mayr 2007). Although our results might be interpreted as *L. decidua* being slightly isohydric (i.e., more actively regulating stomatal conductance to maintain constant leaf water potential) than *P. abies* in mountainous ecosystems, we did not perform continuous stem water potential (ψ_{stem}) measurements to confirm that *L. decidua* maintains more constant ψ_{stem} (see Roman *et al.* 2015). Nevertheless, the more active downregulation of g_s with increasing *D* does support that *L.*

decidua might be more effective in maintaining hydraulic functioning under drier growing conditions compared to *P. abies*.

Next to the environmental regulation of g_s, a species-specific difference was found in the delay between sap flow diurnal fluctuations and the driving meteorological conditions (due to water storage in the stem; Braun *et al.* 2010). When comparing start of sap flow and sunrise, we found that *P. abies* sap flow response to sunrise took one hour longer compared to *L. decidua*. Also, the duration of diel hydraulic functions of *L. decidua* is longer when compared to *P. abies*. As no effect of stem length could be found, one could assume that the earlier stomatal conductance response of *L. decidua* enables this species to transpire longer during the course of the day. Alternatively, the asynchronous delay could be explained by the difference in both xylem and phloem capacitance (Zweifel *et al.* 2001; Meinzer *et al.* 2009; Matheny *et al.* 2015).

Interestingly, asynchronous and contrasting tree hydrodynamics between co-occurring boreal conifers was also found in the southern limit of the boreal ecozone in central Canada (*Larix laricina* and *Picea mariana*; Pappas *et al*. 2018) and have been attributed to whole-plant traits coordination along the 'fast-slow' plant economics spectrum (Reich 2014). More specifically, the deciduous *Larix* is characterised by a "fast" traits strategy with higher rates of resource acquisition and use, resulting also in higher water conductance while the evergreen *Picea* is characterised by a "slow" traits strategy, with slower growth rates and thus lower water conductance (Pappas *et al*. 2018).

Inter-specific variability in stomatal conductance plasticity

We did not find evidence to support a plastic adjustment of the g_s response to *D* for *L. decidua* and *P. abies* when growing under persistently different growing season temperatures, as found by Grossiord *et al.* (2017). When comparing sites across the elevational gradient, only *L. decidua* growing at the tree line site (S22) showed a different g_s response, with higher conductance below 1.5 kPa (Figure 6.5a, b). Although the response-function shift at S22 potentially increases transpiration by ≈10 kg m^{-2} yr^{-1} (Table 6.5), this shift does not appear to relate to increasing elevation (as S19 and S16 show a similar response-function as N13; Figure 6.5a, b) and is thus difficult to attribute to the decreasing growing season temperatures. This lack of apparent plasticity in stomatal response to *D* for high elevation conifers is consistent with Poyatos *et al.* (2007) who found little evidence for *Pinus sylvestris* L. adjusting the g_s sensitivity to *D* when comparing sites with mean annual temperature ranging from -3.7 to 9.8 °C.

We observed that high elevation conifers adjust their g_s response to T_a (Figure 6.5c) and R_g (Figure 6.5e, f) depending on elevation. Surprisingly, only *L. decidua* at higher elevations showed a plastic g_s response to T_a (Figure 6.5c, d), with a significant inflection point shift of +0.87 °C per 1 °C increase in growing season temperature (May-October; similar to the T_s response in Figure S6.3). Crop species have shown a similar plasticity in their g_s response to temperature (e.g., Yamori *et al.* 2010), but to our knowledge, studies showing this plastic g_s response for trees are missing. In this study, we showed that the observed plasticity of the g_s-T_a response enables high-elevation *L. decidua* to transpire up to ≈5 kg m^{-2} yr^{-1} more (Table 6.5). In particular, high-elevation *L. decidua* would benefit from this lower operational temperature at the end of the growing season (Figure 6.6b). At lower elevations, the adjusted g_s-T_a response was marginally beneficial in preventing water loss during cold periods in the beginning of the growing season (Figure 6.6e). Potential reasons for high-elevation *L. decidua* to maintain higher transpiration rates at the end of the growing season include the increase of water transport to facilitate higher carbon assimilation, despite less favourable thermal conditions for photosynthetic activity (Wieser 2007), or the increased facilitation of nutrient transport (Mayr 2007). This type of plasticity could be facilitated by changing enzymatic activity and thus maintaining photosynthetic activity and transpiration under less favourable conditions (see Hikosaka *et al.* 2006). It could also involve a change in osmotic potential to keep stomata open (Badalotti *et al.* 2000). Unlike *L. decidua*, *P. abies* did not show plasticity in its g_s response to temperature. We hypothesize that the difference in plasticity between species could either be explained by the deciduous life strategy of *L. decidua*, with a shorter vegetative season compared to evergreen species, or due to the fact that pioneers need to deal with a larger range of environmental conditions, demanding higher maintenance respiration and protection against freezing damage.

Both species showed a weaker downregulation of g_s with decreasing R_g at higher elevations, highlighted by a decrease in the g_s response slope (Figure 6.5e, f). This plasticity of the g_s-R_g response is likely regulated by an osmotic pressure change within the guard cells, facilitated by specific photoreceptors (Buckley & Mott 2013). The slower g_s increase with increasing R_g at higher elevations for both species, as well as incomplete stomatal closure at night, could facilitate a faster response to sunrise, thus extending the daily transpiration activity and counteracting the shorter growing season at these mesic sites (Daley & Phillips 2006). Another possible explanation could be the interplay between R_g and atmospheric CO_2 concentration, where the mechanisms to open the guard cells

with increasing light change depending upon the CO_2 concentration (Buckley & Mott 2013; Tor-ngern *et al.* 2014).

The study by King *et al.* (2013b) revealed a genetically well-mixed population within the Lötschental, supporting our plasticity hypothesis over adaptation. Yet, transplantation experiments could aid in further testing this hypothesis, as changes in g_s response to environmental drivers might take a considerable amount of time to become apparent (Livingston & Black 1987). Notwithstanding, our results show that models estimating evapotranspiration patterns with generalized g_s response functions might underestimate the transpiration amount at high elevations (and potentially high latitudes). A recent modelling study also pinpointed the importance of plant trait plasticity in explaining the recent increase in forest water-use efficiency (Mastrotheodoros *et al.* 2017). Moreover, the vegetation modelling community acknowledges the fundamental role of inter- and intra-specific plant trait variability and plasticity in the resulting terrestrial carbon, water and energy dynamics and should stimulate the move towards a trait-based representation of vegetation functioning (Scheiter *et al.* 2013; Fyllas *et al*. 2014; Sakschewski *et al*. 2015; Pappas *et al.* 2016). Finally, if we want to fully grasp the effect of climatic change on the hydraulic functioning of different tree species, we should move away from focussing on only one hydraulic mechanism (like g_s) and apply a more holistic approach, including photosynthetic activity, the tree's water storage capacity, wood anatomical structure and other traits defining the hydraulic architecture (e.g., Egea *et al.* 2011; Köcher *et al.* 2013). Thus, more detailed studies on the plasticity of plant functional traits along environmental gradients could help to better quantify the magnitude of plasticity and variability in plant functional traits, as well as the timescales for these functional changes to occur. Such information would improve the parameterization of terrestrial ecosystem models and would result in more constrained predictions of the water, carbon and energy dynamics under changing environmental conditions.

Acknowledgments

We thank Gregory King, Roger Köchli, Daniel Nievergelt and Anne Verstege for their aid in the extensive field- and labwork performed throughout the past years at the Lötschental transect. We also would like to thank Flurin Babst, Niklaus Zimmermann, Rafael Wüest Karpati and Damaris Zurell for discussion. This work was funded by two Swiss National Science Foundation projects (SNSF), LOTFOR (no. 150205). C.P. acknowledges support from the Stavros Niarchos Foundation, the ETH Zurich Foundation, and the SNSF (Grants P2EZP2_162293, P300P2 174477).

Supporting information Chapter 6

Table S6.1 Parameters for the pedotransfer functions established for converting θ into ψ_{soil} at two depths per monitoring site (see Teepe *et al.* 2003). The strength of fit is not high due to high stone content and heterogeneity within the soil. Because of this we do not recommend applying these functions at other locations. The saturated water content (θ_s), residual water content (θ_r) and empirical constants α and n are provided, in addition to the goodness-of-fit of the model.

Site	Soil depth [cm]	θ_s [Vol. %]	θ_r [Vol. %]	α [kPa^{-1}]	n [-]	Goodness of fit [R^2]
N13	10	74.4	7	0.535	5.79	0.408
	70	62.6	0	0.598	3.079	0.852
N13W	10	93	0	2.577	1.344	0.223
	70	-	-	-	-	-
S16	10	66.4	0	2.949	1.706	0.540
	70	40.6	0	1.044	1.704	0.564
S19	10	74.8	0	1.046	2.391	0.583
	70	55.2	0	0.773	2.187	0.539
S22	10	78.4	14	0.794	3.478	0.722
	70	65.7	0	0.713	2.809	0.768

Table S6.2 Results for linear mixed-effect models analysing allometric relationships between diameter at breast height (DBH), sapwood area (A_S) and leaf area (A_L) as presented in Figure 6.1. We selected A_S and A_L as the dependent variables, against DBH and A_S as independent variables, respectively. Random effects include the sites, where we accounted for a random intercept and slope.

Formula	Fixed effects	Estimates	SE	*p*	Random effects
$A_S \sim 0 + DBH + DBH^2 * Species + (DBH \mid Site)$ [Figure 6.1b]	*L. decidua* DBH	4.78	0.82	<0.001	Site (intercept and slope)
	P. abies DBH	5.98	1.20	<0.001	
	L. decidua DBH^2	0.02	0.01	0.081	
	P. abies DBH^2	0.16	0.02	<0.001	
$A_L \sim A_S * species + (A_S \mid Site)$ [Figure 6.1c]	Intercept: *L. decidua*	0.09	0.05	0.068	
	P. abies	-0.14	0.05	0.011	
	A_S	1.00	0.09	<0.001	
	P. abies A_S	-0.09	0.08	0.265	

Note S6.1 Sap flow measurement processing.

Two 20 mm long stainless steel probes with 2 mm diameter were radially inserted into the xylem (below the cambium), with a vertical distance of 10 cm on the slope-facing side of the stem at ≈1.6 m height. The temperature difference between the continuously heated upper and unheated lower probe was measured (ΔT [°C]) and recorded with 15-minute resolution on a data logger (Campbell Scientific, USA, CR1000). The difference (denoted as unitless K [-]) between measured ΔT and zero sap flow conditions (denoted as ΔT_{max}; see Lu *et al.* 2004) was calculated. The method proposed by Oishi *et al.* (2016) was used to determine ΔT_{max}, where pre-dawn ΔT_{max} values (R_g <100 W m^{-2}) were retained when T_a was <1 °C or D was <0.1-0.05 kPa for a period of two hours (D threshold depending on elevation). Also, the coefficient of variation of pre-dawn ΔT should be below 0.5%, to ensure selection of nights with stable zero-flow conditions. The maximum pre-dawn ΔT of the selected days was used as ΔT_{max} and linearly interpolated to provide continuous daily ΔT_{max} series.

For trees showing a reduction in K against time since installation [t], a tree-specific function was fitted to generate a correction curve. Both a seasonality (day of year; DOY) term and t were used as independent variables for the correction curve. A non-linear model was fitted to the daily maximum K, excluding rainy days (<1 mm d^{-1}) and low maximum K values (<0.05) to generate the correction curve (K_{cor}):

$$K_{\mathrm{cor}} = \frac{(a + b \cdot t)}{(1 + c \cdot t + d \cdot t^2)} + e \cdot \mathrm{DOY} + f \cdot \mathrm{DOY}^2 \qquad \text{(Eq. 1.1)}$$

The fitted parameters for t (with a, b, c and d; see Table S6.1.1) were used to correct K and scale them to the maximum value of the first year of installation.

Next, F_d was calculated from K (Granier 1985) using a species-specific calibration curve established with cut-stem calibration for the two species according to Steppe *et al.* (2010; F_d= 26.236 K + 56.495 K^2, see Figure S6.1.1 and Table S6.1.2). The heat conducting properties of the wood (relationship between K and F_d) was established for each tree species using a laboratory calibration experiment on fresh cut-stem segments. The segments were collected from four trees per species, which we harvested at the Centre for Studies on Alpine Environment of the University of Padova located in the Dolomite mountain region (Italy, San Vito di Cadore), as harvesting stems in the Lötschental was logistically difficult. See Peters *et al.* (In press.) for a more detailed description.

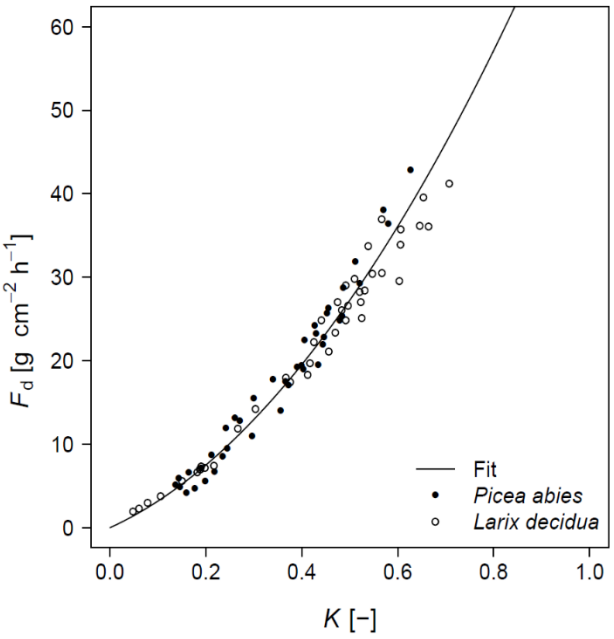

Figure S6.1.1 Results from the laboratory calibration experiment on fresh cut stem segments as described in Steppe *et al.* (2010). Four stems of *Picea abies* and *Larix decidua* were harvested at the Centre for Studies on Alpine Environment of the University of Padova located in the Dolomite mountain region (latitude: 46.45139, longitude: 12.21417) and used within the cut stem segment calibration. The stems had a diameter ranging from 12-20 cm with a length of ≈25 cm. Calibration curves to calculate F_d were established by comparing artificial flows induced gravimetrically through a stem segment against K measured with TDM probes. The calibration curve was established by fitting a second order polynomial function.

Table S6.1.1 Parameter overview for non-linear models when explaining the dampening effect K (pre-dawn ΔT_{max}) with time since installation (t [days]) and seasonality (DOY in day of year) for *Picea abies* (PA) and *Larix decidua* (LD). For every tree values of the variable (*a*-*f*) are provided, in addition to the residual standard error (RSE) and degrees of freedom (df). The final column indicates whether K was corrected, as the tree showed distinct dampening.

Species	Tree	Non-linear model								
		a	***b***	***c***	***d***	***e***	***f***	**RSE**	**df**	**Reduction**
PA	N13WAd_S1	0.14*	0.000*	-0.001*	1.2E-06	2.1E-03	-5.46E-06*	0.038	527	Yes
	N13WAd_S2	-0.33	0.001	1.137	4.2E-04	3.0E-03	-7.55E-06*	0.053	541	No
	N13WBd_S3	0.14*	0.000	0.001	1.8E-06	1.1E-03*	-3.16E-06*	0.028	437	Yes
LD	N13WAd_L1	-1.39*	-0.004	0.002	4.0E-08*	1.8E-02*	-4.13E-05*	0.043	403	Yes
	N13WBd_L2	-0.59*	-0.001	0.001	7.6E-08	1.1E-02*	-2.44E-05*	0.046	375	Yes
	N13WBd_L3	-0.70*	-0.002*	0.002*	6.0E-08	1.2E-02*	-2.72E-05*	0.042	413	Yes
PA	N13Ad_S1	0.28*	0.005*	0.039*	2.4E-06	2.6E-05	-7.39E-07*	0.023	375	Yes
	N13Ad_S2	0.28*	0.002	0.011	-1.7E-06	3.9E-04	-2.07E-06*	0.058	415	Yes
	N13Bd_S3	0.23*	0.003	0.020	1.8E-06	1.5E-03*	-4.76E-06*	0.061	480	Yes
LD	N13Bd_L1	-0.19*	-0.005*	0.007*	1.1E-06*	9.7E-03*	-2.35E-05*	0.094	436	Yes
	N13Bd_L2	-0.31*	-0.002	0.004	-3.6E-07	6.2E-03*	-1.57E-05*	0.051	337	Yes
	N13Ad_L4	-0.58*	-0.005	0.006	8.9E-07	1.2E-02*	-2.67E-05*	0.133	438	No
PA	S16Ad_S2	0.17*	0.000*	0.000	-6.6E-07	1.1E-03*	-3.27E-06*	0.031	277	Yes
	S16Bd_S2	0.21*	0.001	0.007	-7.8E-07	0.6E-03*	-2.29E-06*	0.040	519	No
	S16Bd_S4	0.31*	0.000	0.006*	-3.6E-06	0.6E-03*	-2.30E-06*	0.024	324	Yes
LD	S16Ad_L1	-0.64*	-0.002	0.002	2.2E-07	9.7E-03*	-2.24E-05*	0.036	282	Yes
	S16Bd_L1	-0.11*	-0.003*	0.005*	8.2E-07	5.6E-03*	-1.30E-05*	0.023	407	Yes
	S16Ad_L4	-1.01*	0.000*	0.000	0.0E-07	12.9E-03*	-2.92E-05*	0.034	171	Yes
PA	S19Ad_S2	0.28*	0.008	0.069*	-5.4E-06	6.7E-04	-1.85E-06*	0.041	329	No
	S19Bd_S2	-0.03	0.000	0.002	2.6E-06	5.0E-03*	-1.23E-05*	0.062	478	No
	S19Bd_S3	0.15*	0.000	0.011*	-2.2E-06*	7.8E-04*	-2.12E-06*	0.019	434	Yes
LD	S19Ad_L1	0.02	-0.003*	0.010*	1.9E-06*	2.9E-03*	-6.84E-06*	0.017	249	No
	S19Bd_L1	-1.78*	-0.003	0.001	5.2E-08*	2.1E-02*	-4.64E-05*	0.043	382	Yes
	S19Ad_L3	-0.39*	-0.012*	0.018*	-5.5E-07*	7.5E-03*	-1.71E-05*	0.019	269	No
LD	S22Ad_L1	-1.12*	-0.028	0.025	-1.2E-06	13.1E-03*	-2.98E-05*	0.030	311	Yes
	S22Ad_L2	-0.26*	-0.002*	0.002*	8.3E-07*	6.0E-03*	-1.32E-05*	0.032	321	Yes
	S22Ad_L3	-1.71*	-0.007*	0.003*	2.9E-07*	20.1E-03*	-4.60E-05*	0.037	306	Yes

Table S6.1.2 General statistics of linear mixed-effect modelling for the thermal dissipation calibration curves for *Picea abies* and *Larix decidua* together. The slope (Estimate), standard error of the slope (Std. error), frequentist statistics (t-value, *p*), goodness of fit [R^2] and the Akaike Information Criterion (AIC) is provided.

Formula (in R)	Random effects	Coefficients	Estimate	Std. error	t-value	*p*	R^2	AIC
lmer(SFD ~ 0 + K + I(K^2) + (K | tree))	Tree: Int. var.= 1.3 K var.= 46.4	K	26.236	1.56	16.85	<0.001	0.96	283.9
		I(K^2)	56.495	4.51	12.53	<0.001		

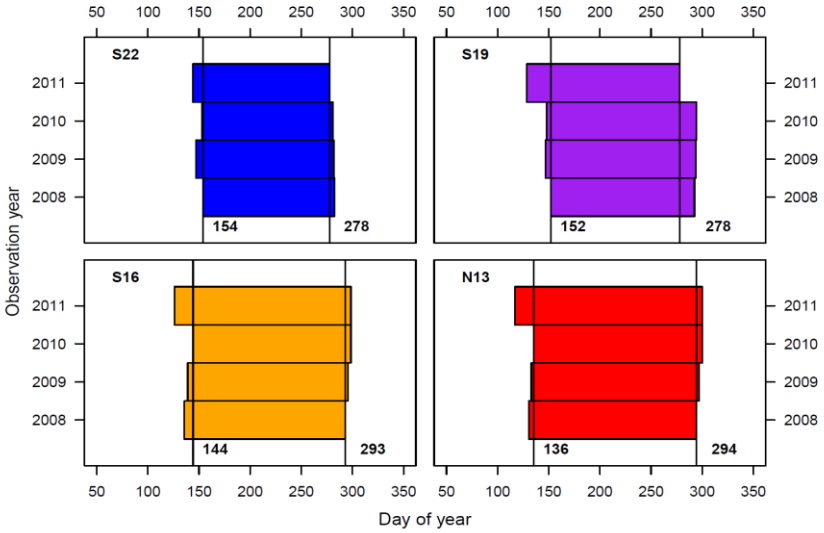

Figure S6.1 Phenological observations when *Larix decidua* showed 50% coverage of its crown with leaves, during leaf development and senescence. The latest observed date of leaf development and earliest data of leaf senescence were used to correct the sap flow data (using a week margin).

Table S6.3 Results for linear mixed-effect models analysing the delay between sunrise and start of sap flow, as presented in Figure S6.2. Relative delay time frequency, as the dependent variable, was tested against species and site as independent variables. After testing overall effects, species were separated and analysed against the site effect. Random effects included the individuals and we corrected for the high first-order auto-correlation. SE, standard error of fixed effect estimates; SD, standard deviation of random factor; Phi, first-order autocorrelation coefficient.

Variable	Fixed effects	Estimates	SE	*p*	Random effects	SD	Phi
Species + Site	Intercept: *L. decidua* N13	120.42	8.77	<0.001	Individual	18.42	0.258
	Species: *P. abies*	65.63	7.90	<0.001			
	Site: N13W	13.85	11.09	0.225			
	Site: S16	5.23	11.18	0.645			
	Site: S19	2.31	11.16	0.838			
	Site: S22	-13.49	14.27	0.355			
Species = *"L. decidua"* + Site	Intercept: N13	126.94	8.31	<0.001	Individual	13.30	0.257
	Site: N13W	7.20	11.83	0.556			
	Site: S16	8.31	12.05	0.506			
	Site: S19	-20.45	12.01	0.119			
	Site: S22	-19.90	11.95	0.127			
Species = *"P. abies"* + Site	Intercept: N13	179.47	11.78	<0.001	Individual	19.68	0.260
	Site: N13W	20.61	16.61	0.250			
	Site: S16	2.36	16.69	0.891			
	Site: S19	24.76	16.67	0.176			

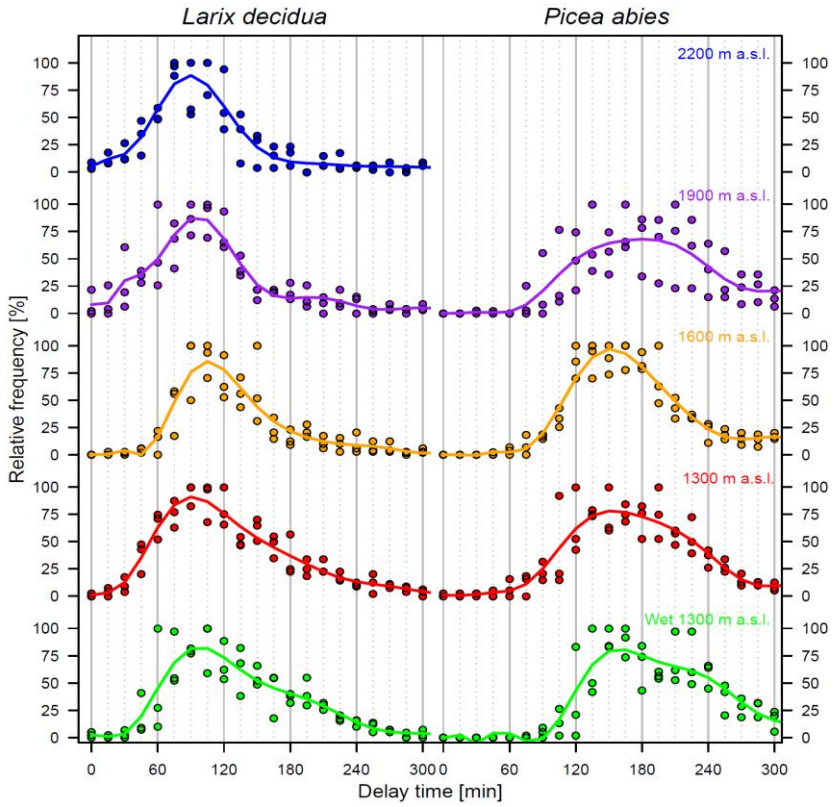

Figure S6.2 Relative frequency of the delay time between sunrise and start of sap flow. Delay time is expressed in 15 minute delay classes and the frequency is defined as the amount of days falling within a class. For every elevation and species three individuals are presented with a cubic smoothing spline.

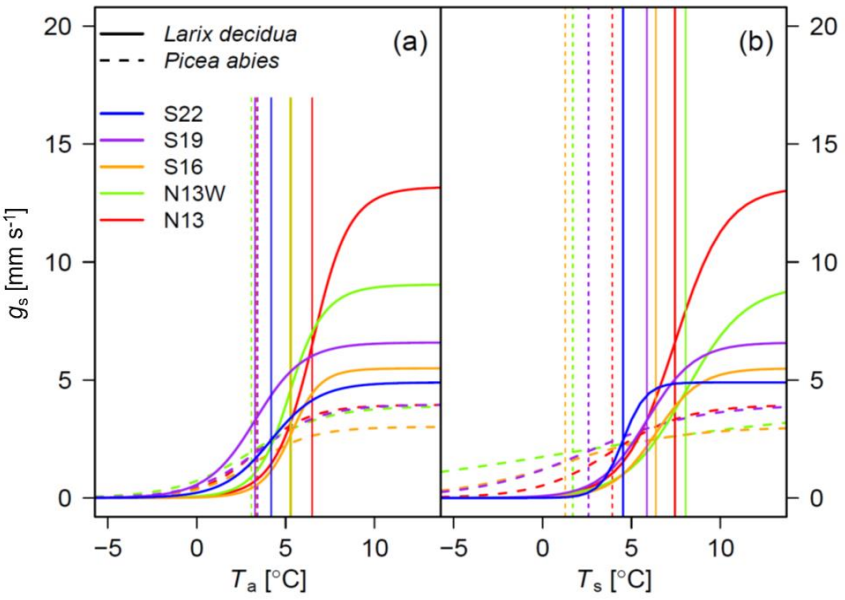

Figure S6.3 Non-linear canopy conductance ($g_s/g_{s.max}$) curves fitted against (a) atmospheric (T_a) and (b) soil temperature (T_s) scaled to the maximum average site conductance ($g_{s.max}$). All species and sites are presented, as the inflection points of the gompertz functions with the vertical lines (see Table 6.3).

Note S6.2 For the stomatal conductance (g_s) we applied the following code within R (software version 3.2.00, R development core team 2013).

```
gs_eImp <- function(e,t,vpd,elv){
#Calculates surface conductance based on imposed evaporation (simplified version of Penman-Monteith for aerodynamically
#well-coupled conditions).
#Input: # vpd: vapor pressure deficit [kPa]
#t: air temperature [°C]
#elv: elevation [m a.s.l.]
#e: transpiration [g m-2 h-1]
# Output:
#gs: canopy conductance [m s-1]
#Set constants
cp <- 1.01                                                    #Heat capacity of air [J g-1 K-1]
#Helper variables
zeroK <- 273.15                                               #0 °C in K
hundredK <- 373.15                                            #100 °C in K
gammaT <- 0.005                                               #Temperature lapse rate [k m-1]
rAir <- 287.04                                                #Gas constant for dry air [J kg-1 K-1]
 rWat <- 461.5                                                #Gas constant for water vapour
 pZero <- 1013.25                                             #Standard air pressure
 g <- 9.81                                                    #Gravitational acceleration [m s-2]
 #Functions of temperature (adapted from PREVAH subroutine EPMONDT / FORHYCS subroutine EVAP)
 tk <- t+zeroK
 tr <- 1.0-(hundredK/tk)
 tp <- tk+gammaT*elv/2.0                                      #Potential temperature
 pt <- pZero * exp(-g*elv/rAir/tp)                            #Atmospheric pressure
 lambda <- 2500.8 - 2.36*t + 0.0016*(t^2) - 0.00006*(t^3) #Latent heat of vaporization of water [J g-1]
 gamma <- (pt*cp/lambda/(rAir/rWat))*100.0                    #Psychrometric "constant" [Pa K-1]
 rhoAir <- (pt/(rAir*tk)) * 100000.0                          #Density of air [g m-3]
 #Unit conversion
 e <- e/3600                                                  # hours to seconds
 vpd <- vpd*1000  #kPa to Pa
 vpd[which(vpd<100)]<-NA                                      #Remove values below 100 Pa
 gs <- (lambda*e*gamma)/(rhoAir*cp*vpd)
 return(gs)}
```

Growth = Ψ^{s}_{p} (turgor) > Γ

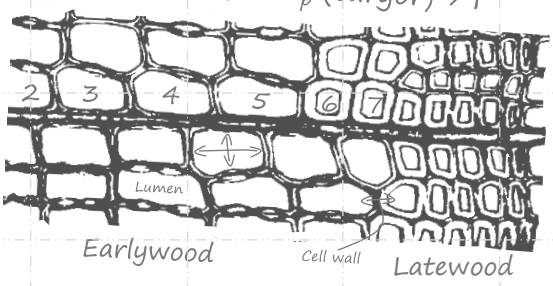

Hydraulics

$$F_{stem} = \frac{(\Psi_{soil} - \Psi^{x}_{stem})}{R^{x}}$$

$\Psi_{soil} = k_{soil} \times$ Tensio

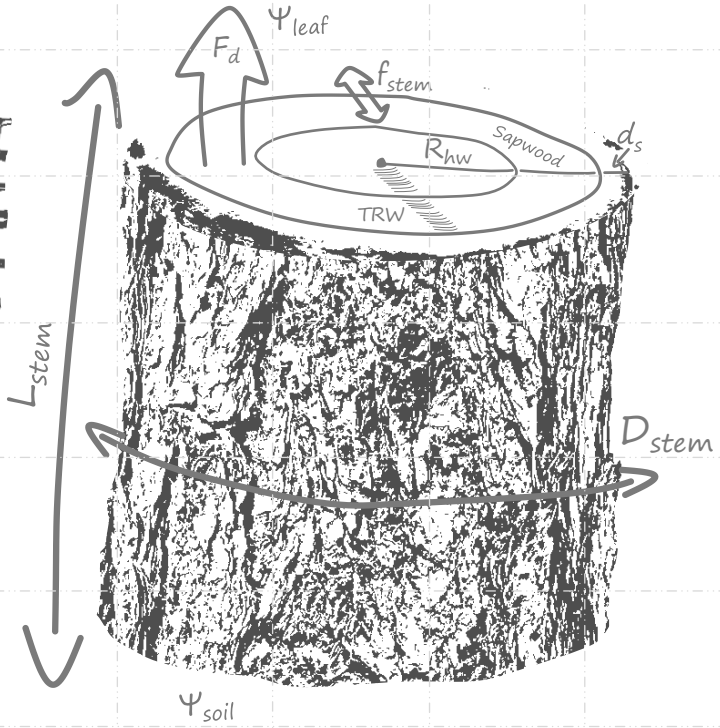

Chapter 7

Turgidity: the engine behind radial wood growth in mature Alpine conifers

Richard L. Peters, Kathy Steppe, Henri E. Cuny, Dirk de Pauw, David C. Frank, Marcus Schaub, Cyrille B.K. Rathgeber, Patrick Fonti

Abstract

Environmental regulation of tree growth is generally modelled with photosynthetic activity, despite the increasing recognition that turgor dynamics in the cambium is a key driver for xylem formation. While mechanistic models can now simulate turgor-driven radial stem growth and potentially improve growth predictions, they lack validation on annual timescales. We modelled turgor-driven growth, by using intra-daily tree hydraulics to simulate diameter variations of the stem, and compared it to weekly xylogenesis observations and ring width. We used four years of sap flow and dendrometer measurements from *Picea abies* (L.) Karst. and *Larix decidua* Mill. along an elevational gradient with contrasting thermal and soil water conditions. The model was used to analyse hydraulic dynamics in the stem and environmental conditions that limit turgor-driven growth. Good agreement was found between simulated and observed radial growth. Growth was unlikely to occur at temperatures below 2 °C or soil water potentials lower than -0.6 MPa, while water transport to the crown was maintained. Furthermore, the model indicated that *P. abies* has difficulty maintaining hydraulic functioning during droughts. Our results suggest that turgor and its environmental drivers are important for regulating radial growth and should be considered when assessing forest productivity under changing environmental conditions.

7.1 Introduction

Woody stems in plants provide a pathway for water and nutrients transport (Sperry *et al*. 2008), mechanical support for the canopy (Fournier *et al*. 2006) and storage room for carbohydrates, water and defence compounds (Kozlowski & Pallardy 1997). In conifers, ≈90% of the stem's xylem is composed of dead tracheids, which are progressively formed via cell division by the cambium (a lateral meristem) and mature through cell enlargement, secondary cell wall formation, lignification and apoptosis (Vaganov *et al*. 2006; Rathgeber *et al*. 2016). The annual increase in stem radius (i.e., radial growth) mainly depends on the number of new cells produced by cambial division and their ability to enlarge under given environmental conditions (Rathgeber *et al*. 2011b; Cuny *et al*. 2015). Considering the impact of climate change on forest productivity and carbon sequestration (Pan *et al*. 2011; Frank *et al*. 2015), the environmental regulation of wood formation is increasingly studied (e.g., Rossi *et al*. 2008; Rossi *et al*. 2013; Cuny *et al*. 2014; Steppe *et al.* 2015).

Wood formation has often been directly associated with the tree's photosynthetic activity and thus linked to trends in CO_2, light, temperature, water and nutrients, i.e., the carbon source (Boisvenue & Running 2006; McMurtrie *et al*. 2008). Based on this principle, dynamic global vegetation models (DGVMs) commonly provide predictions on forest growth and subsequent feedback on future climate (Cox *et al*. 2000; Sitch *et al*. 2008). However, DGVM simulations show a mismatch with tree-ring based estimates of biomass increment, especially when considering the tree's climatic sensitivity, growth and recovery after extreme climatic events (Babst *et al.* 2013; Anderegg *et al.* 2015; Zhang *et al.* 2017). Additionally, when comparing biomass increment with carbon uptake, derived from flux tower measurements, limited agreement between the inter-annual dynamics is found (Rocha *et al.* 2006; Ohtsuka *et al.* 2009; Babst *et al.* 2014c; Delpierre *et al.* 2016). A prominent hypothesis to explain these mismatches is that wood formation might not be solely limited by carbon production (Fatichi *et al.* 2014). For example, experiments comparing apical meristem growth with photosynthetic activity showed that growth under colder and drier conditions decreases earlier than photosynthetic activity (Parent *et al.* 2010; Muller *et al.* 2011). Additionally, observations of cambial activity in mature trees confirmed that cell division only occurs above 5-6 °C (Rossi *et al.* 2016), which is above the photosynthetic minimum of ≈0 °C (Saxe *et al.* 2001; Körner 2008). Thus, our predictions of forest productivity likely depend on a deeper understanding of how environmental drivers regulate wood growth, i.e., the carbon sink (Guillemot *et al.* 2017; Hayat *et al.* 2017; Huntzinger *et al.* 2017).

Although xylogenesis observations provide valuable insights into wood formation dynamics (e.g., Cuny *et al.* 2015), mechanistic models are needed to fully disentangle the mechanisms underlying growth (see Tardieu 2010). Turgor pressure in cambial cell vacuoles has been advanced as an important growth-related mechanism since it can determine the initiation and rate of cell enlargement (Lockhart 1965; Cosgrove 1986; Abe *et al.* 1997). Based on this mechanism, Génard *et al.* (2001) simulated radial growth occurrence when turgor pressure in the cambium exceeds a defined threshold. A recently developed mechanistic whole-tree model, based on internal stem hydraulics, simulated intra-daily growth (of both xylem and phloem) by means of turgor pressure (Steppe *et al.* 2005; De Schepper & Steppe 2010). In addition, the model provided new insights into tree internal hydraulic regulations, e.g., assessing the xylem hydraulic resistance (R_x) and capacitance of tissues facilitating water storage ($C_{storage}$) (e.g., Steppe *et al.* 2008; De Swaef *et al.* 2014; Baert *et al.* 2015; Salomón

et al. 2017). However, so far such models only provide realistic results when applied to short periods of a few months. To validate that turgor pressure is an important mechanism in regulating annual growth, independent wood-formation data on both, inter- and intra-annual time scales are needed to validate extended model simulations (Fonti & Jansen 2012; Steppe *et al.* 2015). Such comparisons should preferably be performed during droughts and at sites where temperature is limiting tree growth (e.g., at the treeline; see Körner 2003; Körner 2012), as then larger discrepancies between photosynthetic activity and growth rate are expected (Fatichi *et al.* 2014).

In this study, we make use of a mechanistic whole-tree model to compare simulated turgor-driven growth of *Larix decidua* Mill. and *Picea abies* (L.) Karst., growing at contrasting site conditions, with benchmarked inter- and intra-annual xylogensis observations. For four years we monitored sub-hourly tree hydraulics (i.e., sap flow and dendrometer measurements) and weekly to annual growth rates of trees along a steep thermal gradient (stretching to the treeline) and contrasting wet and dry growing conditions in a Swiss Alpine valley (see Peters *et al.* In press). We hypothesize that inter- and intra-annual growth patterns can be well explained with turgor dynamics at temperature-limiting growing conditions and during drought events, as low temperatures and low soil water potentials prevent turgor pressure to build-up and initiate growth. Additionally, we assume that growth rates decline more severely than the conductance of water (i.e., needed for facilitating photosynthesis) with decreasing temperature and increasing drought, where little to no growth will occur if temperature decreases below 5° C. Finally, the hydraulic parameters extracted with the model could provide information on the tree's hydraulic integrity. For instance, an increase in R_x during droughts could indicate increased cavitation of xylem conduits (e.g., Salomón *et al.* 2017). We thus expect dry sites to show more dynamic patterns in hydraulic parameters, as embolisms in the water conduction xylem and depletion of storage water occurring during droughts alters the dynamics of both $C_{storage}$ and R_x.

7.2 Materials and methods

Study design and model description

This study makes use of the mechanistic whole-tree model presented in De Schepper & Steppe (2010), simulating turgor-driven radial wood growth. The model requires detailed information on tree-specific allometric characteristics, high-resolution meteorological data and tree physiological measurements and parameters. The model was calibrated for all individuals monitored in the

Lötschental and the simulated radial growth rates were compared to observations of radial growth, water use and environmental conditions (Figure 7.1). Additionally, we compared calibrated hydraulic parameters across sites and species.

Turgor-driven growth was modelled by simulating internal water transport and stem diameter variation (De Schepper & Steppe 2010, excluding carbon transport). In short, the model considers three compartments, including the roots, stem (trunk of the tree until the crown base) and crown (Figure 7.1b). The stem is modelled by three coaxial cylinders including the heartwood (defined by the radius of the heartwood; R_{hw}), water conducting sapwood (which together with R_{hw} defines R_{xyl}) and an elastic stem storage compartment (cambium and phloem tissue; d_s). The model simulates water exchange between stem compartments induced by transpiration, which allows assessment of the differences in water potentials between compartments (or tissues). Water transport from the roots through the sapwood (F_{stem} [g h^{-1}]) is determined by the difference between root water potential (ψ_{root} [MPa]) and stem water potential (ψ_{stem} [MPa]) divided by the hydraulic resistance of the xylem (R_x [MPa h g^{-1}]). The mismatch between F_{stem} and the water transported to the crown (F_{crown} [g h^{-1}]; sap flow measurements) defines the amount of water that is used from the storage compartment ($f_{storage}$), which is calculated with the resistance for radial water transport (R_s [MPa h g^{-1}]) and the capacitance of the tissue to release water ($C_{storage}$ [g MPa^{-1}]). Thus, the model estimates the storage water potential ($\psi_{storage}$ [MPa]) and subsequently the volume of water in the storage compartment ($V_{storage}$ [m^3]). Depending on the initial osmotic potential (Π^i_s [MPa]), these dynamics are used to determine the turgor pressure in the storage tissue (ψ^P_s [MPa]). Growth occurs when ψ^P_s exceeds a threshold value for cell wall yielding (Γ [MPa]; Lockhart 1965), which increases both the dimensions of the phloem and xylem compartment dimensions (which fractional investment is defined by f_{growth}). The amount of irreversible growth is determined by accounting for the extensibility of cell walls (ϕ [MPa^{-1} h^{-1}]), while assuming that enough carbon is available. Daily reversible fluctuations in D_{stem} are determined by pressure changes in sapwood (affected by its elastic modulus; ε_x [MPa]) and storage tissue (determined by the storage tissue elastic modulus; ε_s [MPa]) using Hooke's law (see De Schepper & Steppe 2010). See Table 7.1 for an overview of all the modelling parameters and the supporting information for the model equations (see Note S7.1).

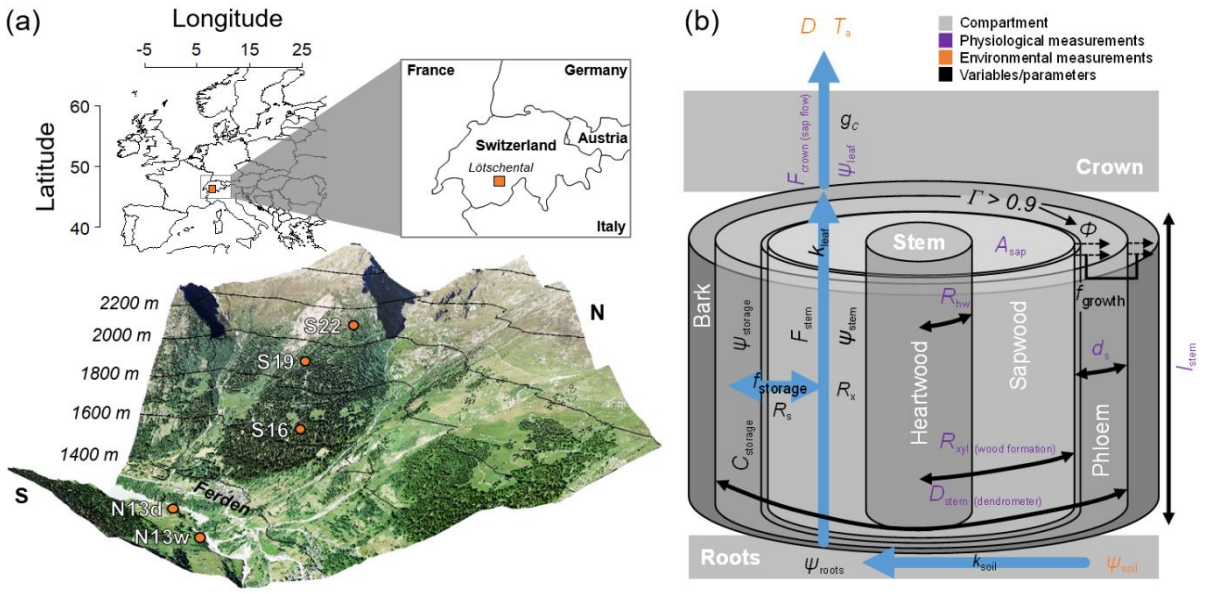

Figure 7.1 Location and experimental setup within the Lötschental (a) and a schematic description of the mechanistic whole-tree model (b). Sites are located at every 300 m a.s.l. from the valley bottom (at ≈1300 m a.s.l.= 13) to the treeline (at ≈2200 m a.s.l.= 22) on either the north- (= N) or south-facing (= S) slope. At the valley bottom, an additional site provides contrast in soil water availability (dry= d and wet= w). The model assesses tree-internal flows when water moves from the soil to the atmosphere and consists of three compartments where water enters (roots) flows (stem) and exits the tree (crown). The stem compartment includes four tissues, where non-functional bark and heartwood are hydraulically inactive, while the sapwood and phloem facilitate water transport and store water, respectively. Water flow is driven by transpiration (F_{crown}) and utilizes either water moving from the soil (F_{stem}) or from the storage compartment ($f_{storage}$), which affects the pressure ($\psi_{storage}$) and turgidity of the storage tissue, and consequently the outer stem diameter (D_{stem}). Flows depend on environmental conditions (indicated in orange) and the tree's allometric and physiological properties (indicated in purple). Xylem growth (R_{xyl}; i.e., radial wood growth) occurs when turgor in the forming tissues exceeds a threshold (Γ). The resulting daily growth rates and crown conductance (g_c) were compared to radial growth observations and environmental conditions. A description of all variables and parameters used by the model are presented in Table 7.1.

Site description and meteorological measurements

The five study sites selected for this study are all located in the Lötschental, a valley situated in the Swiss Alps (46°23′40″ N, 7°45′35″ E; Figure 7.1a). Four sites (N13d, S16, S19 and S22) are distributed along an elevational gradient from the valley bottom (≈1300 m a.s.l.) to the treeline (≈2200 m a.s.l.), in addition to a site with wetter conditions (N13w) to contrast the neighbouring dry site at the valley bottom (N13d). The slopes are covered by a mixed forest of evergreen *Picea abies* (L.) Karst. and deciduous *Larix decidua* Mill. The valley bottom has a mean annual temperature of 5.7° C and mean annual precipitation of 800 mm (data from MeteoSwiss surface observation network). The mean growing season

temperature (May-October temperature from 2007-2015) decreases by 3.2 °C when moving from the valley bottom (N13d) up to the treeline (S22).

At each site, micrometeorological conditions were monitored from April 2012 to October 2015, including 15-min resolved air temperature (Ta [°C]) and relative humidity (RH [%]; Onset, USA, U23-002 Pro; also used to calculate vapour pressure deficit or D [kPa], see WMO 2008), as well as hourly soil volumetric water content (θ [%]; Decagon, USA, EC-5) and soil water potential measurements at 10 and 70 cm depth (ψ_{soil} [MPa]; Decagon, USA, MPS-2). The ψ_{soil} and θ measurements were used to establish soil water retention curves at each site in order to estimate ψ_{soil} from θ for 2012-2015, as ψ_{soil} measurements only started in autumn 2014 (see van Genuchten 1980; Teepe *et al*. 2003). Hourly global radiation (R_g [W m-2]) was measured at N13d using a micro-station (Onset, USA, H21-002 Micro Station) and pyranometer (Onset, USA, S-LIB-M003).

Allometric and physiological measurements

At each site two to three trees per species were selected for the continuous monitoring of stem radius (ΔR_{stem} [µm] of the xylem and bark, 1-h resolution) and sap flux density (F_d [cm^3 m^{-2} h^{-1}], 15-min resolution). In total, 20 dominant and mature trees were monitored (11 *L. decidua* and 9 *P. abies*; see Table 7.2; e.g., Figure 7.2). Allometric properties were collected from the monitored trees, including stem diameter at breast height (DBH [cm]), tree height [m], stem length up to the crown base (l_{stem} [m]; Vertex, Haglöf, Sweden), sapwood and heartwood thickness (R^i_{hw} [cm]) (measured from two increment cores taken perpendicular to the slope; using an increment borer, Haglöf, Sweden) and bark thickness (T_{bark} [cm]) at breast height. Additionally, measurements of phloem thickness (T_{phloem} [mm]; using a Trephor puncher; Tesaf, University of Padova, Italy) of 140 trees were taken across the Alps to obtain robust allometric relationships with DBH (see Table S7.1; T_{phloem} was used to define d_s). See Table 7.2 for an overview of the sampled trees and allometric properties.

Table 7.1 Overview of model parameters. Source indicates if the parameter is measured, given as a standard value or calibrated. For all calibrated parameters, we applied standardized initial values and calibration ranges established from literature.

Sym.	Unit	Description	Values (cal. range)	Source
Constants				
P_w	g m^{-3}	Density of water	$1e^{+06}$	Standard
Tree dimensions				
l_{stem}	m	Length of the stem	Individual specific	Measured
D^i_{stem}	m	Initial diameter of the outer diameter of the stem segment (DBH)	Individual and time specific	Measured
d_s	m	Initial thickness of the stem storage compartment (phloem)	Determined by an allometric equation with DBH (see Figure S7.1 and Table S7.2) and corrected for the offset with the observed thickness (Table 7.1)	Measured
R^i_{hw}	m	Initial radius of the non-conductive xylem (heartwood)	Individual and time specific assuming sapwood thickness stays constant. For each year the original R_{hw} (Table 7.1) is corrected for the ring width	Measured
Water relations				
$C_{storage}$	g MPa^{-1}	Capacitance of the stem storage compartment	1000 (50-10,000)	Wronski *et al.* 1985; Milne & Young 1985; Hunt *et al.* 1991; Kobayashi & Tanaka 2001; Verbeeck *et al*. 2007b; Zweifel *et al.* 2007
R_x	MPa h g^{-1}	Flow resistance in the stem compartment of the active xylem (sapwood)	0.0001 ($1e^{-6}$-0.1)	Milne & Young 1985; Hunt *et al.* 1991; Magnani & Borghetti 1995; Verbeeck *et al.* 2007b; De Schepper & Steppe 2010
R_s	MPa h g^{-1}	Echange resistance between the active xylem of the stem and the storage compartment (bark)	0.01 (1^{e-5}-0.5)	Milne & Young 1985; Hunt *et al.* 1991; Verbeeck *et al.* 2007b
$\prod^i_s$	MPa	Initial osmotic pressure of living tissue of the stem	1.2 (0-5)	Jones 1992
f_{water}	unitless	Water fraction of the stem compartment	0.4	Tyree 1988; Perämäki *et al.* 2001; Kravka & Čermák 1999
k_{leaf}	unitless	Proportionality constant for calculating ψ_{stem}	0.708 Determined by an allometric equation between ψ_{leaf} and ψ_{stem} (see Figure S7.2 and Table S7.3)	Measured
Stem diameter dynamics				
$\mathcal{E}_0$	m^{-1}	Proportionality constant	50 Adopted to let the elastic modulus range around 0-30 MPa	Génard *et al.* 2001; Steppe *et al.* 2005
$\mathcal{E}_x$	MPa	Elastic modulus of the xylem	1500	Irvini & Grace 1997; Hölttä *et al.* 2006; De Schepper & Steppe 2010
ϕ	MPa^{-1} h^{-1}	Extensibility of cell walls in relation to non-reversible dimensional changes (xylogenesis)	0.006	Hsiao *et al.*1998; Génard *et al.* 2001; Steppe *et al.*2005; De Schepper & Steppe 2010
Γ	MPa	Threshold turgor pressure	0.9	Génard *et al.* 2001; Steppe *et al.* 2005; De Schepper & Steppe 2010
f_{growth}	fraction	Fraction of growth contributing to xylem formation	0.9 Determined by recalculating literature values (see Figure S7.3)	Prislan *et al.* 2013; Gričar *et al.* 2016
Climate data				
ψ^i_{soil}	MPa	Initial soil water potential	Site and time specific	Measured
k_{soil}	unitless	Proportionality constant for calculating ψ_{roots}	S22/S19/S16/N13W= 1, N13= 0.25 Established by comparing pre-dawn ψ_{leaf} against ψ_{soil} (see Figure S7.4)	Verbeeck *et al.* 2007b

Measurements of ΔR_{stem} were performed with high-precision point dendrometers (Ecomatik model DR, Munich, Germany) and F_d using commercially available thermal dissipation probes (Tesaf, University of Padova, Italy; according to Granier 1985). Both sensors were installed at the stem height of ≈1.6 m on the side facing slope height. D_{stem} ([cm]; ΔR_{stem} * 2, required for model calibration) was calculated with the tree diameter when considering the xylem and phloem (DBH – T_{bark} * 2 + T_{phloem} * 2). F_d was calculated by using the method described in Peters *et al.* (In press; applying a species-specific calibration, dampening correction and environmental dependent ΔT_{max}). F_d was multiplied by the sapwood area (A_{sap} [cm^2]) to obtain water flow to the crown (F_{crown} [g h-1]) needed as input for the model. To improve model calibration, leaf water potential (ψ_{leaf} [MPa]) measurements were taken at N13d, N13w and S22 during four diurnal campaigns (2-hour interval from 05:00 to 21:00 CET on 19-04-2014, 27-05-2015, 21-07-2015 and 24-09-2015) and weekly at midday (11:00-15:00 CET) during the 2015 growing season. Measurements were performed using a Scholander pressure chamber (Boyer 1967) on four twigs (≈5 cm) per tree. During the diurnal campaigns some twigs were covered with aluminium foil, two hours prior to sampling (see Begg & Turner 1970) to also assess stem water potential (ψ_{stem} [MPa]).

Observations of radial growth

Xylem formation was monitored on inter- and intra-annual timescales, using increment cores collected in November 2015 and weekly micro-cores (see Rossi *et al.* 2006a) collected in 2012 and 2013 from three to four neighbouring trees. Inter-annual growth was established for the monitored trees by measuring ring width [mm] from cross-dated increment cores (as described in Peters *et al.* 2017). Intra-annual wood formation was derived via xylogenesis observations of the collected micro-cores (see Moser *et al.* 2009). Observations included cell-counts of the number of cells in cambial, enlargement, wall thickening and mature zones on thin-sections. These cell-counts were standardized by the total number of cells of the previous ring (see Rossi *et al.* 2006b). Additionally, the lumen area and the cell wall thickness of tracheids were measured on digital images from thin-sections (see von Arx *et al.* 2016) of increment cores from the neighbouring trees using ROXAS (von Arx & Carrer 2014). The anatomical measurements were aggregated into tracheidograms according to Peters *et al.* (2018) and combined with the xylogenesis data to time cell and xylem radius (R_{xyl}) development at each site (see Cuny *et al.* 2014). For the comparison with the modelling output,

R_{xyl} (in µm d^{-1}) was standardized to the annual maximum R_{xyl}, to assess the dynamics rather than the absolute values.

Table 7.2 Characteristics of the monitored trees with an indication of the type of model calibration applied. For each individual the diameter at breast height (DBH), stem length (l_{stem}), initial thickness of the storage tissue (d_s), age and sapwood thickness are provided. Two calibration procedures were applied, including the 2015 weekly calibration using ψ_{leaf} measurements (Cal. 2015) and the moving-window calibration over the entire growing season (Cal. MW).

Elevation [m a.s.l.]	Species	Tree	DBH [cm]	l_{stem} [m]	d_s [cm]	Age [yrs]	Sapwood thickness [cm]	Cal. 2015	Cal. MW
1300 (dry)	*Larix decidua*	N13Bd_L1	29.5	7.2	0.46	131	1.5	X	X
		N13Bd_L2	32.0	10	0.36	128	1.8	X	X
	Picea abies	N13Ad_S1	30.7	2.8	0.48	90	2.5	X	X
		N13Ad_S2	48.1	2.9	0.33	93	5.3	X	X
1300 (wet)	*Larix decidua*	N13WAd_L1	78.0	8.2	0.80	148	2.2	X	X
		N13WBd_L2	89.3	8.8	0.83	164	2.4	X	X
		N13WBd_L3	52.0	5.6	0.37	134	2.4	X	X
	Picea abies	N13WAd_S1	81.0	3.1	0.66	85	9.1	X	X
		N13WAd_S2	62.8	5.8	0.63	81	6.9	X	X
		N13WBd_S3	80.7	4.4	0.71	109	9.0	X	X
1600	*Larix decidua*	S16Bd_L1	75.2	15	0.40	371	3.5		X
		S16Ad_L1	38.5	13	0.39	69	2.6		X
	Picea abies	S16Ad_S2	38.2	6.7	0.74	62	4.2		X
		S16Bd_S2	56.2	13	0.53	461	2		X
1900	*Larix decidua*	S19Ad_L1	48.0	5.3	0.28	200	3.2		X
		S19Bd_L1	48.7	9.8	0.51	326	1.8		X
	Picea abies	S19Ad_S2	34.1	8.8	0.62	137	1.7		X
		S19Bd_S2	47.5	5.5	0.29	229	5.5		X
2200	*Larix decidua*	S22Ad_L1	47.0	8.9	0.59	269	2.4	X	X
		S22Ad_L2	55.7	5.5	0.45	280	3.1	X	X

Modelling and statistical analyses

Model simulations, calibrations, sensitivity and identifiability analyses were performed using the plant modelling software PhytoSim (version 2.1, Phyto-IT, Mariakerke, Belgium). Two different types of model calibrations were used for different subsets of trees. First calibrations were performed for the measurements in 2015 for 7-day periods where ψ_{leaf} was measured (at N13d, N13w and S22). These weekly calibrations were performed to analyse the behaviour of hydraulic parameters (R_x, $C_{storage}$, Π^i_s and R_s). Additionally, as leaf water potential (ψ_{leaf}) measurements were not available for all years, we performed analyses to test model performance when including $C_{storage}$ or R_x, as a fixed parameter. See Note S7.2 for a detailed description on the model performance analyses and calibration procedure. These results supported using $C_{storage}$ as a fixed parameter when

applying the model on periods without ψ_{leaf} measurements (see Note S7.3) Secondly, a 7-day moving-window calibration with fewer calibration parameters (fixing $C_{storage}$ and Π^{i}_{s}) was applied on 4 growing seasons for all trees, referred to as growing season calibrations (see Note S7.2). Sensitivity and identifiability analyses were performed to determine which subset of model parameters was both sensitive enough and not collinear (De Pauw *et al.* 2008).

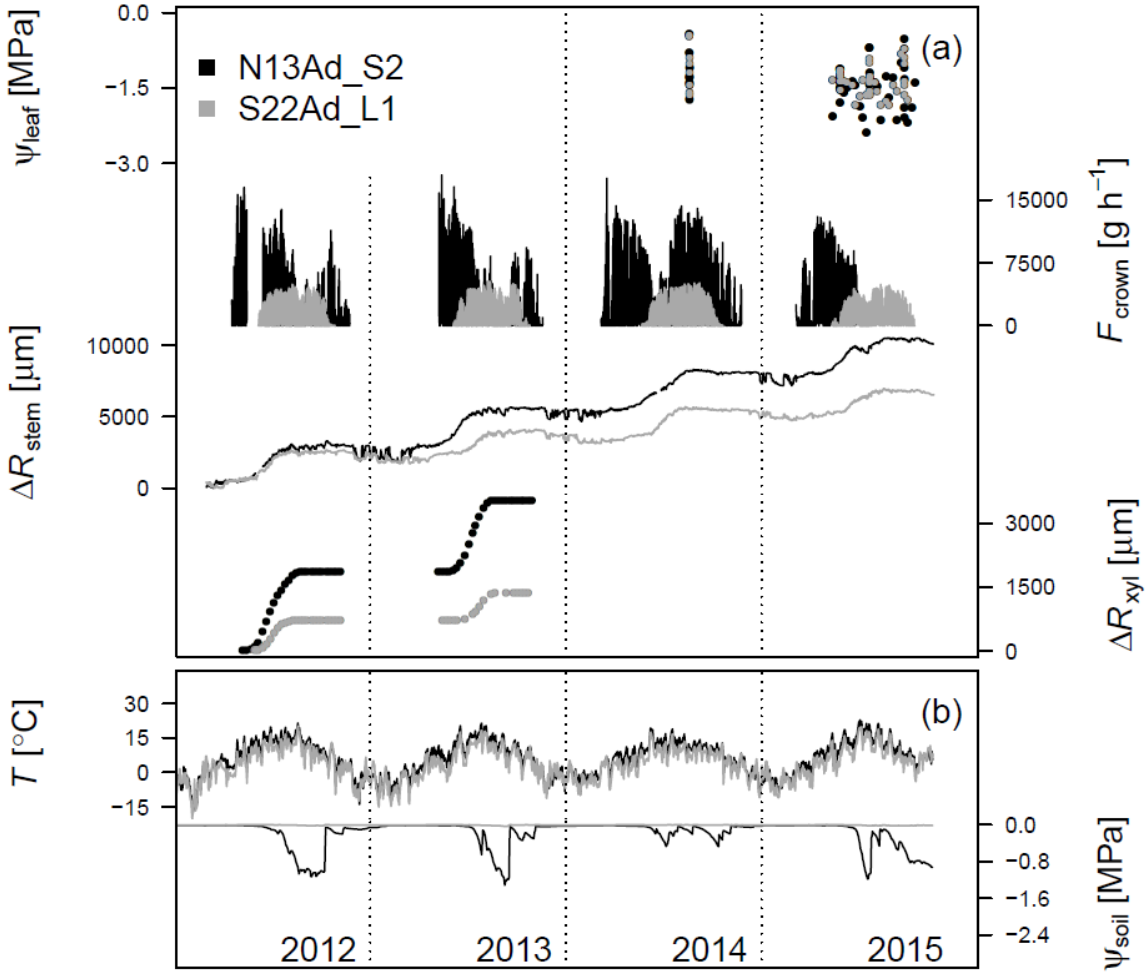

Figure 7.2 Overview of physiological and meteorological measurements from 2012 until 2015 used in the model for two trees at two sites (*Larix decidua* at S22= S22Ad_L1 and *Picea abies* at N13d= N13Ad_S2). (a) Vertical dotted lines indicate the boundary between calendar years. Measurement frequency is weekly for leaf water potential measurements (ψ_{leaf}) and xylogenesis observations (R_{xyl}), 15 min for sap flow (F_{crown}) and hourly for dendrometer (R_{stem}) measurements. (b) Environmental measurements of daily mean air temperature (T) and soil water potential (ψ_{soil}) collected at S22 (in grey) and N13d (in black).

The simulated and weekly-averaged daily growth patterns were compared to xylogenesis observation and annual ring width. To analyse the environmental response of turgor-driven radial stem growth, simulated daily growth rates [mm d^{-1}] were related to daily mean T_a and ψ_{soil}. Additionally, the crown conductance (g_c [g_{water} $m^{-2}_{sapwood}$ s^{-1} kPa^{-1}]) response to T_a and ψ_{soil} was analysed. Daily mean crown conductance was determined by using D and F_d according to Meinzer *et al.* (2013):

$$g_c = \frac{(F_d * 10000/3600)}{D} \quad \text{(Eq. 1)}$$

where we calculated g_c for every 15-min time-step and excluded measurements where R_g is below 500 W m^{-2}, to avoid delay effects between sap flow and transpiration during dawn and dusk. To account for collinear environmental factors, we analysed T_a when removing all data with a ψ_{soil} below -0.2 MPa, while for ψ_{soil} we removed all T_a data below 11 °C. The probability for growth and g_c to occur was calculated by determining the fraction of data points below a threshold (<5 μm d^{-1} for growth and <15 g m^{-2} s^{-1} kPa^{-1} for g_c). Data processing and statistical analysis on the comparison between model output and validation data was performed with linear mixed-effect models (including the site or individual as a random factor) with the software R (version 3.2.00, R development core team 2013).

7.3 Results

Model performance

Hydraulic parameters addressed with weekly model calibrations in 2015 (May-October; see Table 7.2), showed stable fits for 55% (139 out of 252) of the individual calibrations. At N13d, drought periods and data gaps caused difficulties in obtaining stable parameter values (37 out of 48 7-day periods were successfully calibrated). S22 showed less successful calibration due to the late start of the growing season and early start of the dormancy period (21 out of 42), while N13w showed the highest success rate (81 out of 126). Clear differences were found between simulated growth rates at the end of the growing season (little to no R_{xyl} expansion), and periods during the growing season where the xylem diameter increased (Figure 7.3c, d). The identifiability analysis showed that $C_{storage}$, R_x, Π^i_s and R_s where both sensitive and identifiable (e.g., Figure S7.5).

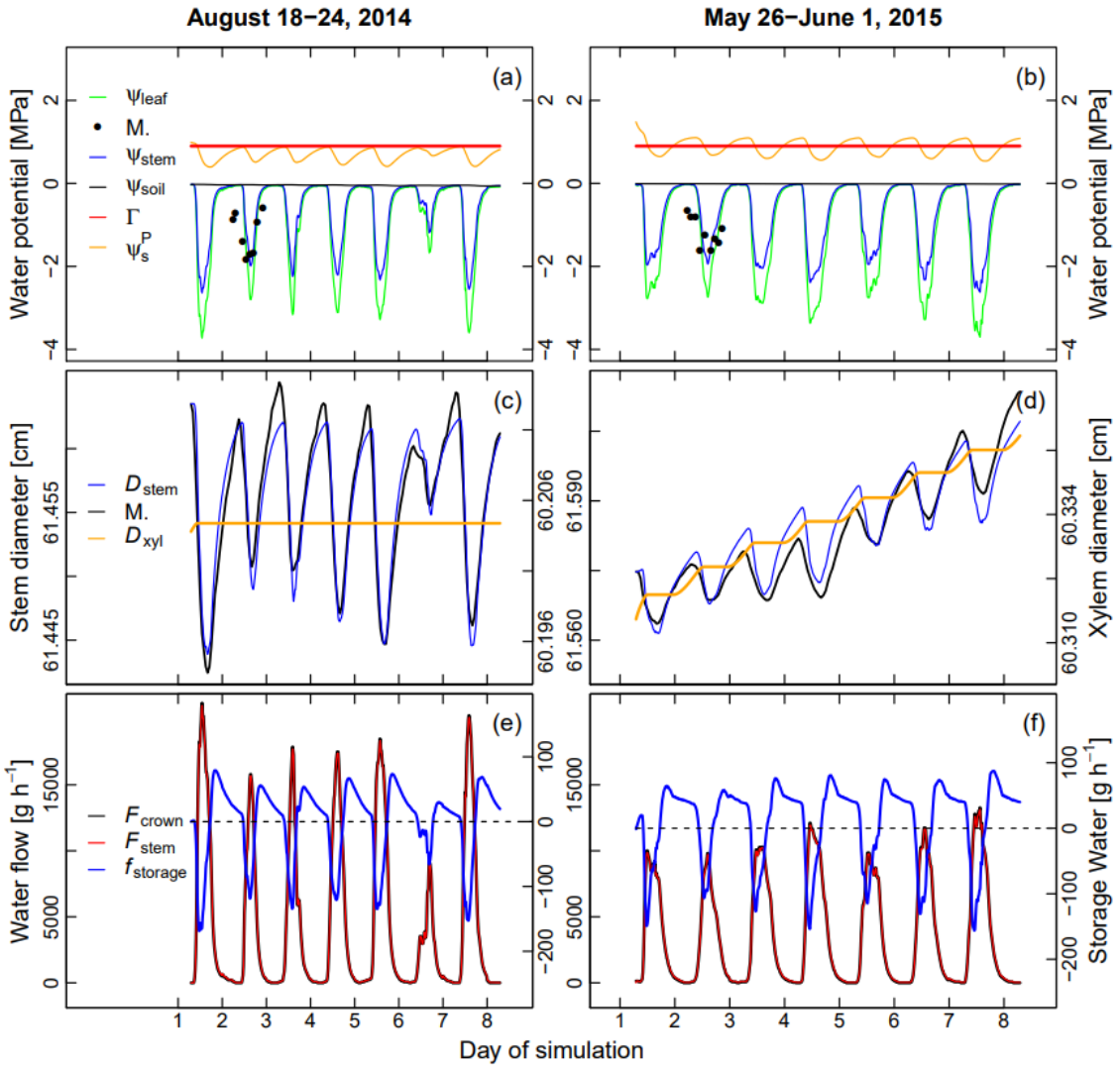

Figure 7.3 Measured and simulated water potentials (a, b), diameter variations (c, d) and water flows (e, f) in *Picea abies* at N13w (N13WAd_S2) during non-growth (a, c, e) and growth (b, d, f) periods. Soil water potential (ψ_{soil}; a, b) and sap flow (F_{crown}; e, f) were used as model inputs, while leaf water potential (ψ_{leaf} indicated by M.; a, b) and diameter variations (D_{stem} indicated by M.; c, d) were measured. Growth of the xylem (D_{xyl}; d) occurs during night-time, when cell turgor pressure (ψ^{p}_{s}; a, b) exceeds the critical value for wall-yielding (Γ). The flow of water to and from the storage tissue ($f_{storage}$) affects the turgor pressure, which is defined by the mismatch between F_{crown} and direct stem water flow (F_{stem}; e, f).

Variability in hydraulic properties

The hydraulic capacitance of the storage tissue ($C_{storage}$) ranged from 50 to 7222 g MPa^{-1}, with the highest values at the lower elevation wet site (N13w). Although higher $C_{storage}$ values was calibrated at wetter and colder sites (N13w and S22, respectively; Figure 7.4a), no significant differences were found when correcting for the size of the storage tissue ($V_{storage}$ in Table 7.3) between sites and species (μ= 0.0221 g MPa^{-1} cm^{-3} and p= 0.128 across species and sites; *L. decidua* μ= 0.0263, p= 0.228 across sites; *P. abies* μ= 0.0152, p= 0.3524 across sites).

Table 7.3 Mean and standard deviation of the model parameters for individual trees and averaged per species obtained from the weekly calibrations during the growing season of 2015 (see Table 7.2). Calibrated parameters include; the hydraulic resistance through the xylem (R_x), storage tissue hydraulic capacitance ($C_{storage}$), initial osmotic potential (Π^i_s) and hydraulic resistance from the storage tissue to the xylem (R_s). Storage tissue volume ($V_{storage}$) and ratio between sapwood area and stem length (A_{sap}/l_{stem}) which are used to standardize to $C_{storage}$ and R_x for Figure 7.4 are also provided.

Site	Species	Tree	$C_{storage}$ [g MPa^{-1}]	R_x [MPa h g^{-1}]	Π^i_s [MPa]	R_s [MPa h g^{-1}]	$V_{storage}$ [cm^3]	A_{sap}/l_{stem} [cm^{-1}]
N13d	*Larix decidua*	N13Bd_L1	$264.2_{\pm 324.7}$	$0.00037_{\pm 0.00016}$	$1.48_{\pm 0.50}$	$0.0207_{\pm 0.0122}$	25107	0.15
		N13Bd_L2	$1218.5_{\pm 1150.2}$	$0.00079_{\pm 0.00051}$	$1.14_{\pm 0.23}$	$0.0019_{\pm 0.0014}$	32512	0.14
	Picea abies	N13Ad_S1	$164.9_{\pm 73.0}$	$0.00260_{\pm 0.00267}$	$0.95_{\pm 0.27}$	$0.0350_{\pm 0.0376}$	12648	0.75
		N13Ad_S2	$125.6_{\pm 59.1}$	$0.00015_{\pm 0.00004}$	$1.42_{\pm 0.11}$	$0.0057_{\pm 0.0064}$	13857	2.35
N13w	*Larix decidua*	N13WAd_L1	$4162.5_{\pm 1820.6}$	$0.00010_{\pm 0.00003}$	$1.35_{\pm 0.17}$	$0.0074_{\pm 0.0048}$	143007	0.57
		N13WBd_L2	$1192.6_{\pm 699.3}$	$0.00013_{\pm 0.00004}$	$1.21_{\pm 0.36}$	$0.0034_{\pm 0.0029}$	169520	0.62
		N13WBd_L3	$1110.8_{\pm 816.0}$	$0.00029_{\pm 0.00011}$	$1.35_{\pm 0.24}$	$0.0124_{\pm 0.0121}$	27937	0.54
	Picea abies	N13WAd_S1	$1058.6_{\pm 721.4}$	$0.00005_{\pm 0.00001}$	$1.53_{\pm 0.43}$	$0.0207_{\pm 0.0087}$	49296	6.14
		N13WAd_S2	$375.3_{\pm 176.5}$	$0.00017_{\pm 0.00003}$	$1.54_{\pm 0.34}$	$0.0117_{\pm 0.0030}$	70277	1.99
		N13WBd_S3	$1751.1_{\pm 1652.1}$	$0.00008_{\pm 0.00003}$	$1.64_{\pm 0.45}$	$0.0094_{\pm 0.0028}$	76463	4.36
S22	*Larix decidua*	S22Ad_L1	$1518.4_{\pm 901.3}$	$0.00041_{\pm 0.00021}$	$1.32_{\pm 0.24}$	$0.0080_{\pm 0.0094}$	69129	0.33
		S22Ad_L2	$1759.8_{\pm 1032.0}$	$0.00014_{\pm 0.00007}$	$1.56_{\pm 0.17}$	$0.0140_{\pm 0.0206}$	37492	0.79
All	***Larix decidua***		$\mathbf{1603.8_{\pm 1220.2}}$	$\mathbf{0.00032_{\pm 0.00024}}$	$\mathbf{1.34_{\pm 0.14}}$	$\mathbf{0.0097_{\pm 0.0065}}$	**72101**	**0.45**
	Picea abies		$\mathbf{695.1_{\pm 699.1}}$	$\mathbf{0.00061_{\pm 0.00111}}$	$\mathbf{1.42_{\pm 0.27}}$	$\mathbf{0.0165_{\pm 0.0117}}$	**44508**	**3.12**

The hydraulic resistance through the xylem (R_x) ranged from 0.00003 to 0.00753 MPa h g^{-1}, with slightly higher average values at N13d (Table 7.3). When calculating the resistivity from R_x using A_{sap}/l_{stem} (Table 7.3), *P. abies* showed a tendency for higher values (μ= 5.79*10^{-4} MPa h g^{-1} cm^{-1}, p= 0.0604) compared to *L. decidua* (μ= 9.94*10^{-5} MPa h g^{-1} cm^{-1}; Figure 7.4b). This difference is more apparent at N13w (*P. abies* μ= 3.28*10^{-4} MPa h g^{-1} cm^{-1}, *L. decidua* μ= 1.01*10^{-4} MPa h g^{-1} cm^{-1}, p= 0.0028). Relatively higher standardized R_x was found during periods with more negative soil water potential only for *P. abies* (slope= -0.0068, p <0.001), and not for *L. decidua* (slope= 1.317*10^{-5}, p= 0.721). However, only five calibrations were possible during drier conditions. A significant higher standardized R_x value was found for *P. abies* at N13d (N13d μ= 0.00142 MPa h g^{-1} cm^{-1}, N13w μ= 0.00033 MPa h g^{-1} cm^{-1}, p= 0.00024), while for *L. decidua* only slightly higher values for S22 (N13d μ= 7.58*10^{-5} MPa h g^{-1} cm^{-1}, N13w μ= 0.0001 MPa h g^{-1} cm^{-1}, S22= 0.00013 MPa h g^{-1} cm^{-1}, p= 0.0189). Yet, there is no significant different between N13w and S22 (p= 0.1289). The initial osmotic potential (Π^i_s) ranged from 0.36 to 2.45 MPa and radial hydraulic resistance to the storage tissue (R_s) ranged from 0.00021 to 0.09238 MPa h g^{-1}. Across species a consistent temporal pattern of decreasing Π^i_s with day of year was found (*P. abies*

slope= -5.44*10^{-3} MPa^{-1}, p= 0.0002, *L. decidua* slope= -2.43*10^{-3} MPa^{-1}, p= 0.0071). No significant difference was found across sites and species for these parameters (p >0.005).

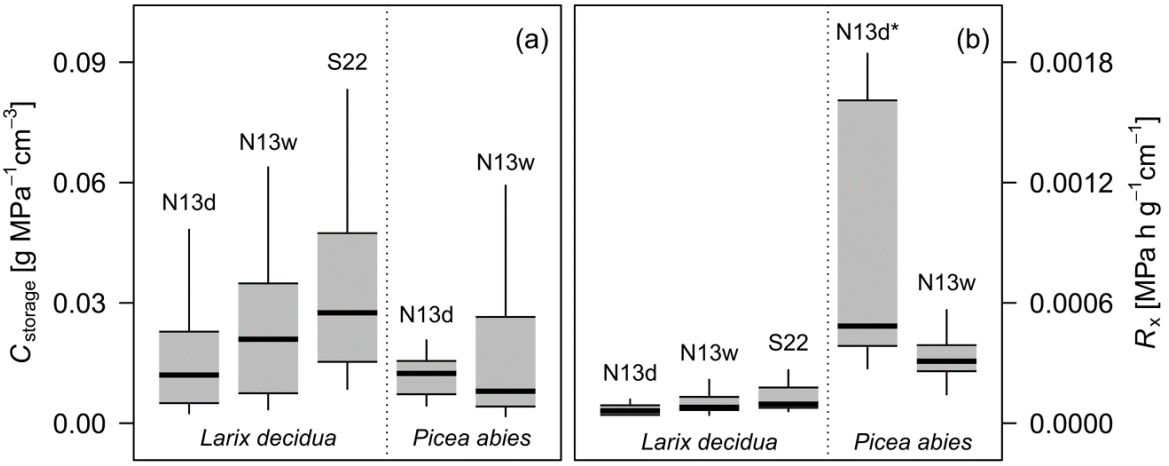

Figure 7.4 Boxplots of 2015 weekly calibrated parameters grouped per site- and species and effect of parameter fixing on model performance. (a) $C_{storage}$, corrected for individual storage tissue volume. (b) R_x recalculated into resistivity, by multiplying it with the ratio between sapwood area and stem length (A_{sap}/l_{stem}). Significant within species difference are highlighted with *.

Growing season R_{xyl} dynamics and simulated ring width

The comparison of weekly-averaged daily xylem growth rates of the growing-season calibrations (e.g., Figure 7.5) with xylogenesis observations for 2012 and 2013 (Figure 7.6a; Table 7.4) shows the highest agreement for *L. decidua* at S22 (R^2= 0.88, p <0.0001). The correlation decreases with elevation, with lowest correlation at N13d for 2013 (R^2= 0.13, p= 0.082). On average, the goodness of fit was slightly lower for *P. abies* compared to *L. decidua* (R^2= 0.53 and 0.68, respectively). For *P. abies*, the highest correlations were found at N13w for 2012 (R^2= 0.81, p <0.0001). The largest mismatches were found at the end of the growing season, where simulated growth stopped earlier than observations at S16 and N13d, especially for *P. abies* (Figure 7.6a).

A comparison of simulated vs. measured ring width from 2012-2015 showed a significant positive linear correlation across sites and species (Figure 7.6b). The slope of 0.85 (p <0.0001, n= 72; with the site as a random factor) indicates a small overestimation of the simulated ring width. A less accurate fit was found for *L. decidua* at S19 (S19Ad_L1), with larger simulated ring widths (only for 2013 and 2014 due to data gaps). The 95% Bayesian credible interval (see Gelman & Hill, 2007) shows an offset of ≈1 mm. For the moving-window calibrations consistent patterns where found for R_s and R_x, with higher values at

the beginning and the end of the growing season (e.g., Figure 7.5). Additionally, higher R_s and R_x values were found at the site with drier conditions (see Figure S7.7).

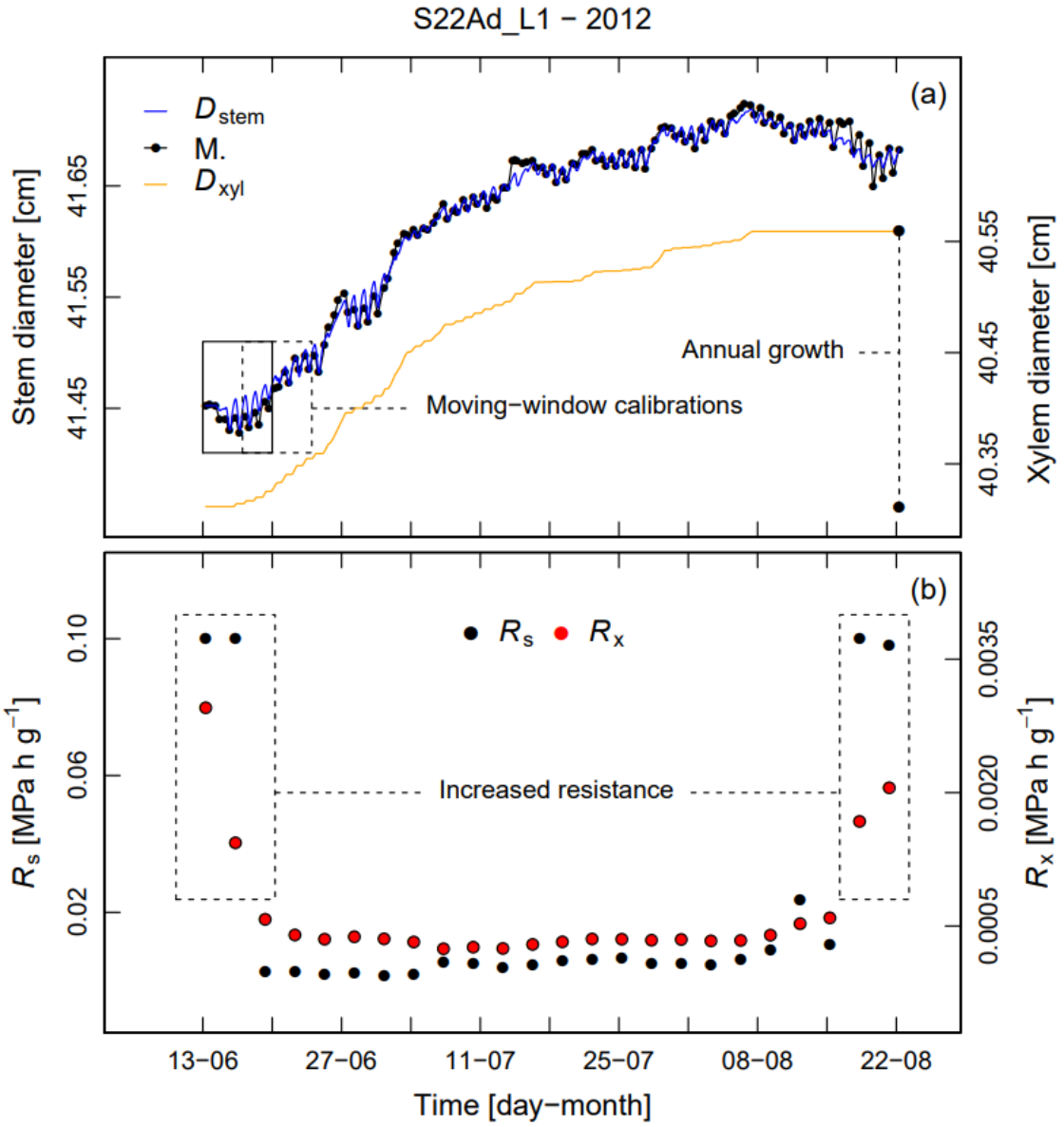

Figure 7.5 Example of a 7-day moving-window calibration with an overlap of 3 days for the growing season of 2012 for a *Larix decidua* tree growing at S22. (a) Simulated stem diameter (blue line) calibrated to stem diameter measurements (black points/line). The simulated xylem diameter increase was used to derive annual and daily growth rates (orange line). (b) R_s (black points) and R_x (red points) have been calculated for each calibration window.

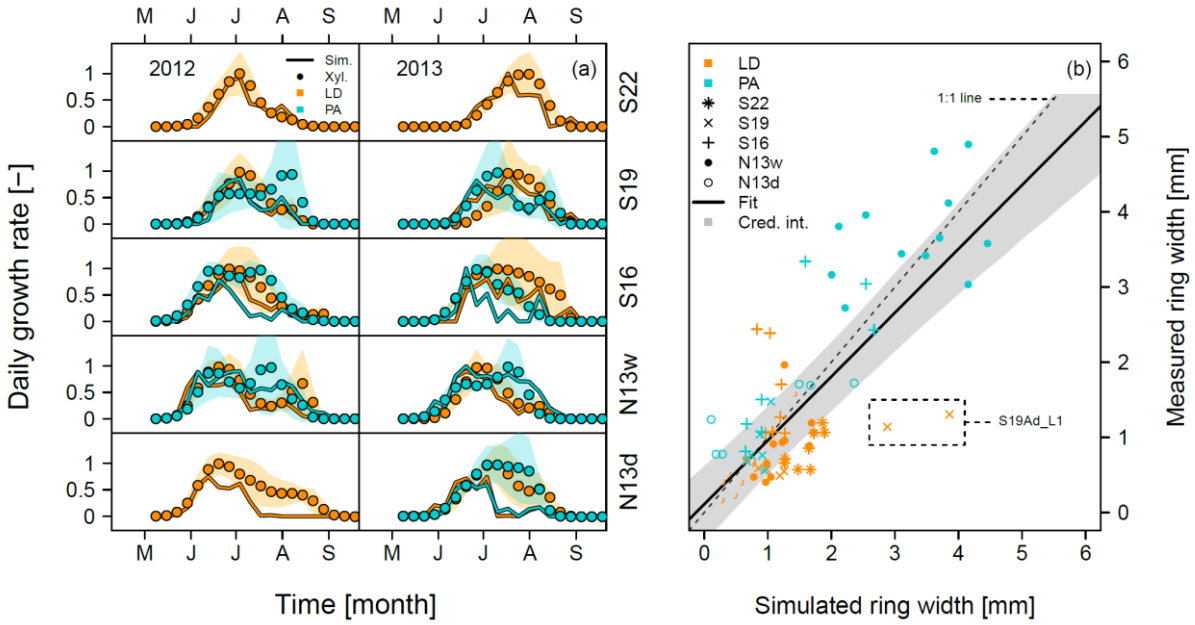

Figure 7.6 Comparison between turgor-driven growth and radial growth observations. (a) Xylogenesis-derived daily xylem growth rate (R_{xyl}; with shading indicating the standard deviation) against simulated values (coloured lines) for the 2012 and 2013 growing seasons. Data are averaged over all measured individuals (see Figure S7.6) and scaled by the maximum daily growth rate for comparison. (b) Simulated ring widths from 2012-2015 compared with observed ring widths from the increment cores per individual and grouped per site (different symbols) and species (*Larix decidua*=LD; in orange; *Picea abies*= PA; in cyan). The solid line indicates a linear regression and the shaded areas show the Bayesian credible interval of the fitted function (see Gelman & Hill 2007). Both 2013 and 2014 ring width for the tree S19Ad_L1 (see Table 7.2) deviate from the other measurements.

Table 7.4 Statistics of linear correlations between weekly standardized daily xylem growth and corresponding model growth grouped for 2012 and 2013. Significant correlations are identified with *. Due to data gaps, no correlations could calculated for *Picea abies* in 2012.

Site	**Species**	**2012**			**2013**		
		R^2	***p***	**n**	**R^2**	***p***	**n**
N13d	*L. decidua*	0.62*	$5.78e^{-05}$	18	0.13	$8.15e^{-02}$	18
	P. abies				0.25*	$1.38e^{-02}$	20
N13w	*L. decidua*	0.55*	$1.41e^{-04}$	20	0.76*	$3.64e^{-07}$	20
	P. abies	0.71*	$1.18e^{-06}$	21	0.81*	$3.54e^{-08}$	20
S16	*L. decidua*	0.86*	$2.47e^{-09}$	20	0.69*	$3.26e^{-06}$	20
	P. abies	0.49*	$3.48e^{-04}$	20	0.32*	$7.13e^{-03}$	19
S19	*L. decidua*	0.82*	$2.39e^{-08}$	20	0.69*	$3.46e^{-06}$	20
	P. abies	0.44*	$1.51e^{-03}$	18	0.71*	$6.58e^{-06}$	18
S22	*L. decidua*	0.88*	$6.70e^{-09}$	18	0.77*	$1.20e^{-06}$	18

Environmental controls on daily growth and crown conductance
The response of daily growth rates, derived from the growing-season simulations, and daily mean crown conductance (g_c) to Ta and ψ_{soil} are shown in Figure 7.7. Daily T_a at the sites along the gradient ranges from ≈0-20 °C for June-July-August (Figure 7.7a), while in the valley bottom the wet and dry sites provided a ψ_{soil} range from ≈0- -1.2 MPa (Figure 7.7b). These conditions fall into the range where offsets between photosynthetic activity and growth would be expected (Figure 7.7c, d), according to Fatichi *et al.* (2014). Below 2 °C the probability of modelled growth to occur is only 15% (Figure 7.7e), while conductance occurs with a probability of 43% (Figure 7.7g). Growth rates increased until 11 °C, after which they stabilized and slowly decreased. Increasing T_a was collinear with the increase in vapour pressure deficit (see D in Figure S7.8). The probability of growth occurring decreased from 66% to 28% between -0.2 and -0.6 MPa, ψ_{soil}, while almost no growth occurred after -0.6 MPa (Figure 7.7f). Yet, g_c appeared to show a less steep decrease with decreasing ψ_{soil}, where sap flow still occurred at -1.2 MPa (Figure 7.7h).

7.4 Discussion

Turgor pressure in the cambium has long been recognized as a key factor for determining the initiation and rate of cell enlargement (see Lochhart 1965; Steppe *et al.* 2005). It has thus been shown that modelling turgor can improve current growth predictions (see Steppe *et al.* 2015), which are still often photosynthesis driven (i.e., carbon source limited; see Sitch *et al.* 2008; Fatichi *et al.* 2014). In this study, we applied a mechanistic model that simulates turgor-driven growth in mature conifers under natural environmental conditions and compared the simulation to independent radial growth observations. Our results reveal the importance of turgor for simulating (intra-)annual radial wood growth. The simulations also helped to elucidate the effect of environmental factors limiting daily growth rates and differences in hydraulic functioning between sites and species.

Species-specific hydraulic functioning
The mechanistic model revealed species-specific differences in hydraulic properties (Steppe & Lemeur 2007), including the hydraulic capacitance of the water storage tissue ($C_{storage}$), hydraulic resistance of the xylem (R_x), hydraulic resistance of water transport from the storage compartment to the xylem (R_s) and the osmotic potential within the storage compartment (Π^i_s). For example, the

dynamic regulation of water release from elastic living tissues (d_s in Figure 7.1b) can reduce xylem tension and hence delay the formation of embolism (Meinzer *et al.* 2008, 2009). Additionally, *in-situ* simulations of R_x and its behaviour during droughts can provide information on species-specific vulnerability to cavitation (Steppe & Lemeur 2007; Choat *et al.* 2012). These hydraulic properties, affected by the trees hydraulic architecture (see Sperry & Love 2015), are thus considered relevant for determining the tree's drought tolerance.

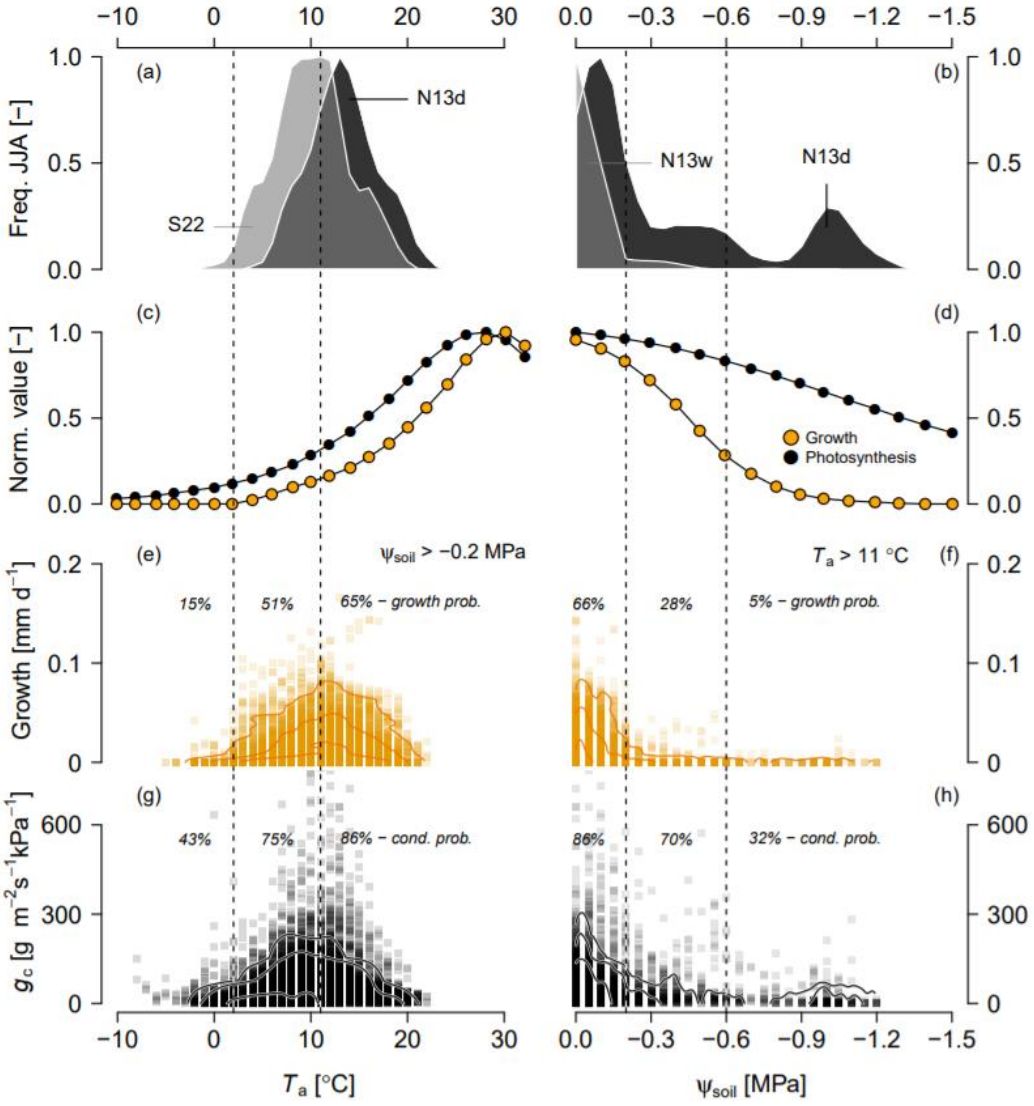

Figure 7.7 Growth and crown conductance (g_c) responses to air temperature (T_a) and soil water potential (ψ_{soil}). (a, b) Frequency of daily mean T_a and ψ_{soil} for contrasted sites regarding temperature (S22 vs. N13d) and soil water availability (N13w vs. N13d). (c, d) Response of primary growth and photosynthesis to T_a and ψ_{soil} as presented by Fatichi *et al.* (2014). (e, f) Modelled growth rates (in mm d^{-1}) as a function of T_a (compiled in 1 °C bins) and ψ_{soil} (compiled in 0.05 MPa bins) for all sites and species. Days where other factors were more limiting were excluded. The same procedure was applied for daily mean g_c (g, h). Solid lines (e-h) show the density contours to better visualize the response. Dotted lines indicate the probability of growth and conductance to occur along T_a and ψ_{soil}.

The calibrated $C_{storage}$ values fell within the range of expected values for mature conifers (Table 7.5), where *L. decidua* showed a 2.3 times higher hydraulic capacitance than *P. abies*. However, when standardizing $C_{storage}$ for the storage-tissue volume, no significant difference was found between species (μ= 0.0221 g MPa^{-1} cm^{-3}; Figure 7.4a), and the values were lower than those found in literature (0.107-0.886 g MPa^{-1} cm^{-3}; Barnard *et al.* 2011; McCulloh *et al.* 2014). This discrepancy could be explained by the fact that we do not account for the capacitance of the xylem to provide water (see Scholz *et al.* 2007; Köcher *et al.* 2013). Moreover, we found stable standardized $C_{storage}$ values during the dry growing season of 2015, which contrasts with decreasing $C_{storage}$ found due to the depletions of the water storage reservoir during droughts in *Quercus ilex* (see Salomón *et al.* 2017). Based on our modelling results, we therefore conclude that monitored high elevation conifers do not show strong dynamics in $C_{storage}$ under occurring drought and that species-specific capacitance differences are most likely caused by the larger storage pool of *L. decidua* (see Table 7.3).

The R_x values determined with the 2015 calibrations corresponded to values from literature (see Table 7.5). Under wet conditions (N13w), *P. abies* showed a 3.3 times higher resistivity compared to *L. decidua* (R_x standardized for A_{sap}/l_{stem}; Figure 7.4b). This difference is in agreement with the xylem-anatomical differences where the potential hydraulic conductivity for *P. abies* is 2.1 times lower than for *L. decidua*, when considering tracheids in the earlywood from 2012-2013 (according to Nonweiler 1975; earlywood= Mork's index <1, see Denne 1989; see Note S7.4). Monitored drought periods seemed to affect *P. abies*, which showed a significant increase in R_x with decreasing ψ_{soil} (slope= -0.0068, p <0.001), indicating a higher risk for cavitation. Although *P. abies* has a relatively smaller lumen area compared to *L. decidua* to improve cavitation resistance, other factors such as its smaller storage tissue, stomatal behaviour and shallow rooting system (Anfodillo *et al.* 1998) potentially make this species more sensitive to drought.

Both Π^i_s and R_s fell within the range of literature values (Table 7.3; Milne & Young 1985; Hunt *et al.* 1991; Jones 1992), with Π^i_s consistently decreasing in both species during the growing season (slope= -0.00544 and -0.00243 MPa^{-1} d^{-1} for *P. abies* and *L. decidua*, respectively). This decrease in Π^i_s is in agreement with the reduction of sugars found in the cambial zone for *L. decidua* in the Lötschental (Simard *et al.* 2013). A mechanism explaining this phenomenon could be sugar loading, where more photosynthetic products are incorporated into woody tissue or starch, or sugars are transported to the roots to increase osmotic

potential (Höllta *et al.* 2006; De Schepper & Steppe 2010; Ryan & Asao 2013). Notwithstanding, the fact that all hydraulic parameters were in agreement with values found in literature supports the validity of mechanisms described with the model.

Table 7.5 Overview of the species average of hydraulic capacitance of the storage tissue ($C_{storage}$) and hydraulic resistance of the stem (R_x) reported in the literature. The average value reported per species is provided.

$C_{storage}$ [g MPa^{-1}]	Species	DBH [cm]	Source	Rx [MPa h g^{-1}]	Species	DBH [cm]	Source
1603.8	*Larix decidua*	54.8	This study	0.00032	*Larix decidua*	54.8	This study
695.1	*Picea abies*	60.7	This study	0.00061	*Picea abies*	60.7	This study
187.1	*Pinus sylvestris*	11.9-23.2	Zweifel *et al.* 2006	0.00039	*Pinus sylvestris*	29.8	Verbeeck *et al.* 2007b
1500	*Picea sitchensis*	≈8.4	Milne & Young 1985	0.00175	*Picea sitchensis*	≈8.4	Milne & Young 1985
1440	*Pinus densiflora*	19.2	Kobayashi & Tanaka 2001	0.00003	*Fagus sylvatica*	57	De Schepper & Steppe 2010
45442.9	*Pinus sylvestris*	29.8	Verbeeck *et al.* 2007b	0.05081	*Fagus sylvatica*	1.68	Steppe & Lemeur 2007
0.2123	*Fagus sylvatica*	≈1.76	Steppe *et al.* 2005	0.02978	*Quercus robur*	1.76	Steppe & Lemeur 2007
0.2123	*Fagus sylvatica*	≈1.76	Steppe & Lemeur 2007	0.00050	*Quercus ilex*	11.7	Salomón *et al.* 2017
0.9398	*Quercus robur*	≈1.68	Steppe & Lemeur 2007	0.00382	*Malus domestica*	2.56	Steppe *et al.* 2008
440	*Quercus mongolica*	19.1	Kobayashi & Tanaka 2001	0.02780	*Malus pumila*	6.5	Landsberg *et al.* 1976
120.9	*Quercus pubescens*	7.2-9.5	Zweifel *et al.* 2006				
314.51	*Quercus ilex*	11.7	Salomón *et al.* 2017				
2.15	*Quercus robur*	1.78	Baert *et al.* 2015				
1.556	*Malus domestica*	2.56	Steppe *et al.* 2008				

The importance of turgor in explaining xylem growth

To the best of our knowledge, our calibrations provide the first validation of turgor-driven growth mechanisms as a proxy for annual and intra-annual growth patterns. The weekly averaged daily growth rates of the xylem show good agreement with the xylogenesis observations, especially for *L. decidua* (mean R^2 of 0.7 and 0.5 for *L. decidua* and *P. abies*, respectively; Table 7.4). The model performed best at high elevations (S22 and S19) and under wet growing conditions (N13w; Figure 7.6a). The fact that turgor-driven cell enlargement processes can explain ring-width patterns is in agreement with xylogenesis observations (e.g., Cuny *et al.* 2014). However, the slight tendency for the model to overestimate the ring width (Figure 7.6a) could be explained by conditions of previous year (or "legacy effects"), where unfavourable environmental conditions reduced the number of cambial cells and affected the cambium division rate (Gregory & Wilson 1967). Additionally, the xylem vs. phloem cell production (see f_{growth} in Table 7.1), which currently is set as a fixed parameter, could change during the growing season (see Prislan *et al*. 2013; Gričar *et al*. 2016). The lower

intra-annual performance observed at lower elevational sites, with drier conditions (S16 and N13d; Figure 7.6a) indicates that we are lacking mechanisms that potentially maintain turgor pressure during a drought period. The current model uses a fixed initial osmotic potential (IT^{i}_{s}) and does not allow for changes due to dynamics of available sugars in the storage tissue. However, phloem osmotic potential has been shown to increase with decreasing soil water potential, due to the mobilization of sugars (Paljakka *et al.* 2017; Schönbeck *et al.* 2018), potentially increasing turgor pressure. Alternatively, dynamic changes in hydraulic parameters (e.g., C_{stem}) during droughts are lacking (e.g., Mencuccini *et al.* 2013; Baert *et al.* 2015; Salomón *et al.* 2017).

A mechanism which could be important to incorporate in the model is the variation in osmolality in the phloem (e.g., Lintunen *et al.* 2016), including the dynamic regulation of sugar production (photosynthesis), transport, loading and unloading (see Daudet *et al.* 2005; De Schepper & Steppe 2010). Additionally, at the beginning and the end of the growth period, R_s, followed by R_x, increased consistently between sites and species (Figure 7.5b; see Figure S7.7). This increase in R_s may well be cause by seasonal dynamics in osmolality, where the concentration of non-structural carbohydrates in the phloem is lower at the beginning and the end of the growing season, reducing the water flow to the storage tissue and reducing osmotic pressure (Simard *et al.* 2013; Martínez-Vilalta *et al.* 2016). Alternatively, hormonal signalling could lead to the observed patterns, where changing auxin concentrations alter cell differentiation in the cambium at the beginning and the end of the growing season (Drew *et al.* 2010; Steppe *et al.* 2015; Hartmann *et al.* 2017), forcing the modelled resistances for xylem water and storage water transport (R_x and R_s, respectively) to increase and reduce refilling of the storage tissue to increase turgidity. However, although these processes were not included, we still found a good relationship between simulated turgor-driven growth and ring-width patterns (Figure 7.6b).

Environmental regulation of turgor-driven growth

Our model allows for the direct comparison between turgor-driven growth and environmental conditions, including air temperature (T_a) and soil water potential (ψ_{soil}). The low probability of cell growth occurring below 2° C (15%; see Figure 7.7e) indicates a temperature threshold which is above the required photosynthetic minimum ≈0 °C (Saxe *et al.* 2001; Körner 2008). However, our value is lower than the ≈5° C determined by Körner (2008) and Rossi *et al.* (2008), which could be due to the higher temporal resolution provided with dendrometer measurements, or the refilling of the storage tissue after shrinkage in winter

(Zweifel & Häsler 2001). We find the latter less likely as most of our simulations start at the end of May when refilling of the storage tissue after winter shrinkage has been completed, especially for *P. abies*, which is hydraulically active before this time.

Stomatal conductance (expressed in crown conductance or g_c) is tightly linked to photosynthetic activity (Damour *et al.* 2010; Dewar *et al.* 2018). When considering the crown conductance derived from sap flow measurements, we find a higher probability for trees to conduct water at temperatures below 2 °C (43%; Figure 7.7e). These results suggest that photosynthesis starts at lower temperature than growth, as discussed by Fatichi *et al.* (2014; see Figure 7.7c), although independent photosynthetic measurements are so far lacking. Interestingly, growth rates appear to decrease above 11 °C, which is in disagreement with the apical meristem growth rates that decrease above ≈30 °C (Figure 7.7c). This 11 °C threshold can be explained by the high vapour pressure deficit (D) at these temperatures that prevents appropriate refilling and subsequently induces lower turgidity (see Figure S7.8), which does not occur in controlled experimental setups (see Parent *et al.* 2010). We also find a steeper decrease with ψ_{soil} in daily growth rates (Figure 7.7f) than crown conductance (Figure 7.7h), confirming the hypothesis stated by Fatichi *et al.* (2014; Figure 7.7d). Yet, the low probability of growth between -0.2 and -0.6 MPa (28%) and almost no growth occurring below -0.6 MPa (5%; see Figure 7.7f) suggest that other factors, like increased D during periods of drought, might have decreased the stem water potential and caused a stronger inhibition of growth than what we would expect from decreasing ψ_{soil} alone (see Muller *et al.* 2011).

Model limitations and implications

Although our model appears to provide appropriate growth patterns when using only ψ_{soil}, sap flow and dendrometer measurements (not requiring continuous ψ_{leaf} measurements), the lack of internal carbon dynamics enforces the use of a 7-day moving-window calibration approach. Although this limits the application of this model family for predictive purposes (often applied on periods ranging from 1-30 days; Steppe *et al.* 2005; Salomón *et al.* 2017), it does provide insight into the dynamic behaviour of the calibrated parameters (e.g., $C_{storage}$, R_x, R_s or Π^i_s). Additionally, the measurements could be repeated at sites with continuously monitored photosynthetic activity (i.e., obtained from flux tower measurements; Chu *et al.* 2017) to integrate water and carbon transport processes on a seasonal basis (e.g., De Schepper & Steppe 2010; Mencuccini *et al.* 2015). Moreover, to provide predictions on the future fate of carbon stored within woody biomass

(Cuny *et al.* 2015), cell wall thickening and other process-based models that define the wood anatomical structures (e.g., Vaganov *et al.* 2006; Drew *et al.* 2010; Hartmann *et al.* 2017) could be incorporated.

The 2 °C threshold and increased growth rate until 11 °C, found with the model, can provide a mechanistic explanation of why ring-width analysis of high-elevation conifers always find positive correlation with June-August temperatures (Peters *et al.* 2017), as this period shows a strong overlap with these T_a ranges (Figure 7.7a). Additionally, the positive correlations between ring width and June-August precipitation (affecting ψ_{soil}; Figure 7.7b) at lower elevations (Peters *et al.* 2017) correspond to conditions where turgor-driven growth is limited by low ψ_{soil} conditions (where it is highly unlikely for growth to occur after -0.6 MPa). As turgidity drives cell enlargement, which heavily dictates the ring width, this process should be considered in global growth models predicting future forest productivity (see Hayat *et al.* 2017). With the increase in the collection of data required for driving the mechanistic model presented in this study (e.g., sap flow data, Poyatos *et al.* 2016; flux tower measurements, Chu *et al.* 2017; tree rings measurements, Babst *et al.* 2017), its application on larger scales should become feasible. Isolating the key mechanisms and conditions under which environmental conditions are limiting should aid in further unravelling the source- vs. sink-limited growth debate and promote the paradigm shift in tree growth mechanisms (Körner 2015; White *et al.* 2016).

Acknowledgments

We thank Gregory King, Roger Köchli, Daniel Nievergelt, Kerstin Treydte and Anne Verstege for their aid in the extensive field- and labwork performed throughout the past years at the Lötschental transect. This work was funded by the Swiss National Science Foundation project LOTFOR (no. 150205).

Supporting information Chapter 7

Table S7.1 Overview of sites sampled for phloem thickness allometric relationships (presented in Figure S7.1).

Country	Site	Site code	(#)	Longitude	Latitude	Elevation (m a.s.l.)	*P. abies* (n)	*L. decidua* (n)
Switzerland	Lötschental	N13d	(1)	7.7613	46.3918	1300	11	11
		N13w	(2)	7.7639	46.3934	1300	7	7
		S16	(3)	7.7554	46.3972	1600	14	17
		S19	(4)	7.7459	46.4000	1900	12	16
		S22	(5)	7.7426	46.3996	2200	8	18
	Davos	D17	(6)	9.8823	46.7735	1750	37	0
		D18	(7)	9.8857	46.7732	1840	40	0
		D20	(8)	9.8902	46.7737	2050	7	28
	Sils Schadenherd	SIS	(9)	9.7326	46.4282	1870	0	31
Italy	San Vito di Cadore	SVC	(10)	12.2142	46.4514	1000	4	5
Slovenia	Kranjska Gora	KGO	(11)	13.7266	46.4454	1800	0	10
						Total (n)	140	143

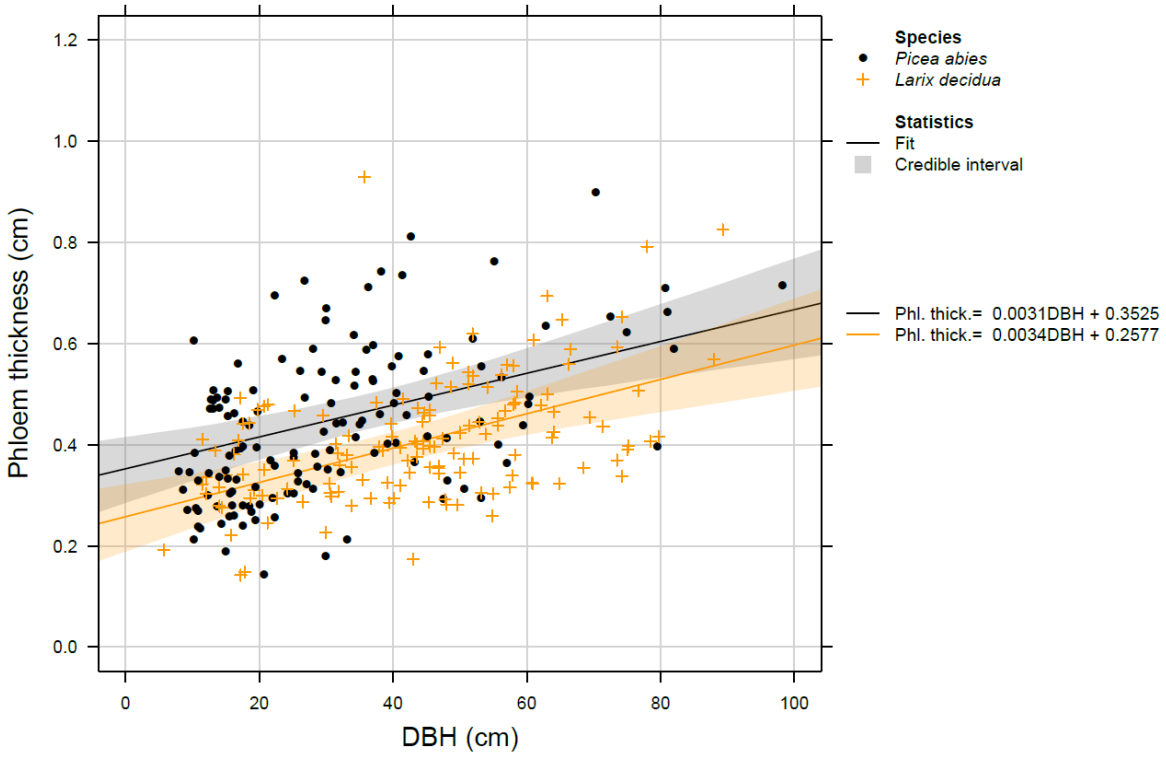

Table S7.1 Species-specific relationship between diameter at breast height (DBH) and phloem thickness. Significant positive linear relationships were found using mixed-effect models which included the site as a random factor. Data originates from 11 sites across the Alps, with a total of 140 individuals for *Picea abies* and 143 individuals for *Larix decidua*. Shaded areas presents the Bayesian credible interval of the fitted function (see Gelman & Hill 2007). For the metadata on sampled sites and statistics, see Table S7.1 and S7.2.

Table S7.2 Summary statistics of linear mixed-effect model applied on diameter at breast height (DBH) versus phloem thickness (presented in Figure S7.1). The applied model structure: Phloem thickness ~ Species * DBH + (DBH | Site), where fixed independent factors included DBH and species, where site is included as a random factor with a variable slope (dependent on DBH) and intercept. * indicates significant variables (*p <0.05*).

Variable	Coefficients	Standard error	Degrees of freedom	*p-value*	Conditional R^2	N
Intercept	0.25769	0.03448	17.63606	7.25E-07*	0.376	183
Species (*Picea*): intercept	0.09480	0.03579	193.28590	8.75E-03*		
DBH	0.00339	0.00074	12.34882	5.87E-04*		
Species (*Picea*): DBH	-0.00025	0.00081	189.22442	7.62E-01		

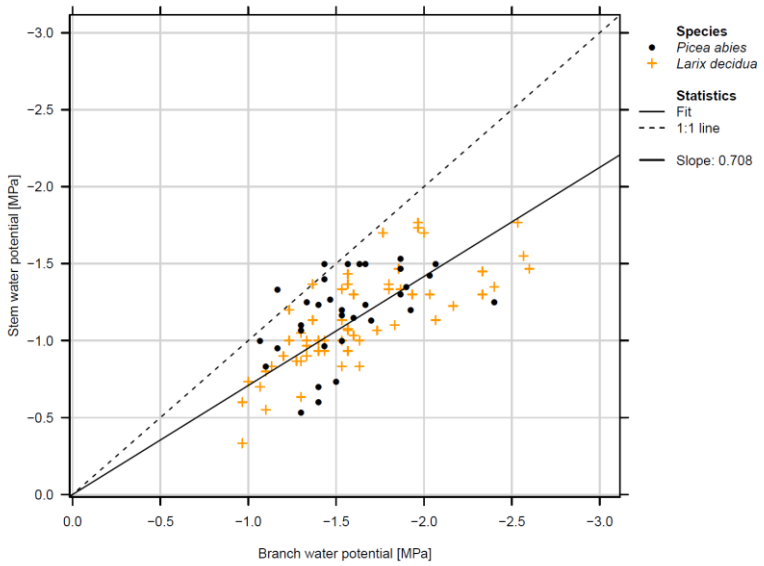

Figure S7.2 Species-specific relationship between branch and stem water potential. No species-specific difference was found (see Table S7.3) between *Picea abies* and *Larix decidua*, thus one linear relationship is presented with a slope of 0.708 MPa^{-1}.

Table S7.3 Summary statistics of linear mixed-effect model applied on stem water potential versus leaf water potential. The applied model structure: Stem water potential ~ Leaf water potential * Species + (Leaf water potential | Site), where fixed independent factors included leaf water potential and species, while site is included as a random factor with a variable slope (dependent on leaf water potential) and intercept. * indicates significant variables (*p <0.05*). No significant species-specific difference was found, therefore both species were compiled and a slope of 0.708 was calculated.

Variable	Coefficients	Standard error	Degrees of freedom	*p-value*	Conditional R^2	N
Intercept	0.17694	0.11977	77.34	0.144	0.574	89
Species (*Picea*): intercept	0.29185	0.23780	82.69	0.223		
Leaf water potential	0.58675	0.07192	37.52	7.78E-10*		
Species (*Picea*): Leaf water potential	-0.13294	0.14766	84.49	0.371		

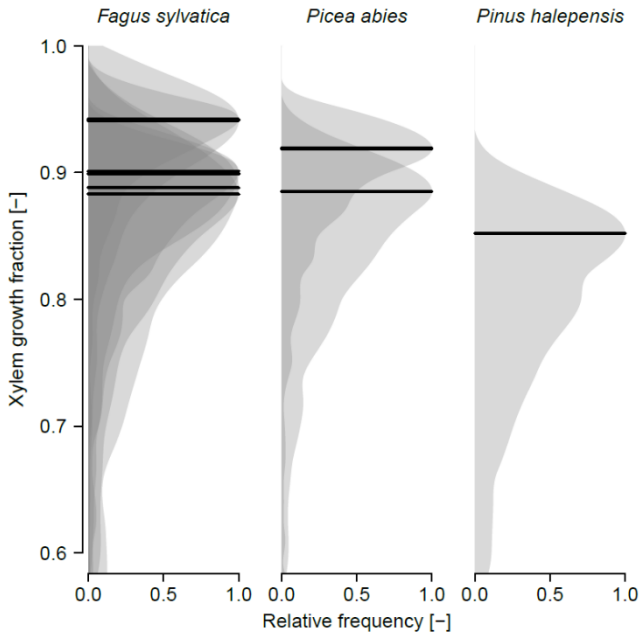

Figure S7.3 The xylem growth faction for three species obtained from literature. The xylem growth fraction was defined as the fraction of annual increment of xylem against the combined annual increment of the xylem and phloem. The mean and standard deviation for both the annual xylem and phloem size (in µm) were obtained from Gričar *et al.* (2016) and Prislan *et al.* (2013) and used within a bootstrap resampling (1000 times) to obtain histograms on the xylem growth fraction (where the mode is highlighted with a bold line).

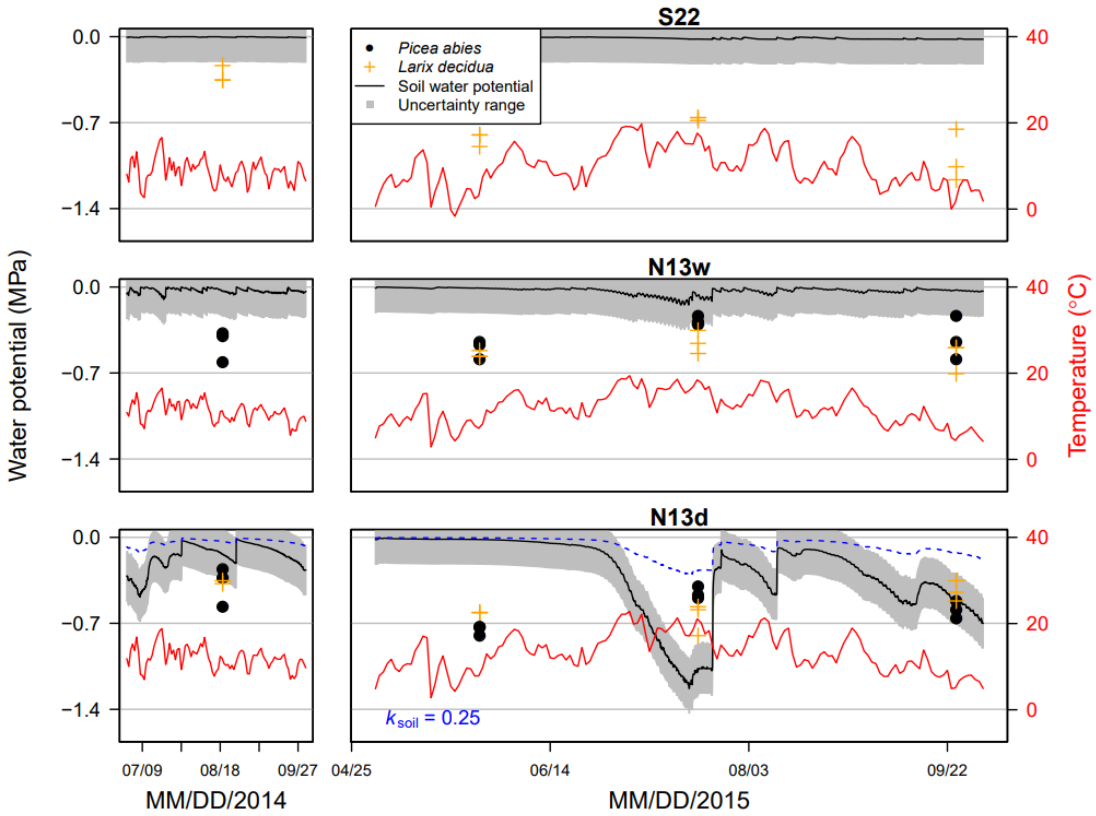

Figure S7.4 Comparison between pre-dawn leaf water potential collected during the diurnal campaigns (ψ_{leaf}; for *Picea abies* and *Larix decidua*) and soil water potential (ψ_{soil}; indicated with black lines) for S22, N13w and N13d. The standard deviation of all ψ_{leaf} (0.2 MPa) is imposed on ψ_{soil} to present the uncertainty range. Daily mean air temperature is present for all sites (in red). As ψ_{soil} at N13d lies below ψ_{leaf} during a drought period in 2015, ψ_{soil} is corrected by 0.25 (k_{soil}; indicated with the dashed blue line) to make the ψ_{leaf} fall within the uncertainty range. The other sites appeared to show little variation in ψ_{soil} and consistency with ψ_{leaf}, therefore a k_{soil} of 1 was applied (adopting the simple assumption that ψ_{root}= ψ_{soil}; see Verbeeck *et al.* 2007b).

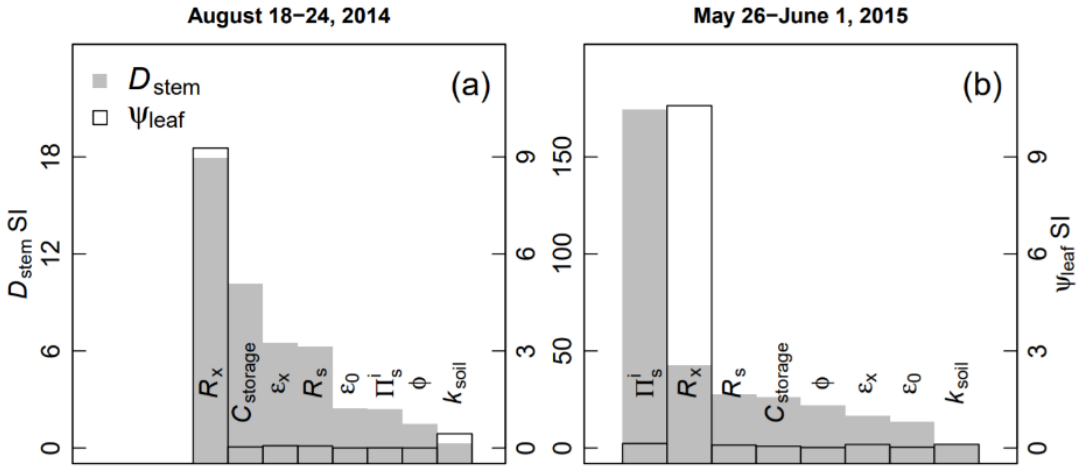

Figure S7.5 Example of a sensitivity analysis for *Picea abies* at N13w (N13WAd_S2) during a non-growth (a) and growth (b) period. The sensitivity index (SI) is provided for multiple parameters when considering dendrometer derived diameter variations (D_{stem}; left axis) and leaf water potential (ψ_{leaf}; right axis) as the target variable. See Table 7.1 for the description of the parameters.

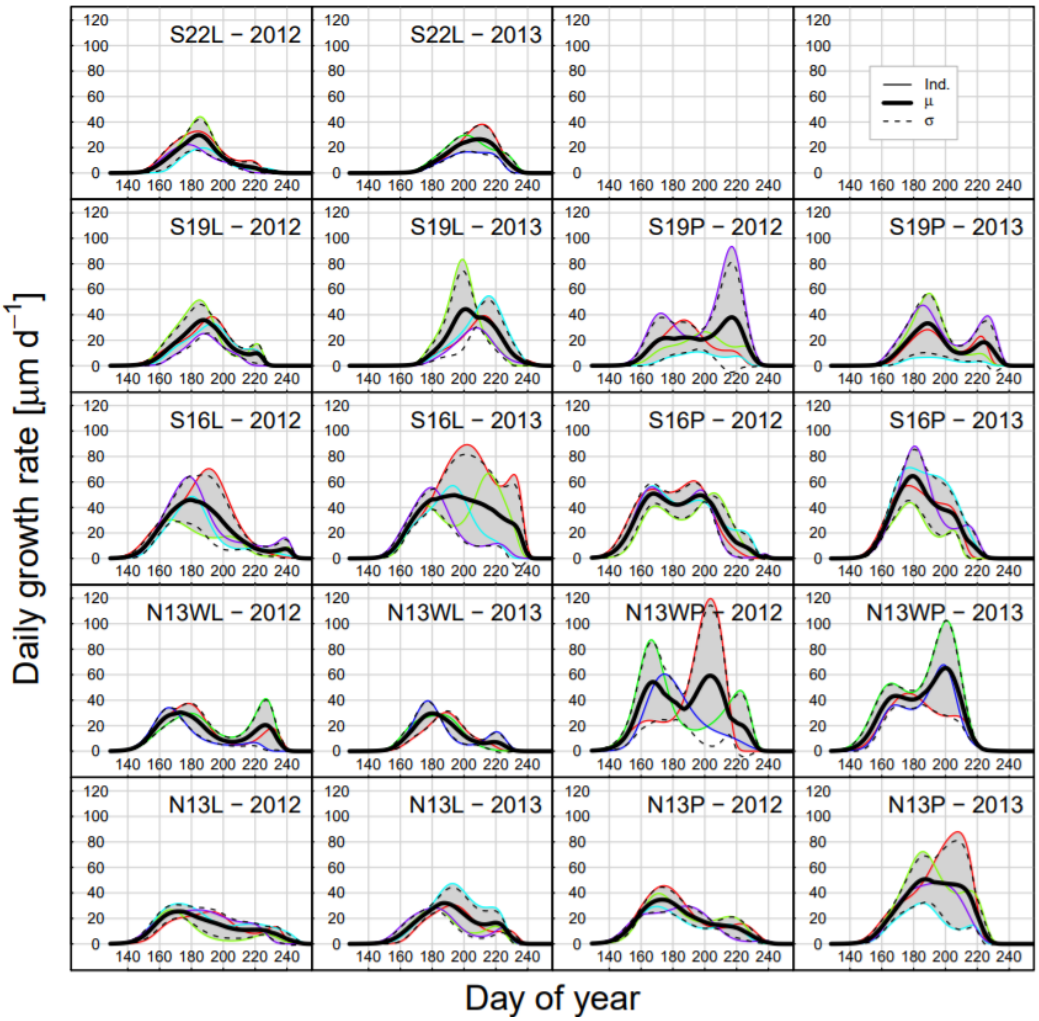

Figure S7.6 Daily growth rates for all sites and species for which xylogenesis observations have been performed in 2012 and 2013. The coloured lines show the daily xylem growth rates for each individual monitored. The bold black lines indicates the mean (μ) per site and species, while the dashed lines indicates the standard deviation (σ).

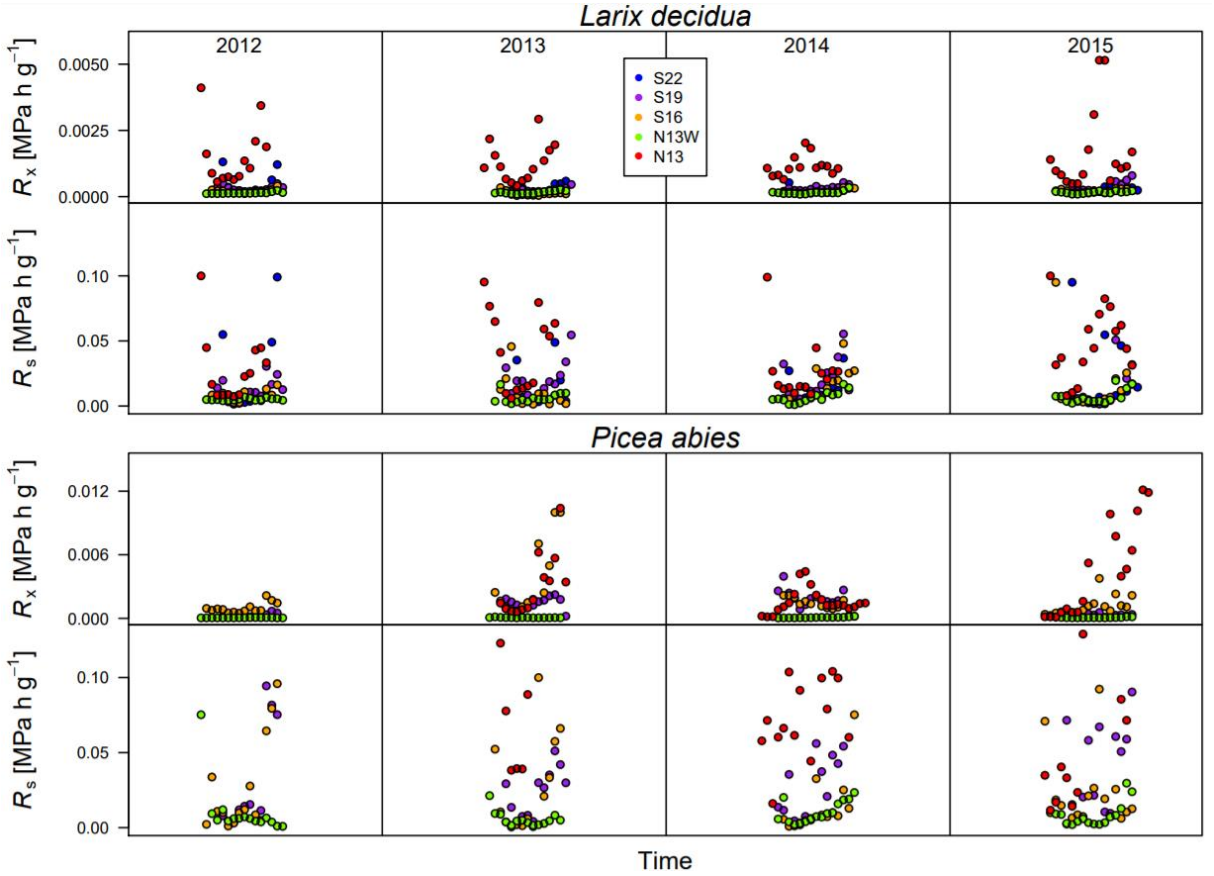

Figure S7.7 Raw outputs of calibrated R_x and R_s from the growing season calibrations for each site and species. A 7-day moving window, which progressively shifts by 3 days, provided R_x and R_s values every 3 days for each individual. These values were aggregated to weekly averages and the mean of those values per site and species are presented.

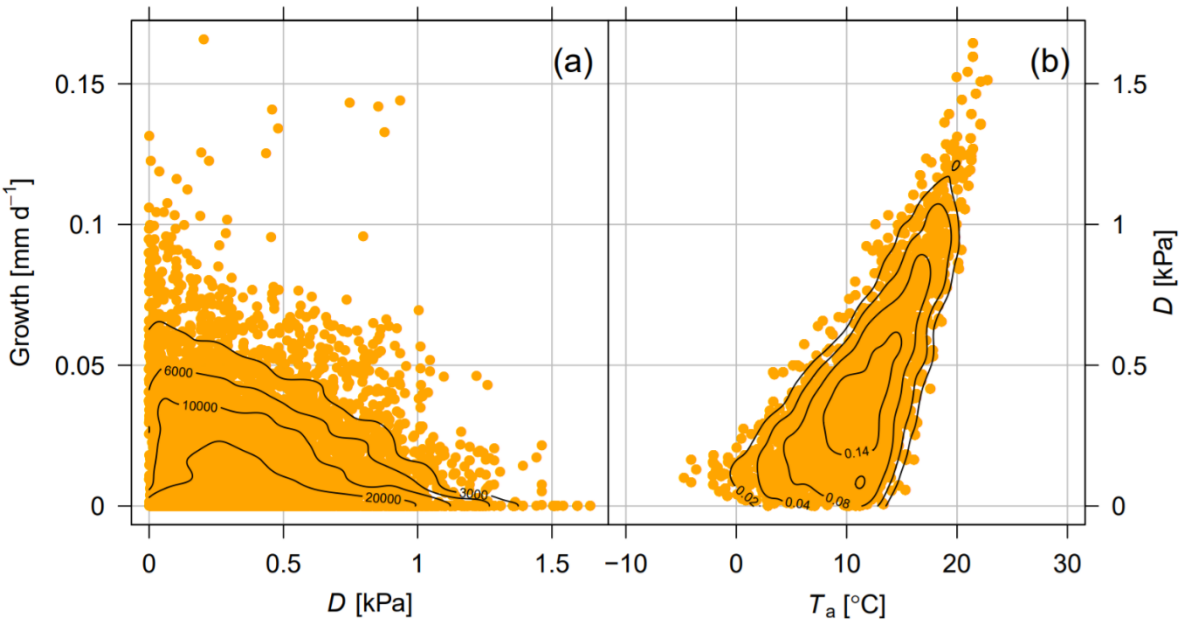

Figure S7.8 (a) Simulated growth rates against vapour pressure deficit (D) for both *Picea abies* and *Larix decidua* from all the sites in the Lötschental. (b) Relationship between D and air temperature (T_a) for all sites. For visual purposes density contours are provided.

Note S7.1 Mathematical equations and components of the growth model.

Water transport model

1. Soil water potential

$\psi_{roots} = k_{soil} * \psi_{soil}$

2. Osmotic water potential of the stem storage compartment

$\psi_{storage} = \psi^{P}_{s} - \Pi^{P}_{s}$

3. Vertical water transport between the soil and the stem

$F_{stem} = (\psi_{soil} - \psi_{stem}) / R_{x}$

4. Radial water exchange between the xylem and the stem storage compartment

$f_{stem} = (\psi_{stem} - \psi_{storage}) / R_{s}$

Stem diameter model

1. Diameters are calculated from the changed volumes

$D^{x}_{stem} = \sqrt{} (R_{hw} * 2 * R_{hw} * 2 + 4 * V^{x}_{stem} / (\pi * l_{stem}))$

$D_{stem} = \sqrt{} (D^{x}_{stem} * D^{x}_{stem} + 4 * V^{s}_{stem} / (\pi * l_{stem}))$

2. Diameter growth by the xylem only

$D^{x}_{growth} = \sqrt{} (R_{hw} * 2 * R_{hw} * 2 + 4 * (\pi * l_{stem} * ((((D^{i}_{stem} - 2 * (d_{s})) / 2) * ((D^{i}_{stem} – 2 * (d_{s})) / 2)) – (R_{hw} * R_{hw})) + V^{x}_{growth}) / (\pi * l_{stem}))$

3. Change in water content

$dW^{s}_{stem} / dt = f_{stem}$

$dW^{x}_{stem} / dt = F_{stem} - F_{crown} - f_{stem}$

4. Change in xylem pressure potential due to change in dimension

$d\psi_{stem} / dt = \mathcal{E}_{x} / W^{x}_{stem} * (dW^{x}_{stem} / dt)$

5. Leaf water potential calculation

$\psi_{leaf} = \psi_{stem} / k_{leaf}$

6. Elastic modulus

$\mathcal{E}_{s} = \mathcal{E}_{0} * \psi^{P}_{s} * D_{stem}$

7. Change in storage pressure potential

if (($\psi^{P}_{s} > \Gamma$)){

Turgor pressure changes due to elastic changes and growth

$d\psi^{P}_{s} / dt = \mathcal{E}_{s} / W^{s}_{stem} * (dW^{s}_{stem} / dt) - \mathcal{E}_{s} * \pi * (\psi^{P}_{s} – \Gamma)$

Changes in total water potential of the stem storage compartment via capacitance C

$dV^{s}_{growth} / dt = \phi * (\psi^{P}_{s} – \Gamma) * W^{s}_{stem} / \rho_{w}$

$d\Pi^{P}_{s} / dt = 0$

}else{

Pressure changes due to elastic changes only

$d\psi^{P}_{s} / dt = \mathcal{E}_{s} / W^{s}_{stem} * (dW^{s}_{stem} / dt)$

$dV^{s}_{growth} / dt = 0$

$d\Pi^{P}_{s} / dt = (d\psi^{P}_{s} / dt) - W^{s}_{stem} / C_{storage}$ }

8. Volume changes and growth component

$dV^{s}_{stem} / dt = (dW^{s}_{stem} / dt) / \rho_{w} - f_{growth} * (dV^{s}_{growth} / dt)$

$dV^{x}_{stem} / dt = (dW^{x}_{stem} / dt) / \rho_{w} + f_{growth} * (dV^{s}_{growth} / dt)$

$dV^{x}_{growth} / dt = f_{growth} * (dV^{s}_{growth} / dt)$

Constant

ρ_w, desnity of water [g m^{-3}]

Parameters

D^i_{stem}, initial stem diameter (including xylem and phloem) [m]

l_{stem}, length of the stem segment to the crown [m]

d_s, thickness of the stem storage tissue (bark, excluding non-living bark) [m]

R_{hw}, radius of the heartwood [m]

$C_{storage}$, stem capacitance [g MPa^{-1}]

R_x, flow resistance in the xylem compartment [MPa h g^{-1}]

R_s, exchange resistance between the stem and storage tissue [MPa h g^{-1}]

f_{water}, water fraction in the stem compartment [-]

$\mathcal{E}_0$, proportionality constant [m^{-1}]

$\mathcal{E}_x$, elastic modulus of the xylem [MPa]

ϕ, extensibility of cell walls in relation to non-reversible dimensional changes [MPa^{-1} h^{-1}]

Γ, critical pressure which must be exceeded to produce growth [MPa]

f_{growth}, fraction of growth contributing to xylem formation [-]

k_{leaf}, the fraction of leaf versus stem water potential [-]

k_{soil}, the fraction between ψ_{soil} and ψ_{roots} [-]

Data variables

F_{crown}, water flow from the stem xylem towards the crown compartment (sap flow) [g h^{-1}]

ψ_{soil}, soil water potential (measurements) [MPa]

D_{stem}, over bark diameter (dendrometer) [m]

Algebraic variables

f_{stem}, water exchange between the xylem and the storage compartment [g h^{-1}]

F_{stem}, water flow from the roots towards the stem xylem compartment [g h^{-1}]

D^x_{stem}, xylem diameter of the stem segment [m]

D_{stem}, outer diameter of the stem [m]

$\mathcal{E}_s$, bulk elastic modulus of living tissue in relation to reversible dimensional changes [MPa]

ψ_{soil}, soil water potential [MPa]

$\psi_{storage}$, water potential in the storage compartment [MPa]

ψ_{leaf}, leaf water potential [MPa]

D^x_{growth}, irreversible growth of the xylem tissue [m]

Derived variables

W^x_{stem}, water content in the stem xylem compartment [g]

W^s_{stem}, water content in the stem storage compartment [g]

ψ_{stem}, pressure component of the xylem water potential [MPa]

ψ^P_s, pressure component of the water potential in the storage compartment [MPa]

V^x_{stem}, volume of the xylem stem tissue [m^3]

V^s_{stem}, volume of the stem storage compartment [m^3]

V^s_{growth}, growth volume for the entire stem [m^3]

Π^P_s, osmotic component of the water potential in the storage compartment [MPa]

V^x_{growth}, growth volume for the xylem [m^3]

Note S7.2 Model calibration and sensitivity and identifiability analysis.

All simulations were conducted with a fourth-order fixed step size integrator (step size = 1 second). Two different types of model calibrations were used for different subsets of trees. First calibrations were performed for the measurements in 2015 for 7-day periods where ψ_{leaf} was measured (at N13d, N13w and S22). Second, a moving-window calibration was applied on 4 growing seasons for all trees with less calibration parameters. The 2015 calibrations were performed to analyse site-specific differences and temporal variability of hydraulic parameters, using the simplex method (accuracy of $1*10^{-5}$ and $1*10^{6}$ maximum evaluations) to minimize the weighted sum of squared errors (SSE) for D_{stem} and ψ_{leaf} (with an objective weight of $1*10^{-5}$ m and 0.2 MPa respectively; see De Pauw *et al.* 2008). All calibration used a starting time of 07:00 CET to ensure that the storage tissue was fully refilled (using initial parameter values presented in Table 7.1). Sensitivity and identifiability analyses were performed to check what subset of model parameters was both sensitive enough and not collinear (as described by De Pauw *et al.* 2008). For the successful calibrations, R_x, $C_{storage}$, Π^i_s and R_s were calibrated within a specified range (provided in Table 7.1), while non-calibrated model parameters were directly measured or assigned from literature (see Table 7.1 for detailed parameter selection).

The calibrated parameter values were analysed for absolute values and temporal patterns between species and sites. For inter-tree comparison we standardized $C_{storage}$ for the volume of the storage tissue, while R_x was recalculated to present the resistivity (using A_{sap} and l_{stem}; see Table 7.2). Additionally, an analysis was performed to test the effect of fixing either $C_{storage}$ or R_x, as these show strong collinearity when no ψ_{leaf} measurements are available for calibration. For the diurnal campaign in 2014 the final predicted error (FPE; see Steppe *et al.* 2005) was calculated for the resulting fit with D_{stem}:

$$FPE = \frac{SSE}{N} + \frac{2pSSE}{(N-p)N} \quad \text{(Eq. 1)}$$

where N is the number of measurements and p is the number of estimated parameters. Normalized final prediction error (FPE) of four tested models with fixed (fix.) or calibrated (cal.) R_x and/or $C_{storage}$ was used to compare model performance, while penalizes for over-parametrized models. The values were normalized to the FPE where both parameter were calibrated. Additionally, the simulated ψ_{leaf} was compared to actually measurements, calculating SSE.

The growing-season calibrations were run from 2012 till 2015 with fixed $C_{storage}$ (dependent on storage tissue volume) and Π^i_s (≈1.3 MPa). The calibrations (of R_x and R_s) were performed with a 7-day moving window approach from May till August. The moving window shifts forward while providing a three day overlap with the previous calibration (to prevent spurious end-effects of the simulated parameters), using both initial conditions and parameters (of R_s and R_x) from the previous calibration.

Note S7.3 Model performance when fixing of $C_{storage}$ or R_x.

As leaf water potential (ψ_{leaf}) measurements are not available for all years, the effect of fixing standardized $C_{storage}$ or R_x was tested on the FPE with D_{stem} and SSE with ψ_{leaf} (Figure 7.3.1a, b). When calibrating both parameters, a FPE of $7.01*10^{-10}\pm4.24*10^{-10}$ and SSE of 3.80±2.76 were found across sites and species. After normalization, the FPE showed consistent lower values when fixing $C_{storage}$ (*L. decidua*= 0.0152 g MPa^{-1} cm^{-3} * $V_{storage}$; *P. abies* 0.0263 g MPa^{-1} cm^{-3} * $V_{storage}$) compared to fixing R_x (*L. decidua*= 0.0001 MPa h g^{-1} cm^{-1} * A_{sap}/l_{stem}; *P. abies*$_{N13d}$= 0.0014 MPa h g^{-1} cm^{-1} * A_{sap}/l_{stem}; *P. abies*$_{N13w}$= 0.0003 MPa h g^{-1} cm^{-1} * A_{sap}/l_{stem}), or both parameters (Figure 7.3.1a). Calibrations without using ψ_{leaf}, showed that normalized SSE was lowest when solely fixing the volume standardized $C_{storage}$. These results support the choice to fix $C_{storage}$ values for the growing-season calibrations.

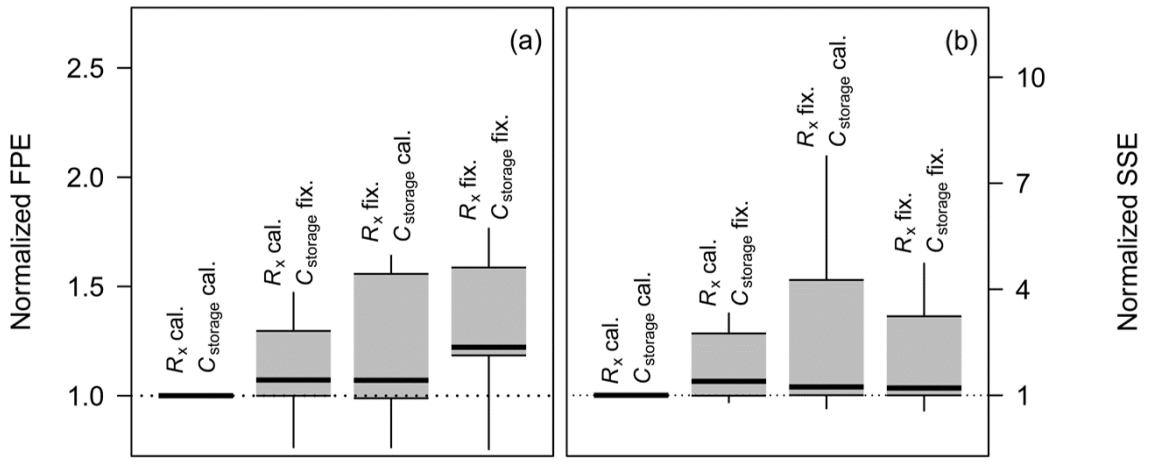

Figure S7.3.1 Boxplots of differences in model performance when fixing parameters. (a) Comparison of model performance for the period from 18-24 August 2014 between four tested models with fixed (fix.) or calibrated (cal.) R_x and/or $C_{storage}$. Normalized final prediction error (FPE) was determined with diameter variation observation from the dendrometer (D_{stem}) and penalized for over-parametrized models. (b) Weighted sum of squared errors (SSE) between simulated and measured leaf water potential (ψ_{leaf}) after calibrating the model to solely D_{stem} for the period from the 18-24 August 2014. SSE was normalized for the models where R_x and $C_{storage}$ were calibrated and presented.

Note S7.4 Description of anatomical measurements.

The potential hydraulic conductivity is determined for each tracheid in the earlywood (Mork's index <1). The average for all measurement taken in 2012 and 2013 was used to calculate the conductivity difference between the species.

1. The hydraulic conductivity of a tracheid

$K_h = (\rho_w * C_a * m) / (v * k)$

2. Hydraulic radius of the selected tracheid

$m = (\pi * \alpha * \beta) / (2 * \pi * \sqrt{} (0.5 * (\alpha^2 + \beta^2)))$

3. Properties of the tracheid

$\alpha = \sqrt{} (C_a * A_c / \pi)$

$\beta = \alpha / A_c$

$k = 4 / (1 + \sqrt{} (1 - \varepsilon^4))$

$\varepsilon = \sqrt{} (\alpha^2 - \beta^2) / \alpha$

Algebraic variables

K_h, potential hydraulic conductivity [kg MPa^{-1} s^{-1}]

α, largest radius [µm]

β, smallest radius [µm]

m, mean hydraulic radius [µm]

k, coefficient depending on the geometry of the cell [-]

ε, eccentricity of the ellipse [-]

Constant

ρ_w, density of water [kg m^{-3}] (998.2 kg m^{-3} at 20 °C)

v, viscosity of water [Pa s] (0.001002 Pa s at 20 °C)

Data variables

C_a, cell size [μm^2]

A_c, aspect of the cell as the ratio between major and minor axis of an ellipse equivalent to the tracheid [-]

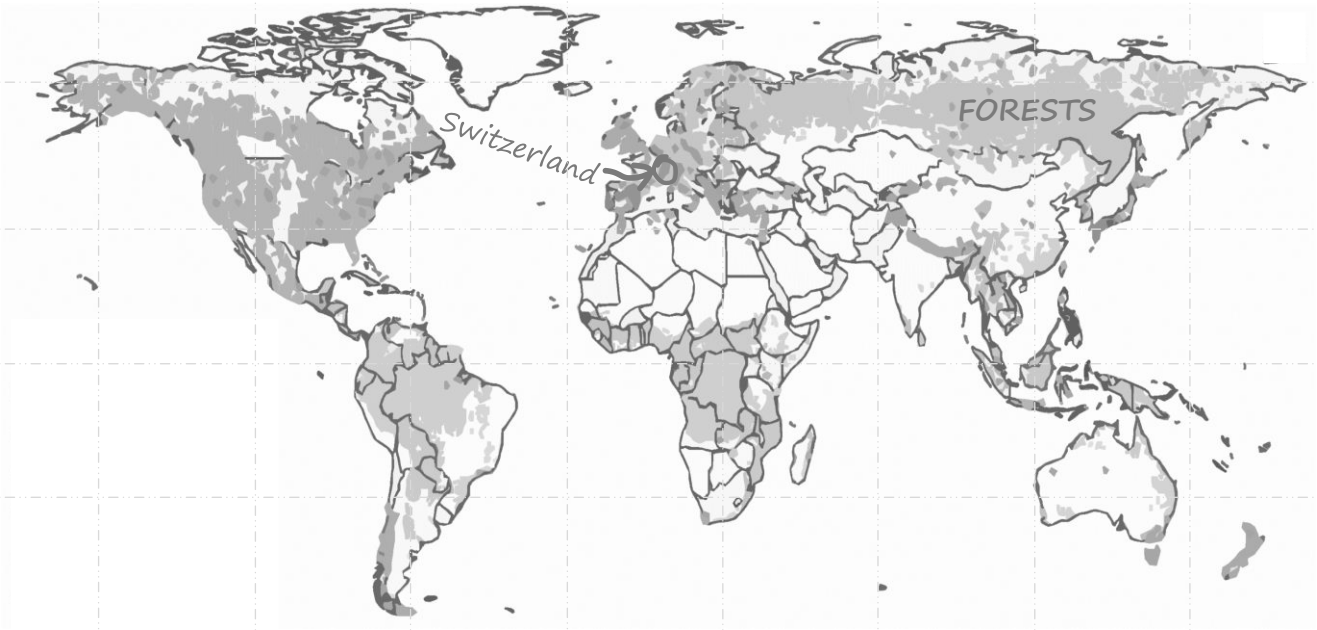
Switzerland
FORESTS

Chapter 8

General discussion

Richard L. Peters

Conifers show a biogeographical distribution across a wide range of contrasting environmental conditions, stretching from the Arctic Circle to the equator and Southern Hemisphere (Farjon & Filer 2014). The extent of the conifer distribution is highlighted within mountainous ecosystems, where they can dominate at high elevations where temperatures severely limit tree growth and survival (Bannister & Neuner 2001; Körner 2012). Conifers growing at sites with temperature limiting conditions are highly sensitive to ongoing climatic change, where warmer and drier conditions will impact their growth, the duration of the vegetative season and subsequently their distribution (Beniston 2003; Soja *et al.* 2007; Thuiller *et al.* 2008; Steltzer & Post 2009). Developing an in-depth understanding on how high-elevation conifers respond to these changes in climate is critical, as they play a role in regulating terrestrial carbon storage (i.e., facilitated by the formation of woody tissue) and water balance within the ecosystem (i.e., by releasing water to the atmosphere via transpiration; Bonan *et al.* 2008).

An interesting property of mountainous ecosystems is the steep contrast in thermal growing conditions, where trees at the treeline are exposed to mean growing season temperatures as low as 5.5 to 7.5 °C (Körner & Paulsen 2004). Decreasing growing season temperatures with increasing elevation provide a unique experimental setup to analyse the tree physiological responses (i.e., wood formation and transpiration dynamics) to warmer climatic conditions (Körner *et al.* 2007). This is particularly relevant when trying to understand how a warmer climate affects wood formation and the ability of conifer species to acclimate their water use accordingly (e.g., Cuny *et al.* 2015; Grossiord *et al.* 2017). A more critical question is which process is limiting and therefore regulating growth dynamics, as models focussing on the production of sugars (via photosynthesis) as the key driver of growth do not appear to produce appropriate predictions of current forest productivity (see Fatichi *et al.* 2014). Combining physiological measurements from an elevational gradient and assessing post-photosynthetic growth mechanisms, such as internal tree hydraulics, is thus crucial to better understand wood formation dynamics (Fonti & Jansen 2012; Steppe *et al.* 2015).

In this thesis I aimed at developing a better mechanistic understanding of how climate affects wood formation dynamics and subsequently shapes tree rings of high-elevation conifers. We studied the growth and transpiration dynamics of *Larix decidua* Mill. and *Picea abies* (L.) Karst. in the Lötschental (Switzerland) in the context of increasing temperature and water scarcity, and combined these processes in a mechanistic growth model. In CHAPTER 2 of this thesis, we assessed more than 150 years of inter-annual growth dynamics (derived from tree

rings) along an elevational gradient in relation to temperature, precipitation and insect activity and showed their impact on forest biomass accumulation. In CHAPTER 3 we developed an algorithm to spatially orient the water conducting cells in conifer wood (tracheids within the xylem) and process large quantities of wood anatomical measurements. In CHAPTER 4 we used cellular-based monitoring of wood formation across an 8 °C thermal gradient to investigate intra-annual dynamics in both xylem cell enlargement dynamics and cell wall thickening in relation to environmental conditions. This analysis included over 7 years of wood anatomical measurements collected from two elevational transects, including the Lötschental and the Vosges Mountains (France). In CHAPTER 5 we quantified the uncertainties generated by commonly applied data processing for sap flow measurement collected from conifers with thermal dissipation probes. The study included a detailed analysis on four years of sap flow measurements collected in the Lötschental, after which the uncertainty was projected on sap flow data collected across the Northern Hemisphere. CHAPTER 6 addressed the transpiration plasticity of *L. decidua* and *P. abies* in the Lötschental across elevations. Transpiration dynamics were addressed by calculating stomatal conductance derived from sap flow measurements. Finally, CHAPTER 7 demonstrated the ability of mechanistic whole-tree models, using turgor-driven growth dynamics, to explain inter- and intra-annual growth dynamics in high-elevation conifers.

In this chapter I discuss the main findings described in this thesis and their consequences. Finally, I provide an outlook for future research on tree hydraulics, wood formation and the integration of these fields.

8.1 Tree growth at high elevations: from biomass to anatomy

Analysing how climate affects tree growth at high elevations requires measurements on annual and intra-annual growth, frequently obtained from tree rings and xylem formation observations, respectively. Tree-ring width is a widely used measure to understand the effects of climate on annual tree growth (Babst *et al*. 2017). As such, tree rings have been used to provide annually resolved climate reconstructions over several thousands of years (e.g., Reinig *et al*. 2018). On a Northern Hemisphere scale, tree rings from different conifer genera have been collected, where *Pinus*, *Picea*, *Pseudotsuga*, *Abies* and *Larix* dominate the records (Figure 8.1a). The large quantity of conifer tree-ring chronologies that have been

established for high elevations (i.e., close to the treeline) and latitudes illustrates the great effort in attempting to understand temperature-limited growth patterns (Figure 8.1b). Studies on high-elevation forests in Europe have shown an increase in tree growth in the recent decades (e.g., Rolland *et al*. 1998; Büntgen *et al*. 2008). As tree-ring width variability at these locations is driven by growing season temperatures (Büntgen *et al*. 2007; Babst *et al*. 2013), the increase has been attributed to more favourable growing conditions due to the recent warming. In CHAPTER 2 we also found that *L. decidua* and *P. abies* showed an increased growth at higher elevations in recent decades. Considering the inter-annual variability in ring width, greater ring widths were observed for years with warmer mean summer temperatures, especially at the upper elevation sites (1900 and 2200 m a.s.l.). Yet, at lower elevation (1300 m a.s.l.) both species showed a negative relationship with summer temperature, where *P. abies*' ring width appeared to respond positively to previous year and current year summer precipitation. These results confirm that conifers at higher elevations will most likely benefit from increasing temperature, while at lower elevations drought stress might become an issue for productivity, especially for *P. abies* (see Frank & Esper 2005; King *et al*. 2013b). The increased growth at higher elevations could have implications for the distribution of the species as higher forest productivity could allow the species to migrate to higher elevations (e.g., Meier *et al*. 2012), although this also depends on other factors, including the increased survival probability of juvenile trees (see Körner 2012).

Tree-ring series have been mainly used for studying climate-growth relationships, although this growth proxy has greater potential if the measurements are complemented with metadata and other global data products, including biometric properties of the trees or satellite derived net primary productivity (Babst *et al.* 2014c; Babst *et al.* 2017). For example, tree rings show great potential in reconstructing aboveground biomass over large time scales, which could be of great value in understanding the temporal variability of the forest carbon pool (Babst *et al.* 2014b; Klesse *et al.* 2016). To obtain appropriate forest biomass estimates, one needs information on tree size and height and an appropriate sampling design (Nehrbass-Ahles *et al*. 2014). Within the Lötschental the biomass reconstruction with tree rings confirms that aboveground biomass increment has increased in the last decades, especially at higher elevations (see Figure 2.2 in CHAPTER 2). Although warmer growing season temperatures play a role, the growth increase was more apparent for *L. decidua*, which was frequently defoliated by larch budmoth outbreaks (*Zeiraphera diniana* Guénée;

see Esper *et al.* 2007) in the past. Our analysis revealed that the recent outbreak absence, possibly induced by climate change (Johnson *et al.* 2010), is a crucial factor in explaining the recent biomass trends, next to climate. These results showed that besides the appropriate use of statistical methods to disentangle long-term growth trends from biological trends related to the size/age of the individuals (Peters *et al.* 2015), biotic drivers such as insect outbreak activity and their interaction with climate should be included when assessing future productivity and carbon sink capacity of forests. This is especially relevant, as many phytophagous insects show increased activity associated with shifts in distribution range (Battisti 2008), improved breeding and growing conditions (Pasztor *et al.* 2014) and increased frequencies and magnitude of outbreaks (Creeden *et al.* 2014).

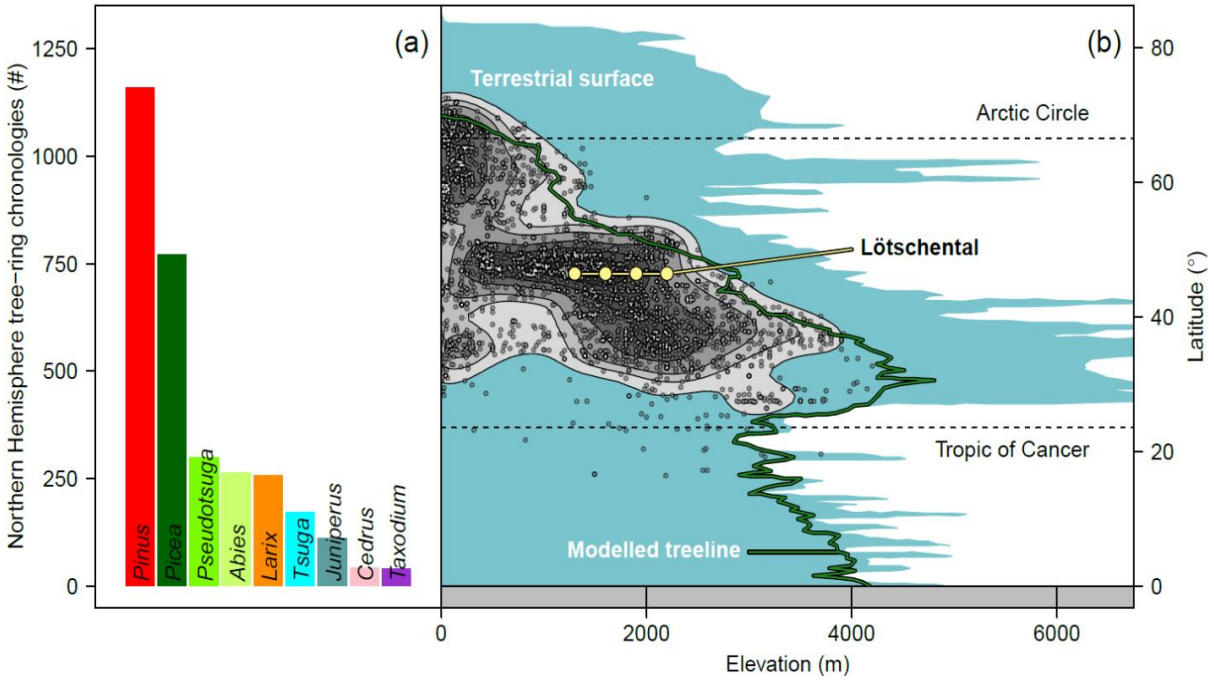

Figure 8.1 Overview of conifer tree-ring chronologies established for the Northern Hemisphere. (a) Number of chronologies per conifer genera. (b) Distribution of sampling locations across elevation and latitude (grey dots). The density contours of the chronology distribution is provided, where darker colours show areas with larger sample sizes. The maximum elevation of the terrestrial surface across latitudes is provide (blue area), in addition to the position of the treeline across latitudes where temperature would support tree growth (≥100 days with air temperature ≥6.5 °C; green lines). The Lötschental sampling sites presented in CHAPTER 2 are included (yellow dots). The data on the chronologies is obtained from Babst *et al.* (2017), while the terrestrial surface and modelled treeline was derived from Körner (2012).

The annual growth variability, as derived from tree rings, represents the integrated signal of the complete growing season, often not considering the intra-annual building block within the tree ring, i.e., the xylem cells. However, knowledge on the wood formation at seasonal and finer timescales is needed to bridge the gap between tree physiological responses and tree-ring width (Fonti & Jansen 2012). Recording xylem formation (or xylogenesis), using (bi-)weekly wood anatomical observations to quantify dividing cambial cells and xylem cells in the enlargement and cell wall thickening phase, has been crucial for bridging this gap (Cuny *et al.* 2014; Rathgeber *et al.* 2016). Multiple studies have focussed on timing the beginning, end, and duration of cambial activity and the wood formation season in relation to the environment (Rossi *et al.* 2008; Deslauriers *et al.* 2008). Strong plasticity of these properties was found in response to temperature, where the growing season is shorter in colder environments due to a later start and earlier ending of wood formation. Yet, recent developments show that high-resolution enlargement and cell wall thickening dynamics (i.e., rate and duration) can be obtained by combining xylogenesis observation with wood anatomical measurements (see CHAPTER 3 about the processing of large quantities of wood anatomical measurements and CHAPTER 4 about the combination of these measurements with xylogenesis observations). Such observations have provided valuable insights into the delay between the enlargement of xylem cells and the deposition of cell wall materials (Cuny *et al.* 2015). In the Lötschental, such analysis revealed that although initial cell division starts later at high elevations, trees growing at higher elevation sites initiate cambial activity at colder temperatures than those growing at lower elevations (see Figure 4.2 in CHAPTER 4).

This acclimation to initial growth conditions could be a key mechanism to extend the trees' growing season, although the underlying mechanism driving the acclimation remains unclear. Additionally, the rate of cell enlargement and wall thickening decreases towards colder sites while the duration increases (see Figure 4.3 in CHAPTER 4). The increased duration most likely compensates for the lower enlargement rate and results in a similar anatomical structure, which is crucial for maintaining large xylem cells which can transport water efficiently (see Figure 4.6 in CHAPTER 4; e.g., Sutera & Skalak 1993). Although labour intensive, these measurements are essential for understanding ring width and wood structure, and provide valuable validation for growth modelling purposes (as done in CHAPTER 7).

8.2 Tree water use under warmer conditions: what can sap flow tell us?

The production of carbohydrates and generation of turgidity within the cambium to initiate growth are tightly linked to the way a tree regulates the flow of water through the soil-plant-atmosphere continuum. Tree hydraulic functioning has received great attention in literature, where environmental responses of multiple components within the tree's hydraulic architecture have been analysed. Woody plants show a large variety of xylem anatomical structures, which aid in the effective transportation of water to the crown under different environmental conditions (Anderegg & Meinzer 2015). Special attention has been given to the efficiency at which the xylem architecture aids in preventing cavitations within xylem conduits, which hamper the transport of water to the crown (Meinzer *et al.* 2009; Bouche *et al.* 2014). Additionally, trees are able to use water from different compartments, such as bark tissue (Zweifel *et al.* 2001), to provide additional water when the atmospheric demand for water is high (i.e., during drought events). Multiple studies have thus focussed on the dynamics of the storage water capacity, which can provide information on species-specific strategies to optimize hydraulic performance under varying climatic conditions (e.g., King *et al.* 2013a; Matheny *et al.* 2015; Dietrich *et al.* 2018). Moreover, the regulation of stomatal conductance (g_s) under different environmental conditions is a key mechanism for plants to optimize the exchange of water to the atmosphere with the fixation of carbon for photosynthesis (Nobel 2009). Interestingly, sap flow measurements can be used to derive g_s (Ewers & Oren 2000) and analyse the stomatal behaviour against vapour pressure deficit (D), air temperature (T_a), solar irradiance (R_g) and soil water potential (ψ_{soil}) in order to define the hydraulic operational space. Yet, this application requires appropriate data processing of raw sap flow measurements to reduce uncertainties.

The development of heat-based sap flow methods applied at the tree-stem level provides valuable information on whole-tree water use across a wide range of spatiotemporal scales (Poyatos *et al.* 2016). The thermal dissipation method (TDM) is, and most likely will continue to be, a widely applied sap flow measurement method (Granier 1985), which estimates the sap flux density (F_d) in the water-conducting xylem on sub-hourly timescales. To calculate F_d from the temperature difference between a heated and reference probes inserted into the stem (expressed as ΔT), a large variety of different data-processing techniques have been proposed (see Figure 5.1 in CHAPTER 5). Three important steps in

data processing include: defining conditions with zero flow (to determine the relative temperature difference expressed in *K*; Rabbel *et al*. 2016), dealing with signal dampening over time (Wiedemann *et al.* 2016) and selecting the appropriate calibration curve (the relationship between *K* and F_d; Steppe *et al.* 2010). Yet, a systematic quantification on the impact of the different combinations of data processing on TDM sap flow data is lacking.

For TDM measurements collected from conifers across the Northern Hemisphere (18 sites; including the Lötschental), the large variety of available calibration curves creates a large uncertainty in F_d calculations, which is amplified by different zero-flow condition calculations (see Figure 5.7 in CHAPTER 5). Additionally, the determination of zero-flow conditions and the absence of a dampening correction affects the inter-daily variability, which is often of interest when analysing the climate-water use relationship and inter-specific sap flow responses (e.g., Poyatos *et al.* 2005; Brinkmann *et al.* 2016). Although CHAPTER 5 proposes a novel empirical approach to deal with signal dampening, which is likely caused by wound reactions (Marañón-Jiménez *et al.* 2017), there is a clear need for a better mechanistic understanding of wound reactions (see Wiedemann *et al.* 2016). Additionally, the large variation in calibration curves (see Figure 5.4 in CHAPTER 5) highlights our poor understanding of how wood properties affect the heat dissipation. However, I anticipate a strong relationship between wood density and steepness of the calibration curve, which could partially explain this large deviation (e.g., smaller or wider rings that have specific anatomical features; see Figure 8.2). Additionally, we should investigate whether cut-segment calibration experiments can mimic sap flow conditions occurring *in situ*, using either gravitational force or suction (e.g., Steppe *et al.* 2010 and Fuchs *et al.* 2017, respectively). Finally, I would like to stress the need for a more systematic assessment of these data-processing uncertainties (as presented in CHAPTER 5) to improve the conclusions drawn from TDM measurements.

At high elevations, stomatal regulation is important as transpiration has to be optimised for minimal winter water losses and maximum photosynthetic yield during the short vegetative season (see Mayr 2007). More specifically, due to low temperatures and reduced partial pressure of CO_2 at higher elevations (Körner 2012), a strategy to optimize carbon assimilation could include allowing higher g_s at low temperatures, despite thermal conditions being less favourable for photosynthetic activity (Wieser 2007; Damour *et al.* 2010). In addition, due to low water stress conditions (Körner 2012), high elevation conifers could faciliate incomplete stomatal closure during the night to allow a faster supply of water for

photosynthesis at sunrise (e.g., Daley & Phillips 2006). Yet, previous studies reveal species-specific differences in conductance response strategies to face droughts (e.g., Oren *et al.* 1999b; Day 2000; Roman *et al.* 2015) or low temperatures (e.g., Anfodillo *et al.* 1998; Mayr 2007). Furthermore, observations of drought responses indicate that individuals of the same species might be able to adjust their stomatal response to persistent drier conditions (e.g., Grossiord *et al.* 2017), raising the question whether different conifers species show similar plasticity in their g_s response to temperature-limiting growth conditions at the treeline.

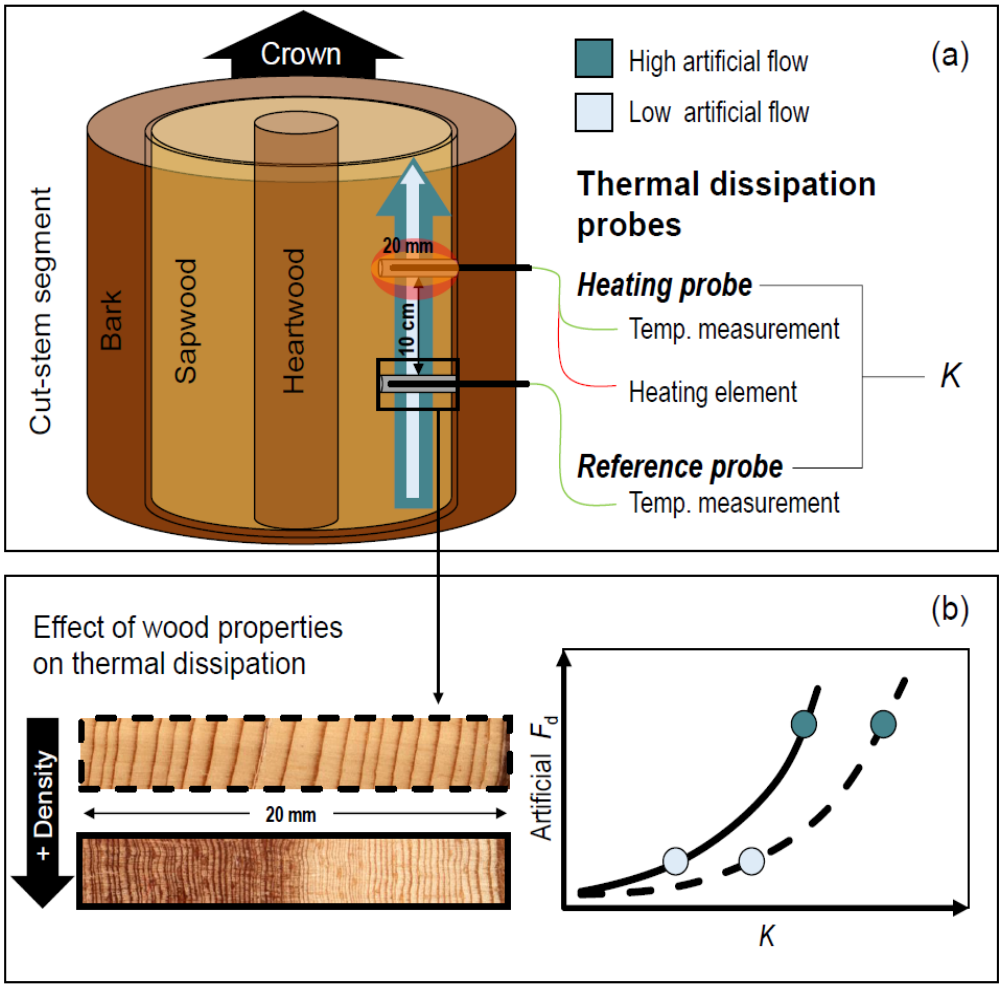

Figure 8.2 Hypothesis on the effect of wood properties on the TDM calibration curve. (a) Graphical representation of a cut-segment calibration experiment (as done in CHAPTER 5). Thermal dissipation probes are installed on the stem segment, measuring the temperature difference between a heated and a reference probe (ΔT recalculated to K; see Steppe *et al.* 2010). During the experiment different velocities of artificial flow are generated, either gravimetrically or with suction (see Fuchs *et al.* 2017). (b) The artificial flow velocities (as presented in a) are plotted against K to derive the calibration curve. We hypothesize that when the wood is denser at the location of probe installation (narrower rings or smaller lumen area), the calibration curve will show lower heat conductance (or K) with increasing artificial sap flux density (or F_d).

In CHAPTER 6, we compared the conductance response (derived from sap flow measurements using a species-specific calibration curve) of deciduous *L. decidua* and evergreen *P. abies* which show a pioneer and climax life strategy, respectively. *L. decidua* clearly showed a higher conductance than *P. abies*, likely due to the fact that this species has to deal with a shorter growing season caused by its deciduous life strategy (see Figure 6.3 in CHAPTER 6; as found by Anfodillo *et al.* 1998). We did not find a within-species increase in maximum conductance with increasing elevation, although commonly reported and attributed to wider tree spacing and more intense radiation (Körner 2012). However, the g_s response to R_g revealed that individuals growing at higher elevations allowed their stomata to stay open during the night (see Figure 6.5e, f in CHAPTER 6), which could facilitate the faster response to sunrise and maximize transpiration during the day (Daley & Phillips 2006). Surprisingly, we found that only *L. decidua* showed the ability to adjust its stomatal dynamics to T_a under different thermal growing conditions (see Figure 6.5c, d in CHAPTER 6), opening the stomata at lower temperatures at the treeline (with 3.2 °C colder growing conditions than in the valley bottom). These results highlight that *L. decidua* is able to adjust its conductance response to different thermal conditions and indicates that this species may be well equipped to function under changing future climatic conditions, compared to a climax species such as *P. abies*. Despite the drought in the summer of 2015 (see Figure 6.1 in CHAPTER 6), neither species showed plasticity in their stomatal behaviour (when comparing dry and wet growing conditions). However, we did find that *L. decidua* appeared to respond slightly faster in closing its stomata with increasing *D* (see Figure 6.5 in CHAPTER 6). Although the low severity and frequency of droughts within the Lötschental might not have been sufficient to initiate adjustment of the g_s response to environmental conditions, this generates an uncertain image about the ability of these species to cope with more frequent droughts.

In CHAPTER 6, we focussed on the regulation of stomatal conductance which showed that a species with a pioneer life strategy (*L. decidua*) adjusts its stomatal behaviour to colder conditions more than a climax species (*P. abies*; see Figure 8.3a, b, c). Yet, to fully grasp the hydraulic life-strategies and its plasticity to different environmental conditions, we have to adopt a more holistic approach and include anatomical features and the dynamics of storage-water capacitance (e.g., Köcher *et al.* 2013). Although we did not find a significant difference between the size of storage tissue (e.g., Phloem in Figure 8.3d), *L. decidua* and *P. abies* could show differences in their dynamic use of the storage pool, which could

be addressed with dendrometers (e.g., King *et al.* 2013a). Also, we see a clear difference in the anatomical features between the species (see Carrer *et al.* 2017), with larger lumen area for *L. decidua*, which allows for more efficient water transport to the crown (Figure 8.3e). However, the temporal variability and plasticity of wood anatomical properties should be addressed (e.g., Eilmann *et al.* 2014).

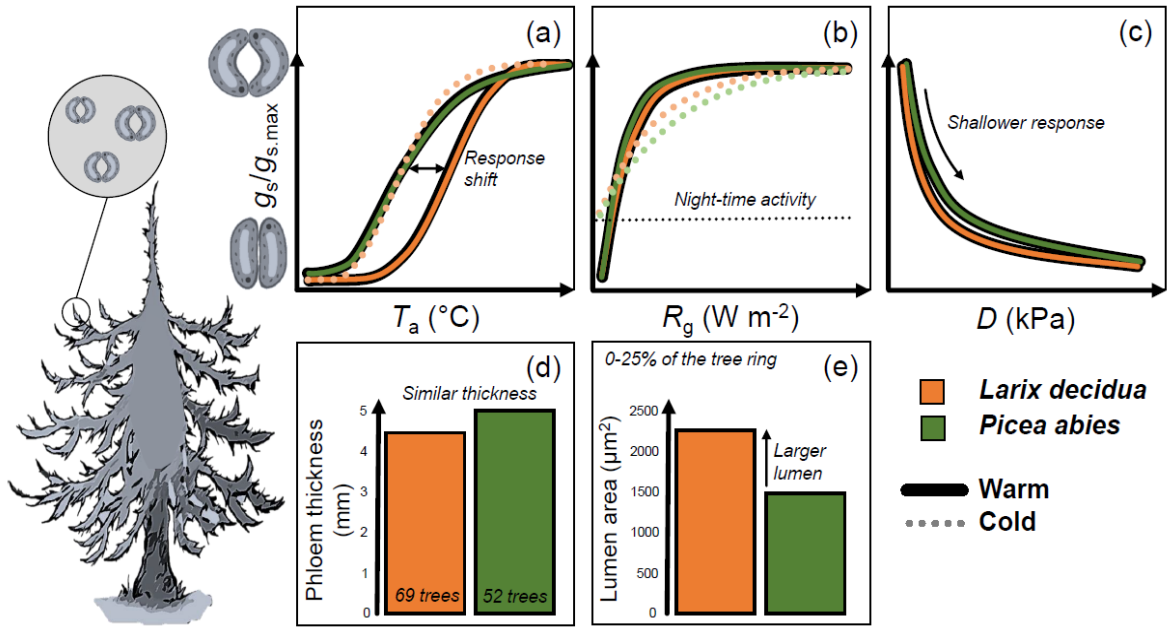

Figure 8.3 Graphical presentation of the ability of *Larix decidua* and *Picea abies* to adjust stomatal conductance (g_s) to warm and cold growing conditions (as discussed in CHAPTER 6). Hypothetical response of normalized g_s to air temperature (Ta; a), solar irradiance (R_g; b) and vapour pressure deficit (D; c). These responses show a larger potential to adjust g_s response to different environmental conditions for *L. decidua* than *P. abies*. No significant difference was found for phloem thickness measurements collected across the Alpine range (see CHAPTER 7; d). Wood anatomical measurements reveal a larger lumen area for *L. decidua*, when considering the first quarter of the tree ring (see CHAPTER 4).

8.3 An important mechanism for explaining wood formation: Turgidity

The environmental regulation of wood formation, dictating annual ring-width patterns, is commonly associated with the tree's photosynthetic activity, while other growth-limiting factors might also be relevant. For example, global forest productivity models (i.e., dynamics global vegetation models; DVGMs) use the changes in CO_2, light, temperature, water and nutrients to simulate photosynthetic activity and subsequently predict the future fate of forests as a carbon sink or source (Cox *et al.* 2000; Sitch *et al.* 2008). Although these models are continuously being expanded with post-photosynthetic mechanisms (Hayat *et al.*

2017; Huntzinger *et al.* 2017) to reduce the observed mismatch between simulations and observations (Babst *et al.* 2013; Anderegg *et al.* 2015), growth within these models remains largely driven by carbon production. Yet, increasing evidence points towards direct drivers of cambial activity regulating growth (or sink-limited growth; White *et al.* 2016), especially for trees growing in cold or dry conditions (Körner 2008; Parent *et al.* 2010; Muller *et al.* 2011). A key mechanism for initiating and regulating wood cell enlargement are internal tree hydraulics, which drives the turgidity in the cambial zone (Lockhart 1965).

In CHAPTER 7, we explored the potential of "turgor-driven" growth in explaining intra-annual growth patterns for conifers exposed to cold growing condition and droughts. We adopted an individual-based mechanistic growth model (see De Schepper & Steppe 2010) and applied it to 20 individual trees monitored along the elevational gradient and in contrasting dry and wet sites in the Lötschental. For both *L. decidua* and *P. abies*, we found good agreement between the simulated growth and independent growth measurements (including annual ring-width measurements and weekly xylogensis observations). The fact that turgor-driven cell enlargement can explain ring-width patterns is in agreement with observations that the final ring width largely depends on the enlargement rate (Cuny *et al.* 2014). Cambial activity monitoring revealed that woody cell division starts around 5-6 °C, which is above the photosynthetic minimum (of ≈0 °C; Saxe *et al.* 2001; Körner 2008). Interestingly, the turgor-driven growth simulations show a similar offset, where growth is highly unlikely to occur at temperatures below 2 °C, while the tree can still transpire water (see Figure 7.7 in CHAPTER 7). Additionally, correlations between climate and ring width show that individuals at the treeline are sensitive to the mean temperature for the period from June to August (S22 in CHAPTER 2), which overlaps with the temperature range where turgor-driven growth is limited. Soil droughts (or low soil water potential), occurring in the valley bottom of the Lötschental, appeared to heavily reduce growth, where growth was unlikely to occur below -0.6 MPa, while even drier conditions are needed to halt photosynthesis (Muller *et al.* 2011). The observed offset between growth and photosynthetic responsed to temperature could explain why DVGMs show a stronger positive climatic sensitivity than tree rings at higher elevations (Babst *et al.* 2013; Fatichi *et al.* 2014). This offset suggests that trees growing under temperature-limited conditions (e.g., at the treeline) will benefit less from the expected temperature increase (Collins *et al.* 2013) than they would if growth was directly controlled by photosynthesis. Additionally, the increased frequency and intensity of

droughts will likely cause more severe reductions if growth is driven by turgidity instead of photosynthesis (see Muller *et al.* 2011). This reduction might be partially driven by increased vapour pressure deficit, which reduces turgor-driven growth, as it heavily affects the release of water to the atmosphere and the refilling of the storage tissue that generates positive turgor (Damour *et al.* 2010). Disentangling these environmental drivers will be needed to fully grasp the consequences of climate change on future tree growth.

The modelling paradigm presented in CHAPTER 7 shows great promise in improving our predictions on future forest productivity. Yet, before the improvements can be incorporated into models operating on large spatial scales, additional steps have to be considered. The model is currently quite data demanding, requiring intra-daily measurements on both environmental and physiological conditions, which are not always available. First, as soils are highly heterogeneous and soil volumetric water content (θ) measurements are not always available, water balance models should be incorporated (Figure 8.4.1; e.g., Salomón *et al.* 2017). Additionally, soil-water retention curves need to be established to translate θ into ψ_{soil}, which is a required model input (applied in CHAPTER 4; e.g., Teepe *et al.* 2003).

Second, data on transpiration and photosynthesis should be available (Figure 8.4.2). Although data collection initiatives like TreeWatch.net (Steppe *et al.* 2016) will advance the availability of sap flow data needed for driving the model, the improvement of transpiration models is more likely to improve the temporal and spatial applicability of the model. The g_s response (used to model transpiration; Monteith & Unsworth 2013) to environmental conditions and the inter- and intra-specific dynamics should be addressed (e.g., CHAPTER 6; Grossiord *et al.* 2007). Additionally, the effect of precipitation on g_s and the mechanisms which regulate nighttime transpiration should be investigated (Caird *et al.* 2007), as they affect the stem storage refilling process, which is crucial for generating positive turgor pressure. Next, as carbon dynamics interact with turgor-driven growth mechanisms (De Schepper & Steppe 2010), models simulating photosynthetic activity under different environmental conditions should be calibrated and validated (e.g., Farquhar *et al.* 1980; Maire *et al.* 2012).

Third, we need a better understanding of the regulation of internal hydraulics and carbon dynamics within the stem under different environmental conditions (Figure 8.4.3). Currently, the presented mechanistic models require a calibration procedure for a multitude of parameters (De Pauw *et al.* 2008), which does not promote its use for predictive purposes. There is thus a clear need to

improve our understanding on the behaviour of these parameters under different environmental conditions across different species (e.g., Steppe & Lemeur 2007; Salomón *et al*. 2017; CHAPTER 7). For example, although the extensibility of cell walls during cell enlargement (ϕ) could affect annual growth patterns, this parameter is often fixed without seasonal dynamics (e.g., CHAPTER 7; Génard *et al.* 2001), which seems unrealistic.

Finally, the structural development of wood-anatomical features has to be considered (Figure 8.4.4). With the mechanistic model, the xylem diameter dynamics are simulated, not distinguishing between the number and dimensions of wood cells (or tracheids for conifers; Vaganov *et al.* 2006). Predicting the anatomical properties is important, as these affect the hydraulic functioning and structural integrity of the stem (Fournier *et al*. 2006; Sperry *et al*. 2008). Although turgor drives the enlargement of xylem cells, originating from the cambium, our understanding of the process of cambial cell production and division to form xylem cells has to be improved (Gregory & Wilson 1967; Shishov *et al*. 2015). Additionally, the process of cell wall thickening shows diverging dynamics from radial growth (Cuny *et al.* 2015), which should be appropriately incorporated if we want to predict structural properties of the wood.

8.4 Outlook

In this thesis I showcase the potential of elevational transect studies to provide crucial insights into the effect of persistent changes in growing season temperature on annual tree growth patterns, wood formation dynamics and tree hydraulics. Furthermore, collecting a large variety of tree physiological measurements (e.g., stem diameter variations, sap flow, leaf water potential, wood anatomical properties and tree-ring width) allow us to calibrate and validate mechanistic growth models. I illustrated that tree-ring width can provide insights into the aboveground biomass dynamics of high-elevation conifer forests and explain how inter-annual climatic variability and insect activity dictate tree-ring variability. Weekly xylogenesis observations provided information on the interplay between climate and the duration and rate of cell enlargement and wall thickening and can validate mechanistic growth models. Besides revealing differences in stomatal regulation between two conifer species, sap flow is a key input for mechanistic growth models. Such mechanistic growth models show that turgidity is an important driver to explain wood formation dynamics, wich could help to improve predicting future forest productivity.

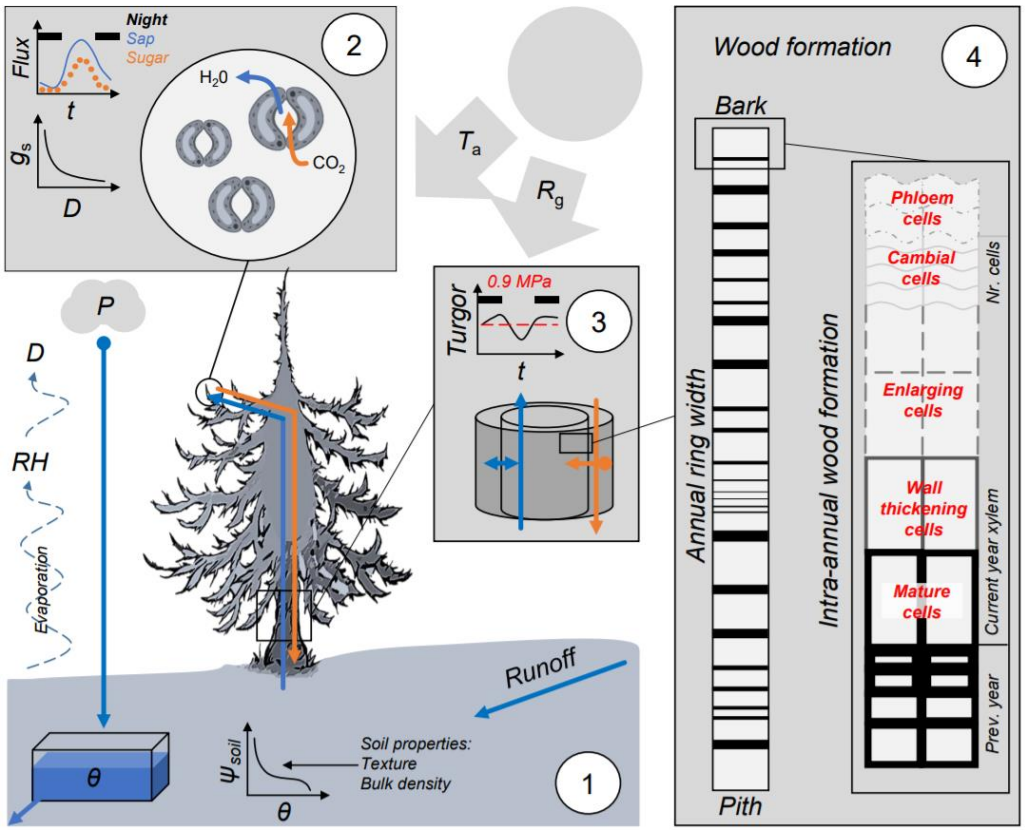

Figure 8.4 Schematics for the future application of mechanistic growth models for simulating intra-annual growth patterns in trees (conifers in this example). The numbers indicate the specific steps which are needed to improve the model, including; 1) soil water balance processes, 2) stomatal conductance regulation and photosynthesis, 3) mechanistic regulation of internal hydraulics and carbon dynamics, and 4) structural development of wood anatomy. Symbols used include; stomatal conductance (g_s), vapour pressure deficit (D), air temperature (T_a), solar irradiance (R_g), precipitation (P), relative humidity (RH), soil water potential (ψ_{soil}), soil moisture content (θ) and time (t). Orange symbols and arrows indicate processes related to carbon dynamics while blue object present water related processes. This figure provides a schematic overview of the processes discussed in the text.

An important message of this thesis is that solely internal tree hydraulics, affecting turgidity within the cambium, can largely explain intra-annual growth dynamics and ring-width patterns. This finding should stimulate the revision of growth models that are solely driven by photosynthetic activity to predict growth patterns (see Fatichi *et al.* 2014; Friend *et al.* 2014). Besides benchmarking modelled inter-annual growth patterns against measurements performed in the field (e.g., Babst *et al.* 2013), more validation is needed on an intra-annual scale. This is especially relevant as there is a clear difference between radial wood increment and the allocation of carbon to cell walls at an intra-annual scale (Cuny *et al.* 2015), which indicates that cell wall production might be regulated by a different mechanism than radial size. It is important to note that our modelling effort does not imply that photosynthesis is not relevant for growth. For example, there is a clear link between the presence of photosynthetic products, which affect

the osmotic potential, and subsequently the turgidity within the cambium (De Schepper & Steppe 2010). Including photosynthesis within the mechanistic model presented in this thesis would aid in identifying these interactions, although this requires continuous measurements of photosynthetic activity for validation. A logical next step would thus be to apply our mechanistic modelling framework on trees growing near eddy covariance flux tower sites, which could provide long-term records of photosynthethic activity (Chu *et al.* 2017) and independent validation of the water use derived from sap flow measurements (e.g., Wilson *et al.* 2001).

Within this thesis, I focussed on the Lötschental, which covers the thermal distribution limits of both *L. decidua* and *P. abies*. Yet, other environmental gradients, could be addressed within the measurement and modelling framework applied in this thesis, for example considering the relative position in species-specific climatic envelopes (i.e., species range projections; Zurell *et al.* 2016). Valuable initiatives are currently collecting global databases of important tree physiological parameters (Figure 8.5), which could be utilized within the presented mechanistic modelling framework. The task at hand is to identify the "hotspots" where multiple parameters are available to model intra-annual growth dynamics, including tree hydraulics and photosynthetic activity. However, when considering the distribution of measurements in climate space (mean annual temperature and precipitation; Figure 8.5), it is clear that the monitoring is not performed evenly. There is a clear gap in data collection in warm and humid ecosystems, while tropical forest ecosystems are critical for the global carbon balance (as discussed by Zuidema *et al.* 2013). Additionally, wood anatomical measurements are more often performed on sites with colder climatic conditions, while sap flow is mainly monitored under warmer conditions. These data gaps and mismatches in climate-space distribution should be resolved in order to provide a base for a more holistic analysis on tree hydraulics, photosynthetic activity and wood formation. Combined with such global datasets, our modelling approach can help to understand the future fate of forests exposed to environmental changes.

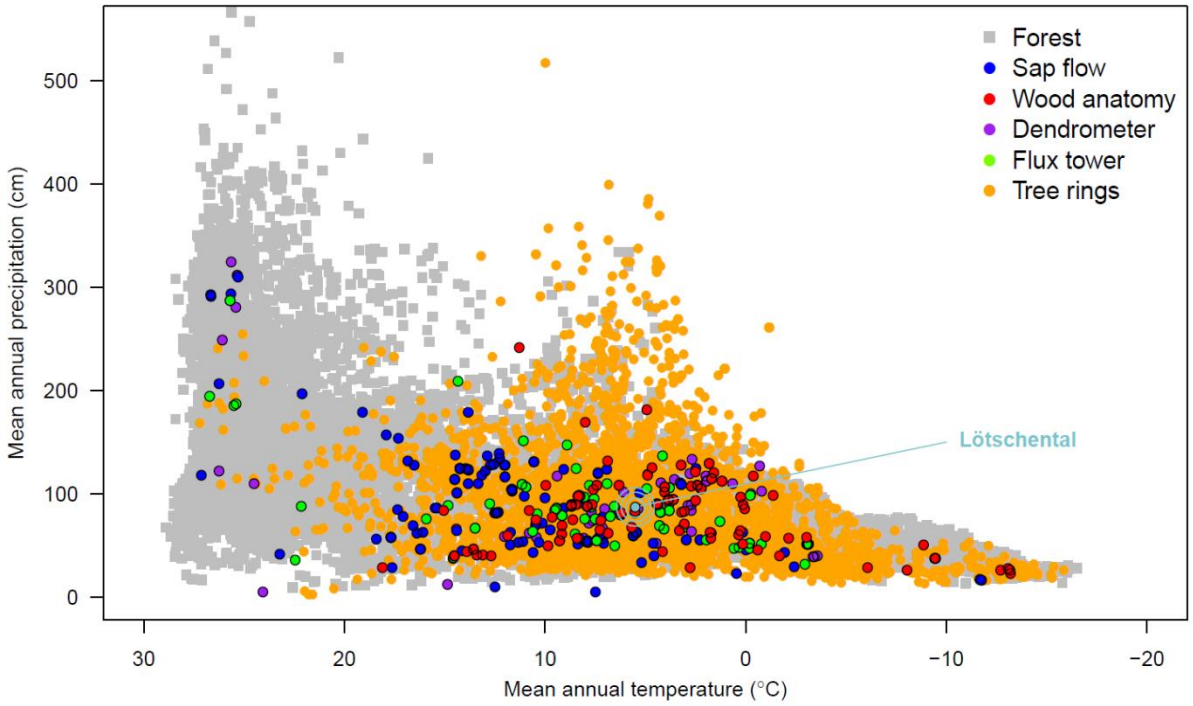

Figure 8.5 Distribution of sites with relevant tree physiological measurements in climate space (mean annual temperature and precipitation), including sap flow (SAPFLUXNET; Poyatos *et al.* 2016), wood anatomy (XCELL and GLOBOXYLO database), dendrometer (DendroGlobal database), flux tower (FLUXNET; Chu *et al.* 2017) and tree-ring width measurements (The International Tree-Ring Data Bank; Babst *et al.* 2017). The forest data was extracted from the MODIS land cover data products (Forest= fractional forest cover >60%; Friedl *et al*. 2010). The mean annual temperature and precipitation were obtained from WorldClim data products (Fick & Hijmans 2017). The location of the Lötschental in the climate space has been highlighted.

Acknowledgements

The author would like to thank Georg von Arx, Flurin Babst, Patrick Fonti, Stefan Klesse, Rafael Poyatos, Cyrille Rathgeber, Ana Stritih and Anne Uilhoorn for providing data, valuable comments on earlier versions of this chapter and for the stimulating discussions.

References

Abe H, Funada R, Ohtani J, Fukazawa K. **1997**. Changes in the arrangement of cellulose microfibrils associated with the cessation of cell expansion in tracheids. *Trees* **11**: 328–332.
Aguadé D, Poyatos R, Rosas T, Martínez-Vilalta J. **2015**. Comparative drought responses of *Quercus ilex* L. and *Pinus sylvestris* L. in a montane forest undergoing a vegetation shift. *Forests* **6**: 2505–2529.
Allen CD, Macalady AK, Chenchouni H, Bachelet D, Mcdowell N, Vennetier M, Kitzberger T, Rigling A, Breshears DD, Hogg EHT, *et al.* 2010. A global overview of drought and heat-induced tree mortality reveals emerging climate change risks for forests. *Forest Ecology and Management* **259**: 660–684.
Anav A, Friedlingstein P, Kidston M, Bopp L, Ciais P, Cox P, Jones C, Jung M, Myneni R, Zhu Z. **2013**. Evaluating the land and ocean components of the global carbon cycle in the CMIP5 earth system models. *Journal of Climate* **26**: 6801–6843.
Anchukaitis KJ, Evans MN, Kaplan A, Vaganov EA, Hughes MK, Grissino-Mayer HD, Cane MA. **2006**. Forward modeling of regional scale tree-ring patterns in the southeastern United States and the recent influence of summer drought. *Geophysical Research Letters* **33**: 1–4.
Anderegg WRL, Berry JA, Field CB. **2012**. Linking definitions, mechanisms, and modeling of drought-induced tree death. *Trends in Plant Science* **17**: 693–700.
Anderegg WRL, Klein T, Bartlett M, Sack L, Pellegrini AFA, Choat B, Jansen S. **2016**. Meta-analysis reveals that hydraulic traits explain cross-species patterns of drought-induced tree mortality across the globe. *Proceedings of the National Academy of Sciences* **113**: 5024–5029.
Anderegg WRL, Meinzer FC. **2015**. Wood Anatomy and Plant Hydraulics in a Changing Climate. In: Hacke U. Eds. Functional and Ecological Xylem Anatomy. New York, USA: Springer, 235–253.
Anderegg WRL, Schwalm C, Biondi F, Camarero JJ, Koch G, Litvak M, Ogle K, Shaw JD, Shevliakova E, Williams AP, *et al.* 2015. Pervasive drought legacies in forest ecosystems and their implications for carbon cycle models. *Science* **349**: 528–532.
Anderegg WRL. **2015**. Spatial and temporal variation in plant hydraulic traits and their relevance for climate change impacts on vegetation. *New Phytologist* **205**: 1008–1014.
Anderson RG, Canadell JG, Randerson JT, Jackson RB, Hungate BA, Baldocchi DD, Ban-Weiss GA, Bonan GB, Caldeira K, Cao L, *et al.* 2011. Biophysical considerations in forestry for climate protection. *Frontiers in Ecology and the Environment* **9**: 174–182.
Anfodillo T, Petit G, Carraro V. **2013**. The effect of axial conduit widening on sap flow sensors readings. *Acta Horticulturae* **991**: 25–30.
Anfodillo T, Rento S, Carraro V, Furlanetto L, Urbinati C, Carrer M. **1998**. Tree water relations and climatic variations at the alpine timberline: seasonal changes of sap flux and xylem water potential in *Larix decidua* Miller, *Picea abies* (L.) Karst. and *Pinus cembra* L. *Annals of Forest Science* **55**: 159–172.
Ansley RJ, Dugas WA, Heuer ML, Trevino BA. **1994**. Stem flow and porometer measurements of transpiration from honey mesquite (*Prosopis glandulosa*). *Journal of Experimental Botany* **45**: 847–856.
Arneth A, Kelliher FM, Bauer G, Hollinger DY, Byers JN, Hunt JE, Seveny TMMC, Ziegler W, Vygodskaya NN, Milukova I, *et al.* 1996. Environmental regulation of xylem sap flow and total conductance of *Larix gmelinii* trees in eastern Siberia. *Tree Physiology* **16**: 247–255.
Asshoff R, Hättenschwiler S. **2006**. Changes in needle quality and larch bud moth performance in response to CO_2 enrichment and defoliation of treeline larches. *Ecological Entomology* **31**: 84–90.
Auer I, Böhm R, Jurkovic A, Lipa W, Orlik A, Potzmann R, Schöner W, Ungersböck M, Matulla C, Briffa K, *et al.* 2007. HISTALP - historical instrumental climatological surface time series of the Greater Alpine Region. *Encyclopedia of Atmospheric Sciences* **27**: 17–46.
Axelson JN, Smith DJ, Daniels LD, Alfaro RI. **2015**. Multicentury reconstruction of western spruce budworm outbreaks in central British Columbia, Canada. *Forest Ecology and Management* **335**: 235–248.
Babst F, Alexander MR, Szejner P, Bouriaud O, Klesse S, Roden J, Ciais P, Poulter B, Frank D, Moore DJP, *et al.* 2014a. A tree-ring perspective on the terrestrial carbon cycle. *Oecologia* **176**: 307–322.
Babst F, Bouriaud O, Alexander R, Trouet V, Frank D. **2014b**. Toward consistent measurements of carbon accumulation: A multi-site assessment of biomass and basal area increment across Europe. *Dendrochronologia* **32**: 153–161.
Babst F, Bouriaud O, Papale D, Gielen B, Janssens IA, Nikinmaa E, Ibrom A, Wu J, Bernhofer C, Köstner B, *et al.* 2014c. Above-ground woody carbon sequestration measured from tree rings is coherent with net ecosystem productivity at five eddy-covariance sites. *New Phytologist* **201**: 1289–1303.
Babst F, Poulter B, Bodesheim P, Mahecha MD, Frank DC. **2017**. Improved tree-ring archives will support earth-system science. *Nature Ecology & Evolution* **1**: 1–2.
Babst F, Poulter B, Trouet V, Tan K, Neuwirth B, Wilson R, Carrer M, Grabner M, Tegel W, Levanic T, *et al.* 2013. Site- and species-specific responses of forest growth to climate across the European continent. *Global Ecology and Biogeography* **22**: 706–717.

Badalotti A, Anfodillo T, Grace J. **2000**. Evidence of osmoregulation in *Larix decidua* at Alpine treeline and comparative responses to water availability of two co-occurring evergreen species. *Annals of Forest Science* **57**: 623–633.

Baert A, Schepper V De, Steppe K. **2015**. Variable hydraulic resistances and their impact on plant drought response modelling. *Tree Physiology* **35**: 439–449.

Bakkenes M, Alkemade JRM, Ihle F, Leemans R, Latour JB. **2002**. Assessing effects of forecasted climate change on the diversity and distribution of European higher plants for 2050. *Global Change Biology* **8**: 390–407.

Bakker JD. **2005**. A new, proportional method for reconstructing historical tree diameters. *Canadian Journal of Forest Research* **35**: 2515–2520.

Balducci L, Cuny HE, Rathgeber CBK, Deslauriers A, Giovannelli A, Rossi S. **2016**. Compensatory mechanisms mitigate the effect of warming and drought on wood formation. *Plant Cell and Environment* **39**: 1338–1352.

Bale JS, Masters GJ, Hodkinson ID, Awmack C, Bezemer TM, Brown VK, Butterfield J, Buse A, Coulson JC, Farrar J, *et al.* 2002. Herbivory in global climate change research: direct effects of rising temperature on insect herbivores. *Global Change Biology* **8**: 1–16.

Baltensweiler W, Rubli D. **1999**. Dispersal: an important driving force of the cyclic population dynamics of the larch bud moth, *Zeiraphera diniana* Gn. *Forest Snow and Landscape. Research* **74**: 1–153.

Baltensweiler W, Weber UM, Cherubini P. **2008**. Tracing the influence of larch-bud-moth insect outbreaks and weather conditions on larch tree-ring growth in Engadine (Switzerland). *Oikos* **117**: 161–172.

Bannister P, Neuner G. **2001**. Frost resistance and the distribution of Conifers. In: Bigras FJ, Colombo SJ. Eds. Conifer Cold Hardiness. Tree Physiology. Dordrecht, The Netherlands: Springer, 3–21.

Barber VA, Juday GP, Finney BP. **2000**. Reduced growth of Alaskan white spruce in the twentieth century from temperature-induced drought stress. *Nature* **405**: 668–673.

Barbour MM, Whitehead D. **2003**. A demonstration of the theoretical prediction that sap velocity is related to wood density in the conifer *Dacrydium cupressinum*. *New Phytologist* **158**: 477–488.

Barigah TS, Ibrahim T, Bogard A, Faivre-Vuillin B, Lagneau LA, Montpied P, Dreyer E. **2006**. Irradiance-induced plasticity in the hydraulic properties of saplings of different temprerate broad-leaved forest tree species. *Tree Physiology* **26**: 1–11.

Barnard DM, Meinzer FC, Lachenbruch B, McCulloh KA, Johnson DM, Woodruff DR. **2011**. Climate-related trends in sapwood biophysical properties in two conifers: avoidance of hydraulic dysfunction through coordinated adjustments in xylem efficiency, safety and capacitance. *Plant, Cell & Environment* **34**: 643–654.

Bates D, Mächler M, Bolker B, Walker S. **2014**. Fitting Linear Mixed-Effects Models using lme4. *Journal of Statistical Software* **67**: 1–48.

Battipaglia G, Büntgen U, McCloskey S, Blarquez O, Denis N, Paradis L, Brossier B, Fournier T, Carcaillet C. **2014**. Long-term effects of climate and land-use change on larch budmoth outbreaks in the French Alps. *Climate Research* **62**: 1–14.

Battisti A, Boato A, Masutti L. **2000**. Influence of silvicultural practices and population genetics on management of the spruce sawfly, *Cephalcia arvensis*. *Forest Ecology and Management* **128**: 159–166.

Battisti A. **2008**. Forests and climate change - Lessons from insects. *IForest* **1**: 1–5.

Beauchamp K, Mencuccini M, Perks M, Gardiner B. **2013**. The regulation of sapwood area, water transport and heartwood formation in Sitka spruce. *Plant Ecology and Diversity* **6**: 45–56.

Beer C, Reichstein M, Tomelleri E, Ciais P, Jung M, Carvalhais N, Rödenbeck C, Arain MA, Baldocchi D, Bonan GB, *et al.* 2010. Terrestrial Gross Carbon Dioxide Uptake: Global Distribution and Covariation with Climate. *Science* **329**: 834–839.

Begg JE, Turner NC. **1970**. Water Potential Gradients in Field Tobacco. *Plant Physiology* **46**: 343–346.

Beniston M. **2003**. Climatic change in mountain regions: A review of possible impacts. *Climatic Change* **59**: 5–31.

Berdanier AB, Miniat CF, Clark JS. **2016**. Predictive models for radial sap flux variation in coniferous, diffuse-porous and ring-porous temperate trees. *Tree physiology* **36**: 932–941.

Berkelhammer M, Hu J, Bailey A, Noone DC, Still CJ, Barnard H, Gochis D, Hsiao GS, Rahn T, Turnipseed A. **2013**. The nocturnal water cycle in an open-canopy forest. *Journal of Geophysical Research Atmospheres* **118**: 10225–10242.

Boisvenue C, Running SW. **2006**. Impacts of climate change on natural forest productivity - Evidence since the middle of the 20th century. *Global Change Biology* **12**: 862–882.

Bonan GB, Lawrence PJ, Oleson KW, Levis S, Jung M, Reichstein M, Lawrence DM, Swenson SC. **2011**. Improving canopy processes in the Community Land Model version 4 (CLM4) using global flux fields empirically inferred from FLUXNET data. *Journal of Geophysical Research* **116**: 1–22.

Bonan GB. **2008**. Forests and Climate Change: Forcings, Feedbacks, and the Climate Benefits of Forests. *Science* **320**: 1444–1449.

Bosch DD, Marshall LK, Teskey R. **2014**. Forest transpiration from sap flux density measurements in a Southeastern Coastal Plain riparian buffer system. *Agricultural and Forest Meteorology* **187**: 72–82.
Bouche PS, Larter M, Domec J, Burlett R, Gasson P, Jansen S, Delzon S. **2014**. A broad survey of hydraulic and mechanical safety in the xylem of conifers. *Journal of Experimental Botany* **65**: 4419–4431.
Bowman DMJS, Brienen RJW, Gloor E, Phillips OL, Prior LD. **2013**. Detecting trends in tree growth: not so simple. *Trends in Plant Science* **18**: 11–17.
Boyer JS. **1967**. Leaf water potential measure with a pressure chamber. *Plant Physiology* **42**: 133–137.
Brändli UB. **2010**. *Schweizerisches Landesforstinventar. Ergebnisse der dritten Erhebung 2004–2006.* Birmensdorf, Switzerland: Swiss Federal Institute for Forest, Snow and Landscape Research (WSL).
Brassel P, Lischke H. **2001**. *Swiss National Forest Inventory: Methods and Models of the Second Assessment.* Birmensdorf, Switzerland: Swiss Federal Institute for Forest, Snow and Landscape Research (WSL).
Braun S, Schindler C, Leuzinger S. **2010**. Use of sap flow measurements to validate stomatal functions for mature beech (*Fagus sylvatica*) in view of ozone uptake calculations. *Environmental Pollution* **158**: 2954–2963.
Breshears DD, Myers OB, Meyer CW, Barnes FJ, Zou CB, Allen CD, McDowell NG, Pockman WT. **2009**. Tree die-off in response to global change-type drought: Mortality insights from a decade of plant water potential measurements. *Frontiers in Ecology and the Environment* **7**: 185–189.
Briffa KR, Melvin TM. **2011**. A closer look at regional curve standardization of tree-ring records: justification of the need, a warning of some pitfalls, and suggested improvements in its application. In: Hughes MK, Swetnam TW, Diaz HF. Eds. Dendroclimatology: Progress and Prospects. New York, USA: Springer, 113–145.
Briffa KR, Schweingruber FH, Jones PD, Osborn TJ, Shiyatov SG, Vaganov EA. **1998**. Reduced sensitivity of recent tree-growth to temperature at high northern latitudes. *Nature* **391**: 678–682.
Brinkmann N, Eugster W, Zweifel R, Buchmann N, Kahmen A. **2016**. Temperate tree species show identical response in tree water deficit but different sensitivities in sap flow to summer soil drying. *Tree Physiology* **36**: 1508–1519.
Brodribb TJ, Mcadam SAM, Jordan GJ, Martins SC V. **2014**. Conifer species adapt to low-rainfall climates by following one of two divergent pathways. *Proceedings of the National Academy of Sciences* **111**: 14489–14493.
Brown-Mitic C, Shuttleworth WJ, Chawn Harlow R, Petti J, Burke E, Bales R. **2007**. Seasonal water dynamics of a sky island subalpine forest in semi-arid southwestern United States. *Journal of Arid Environments* **69**: 237–258.
Buckley TN, Mott KA. **2013**. Modelling stomatal conductance in response to environmental factors. *Plant, Cell and Environment* **36**: 1691–1699.
Buckley TN. **2005**. The control of stomata by water balance. *New Phytologist* **168**: 275–292.
Bunn AG, Waggoner L a, Graumlich LJ. **2005**. Topographic mediation of growth in high elevation foxtail pine. *Global Ecology and Biogeography* **14**: 103–114.
Bunn AG. **2008**. A dendrochronology program library in R (dplR). *Dendrochronologia* **26**: 115–124.
Büntgen U, Frank D, Liebhold A, Johnson D, Carrer M, Urbinati C, Grabner M, Nicolussi K, Levanic T, Esper J. **2009**. Three centuries of insect outbreaks across the European Alps. *New Phytologist* **182**: 929–941.
Büntgen U, Frank D, Wilson R, Carrer M, Urbinati C, Esper J. **2008**. Testing for tree-ring divergence in the European Alps. *Global Change Biology* **14**: 2443–2453.
Büntgen U, Frank DC, Kaczka RJ, Verstege A, Zwijacz-Kozica T, Esper J. **2007**. Growth responses to climate in a multi-species tree-ring network in the Western Carpathian Tatra Mountains, Poland and Slovakia. *Tree Physiology* **27**: 689–702.
Burger H. **1953**. *Holz, Blattmenge und Zuwachs. Fichten in gleichaltrigen Hochwald. Mitt. Schweiz.* Mitteilungen der Schweizerischen Anstalt für das forstliche Versuchswesen, 29.
Burgess S, Adams MA, Turner NC, Beverly CR, Ong CK, Khan AAH, Bleby TM. **2001**. An improved heat pulse method to measure low and reverse rates of sap flow in woody plants. *Tree Physiology* **21**: 589–598.
Burnham KP, Anderson DR. **2003**. *Model Selection and Multimodel Inference: A Practical Information-Theoretic Approach*. New York, USA: Springer.
Bush SE, Hultine KR, Sperry JS, Ehleringer JR. **2010**. Calibration of thermal dissipation sap flow probes for ring- and diffuse-porous trees. *Tree Physiology* **30**: 1545–1554.
Cabibel BDF. **1991**. Mesures thermiques des flux de sève dans les troncs et les racines et fonctionnement hydriques des arbres. *Agronomie* **8**: 669–678.
Caird MA, Richards JH, Donovan LA. **2006**. Nighttime Stomatal Conductance and Transpiration in C3 and C4 Plants. *Plant Physiology* **143**: 4–10.
Camarero JJ, Gazol A, Tardif JC, Conciatori F. **2015**. Attributing forest responses to global-change drivers: limited evidence of a CO_2-fertilization effect in Iberian pine growth. *Journal of Biogeography* **42**: 2220–2233.
Camarero JJ, Olano JM, Parras A. **2010**. Plastic bimodal xylogenesis in conifers from continental Mediterranean climates. *New Phytologist* **185**: 471–480.

Campelo F, Nabais C, Carvalho A, Vieira J. **2016**. tracheideR - An R package to standardize tracheidograms. *Dendrochronologia* **37**: 64–68.

Canadell JG, Le Quéré C, Raupach MR, Field CB, Buitenhuis ET, Ciais P, Conway TJ, Gillett NP, Houghton RA, Marland G. **2007**. Contributions to accelerating atmospheric CO_2 growth from economic activity, carbon intensity, and efficiency of natural sinks. *Proceedings of the National Academy of Sciences of the United States of America* **104**: 18866–18870.

Carrer M, Castagneri D, Prendin AL, Petit G, von Arx G. **2017**. Retrospective Analysis of Wood Anatomical Traits Reveals a Recent Extension in Tree Cambial Activity in Two High-Elevation Conifers. *Frontiers in Plant Science* **8**: 1–13.

Castagneri D, Fonti P, von Arx G, Carrer M. **2017**. How does climate influence xylem morphogenesis over the growing season? Insights from long-term intra-ring anatomy in *Picea abies*. *Annals of Botany* **119**: 1011–1020.

Čermák J, Cienciala E, Kucera J, Lindroth a, Bednárová E. **1995**. Individual variation of sap-flow rate in large pine and spruce trees and stand transpiration: a pilot study at the central NOPEX site. *Journal of Hydrology* **168**: 17–27.

Čermák J, Kučera J, Nadezhdina N. **2004**. Sap flow measurements with some thermodynamic methods, flow integration within trees and scaling up from sample trees to entire forest stands. *Trees - Structure and Function* **18**: 529–546.

CH2011. **2011**. *Swiss Climate Change Scenarios CH2011*. C2SM, MeteoSwiss, ETH, NCCR Climate, and OcCC, Zurich, Switzerland.

Chambers JL, Hinckley TM, Hinckley TM. **1985**. Boundary-Line Analysis and Models of Leaf Conductance for Four Oak-Hickory Forest Species. *Forest Science* **31**: 437–450.

Chambers JM, Freeny A, Heiberger RM. **1992**. Analysis of variance; designed experiments. In: Chambers JM, Hastie TJ. Eds. Statistical Models in S. Pacific Grove, USA: Wadsworth & Brooks/Cole, 624.

Chang X, Zhao W, Liu H, Wei X, Liu B, He Z. **2014**. Agricultural and Forest Meteorology Qinghai spruce (*Picea crassifolia*) forest transpiration and canopy conductance in the upper Heihe River Basin of arid northwestern China. *Agricultural and Forest Meteorology* **198**–**199**: 209–220.

Chapin FS, Randerson JT, McGuire AD, Foley JA, Field CB. **2008**. Changing feedbacks in the climate-biosphere system. *Frontiers in Ecology and the Environment* **6**: 313–320.

Charney ND, Babst F, Poulter B, Record S, Trouet VM, Frank D, Enquist BJ, Evans MEK. **2016**. Observed forest sensitivity to climate implies large changes in 21st century North American forest growth. *Ecology letters* **19**: 1119–1128.

Charra-Vaskou K, Badel E, Charrier G, Ponomarenko A, Bonhomme M, Foucat L, Mayr S, Améglio T. **2016**. Cavitation and water fluxes driven by ice water potential in Juglans regia during freeze-thaw cycles. *Journal of Experimental Botany* **67**: 739–750.

Chatterjee S, Hardi AS. **2012**. *Regression Analysis by Example*. Hoboken, USA: John Wiley & Sons.

Chave J, Coomes D, Jansen S, Lewis SL, Swenson NG, Zanne AE. **2009**. Towards a worldwide wood economics spectrum. *Ecology Letters* **12**: 351–366.

Choat B, Jansen S, Brodribb TJ, Cochard H, Delzon S, Bhaskar R, Bucci SJ, Feild TS, Gleason SM, Hacke UG, *et al.* 2012. Global convergence in the vulnerability of forests to drought. *Nature* **491**: 752–756.

Chu H, Baldocchi DD, John R, Wolf S, Reichstein M. **2017**. Fluxes all of the time? A primer on the temporal representativeness of FLUXNET. *Journal of Geophysical Research: Biogeosciences* **122**: 289–307.

Clark KL, Skowronski N, Hom J. **2010**. Invasive insects impact forest carbon dynamics. *Global Change Biology* **16**: 88–101.

Clearwater MJ, Meinzer FC, Andrade JL, Goldstein G, Holbrook NM. **1999**. Potential errors in measurement of nonuniform sap flow using heat dissipation probes. *Tree Physiology* **19**: 681–688.

Collins M, Knutti R, Arblaster J, Dufresne JL, Fichefet T, Friedlingstein P, Gao X, Gutowski WJ, Johns T, Krinner G, *et al.* 2013. Long-term Climate Change: Projections, Commitments and Irreversibility. In: Climate Change 2013: The Physical Science Basis. Contribution of Working Group I to the Fifth Assessment Report of the Intergovernmental Panel on Climate Change. New York, USA: Cambridge University Press, 1029–1136.

Cook ER, Peters K. **1981**. The smoothing spline: A new approach to standardizing forest interior tree-ring width series for dendroclimatic studies. *Tree-Ring Bulletin* **41**: 45–53.

Cordell S, Goldstein G, Mueller-Dombois D, Webb D, Vitousek PM. **1998**. Physiological and morphological variation in *Metrosideros polymorpha*, a dominant Hawaiian tree species, along an altitudinal gradient: The role of phenotypic plasticity. *Oecologia* **113**: 188–196.

Cosgrove DJ. **2000**. Loosening of plant cell walls by expansins. *Nature* **407**: 321–326.

Cox PM, Betts RA, Jones CD, Spall SA, Totterdell IJ. **2000**. Acceleration of global warming due to carbon-cycle feedbacks in a coupled climate model. *Nature* **408**: 184–187.

Cramer W, Bondeau A, Woodward FI, Prentice IC, Betts RA, Brovkin V, Cox PM, Fisher V, Foley JA, Friend AD, *et al.* 2001. Global response of terrestrial ecosystem structure and function to CO_2 and climate change: Results from six dynamic global vegetation models. *Global Change Biology* **7**: 357–373.

Crawley MJ. **2007**. *The R book*. West Sussex, England: John Wiley & Sons Ltd.
Creeden EP, Hicke JA, Buotte PC. **2014**. Climate, weather, and recent mountain pine beetle outbreaks in the western United States. *Forest Ecology and Management* **312**: 239–251.
Cuny HE, Rathgeber CBK, Frank D, Fonti P, Fournier M. **2014**. Kinetics of tracheid development explain conifer tree-ring structure. *New Phytologist* **203**: 1231–1241.
Cuny HE, Rathgeber CBK, Frank D, Fonti P, Mäkinen H, Prislan P, Rossi S, del Castillo EM, Campelo F, Vavrčík H, *et al.* 2015. Woody biomass production lags stem-girth increase by over one month in coniferous forests. *Nature Plants* **1**: 1–6.
Cuny HE, Rathgeber CBK, Kiessé TS, Hartmann FP, Barbeito I, Fournier M. **2013**. Generalized additive models reveal the intrinsic complexity of wood formation dynamics. *Journal of Experimental Botany* **64**: 1983–1994.
Cuny HE, Rathgeber CBK. **2016**. Xylogenesis: Coniferous Trees of Temperate Forests Are Listening to the Climate Tale during the Growing Season But Only Remember the Last Words! *Plant Physiology* **171**: 306–317.
Daley MJ, Phillips NG. **2006**. Interspecific variation in nighttime transpiration and stomatal conductance in a mixed New England deciduous forest. *Tree Physiology* **26**: 411–419.
Damour G, Simonneau T, Cochard H, Urban L. **2010**. An overview of models of stomatal conductance at the leaf level. *Plant, Cell & Environment* **33**: 1419–1438.
Darikova YA, Vaganov EA, Kuznetsova G V., Grachev AM. **2013**. Changes in the anatomical structure of tree rings of the rootstock and scion in the heterografts of Siberian pine. *Trees - Structure and Function* **27**: 1621–1631.
Daudet F, Améglio T, Cochard H, Archilla O, Lacointe A. **2005**. Experimental analysis of the role of water and carbon in tree stem diameter variations. *Journal of Experimental Botany* **56**: 135–144.
Day ME. **2000**. Influence of temperature and leaf-to-air vapor pressure deficit on net photosynthesis and stomatal conductance in red spruce (*Picea rubens*). *Tree Physiology* **20**: 57–63.
de la Cruz M, DeSoto L. **2015**. tgram: Functions to compute and plot tracheidograms. CRAN: https://cran.r-project.org/web/packages/tgram/tgram.pdf.
De Pauw DJW, Steppe K, De Baets B. **2008**. Identifiability analysis and improvement of a tree water flow and storage model. *Mathematical Biosciences* **211**: 314–332.
De Schepper V, Steppe K. **2010**. Development and verification of a water and sugar transport model using measured stem diameter variations. *Journal of Experimental Botany* **61**: 2083–2099.
De Swaef T, Mellisho CD, Baert A, Schepper V De, Torrecillas A, Conejero W, Steppe K. **2014**. Model-assisted evaluation of crop load effects on stem diameter variations and fruit growth in peach. *Trees* **28**: 1607–1622.
De Swaef T, Steppe K, Verbist K, Cornelis W. **2012**. Tomato stem and fruit diameter dynamics in response to changing water availability. *Acta Horticulturae* **952**: 953–957.
De Wit CT. **1959**. Potential photosynthesis of crop surfaces. *Netherlands Journal of Agricultural Science* **7**: 141–149.
Delpierre N, Berveiller D, Granda E, Dufrêne E. **2016**. Wood phenology, not carbon input, controls the interannual variability of wood growth in a temperate oak forest. *New Phytologist* **210**: 459–470.
Delpierre N, Dufrêne E, Soudani K, Ulrich E, Cecchini S, Boé J, François C. **2009**. Modelling interannual and spatial variability of leaf senescence for three deciduous tree species in France. *Agricultural and Forest Meteorology* **149**: 938–948.
Denne MP. **1989**. Definition of Latewood According to Mork (1928). *IAWA Bulletin* **10**: 59–62.
Deslauriers A, Giovannelli A, Rossi S, Castro G, Fragnelli G, Traversi L. **2009**. Intra-annual cambial activity and carbon availability in stem of poplar. *Tree Physiology* **29**: 1223–1235.
Deslauriers A, Morin H. **2005**. Intra-annual tracheid production in balsam fir stems and the effect of meteorological variables. *Trees - Structure and Function* **19**: 402–408.
Deslauriers A, Rossi S, Anfodillo T, Saracino A. **2008**. Cambial phenology, wood formation and temperature thresholds in two contrasting years at high altitude in southern Italy. *Tree Physiology* **28**: 863–871.
DeSoto L, De la Cruz M, Fonti P. **2011**. Intra-annual patterns of tracheid size in the Mediterranean tree *Juniperus thurifera* as an indicator of seasonal water stress. *Canadian Journal of Forest Research* **41**: 1280–1294.
Dewar R, Mauranen A, Mäkelä A, Hölttä T, Medlyn B, Vesala T. **2018**. New insights into the covariation of stomatal, mesophyll and hydraulic conductances from optimization models incorporating nonstomatal limitations to photosynthesis. *New Phytologist* **217**: 571–585.
Dietrich L, Zweifel R, Kahmen A. **2018**. Daily stem diameter variations can predict the canopy water status of mature temperate trees. *Tree Physiology* **38**: 941–952.
Do F, Rocheteau A. **2002**. Influence of natural temperature gradients on measurements of xylem sap flow with thermal dissipation probes. 2. Advantages and calibration of a noncontinuous heating system. *Tree physiology* **22**: 649–654.

Downes GM, Drew D, Battaglia M, Schulze D. **2009**. Measuring and modelling stem growth and wood formation: An overview. *Dendrochronologia* **27**: 147–157.

Drew DM, Downes GM, Battaglia M. **2010**. CAMBIUM, a process-based model of daily xylem development in Eucalyptus. *Journal of Theoretical Biology* **264**: 395–406.

Egea G, Verhoef A, Luigi P. **2011**. Towards an improved and more flexible representation of water stress in coupled photosynthesis-stomatal conductance models. *Agricultural and Forest Meteorology* **151**: 1370–1384.

Eilmann B, Sterck F, Wegner L, De Vries SMG, Von Arx G, Mohren GMJ, Den Ouden J, Sass-Klaassen U. **2014**. Wood structural differences between northern and southern beech provenances growing at a moderate site. *Tree Physiology* **34**: 882–893.

Ellenberg H, Leuschner C. **2010**. *Vegetation Mitteleuropas mit den Alpen in ökologischer, dynamischer und historischer Sicht*. Stuttgart, Germany: Ulmer.

Esper J, Buntgen U, Frank DC, Nievergelt D, Liebhold A. **2007**. 1200 Years of Regular Outbreaks in Alpine Insects. *Proceedings of the Royal Society B: Biological Sciences* **274**: 671–679.

Esper J, Schweingruber FH. **2004**. Large-scale treeline changes recorded in Siberia. *Geophysical Research Letters* **31**: 1–5.

Etzold S, Waldner P, Thimonier A, Schmitt M, Dobbertin M. **2014**. Tree growth in Swiss forests between 1995 and 2010 in relation to climate and stand conditions: Recent disturbances matter. *Forest Ecology and Management* **311**: 41–55.

Evans MN, Reichert BK, Kaplan A, Anchukaitis KJ, Vaganov EA, Hughes MK, Cane MA. **2006**. A forward modeling approach to paleoclimatic interpretation of tree-ring data. *Journal of Geophysical Research* **111**: 1–13.

Ewers BE, Oren R. **2000**. Analysis of assumptions and errors in the calculation of stomatal conductance from sap-flow measurements. *Tree Physiology* **20**: 579–589.

Fan J, Guyot A, Ostergaard KT, Lockington DA. **2018**. Effects of earlywood and latewood on sap flux density-based transpiration estimates in conifers. *Agricultural and Forest Meteorology* **249**: 264–274.

Fang J, Chen A, Peng C, Zhao S, Ci L. **2001**. Changes in Forest Biomass Carbon Storage in China between 1949 and 1998. *Science* **292**: 2320–2322.

Farjon A, Filer D. **2013**. *An atlas of the world's conifers: an analysis of their distribution, biogeography, diversity and conservation status*. United Kingdom: BRILL.

Farquhar GD, Caemmerer S Von, Berry JA. **1980**. A Biochemical Model of Photosynthetic CO_2 Assimilation in Leaves of C3 Species. *Planta* **149**: 78–90.

Fatichi S, Leuzinger S, Körner C. **2014**. Letters Moving beyond photosynthesis: from carbon source to sink-driven vegetation modeling. *New Phytologist* **201**: 1086–1095.

Fatichi S, Pappas C, Ivanov VY. **2016**. Modeling plant-water interactions: an ecohydrological overview from the cell to the global scale. *WIREs Water* **3**: 327–368.

Fatichi S, Pappas C. **2017**. Constrained variability of modeled T:ET ratio across biomes. *Geophysical Research Letters* **44**: 6795–6803.

Fick SE, Hijmans RJ. **2017**. WorldClim 2: new 1-km spatial resolution climate surfaces for global land areas. *International Journal of Climatology* **37**: 4302–4315.

Fiora A, Cescatti A. **2006**. Diurnal and seasonal variability in radial distribution of sap flux density: Implications for estimating stand transpiration. *Tree Physiology* **26**: 1217–1225.

Fonti P, Babushkina EA. **2016**. Tracheid anatomical responses to climate in a forest-steppe in Southern Siberia. *Dendrochronologia* **39**: 32–41.

Fonti P, Heller O, Cherubini P, Rigling A, Arend M. **2013**. Wood anatomical responses of oak saplings exposed to air warming and soil drought. *Plant Biology* **15**: 210–219.

Fonti P, Jansen S. **2012**. Xylem plasticity in response to climate. *New Phytologist* **195**: 734–736.

Ford CR, Hubbard RM, Kloeppel BD, Vose JM. **2007**. A comparison of sap flux-based evapotranspiration estimates with catchment-scale water balance. *Agricultural and Forest Meteorology* **145**: 176–185.

Ford CR, McGuire MA, Mitchell RJ, Teskey RO. **2004**. Assessing variation in the radial profile of sap flux density in *Pinus* species and its effect on daily water use. *Tree Physiology* **24**: 241–249.

Foster JR, D'Amato AW, Bradford JB. **2014**. Looking for age-related growth decline in natural forests: Unexpected biomass patterns from tree rings and simulated mortality. *Oecologia* **175**: 363–374.

Fournier M, Stokes A, Coutand C, Fourcaud T, Moulia B. **2006**. Tree biomechanics and growth strategies in the context of forest functional ecology. In: Herrel A, Speck T, Rowe NP. Eds. Ecology and biomechanics: a mechanical approach to the ecology of animals and plants. Boca Raton, USA: CRC Press, 1–33.

Frank D, Esper J, Cook ER. **2007**. Adjustment for proxy number and coherence in a large-scale temperature reconstruction. *Geophysical Research Letters* **34**: 1–5.

Frank D, Esper J. **2005**. Characterization and climate response patterns of a high-elevation, multi-species tree-ring network in the European Alps. *Dendrochronologia* **22**: 107–121.

Frank D, Reichstein M, Bahn M, Thonicke K, Frank D, Mahecha MD, Smith P, van der Velde M, Vicca S, Babst F, *et al.* 2015. Effects of climate extremes on the terrestrial carbon cycle: concepts, processes and potential future impacts. *Global Change Biology* **21**: 2861–2880.

Frank DC, Esper J, Raible CC, Büntgen U, Trouet V, Stocker B, Joos F. 2010. Ensemble reconstruction constraints on the global carbon cycle sensitivity to climate. *Nature* **463**: 527–530.

Friedl MA, Sulla-Menashe D, Tan B, Schneider A, Ramankutty N, Sibley A, Huang X. 2010. *MODIS Collection 5 global land cover: Algorithm refinements and characterization of new datasets, 2001-2012, Collection 5.1 IGBP Land Cover*. Boston, USA: Boston University.

Friedlingstein P, Cox P, Betts R, Bopp L, von Bloh W, Brovkin V, Cadule P, Doney S, Eby M, Fung I, *et al.* 2006. Climate-Carbon Cycle Feedback Analysis: Results from the C4 MIP Model Intercomparison. *Journal of Climate* **19**: 3337–3353.

Friedlingstein P, Houghton RA, Marland G, Hackler J, Boden TA, Conway TJ, Canadell JG, Raupach MR, Ciais P, Le Quéré C. 2010. Update on CO_2 emissions. *Nature Geoscience* **3**: 811–812.

Friend AD, Lucht W, Rademacher TT, Keribin R, Betts R, Cadule P, Ciais P, Clark DB, Dankers R, Falloon PD, *et al.* 2014. Carbon residence time dominates uncertainty in terrestrial vegetation responses to future climate and atmospheric CO2. *Proceedings of the National Academy of Sciences* **111**: 3280–3285.

Fritts HC, Shaskin A, Downes GM. 1999. A simulation model of conifer ring growth and cell structure. In: Wimmer R, Vetter RE. Eds. Tree Ring Analysis: Biological, Methodological and Environmental Aspects. New York, USA: CABI, 320.

Fritts HC, Vaganov EA, Sviderskaya I V, Shashkin A V. 1991. Climatic variation and tree ring structure in conifers: empirical and mechanistic models of tree ring width, number of cells, cell size, cell wall thickness and wood density. *Climate Research* **1**: 97–116.

Fuchs S, Leuschner C, Link R, Coners H, Schuldt B. 2017. Calibration and comparison of thermal dissipation, heat ratio and heat field deformation sap flow probes for diffuse-porous trees. *Agricultural and Forest Meteorology* **244**–**245**: 151–161.

Fyllas NM, Gloor E, Mercado LM, Sitch S, Quesada CA, Domingues TF, Galbraith DR, Torre-Lezama A, Vilanova E, Ramírez-Angulo H, *et al.* 2014. Analysing Amazonian forest productivity using a new individual and trait-based model (TFS v.1). *Geoscientific Model Development* **7**: 1251–1269.

Galván DJ, Büntgen U, Ginzler C, Grudd H, Gutiérrez E, Labuhn I, Julio Camarero J. 2015. Drought-induced weakening of growth-temperature associations in high-elevation Iberian pines. *Global and Planetary Change* **124**: 95–106.

Gärtner H, Schweingruber FH. 2013. *Microscopic preparation techniques for plant stem analysis*. Remagen-Oberwinter, Germany: Verlag Dr. Kessel.

Gelman A, Hill J. 2007. *Data analysis using regression and multilevel/hierarchical models*. Cambridge, United Kingdom: Cambridge University Press.

Génard M, Fishman S, Vercambre G, Huguet J-G, Bussi C, Besset J, Habib R. 2001. A biophysical analysis of stem and root diameter variations in woody plants. *Plant Physiology* **126**: 188–202.

Girardin MP, Hogg EH, Bernier PY, Kurz WA, Guo XJ, Cyr G. 2016. Negative impacts of high temperatures on growth of black spruce forests intensify with the anticipated climate warming. *Global Change Biology* **22**: 627–643.

Girardin MP, Raulier F, Bernier PY, Tardif JC. 2008. Response of tree growth to a changing climate in boreal central Canada: A comparison of empirical, process-based, and hybrid modelling approaches. *Ecological Modelling* **213**: 209–228.

Gómez-Guerrero A, Silva LCR, Barrera-Reyes M, Kishchuk B, Velázquez-Martínez A, Martínez-Trinidad T, Plascencia-Escalante FO, Horwath WR. 2013. Growth decline and divergent tree ring isotopic composition ($\delta^{13}C$ and $\delta^{18}O$) contradict predictions of CO_2 stimulation in high altitudinal forests. *Global Change Biology* **19**: 1748–1758.

González-Altozano P, Pavel EW, Oncins JA, Doltra J, Cohen M, Paço T, Massai R, Castel JR. 2008. Comparative assessment of five methods of determining sap flow in peach trees. *Agricultural Water Management* **95**: 503–515.

Good SP, Noone D, Bowen G. 2015. Hydrologic connectivity constrains partitioning of global terrestrial water fluxes. *Science* **349**: 175–177.

Gower ST, Richards JH. 1990. Larches: Deciduous conifers in an evergreen world. *BioScience* **40**: 818–826.

Graham MH. 2003. Confronting multicollinearity in ecological multiple regression. *Ecology* **84**: 2809–2815.

Granier A, Biron P, Kiistner B, Gay LW, Najjar G. 1996. Comparisons of Xylem Sap Flow and Water Vapour Flux at the Stand Level and Derivation of Canopy Conductance for Scots Pine. *Theoretical and Applied Climatology* **53**: 115–122.

Granier A, Bréda N, Biron P, Villette S. 1999. A lumped water balance model to evaluate duration and intensity of drought constraints in forest stands. *Ecological Modelling* **116**: 269–283.

Granier A, Loustau D. **1994**. Measuring and modelling the transpiration of a maritime pine canopy from sap-flow data. *Agricultural and Forest Meteorology* **71**: 61–81.

Granier A. **1985**. Une nouvelle méthode pour la mesure du flux de sève brute dans le tronc des arbres. *Annals of Forest Science* **42**: 193–200.

Granier A. **1987**. Evaluation of transpiration in a Douglas-fir stand by means of sap flow measurements. *Tree Physiology* **3**: 309–320.

Green S, Clothier B, Jardine B. **2003**. Theory and Practical Application of Heat Pulse to Measure Sap Flow. *Agronomy Journal* **95**: 1371–1379.

Greenwood S, Ruiz-Benito P, Martínez-Vilalta J, Lloret F, Kitzberger T, Allen CD, Fensham R, Laughlin DC, Kattge J, Bönisch G, *et al.* 2017. Tree mortality across biomes is promoted by drought intensity, lower wood density and higher specific leaf area. *Ecology Letters* **20**: 539–553.

Gregory RA, Wilson BF. **1968**. A comparison of cambial activity of white spruce in Alaska and New England. *Canadian Journal of Botany* **46**: 733–734.

Gričar J, Prislan P, De Luis M, Novak K, Longares LA, del Castillo EM, Čufar K. **2016**. Lack of annual periodicity in cambial production of phloem in trees from Mediterranean areas. *IAWA Journal* **37**: 349–364.

Groenendijk P, van der Sleen P, Vlam M, Bunyavejchewin S, Bongers F, Zuidema PA. **2015**. No evidence for consistent long-term growth stimulation of 13 tropical tree species: results from tree-ring analysis. *Global Change Biology* **21**: 3762–3776.

Groover A, Jones AM. **1999**. Tracheary Element Differentiation Uses a Novel Mechanism Coordinating Programmed Cell Death and Secondary Cell Wall Synthesis. *Plant Physiology* **119**: 375–384.

Grossiord C, Sevanto S, Borrego I, Chan AM, Collins AD, Dickman LT, Hudson PJ, Mcbranch N, Michaletz ST, Pockman WT, *et al.* 2017. Tree water dynamics in a drying and warming world. *Plant, Cell & Environment* **40**: 1861–1873.

Guillemot J, Francois C, Hmimina G, Dufrêne E, Martin-StPaul NK, Soudani K, Marie G, Ourcival JM, Delpierre N. **2017**. Environmental control of carbon allocation matters for modelling forest growth. *New Phytologist* **214**: 180–193.

Hacke UG, Sperry JS, Pockman WT, Davis SD, McCulloh KA. **2001**. Trends in wood density and structure are linked to prevention of xylem implosion by negative pressure. *Oecologia* **126**: 457–461.

Handa IT, Körner C, Hättenschwiler S. **2005**. A test of the treeline carbon limitation hypothesis by in situ CO_2 enrichment and defoliation. *Ecology* **86**: 1288–1300.

Hanewinkel M, Cullmann DA, Schelhaas M-J, Nabuurs G-J, Zimmermann NE. **2012**. Climate change may cause severe loss in the economic value of European forest land. *Nature Climate Change* **3**: 203–207.

Hansen MCC, Potapov P V, Moore R, Hancher M, Turubanova SA, Tyukavina A, Thau D, Stehman S V, Goetz SJ, Loveland TR, *et al.* 2013. High-Resolution Global Maps of 21st-Century Fores Cover Change. *Science* **342**: 850–854.

Hartl-Meier C, Dittmar C, Zang C, Rothe A. **2014**. Mountain forest growth response to climate change in the Northern Limestone Alps. *Trees* **28**: 819–829.

Hartl-Meier C, Esper J, Liebhold A, Konter O, Rothe A, Büntgen U. **2017**. Effects of host abundance on larch budmoth outbreaks in the European Alps. *Agricultural and Forest Entomology* **19**: 376–387.

Hartmann F, Rathgeber C, Fournier M, Moulia B. **2017**. Modelling wood formation and structure: power and limits of a morphogenetic gradient in controlling xylem cell proliferation and growth. *Annals of Forest Science* **74**: 1–15.

Hatton TJ, Wu H. **1995**. A scaling theory to extrapolate individual tree water use to stand water use. *Hydrological Processes* **9**: 527–540.

Hayat A, Hacket-pain AJ, Pretzsch H, Rademacher TT, Friend AD. **2017**. Modeling Tree Growth Taking into Account Carbon Source and Sink Limitations. *Frontiers in Plant Science* **8**: 1–15.

Hember RA, Kurz WA, Metsaranta JM, Black TA, Guy RD, Coops NC. **2012**. Accelerating regrowth of temperate-maritime forests due to environmental change. *Global Change Biology* **18**: 2026–2040.

Herbst M, Rosier PTW, Morecroft MD, Gowlng DJ. **2008**. Comparative measurements of transpiration and canopy conductance in two mixed deciduous woodlands differing in structure and species composition. *Tree Physiology* **28**: 959–970.

Hetherington A, Woodward FI. **2003**. The role of stomata in sensing and driving environmental change. *Nature* **424**: 901–908.

Hicke JA, Allen CD, Desai AR, Dietze MC, Hall RJ, Ted Hogg EH, Kashian DM, Moore D, Raffa KF, Sturrock RN, *et al.* 2012. Effects of biotic disturbances on forest carbon cycling in the United States and Canada. *Global Change Biology* **18**: 7–34.

Hikosaka K, Ishikawa K, Borjigidai A, Muller O, Onoda Y. **2006**. Temperature acclimation of photosynthesis: mechanisms involved in the changes in temperature dependence of photosynthetic rate. *Journal of Experimental Botany* **57**: 291–302.

Holbrook NM, Zwieniecki M a. **2003**. Plant biology: water gate. *Nature* **425**: 361.

Holmes RL. **1983**. Computer-assisted quality control in tree-ring dating and measurement. *Tree-ring Bulletin* **43**: 69–78.
Hölttä T, Vesala T, Sevanto S, Perämäki M, Nikinmaa E. **2006**. Modeling xylem and phloem water flows in trees according to cohesion theory and Münch hypothesis. *Trees* **20**: 67–78.
Hsiao TC, Acevedo E, Fereres E, Henderson DW. **1976**. Stress Metabolism: Water stress, growth, and osmotic adjustment. *Philosophical Transactions of the Royal Society of London. Series B, Biological Sciences* **273**: 479–500.
Hsiao TC, Frensch J, Raja-Lara BA. **1998**. The pressure-jump technique shows maize leaf growth to be enhanced by increases in turgor only when water status is not too high. *Plant, Cell and Environment* **21**: 33–42.
Huang J-G, Bergeron Y, Denneler B, Berninger F, Tardif J. **2007**. Response of Forest Trees to Increased Atmospheric CO_2. *Critical Reviews in Plant Sciences* **26**: 265–283.
Hubbard RM, Stape J, Ryan MG, Almeida AC, Rojas J. **2010**. Effects of irrigation on water use and water use efficiency in two fast growing *Eucalyptus* plantations. *Forest Ecology and Management* **259**: 1714–1721.
Hughes MK, Schweingruber FH, Cartwright D, Kelly PM. **1984**. July-August temperature at Edinburgh between 1721 and 1975 from tree-ring density and width data. *Nature* **308**: 341–344.
Hultine KR, Nagler PL, Morino K, Bush SE, Burtch KG, Dennison PE, Glenn EP, Ehleringer JR. **2010**. Sap flux-scaled transpiration by tamarisk (*Tamarix* spp.) before, during and after episodic defoliation by the saltcedar leaf beetle (*Diorhabda carinulata*). *Agricultural and Forest Meteorology* **150**: 1467–1475.
Hunt ER, Running SW, Federer CA. **1991**. Extrapolating plant water flow resistances and capacitances to regional scales. *Agricultural and Forest Meteorology* **54**: 169–195.
Huntzinger DN, Michalak AM, Schwalm C, Ciais P, King AW, Fang Y, Schaefer K, Wei Y, Cook RB, Fisher JB, *et al.* 2017. Uncertainty in the response of terrestrial carbon sink to environmental drivers undermines carbon-climate feedback predictions. *Scientific Reports* **7**: 1–8.
Hutcheson G. **2012**. *Data Analysis in R and the R-commander (Rcmdr)*. Manchester, United Kingdom: Manchester University.
Hutjes RWA, Kabat P, Running SW, Shuttleworth WJ, Field C, Bass B, Silva MAF, Avissar R, Becker A, Claussen M, *et al.* 1998. Biospheric Aspects of the Hydrological Cycle. *Journal of Hydrology* **212**–**213**: 1–21.
Hyvonen R, Agren GI, Linder S, Persson T, Cotrufo MF, Ekblad A, Freeman M, Grelle A, Janssens IA, Jarvis PG, *et al.* 2007. The likely impact of elevated [CO_2], nitrogen deposition, increased temperature and management on carbon sequestration in temperate and boreal forest ecosystems: a literature review. *New Phytol* **173**: 463–480.
IPCC. **2007**. *Climate Change 2007: The Physical Science Basis. Contribution of Working Group I to the Fourth Assessment Report of the Intergovernmental Panel on Climate Change*. Cambridge, United Kingdom: Cambridge University Press.
IPCC. **2013**. *Climate Change 2013: The Physical Science Basis. Contribution of Working Group I to the Fifth Assessment Report of the Intergovernmental Panel on Climate Change*. Cambridge, United Kingdom and New York: Cambridge University Press.
Irvine J, Grace J. **1997**. Continuous measurements of water tensions in the xylem of trees based on the elastic properties of wood. *Planta* **202**: 455–461.
Isarangkool Na Ayutthaya S, Do FC, Pannengpetch K, Junjittakarn J, Maeght JL, Rocheteau A, Cochard H. **2010**. Transient thermal dissipation method of xylem sap flow measurement: Multi-species calibration and field evaluation. *Tree Physiology* **30**: 139–148.
Iyengar S V, Balakrishnan J, Kurths J. **2016**. Impact of climate change on larch budmoth cyclic outbreaks. *Scientific Reports* **6**: 1–8.
Jacoby GC, D'Arrigo RD, Davaajamts T. **1996**. Mongolian Tree Rings and 20th-Century Warming. *Science* **273**: 771–773.
Jarvis PG. **1976**. The interpretation of the variations in leaf water potential and stomatal conductance found in canopies in the field. *Philosophical Transactions of the Royal Society of London. Series B, Biological Sciences* **273**: 593–610.
Ježík M, Blaženec M, Letts MG, Ditmarová Ľ, Sitková Z, Střelcová K. **2015**. Assessing seasonal drought stress response in Norway spruce (*Picea abies* (L.) Karst.) by monitoring stem circumference and sap flow. *Ecohydrology* **386**: 378–386.
Johnson DM, Bjørnstad ON, Liebhold AM. **2004**. Landscape geometry and travelling waves in the larch budmoth. *Ecology Letters* **7**: 967–974.
Johnson DM, Buntgen U, Frank DC, Kausrud K, Haynes KJ, Liebhold AM, Esper J, Stenseth NC. **2010**. Climatic warming disrupts recurrent Alpine insect outbreaks. *Proceedings of the National Academy of Sciences* **107**: 20576–20581.

Jones HG. **1992**. *Plants and microclimate, a quantitative approach to environmental plant physiology*. Cambridge, United Kingdom: Cambridge University Press.

Kallarackal J, Otieno DO, Reineking B, Jung EY, Schmidt MWT, Granier A, Tenhunen JD. **2013**. Functional convergence in water use of trees from different geographical regions: A meta-analysis. *Trees - Structure and Function* **27**: 787–799.

Kaufmann E. **2001**. Estimating standing timber, growth and cut. In: Brassel P, Lischke H. Eds. Swiss National Forest Inventory: Methods and Models of the Second Assessment. Birmensdorf, Switzerland: Swiss Federal Institute for Forest, Snow and Landscape Research (WSL), 162–196.

Kavanagh KL, Pangle R, Schotzko AD. **2007**. Nocturnal transpiration causing disequilibrium between soil and stem predawn water potential in mixed conifer forests of Idaho. *Tree Physiology* **27**: 621–629.

Kelliher M, Leuning R, Schulze D. **1993**. Evaporation and canopy characteristics of coniferous forests and grasslands. *Oecologia* **95**: 153–163.

King G, Fonti P, Nievergelt D, Büntgen U, Frank D. **2013a**. Climatic drivers of hourly to yearly tree radius variations along a 6°C natural warming gradient. *Agricultural and Forest Meteorology* **168**: 36–46.

King GM, Gugerli F, Fonti P, Frank DC. **2013b**. Tree growth response along an elevational gradient: climate or genetics? *Oecologia* **173**: 1587–1600.

Kirdyanov A, Hughes M, Vaganov E, Schweingruber F, Silkin P. **2003**. The importance of early summer temperature and date of snow melt for tree growth in the Siberian Subarctic. *Trees - Structure and Function* **17**: 61–69.

Kirtman B, Power SB, Adedoyin AJ, Boer GJ, Bojariu R, Camilloni I, Doblas-Reyes F, Fiore AM, Kimoto M, Meehl GA, *et al.* 2013. Near-term climate change: projections and predictability. In: Stocker TF, Qin D, Plattner GK, Tignor M, Allen SK, Boschung J, Nauels A, Xia Y, Bex V, Midgley PM. Eds. Climate Change 2013: The Physical Science Basis. Contribution of Working Group I to the Fifth Assessment Report of the Intergovernme. Cambridge, United Kingdom: Cambridge University Press, 953–1028.

Klein T. **2014**. The variability of stomatal sensitivity to leaf water potential across tree species indicates a continuum between isohydric and anisohydric behaviours. *Functional Ecology* **28**: 1313–1320.

Klesse S, Etzold S, Frank D. **2016**. Integrating tree-ring and inventory-based measurements of aboveground biomass growth: research opportunities and carbon cycle consequences from a large snow breakage event in the Swiss Alps. *European Journal of Forest Research* **135**: 297–311.

Kobayashi Y, Tanaka T. **2001**. Water flow and hydraulic characteristics of Japanese red pine and oak trees. *Hydrological Processes* **15**: 1731–1750.

Köcher P, Horna V, Leuschner C. **2013**. Stem water storage in five coexisting temperate broad-leaved tree species: Significance, temporal dynamics and dependence on tree functional traits. *Tree Physiology* **33**: 817–832.

Konter O, Esper J, Liebhold A, Kyncl T, Schneider L, Düthorn E, Büntgen U. **2015**. Tree-ring evidence for the historical absence of cyclic larch budmoth outbreaks in the Tatra Mountains. *Trees* **29**: 809–814.

Körner C, Bannister P, Mark AF. **1986**. Altitudinal variation in stomatal conductance, nitrogen content and leaf anatomy in different plant life forms in New Zealand. *Oecologia* **69**: 577–588.

Körner C, Cochrane PM. **1985**. Stomatal responses and water relations of *Eucalyptus paucitlora* in summer along an elevational gradient. *Oecologia* **66**: 443–455.

Körner C, Paulsen J. **2004**. A world-wide study of high altitude treeline temperatures. *Journal of Biogeography* **31**: 713–732.

Körner C. **1998**. A re-assessment of high elevation treeline positions and their explanation. *Oecologia* **115**: 445–459.

Körner C. **2003**. Carbon limitation in trees. *Journal of Ecology* **91**: 4–17.

Körner C. **2007**. Climatic treelines: conventions, global patterns, causes. *Erdkunde* **61**: 316–324.

Körner C. **2008**. Winter crop growth at low temperature may hold the answer for alpine treeline formation. *Plant Ecology and Diversity* **1**: 3–11.

Körner C. **2012**. *Alpine treelines: Functional Ecology of the global high elevation tree limits*. Basel, Switzerland: Springer.

Körner C. **2015**. Paradigm shift in plant growth control. *Plant Biology* **25**: 107–114.

Körner C. **2017**. A matter of tree longevity. *Science* **355**: 130–131.

Köstner B, Granier A, Cermák J. **1998**. Original article Sapflow measurements in forest stands: methods and uncertainties. *Annals of Forest Science* **55**: 13–27.

Kozlowski TT, Pallardy SG. **1997**. *Physiology of woody plants*. San Diego, USA: Academic Press.

Kozlowski TT. **1962**. *Tree Growth*. New York, USA: Ronald Press Company.

Kravka M, Krejzar T, Čermák KJ. **1999**. Water content in stem wood of large pine and spruce trees in natural forests in central Sweden. *Agricultural and Forest Meteorology* **99**: 555–562.

Kress A, Saurer M, Büntgen U, Treydte KS, Bugmann H, Siegwolf RTW. **2009**. Summer temperature dependency of larch budmoth outbreaks revealed by Alpine tree-ring isotope chronologies. *Oecologia* **160**: 353–365.

Kunert N, Schwendenmann L, Hölscher D. **2010**. Agricultural and Forest Meteorology Seasonal dynamics of tree sap flux and water use in nine species in Panamanian forest plantations. *Agricultural and Forest Meteorology* **150**: 411–419.

Kurz WA, Dymond CC, Stinson G, Rampley GJ, Neilson ET, Carroll AL, Ebata T, Safranyik L. **2008**. Mountain pine beetle and forest carbon feedback to climate change. *Nature* **452**: 987–990.

Landsberg JJ, Blanchard TW, Warrit B. **1976**. Studies on the Movement of Water through Apple Trees. *Journal of Experimental Botany* **27**: 579–596.

Langensiepen M, Kupisch M, Graf A, Schmidt M, Ewert F. **2014**. Improving the stem heat balance method for determining sap-flow in wheat. *Agricultural and Forest Meteorology* **186**: 34–42.

Larocque SJ, Smith DJ. **2005**. A dendroclimatological reconstruction of climate since AD 1700 in the Mt. Waddington area, British Columbia Coast Mountains, Canada. *Dendrochronologia* **22**: 93–106.

Lawrence DM, Thornton PE, Oleson KW, Bonan GB. **2007**. The Partitioning of Evapotranspiration into Transpiration, Soil Evaporation, and Canopy Evaporation in a GCM: Impacts on Land-Atmosphere Interaction. *Journal of Hydrometeorology* **8**: 862–880.

Leo M, Oberhuber W, Schuster R, Grams TEE, Matyssek R, Wieser G. **2014**. Evaluating the effect of plant water availability on inner alpine coniferous trees based on sap flow measurements. *European Journal for Forest Research* **133**: 691–698.

Liang W, Heinrich I, Helle G, Liñán ID, Heinken T. **2013**. Applying CLSM to increment core surfaces for histometric analyses: A novel advance in quantitative wood anatomy. *Dendrochronologia* **31**: 140–145.

Lin Y, Medlyn BE, Duursma RA, Prentice IC, Wang H, Baig S, Eamus D, Resco de Dios V, Mitchel P, Ellsworth DS, *et al.* 2015. Optimal stomatal behaviour around the world. *Nature Climate Change* **5**: 459–464.

Lindner M, Maroschek M, Netherer S, Kremer A, Barbati A, Garcia-Gonzalo J, Seidl R, Delzon S, Corona P, Kolström M, *et al.* 2010. Climate change impacts, adaptive capacity, and vulnerability of European forest ecosystems. *Forest Ecology and Management* **259**: 698–709.

Lindroth A. **1985**. Canopy Conductance of Coniferous Forests Related to Climate. *Water Resources Research* **21**: 297–304.

Lintunen A, Paljakka T, Jyske T, Peltoniemi M, Sterck F, von Arx G, Cochard H, Copini P, Caldeira MC, Delzon S, *et al.* 2016. Osmolality and Non-Structural Carbohydrate Composition in the Secondary Phloem of Trees across a Latitudinal Gradient in Europe. *Frontiers in Plant Science* **7**: 1–15.

Livingston NJ, Black TA. **1987**. Stomatal characteristics and transpiration of three species of conifer seedlings planted on a high elevation south-facing clear-cut. *Canadian Journal of Forest Research* **17**: 1273–1282.

Lockhart JA. **1965**. An Analysis of Irreversible Plant Cell Elongation. *Journal of Theoretical Biology* **8**: 264–275.

Locosselli GM, Ceccantini G. **2012**. Plasticity of stomatal distribution pattern and stem tracheid dimensions in Podocarpus lambertii: An ecological study. *Annals of Botany* **110**: 1057–1066.

Longuetaud F, Mothe F, Leban J, Mäkelä A. **2007**. *Picea abies* sapwood width: Variations within and between trees. *Scandinavian Journal of Forest Research* **21**: 41–53.

López R, López De Heredia U, Collada C, Cano FJ, Emerson BC, Cochard H, Gil L. **2013**. Vulnerability to cavitation, hydraulic efficiency, growth and survival in an insular pine (*Pinus canariensis*). *Annals of Botany* **111**: 1167–1179.

Lu P, Chacko E. **1998**. Evaluation of Granier's sap flux in young mango trees sensor. *Agronomie* **18**: 461–471.

Lu P, Müller WJ, Chacko EK. **2000**. Spatial variations in xylem sap flux density in the trunk of orchard-grown, mature mango trees under changing soil water conditions. *Tree Physiology* **20**: 683–692.

Lu P, Urban L, Zhao P. **2004**. Granier's Thermal Dissipation Probe (TDP) method for measuring sap flow in trees: Theory and practice. *Acta Botanica Sinica* **46**: 631–646.

Lubczynski MW, Chavarro-Rincon D, Roy J. **2012**. Novel, cyclic heat dissipation method for the correction of natural temperature gradients in sap flow measurements. Part 1. Theory and application. *Tree Physiology* **32**: 894–912.

Lundblad M, Lagergen F, Lindroth A. **2001**. Evaluation of heat balance and heat dissipation methods for sapflow measurements in pine and spruce. *Annals of Forest Science* **58**: 625–638.

Luomala E, Laitinen K, Sutinen S, Kellomäki S, Vapaavuori E. **2002**. Stomatal density, anatomy and nutrient concentrations of Scots pine needles are affected by elevated CO_2. *Plant, Cell and Environment* **28**: 733–749.

Lupi C, Morin H, Deslauriers A, Rossi S. **2010**. Xylem phenology and wood production: Resolving the chicken-or-egg dilemma. *Plant, Cell and Environment* **33**: 1721–1730.

Ma C, Luo Y, Shao M, Li X, Sun L, Jia X. **2017**. Environmental controls on sap flow in black locust forest in Loess Plateau, China. *Scientific Reports* **7**: 1–12.

Macinnis-Ng C, Webb T, Lin YS, Schwendenmann L, Medlyn B. **2017**. Leaf age-related and diurnal variation in gas exchange of kauri (*Agathis australis*). *New Zealand Journal of Botany* **55**: 80–99.

Magnani F, Borghettt M. **1995**. Interpretation of seasonal changes of xylem embolism and plant hydraulic resistance in *Fagus sylvatica*. *Plant, Cell and Environment* **18**: 689–696.

Mahan JR, McMichael BL, Wanjura DF. **1997**. Reduction of high temperature stress in plants. In: Basra AS, Basra RK. Eds. Mechanisms of environmental stress resistance in plants. Amsterdam, The Netherlands: Harwood Academic Publishers, 137–150.

Maire V, Martre P, Kattge J, Gastal F, Esser G, Fontaine S, Soussana JF. **2012**. The coordination of leaf photosynthesis links C and N fluxes in C3 plant species. *PLoS ONE* **7**: 1–15.

Marañón-Jiménez S, Van Den Bulcke J, Piayda A, Van Acker J, Cuntz M, Rebmann C, Steppe K. **2018**. X-ray computed microtomography characterizes the wound effect that causes sap flow underestimation by thermal dissipation sensors. *Tree Physiology* **38**: 288–302.

Martin-Benito D, Anchukaitis KJ, Evans MN, del Río M, Beeckman H, Cañellas I. **2017**. Effects of drought on xylem anatomy and water-use efficiency of two co-occurring pine species. *Forests* **8**: 1–19.

Martin-Benito D, Beeckman H, Cañellas I. **2013**. Influence of drought on tree rings and tracheid features of *Pinus nigra* and *Pinus sylvestris* in a mesic Mediterranean forest. *European Journal of Forest Research* **132**: 33–45.

Martínez-Vilalta J, Cochard H, Mencuccini M, Sterck F, Herrero A, Korhonen JFJ, Llorens P, Nikinmaa E, Nolè A, Poyatos R, *et al.* 2009. Hydraulic adjustment of Scots pine across Europe. *New Phytologist* **184**: 353–364.

Martínez-Vilalta J, Sala A, Asensio D, Galiano L, Hoch G, Palacio S, Piper FI, Lloret F. **2016**. Dynamics of non-structural carbohydrates in terrestrial plants: A global synthesis. *Ecological Monographs* **86**: 495–516.

Maseyk KS, Lin T, Rotenberg E, Grünzweig JM, Schwartz A, Yakir D. **2008**. Physiology-phenology interactions in a productive semi-arid pine forest. *New Phytologist* **178**: 603–616.

Mastrotheodoros T, Pappas C, Molnar P, Burlando P, Keenan TF, Gentine P, Gough CM, Fatichi S. **2017**. Linking plant functional trait plasticity and the large increase in forest water use efficiency. *Journal of Geophysical Research: Biogeosciences* **122**: 2393–2408.

Matheny AM, Bohrer G, Garrity SR, Morin TH, Howard CJ, Vogel CS. **2015**. Observations of stem water storage in trees of opposing hydraulic strategies. *Ecosphere* **6**: 1–13.

Matheny AM, Bohrer G, Vogel CS, Morin TH, He L, Prata de moraes Frasson R, Mirfenderesgi G, Schäfer KVR, Gough CM, Ivanov VY, *et al.* 2014. Species-specific transpiration responses to intermediate disturbance in a northern hardwood forest. *Journal of Geophysical Research: Biogeosciences* **119**: 2292–2311.

Mayr S, Hacke U, Schmid P, Schienbacher F, Gruber A. **2006**. Frost drought in conifers at the alpine timberline: Xylem disfunction and adaptations. *Ecology* **87**: 3175–3185.

Mayr S. **2007**. Limits in water relations. In: Wieser G, Tausz M. Eds. Trees at their upper limit. Dordrecht, The Netherlands: Springer, 145–162.

McCarroll D, Loader NJ. **2004**. Stable isotopes in tree rings. *Quaternary Science Reviews* **23**: 771–801.

McCulloh KA, Johnson DM, Meinzer FC, Woodruff DR. **2014**. The dynamic pipeline: hydraulic capacitance and xylem hydraulic safety in four tall conifer species. *Plant, Cell & Environment* **37**: 1171–1183.

McCulloh KA, Winter K, Meinzer FC, Aranda GJ, Lachenbruch B. **2007**. A comparison of daily water use estimates derived from constant-heat sap-flow probe values and gravimetric measurements in pot-grown saplings. *Tree physiology* **27**: 1355–1360.

McMahon SM, Parker GG, Miller DR. **2010**. Evidence for a recent increase in forest growth. *Proceedings of the National Academy of Sciences* **107**: 3611–3615.

McMurtrie RE, Norby RJ, Medlyn BE, Dewar RC, Pepper DA, Reich PB, Barton CVM. **2008**. Why is plant-growth response to elevated CO_2 amplified when water is limiting, but reduced when nitrogen is limiting? A growth-optimisation hypothesis. *Functional Plant Biology* **35**: 521–534.

Medvigy D, Clark KL, Skowronski NS, Schäfer KVR. **2012**. Simulated impacts of insect defoliation on forest carbon dynamics. *Environmental Research Letters* **7**: 1–9.

Meier ES, Lischke H, Schmatz DR, Zimmermann NE. **2012**. Climate, competition and connectivity affect future migration and ranges of European trees. *Global Ecology and Biogeography* **21**: 164–178.

Meinzer FC, Johnson DM, Lachenbruch B, Mcculloh KA, Woodruff DR. **2009**. Xylem hydraulic safety margins in woody plants: coordination of stomatal control of xylem tension with hydraulic capacitance. *Functional Ecology* **23**: 922–930.

Meinzer FC, Woodruff DR, Domec J-C, Goldstein G, Campanello PI, Gatti MG, Villalobos-vega R. **2008**. Coordination of leaf and stem water transport properties in tropical forest trees. *Oecologia* **156**: 31–41.

Meinzer FC, Woodruff DR, Eissenstat DM, Lin HS, Adams TS, McCulloh KA. **2013**. Above- and belowground controls on water use by trees of different wood types in an eastern US deciduous forest. *Tree Physiology* **33**: 345–356.

Mellerowicz E, Coleman W, Riding R, Little C. **1992**. Periodicity of cambial activity in Abies balsamea. I. Effects of temperature and photoperiod on cambial dormancy and frost hardiness. *Physiologia Plantarum* **85**: 515–525.

Mencuccini M, Hölttä T, Sevanto S, Nikinmaa E. **2013**. Concurrent measurements of change in the bark and xylem diameters of trees reveal a phloem-generated turgor signal. *New Phytologist* **198**: 1143–1154.

Mencuccini M. **2003**. The ecological significance of long-distance water transport: Short-term regulation, long-term acclimation and the hydraulic costs of stature across plant life forms. *Plant, Cell and Environment* **26**: 163–182.

Milne R, Young P. **1982**. Modelling of Water Movement in Trees. *IFAC Proceedings Volumes* **18**: 463–468.

Monteith JL, Unsworth M. **2013**. *Principles of Environmental Physics*. Oxford, UK: Academic Press.

Monteith JL. **1965**. Evaporation and environment. *Symposia of the Society for Experimental Biology* **19**: 205–234.

Moore DJP, Trahan NA, Wilkes P, Quaife T, Stephens BB, Elder K, Desai AR, Negron J, Monson RK. **2013**. Persistent reduced ecosystem respiration after insect disturbance in high elevation forests. *Ecology Letters* **16**: 731–737.

Moore GW, Bond BJ, Jones JA, Meinzer FC. **2010**. Thermal-dissipation sap flow sensors may not yield consistent sap-flux estimates over multiple years. *Trees - Structure and Function* **24**: 165–174.

Moser L, Fonti P, Büntgen U, Esper J, Luterbacher J, Franzen J, Frank D. **2009**. Timing and duration of European larch growing season along altitudinal gradients in the Swiss Alps. *Tree Physiology* **30**: 225–233.

Muller B, Pantin F, Génard M, Turc O, Freixes S, Piques M, Gibon Y. **2011**. Water deficits uncouple growth from photosynthesis, increase C content, and modify the relationships between C and growth in sink organs. *Journal of Experimental Botany* **62**: 1715–1729.

Murray MB, Cannell MGR, Smith RI. **1989**. Date of Budburst of Fifteen Tree Species in Britain Following Climatic Warming. *Journal of Applied Ecology* **26**: 693–700.

Myneni RB, Dong J, Tucker CJ, Kaufmann RK, Kauppi PE, Liski J, Zhou L, Alexeyev V, Hughes MK. **2001**. A large carbon sink in the woody biomass of Northern forests. *Proceedings of the National Academy of Sciences* **98**: 14784–14789.

Nabuurs G-J, Lindner M, Verkerk PJ, Gunia K, Deda P, Michalak R, Grassi G. **2013**. First signs of carbon sink saturation in European forest biomass. *Nature Climate Change* **3**: 792–796.

Nadezhdina N, Cermák J, Ceulemans R. **2002**. Radial patterns of sap flow in woody stems of dominant and understory species: scaling errors associated with positioning of sensors. *Tree physiology* **22**: 907–18.

Nardin M, Musch B, Rousselle Y, Guérin V, Sanchez L, Rossi JP, Gerber S, Marin S, Pâques LE, Rozenberg P. **2015**. Genetic differentiation of European larch along an altitudinal gradient in the French Alps. *Annals of Forest Science* **72**: 517–527.

Nawrot M, Pazdrowski W, Szymański M. **2008**. Dynamics of heartwood formation and axial and radial distribution of sapwood and heartwood in stems of European larch (*Larix decidua* Mill.). *Journal of Forest Science* **54**: 409–417.

Nehrbass-Ahles C, Babst F, Klesse S, Nötzli M, Bouriaud O, Neukom R, Dobbertin M, Frank D. **2014**. The influence of sampling design on tree-ring-based quantification of forest growth. *Global Change Biology* **20**: 2867–2885.

Nemani RR, Keeling CD, Hashimoto H, Jolly WM, Piper SC, Tucker CJ, Myneni RB, Running SW. **2003**. Climate-driven increases in global terrestrial net primary production from 1982 to 1999. *Science* **300**: 1560–1563.

Nobel PS. **2009**. *Physicochemical and Environmental Plant Physiology*. United Kingdom, Oxford: Elsevier Inc.

Nonweiler TRF. **1975**. Appendix 1: Flow of biological fluids through non-ideal capillaries. In: Zimmermann MH, Milburn JA. Eds. Transport in plants 1. Phloem transport. New York, USA: Springer Berlin Heidelberg, 474–477.

Norby RJ, Zak DR. **2011**. Ecological Lessons from Free-Air CO_2 Enrichment (FACE) Experiments. *Annual Review of Ecology, Evolution, and Systematics* **42**: 181–203.

Nourtier M, Chanzy A, Granier A, Huc R. **2011**. Sap flow measurements by thermal dissipation method using cyclic heating: A processing method accounting for the non-stationary regime. *Annals of Forest Science* **68**: 1255–1264.

Novick KA, Oren R, Stoy PC, Siqueira MBS, Katul GG. **2009**. Nocturnal evapotranspiration in eddy-covariance records from three co-located ecosystems in the Southeastern U.S.: Implications for annual fluxes. *Agricultural and Forest Meteorology* **149**: 1491–1504.

Oberhuber W, Kofler W, Schuster R, Wieser G. **2015**. Environmental effects on stem water deficit in co-occurring conifers exposed to soil dryness. *International Journal of Biometeorology* **417**–**426**: 417–426.

Ohtsuka T, Saigusa N, Koizumi H. **2009**. On linking multiyear biometric measurements of tree growth with eddy covariance-based net ecosystem production. *Global Change Biology* **15**: 1015–1024.

Oishi AC, Hawthorne DA, Oren R. **2016**. Baseliner: An open-source, interactive tool for processing sap flux data from thermal dissipation probes. *SoftwareX* **5**: 139–143.

Oishi AC, Oren R, Stoy PC. **2008**. Estimating components of forest evapotranspiration: A footprint approach for scaling sap flux measurements. *Agricultural and Forest Meteorology* **148**: 1719–1732.

Olano JM, González-Muñoz N, Arzac A, Rozas V, Von Arx G, Delzon S, García-Cervigón AI. **2017**. Sex determines xylem anatomy in a dioecious conifer: hydraulic consequences in a drier world. *Tree Physiology* **37**: 1493–1502.

Oliveras I, Llorens P. **2001**. Medium-term sap flux monitoring in a Scots pine stand: analysis of the operability of the heat dissipation method for hydrological purposes. *Tree physiology* **21**: 473–480.

Oren R, Phillips N, Ewers BE, Pataki DE, Megonigal JP. **1999a**. Sap-Flux-Scaled Transpiration Responses To Light, Vapor Pressure Deficit, and Leaf Area Reduction in a flooded *Taxodium distichum* forest. *Tree Physiology* **19**: 337–347.

Oren R, Sperry JS, Katul GG, Pataki DE, Ewers BE, Phillips N, Schäfer KVR. **1999b**. Survey and synthesis of intra- and interspecific variation in stomatal sensitivity to vapour pressure deficit. *Plant, Cell & Environment* **22**: 1515–1526.

Osborn TJ, Briffa KR, Jones PD. **1997**. Adjusting variance for sample-size in tree-ring chronologies and other regional mean timeseries. *Dendrochronologia* **15**: 89–99.

Paljakka T, Jyske T, Lintunen A, Aaltonen H, Nikinmaa E, Hölttä T. **2017**. Gradients and dynamics of inner bark and needle osmotic potentials in Scots pine (*Pinus sylvestris* L.) and Norway spruce (*Picea abies* L. Karst). *Plant Cell and Environment* **40**: 2160–2173.

Pan Y, Birdsey RA, Fang J, Houghton R, Kauppi PE, Kurz WA, Phillips OL, Shvidenko A, Lewis SL, Canadell JG, *et al.* 2011. A Large and Persistent Carbon Sink in the World's Forests. *Science* **333**: 988–994.

Pappas C, Fatichi S, Burlando P. **2016**. Modeling terrestrial carbon and water dynamics across climatic gradients: Does plant trait diversity matter? *New Phytologist* **209**: 137–151.

Pappas C, Matheny AM, Baltzer JL, Barr A, Black TA, Bohrer G, Detto M, Maillet J, Roy A, Sonnentag O, *et al.* 2018. Boreal tree hydrodynamics: asynchronous, diverging, yet complementary. *Tree physiology* **38**: 953–964.

Parent B, Turc O, Gibon Y, Stitt M, Tardieu F. **2010**. Modelling temperature-compensated physiological rates, based on the co-ordination of responses to temperature of developmental processes. *Journal of Experimental Botany* **61**: 2057–2069.

Park WK, Vaganov EA, Shashkin A V, Pusingha P. 1998. Influence of global warming on radial growth in Korean conifers: simulation models using intra-annual variations of tracheid dimensions. *IAWA Journal*: 19–478.

Park Y-ID, Spiecker H. **2005**. Variations in the tree-ring structure of Norway spruce (*Picea abies*) under contrasting climates. *Dendrochronologia* **23**: 93–104.

Pasztor F, Matulla C, Rammer W, Lexer MJ. **2014**. Drivers of the bark beetle disturbance regime in Alpine forests in Austria. *Forest Ecology and Management* **318**: 349–358.

Paudel I, Kanety T, Cohen S. **2013**. Inactive xylem can explain differences in calibration factors for thermal dissipation probe sap flow measurements. *Tree Physiology* **33**: 986–1001.

Paulsen J, Weber UM, Körner C. **2000**. Tree Growth near Treeline: Abrupt or Gradual Reduction with Altitude? *Arctic, Antarctic, and Alpine Research* **32**: 14–20.

Peñuelas J, Canadell JG, Ogaya R. **2011**. Increased water-use efficiency during the 20th century did not translate into enhanced tree growth. *Global Ecology and Biogeography* **20**: 597–608.

Peñuelas J, Rutishauser T, Filella I. **2010**. Phenology Feedbacks on Climate Change. *Science* **324**: 887–889.

Pepin S, Körner C. **2002**. Web-FACE: A new canopy free-air CO_2 enrichment system for tall trees in mature forests. *Oecologia* **133**: 1–9.

Perämäki M, Nikinmaa E, Sevanto S, Ilvesniemi H, Siivola E, Hari P, Vesala T. **2001**. Tree stem diameter variations and transpiration in Scots pine: an analysis using a dynamic sap flow model. *Tree Physiology* **21**: 889–897.

Peters RL, Balanzategui D, Hurley AG, Arx G Von, Luisa A, Cuny HE, Björklund J, Frank DC, Fonti P. **2018**. RAPTOR : Row and position tracheid organizer in R. *Dendrochronologia* **47**: 10–16.

Peters RL, Fonti P, Frank DC, Poyatos R, Pappas C, Kahmen A, Carraro V, Prendin AL, Schneider L, Baltzer JL, *et al.* In press. Quantification of uncertainties in conifer sap flow measured with the thermal dissipation method. *New Phytologist*

Peters RL, Groenendijk P, Vlam M, Zuidema PA. **2015**. Detecting long-term growth trends using tree rings: A critical evaluation of methods. *Global Change Biology* **21**: 2040–2054

Peters RL, Klesse S, Fonti P, Frank DC. **2017**. Contribution of climate vs. larch budmoth outbreaks in regulating biomass accumulation in high-elevation forests. *Forest Ecology and Management* **401**: 147–158.

Petrucco L, Nardini A, Arx G Von, Saurer M, Cherubini P. **2016**. Isotope signals and anatomical features in tree rings suggest a role for hydraulic strategies in diffuse drought-induced die-back of *Pinus nigra*. *Tree physiology* **37**: 523–535.

Phillips N, Oren R, Zimmermann R. **1996**. Radial patterns of xylem sap flow in non-, diffuse- and ring-porous tree species. *Plant, Cell and Environment* **19**: 983–990.

Phillips N, Oren R. **1997**. Comparison of daily representations of canopy conductance based on two conditional time-conductance on environmental factors. *Annals of Forest Science* **55**: 217–235.

Piao SL, Cescatti A, Liski J, Luyssaert S, Le-Maire G, Schulze ED, Bouriaud O, Freibauer A, Valentini R, Nabuurs GJ. **2008**. Carbon accumulation in European forests. *Nature Geoscience* **1**: 425–429.

Pinheiro J, Bates D, DebRoy S, Sarkar D, Team RC. **2017**. nlme: Linear and Nonlinear Mixed Effects Models. R package version 3.1-131, https://CRAN.R-project.org/package=nlme.

Pirie MR, Fowler AM, Triggs CM. **2015**. Assessing the accuracy of three commonly used pith offset methods applied to *Agathis australis* (Kauri) incremental cores. *Dendrochronologia* **36**: 60–68.

Poulter B, Pederson N, Liu H, Zhu Z, D'Arrigo R, Ciais P, Davi N, Frank D, Leland C, Myneni R, *et al.* 2013. Recent trends in Inner Asian forest dynamics to temperature and precipitation indicate high sensitivity to climate change. *Agricultural and Forest Meteorology* **178**–**179**: 31–45.

Poyatos R, Aguadé D, Galiano L, Mencuccini M, Martínez-Vilalta J. **2013**. Drought-induced defoliation and long periods of near-zero gas exchange play a key role in accentuating metabolic decline of Scots pine. *New Phytologist* **200**: 388–401.

Poyatos R, Granda V, Molowny-Horas R, Mencuccini M, Steppe K, Martínez-Vilalta J. **2016**. SAPFLUXNET: Towards a global database of sap flow measurements. *Tree Physiology* **36**: 1449–1455.

Poyatos R, Llorens P, Gallart F. **2005**. Transpiration of montane *Pinus sylvestris* L. and *Quercus pubescens* Willd. forest stands measured with sap flow sensors in NE Spain. *Hydrology and Earth System Sciences Discussions* **2**: 1011–1046.

Poyatos R, Martínez-Vilalta J, Čermák J, Ceulemans R, Granier A, Irvine J, Köstner B, Lagergren F, Meiresonne L, Nadezhdina N, *et al.* 2007. Plasticity in hydraulic architecture of Scots pine across Eurasia. *Oecologia* **153**: 245–259.

Pregitzer KS, King JS, Burton AJ, Brown SE. **2000**. Responses of tree fine roots to temperature. *New Phytologist* **147**: 105–115.

Prendin AL, Petit G, Carrer M, Fonti P, Björklund J, Arx G Von. **2016**. New research perspectives from a novel approach to quantify tracheid wall thickness. *Tree physiology* **37**: 976–983.

Prentice IC, Heimann M, Sitch S. **2000**. The Carbon Balance of the Terrestial Biosphere: Ecosystem Models and Atmospheric Observations. *Ecological Applications* **10**: 1553–1573.

Pretzsch H, Biber P, Schütze G, Uhl E, Rötzer T. **2014**. Forest stand growth dynamics in Central Europe have accelerated since 1870. *Nature Communications* **5**: 1–10.

Price DT, Black TA. **1989**. Estimation of forest transpiration and C0 2 uptake using the Penman-Monteith equation and a physiological photosynthesis model. In: Black TA, Spittlehouse DL, Novak MD, Price DT. Eds. Estimation of Areal Evapotranspiration, Publ. No. 177. Wallingford, UK: International Association of Hydrological Sciences, 213–228.

Prislan P, Gričar J, de Luis M, Smith KT, Čufar K. **2013**. Phenological variation in xylem and phloem formation in *Fagus sylvatica* from two contrasting sites. *Agricultural and Forest Meteorology* **180**: 142–151.

Proseus TE, Boyer JS. **2006**. Periplasm turgor pressure controls wall deposition and assembly in growing Chara corallina cells. *Annals of Botany* **98**: 93–105.

Proseus TE, Ortega JKE, Boyer JS. **1999**. Separating Growth from Elastic Deformation during Cell Enlargement. *Plant physiology* **119**: 775–784.

Proseus TE, Zhu GL, Boyer JS. **2000**. Turgor, temperature and the growth of plant cells: using *Chara corallina* as a model system. *Journal of experimental botany* **51**: 1481–1494.

Qi Z, Liu H, Wu X, Hao Q. **2015**. Climate-driven speedup of alpine treeline forest growth in the Tianshan Mountains, Northwestern China. *Global Change Biology* **21**: 816–826.

R development core team. **2015**. *R: A language and environment for statistical computing*. Vienna, Austria: R Foundation for Statistical Computing.

Rabbel I, Diekkrüger B, Voigt H, Neuwirth B. **2016**. Comparing ΔTmax determination approaches for Granier-based sapflow estimations. *Sensors* **16**: 1–16.

Rathgeber CBK, Cuny HE, Fonti P. **2016**. Biological Basis of Tree-Ring Formation: A Crash Course. *Frontiers in Plant Science* **7**: 1–7.

Rathgeber CBK, Longuetaud F, Mothe F, Cuny H, Le Monguédec G. **2011a**. Phenology of wood formation: Data processing, analysis and visualisation using R (package CAVIAR). *Dendrochronologia* **29**: 139–149.

Rathgeber CBK, Rossi S, Bontemps J. **2011b**. Cambial activity related to tree size in a mature silver-fir plantation. *Annals of Botany* **108**: 429–438.

Regalado CM, Ritter A. **2007**. An alternative method to estimate zero flow temperature differences for Granier. *Tree Physiology* **27**: 1093–1102.

Reich PB. **2014**. The world-wide "fast-slow" plant economics spectrum: A traits manifesto. *Journal of Ecology* **102**: 275–301.

Reinig F, Nievergelt D, Esper J, Friedrich M, Helle G, Hellmann L, Kromer B, Morganti S, Pauly M, Sookdeo A, *et al.* 2018. New tree-ring evidence for the Late Glacial period from the northern pre-Alps in eastern Switzerland. *Quaternary Science Reviews* **186**: 215–224.

Reitalu T, Seppä H, Sugita S, Kangur M, Koff T, Avel E, Kihno K, Vassiljev J, Renssen H, Hammarlund D, *et al.* 2013. Long-term drivers of forest composition in a boreonemoral region: the relative importance of climate and human impact. *Journal of Biogeography* **40**: 1524–1534.

Renninger HJ, Schäfer KVR. **2012**. Comparison of Tissue Heat Balance- and Thermal Dissipation-Derived Sap Flow Measurements in Ring-Porous Oaks and a Pine. *Frontiers in Plant Science* **3**: 1–9.

Reyes-Acosta JL, Lubczynski MW. **2013**. Mapping dry-season tree transpiration of an oak woodland at the catchment scale, using object-attributes derived from satellite imagery and sap flow measurements. *Agricultural and Forest Meteorology* **174**–**175**: 184–201.

Rigling A, Bigler C, Eilmann B, Feldmeyer-Christe E, Gimmi U, Ginzler C, Graf U, Mayer P, Vacchiano G, Weber P, *et al.* 2013. Driving factors of a vegetation shift from Scots pine to pubescent oak in dry Alpine forests. *Global Change Biology* **19**: 229–240.

Rocha A V, Goulden ML, Dunn AL, Wofsy SC. **2006**. On linking interannual tree ring variability with observations of whole-forest CO_2 flux. *Global Change Biology* **12**: 1378–1389.

Roderick ML, Berry SL. **2001**. Linking wood density with tree growth and environment: a theoretical analysis based on the motion of water. *New Phytologist* **149**: 473–485.

Rolland C, Petitcolas V, Michalet R. **1998**. Changes in radial tree growth for *Picea abies*, *Larix decidua*, *Pinus cembra* and *Pinus uncinata* near the alpine timberline since 1750. *Trees - Structure and Function* **13**: 40–53.

Roman DT, Novic KA, Brzostek ER, Dragoni D, Rahman F, Phillips RP. **2015**. The role of isohydric and anisohydric species in determining ecosystem-scale response to severe drought. *Oecologia* **179**: 641–654.

Rossi S, Anfodillo T, Čufar K, Cuny HE, Deslauriers A, Fonti P, Frank D, Gričar J, Gruber A, Huang JG, *et al.* 2016. Pattern of xylem phenology in conifers of cold ecosystems at the Northern Hemisphere. *Global Change Biology* **22**: 3804–3813.

Rossi S, Anfodillo T, Čufar K, Cuny HE, Deslauriers A, Fonti P, Frank D, Gričar J, Gruber A, King GM, *et al.* 2013. A meta-analysis of cambium phenology and growth: linear and non-linear patterns in conifers of the northern hemisphere. *Annals of Botany* **112**: 1911–1920.

Rossi S, Anfodillo T, Menardi R. **2006a**. Trephor: A new tool for sampling microcores from tree stems. *IAWA Journal* **27**: 89–97.

Rossi S, Deslauriers A, Anfodillo T, Carraro V. **2007**. Evidence of threshold temperatures for xylogenesis in conifers at high altitudes. *Oecologia* **152**: 1–12.

Rossi S, Deslauriers A, Anfodillo T. **2006b**. Assessment of Cambial Activity and Xylogenesis By Microsampling Tree Species: An Example At The Alpine Timberline. *IAWA Journal* **27**: 383–394.

Rossi S, Deslauriers A, Griçar J, Seo JW, Rathgeber CBK, Anfodillo T, Morin H, Levanic T, Oven P, Jalkanen R. **2008**. Critical temperatures for xylogenesis in conifers of cold climates. *Global Ecology and Biogeography* **17**: 696–707.

Rossi S, Deslauriers A, Morin H. **2003**. Application of the Gompertz equation for the study of xylem cell development. *Dendrochronologia* **21**: 33–39.

Rossi S, Morin H, Deslauriers A. **2012**. Causes and correlations in cambium phenology: Towards an integrated framework of xylogenesis. *Journal of Experimental Botany* **63**: 2117–2126.

Ryan MG, Asao S. **2014**. Phloem transport in trees. *Tree Physiology* **34**: 1–4.

Sakschewski B, von Bloh W, Boit A, Rammig A, Kattge J, Poorter L, Peñuelas J, Thonicke K. **2015**. Leaf and stem economics spectra drive diversity of functional plant traits in a dynamic global vegetation model. *Global Change Biology* **21**: 2711–2725.

Sala A, Woodruff DR, Meinzer FC. **2012**. Carbon dynamics in trees: Feast or famine? *Tree Physiology* **32**: 764–775.

Salomón RL, Limousin J-M, Ourcival J-M, Rodríguez-Calcerrada J, Steppe K. **2017**. Stem hydraulic capacitance decreases with drought stress: implications for modelling tree hydraulics in the Mediterranean oak *Quercus ilex*. *Plant, Cell & Environment* **40**: 1379–1391.

Salzer MW, Hughes MK, Bunn AG, Kipfmueller KF. **2009**. Recent unprecedented tree-ring growth in bristlecone pine at the highest elevations and possible causes. *Proceedings of the National Academy of Sciences* **106**: 20348–20353.

Sánchez-costa E, Poyatos R, Sabaté S. **2015**. Contrasting growth and water use strategies in four co-occurring Mediterranean tree species revealed by concurrent measurements of sap flow and stem diameter variations. *Agricultural and Forest Meteorology* **207**: 24–37.

Saveyn A, Steppe K, Lemeur R. **2008**. Spatial variability of xylem sap flow in mature beech (*Fagus sylvatica*) and its diurnal dynamics in relation to microclimate. *Botany* **86**: 1440–1448.
Saxe H, Cannell MGR, Johnsen Ø, Ryan MG, Vourlitis G. **2001**. Tree and forest functioning in response to global warming. *New Phytologist* **149**: 369–400.
Scheiter S, Langan L, Higgins SI. **2013**. Next-generation dynamic global vegetation models: learning from community ecology. *New Phytologist* **198**: 957–69.
Schlesinger WH, Jasechko S. **2014**. Transpiration in the global water cycle. *Agricultural and Forest Meteorology* **189**–**190**: 115–117.
Schmidt-Walter P, Richter F, Herbst M, Schuldt B, Lamersdorf NP. **2014**. Transpiration and water use strategies of a young and a full-grown short rotation coppice differing in canopy cover and leaf area. *Agricultural and Forest Meteorology* **195**–**196**: 165–178.
Schoch W, Heller I, Schweingruber FH, Kienast F. **2004**. Wood anatomy of central European species. *Online version: www.woodanatomy.ch.*
Scholz FG, Bucci SJ, Goldstein G, Meinzer FC, Franco AC, Miralles-Wilhelm F. **2007**. Biophysical properties and functional significance of stem water storage tissues in Neotropical savanna trees. *Plant, Cell and Environment* **30**: 236–248.
Schönbeck L, Gessler A, Günter H, McDowell N, Rigling A, Schaub M, Li M-H. **2018**. Homeostatic levels of non -structural carbohydrates after 13 years of drought and irrigation in *Pinus sylvestris* L. *New Phytologist* **219**: 1314–1324.
Schrader J, Baba K, May ST, Palme K, Bennett M, Bhalerao RP, Sandberg G. **2003**. Polar auxin transport in the wood-forming tissues of hybrid aspen is under simultaneous control of developmental and environmental signals. *Proceedings of the National Academy of Sciences of the United States of America* **100**: 10096–10101.
Schuldt B, Leuschner C, Brock N, Horna V. **2013**. Changes in wood density, wood anatomy and hydraulic properties of the xylem along the root-to-shoot flow path in tropical rainforest trees. *Tree Physiology* **33**: 161–174.
Schweingruber FH. **1996**. *Tree Rings and Environment: Dendroecology*. Bern, Switzerland: Paul Haupt.
Seidl R, Fernandes PM, Fonseca TF, Gillet F, Jönsson AM, Merganičová K, Netherer S, Arpaci A, Bontemps J-D, Bugmann H, *et al.* 2011. Modelling natural disturbances in forest ecosystems: a review. *Ecological Modelling* **222**: 903–924.
Seidl R, Schelhaas MJ, Rammer W, Verkerk PJ. **2014**. Increasing forest disturbances in Europe and their impact on carbon storage. *Nature Climate Change* **4**: 806–810.
Seneviratne SI, Lüthi D, Litschi M, Schär C. **2006**. Land-atmosphere coupling and climate change in Europe. *Nature* **443**: 205–209.
Seo JW, Smiljanić M, Wilmking M. **2014**. Optimizing cell-anatomical chronologies of Scots pine by stepwise increasing the number of radial tracheid rows included-Case study based on three Scandinavian sites. *Dendrochronologia* **32**: 205–209.
Shashkin A V, Vaganov EA. **1993**. Simulation-Model of Climatically Determined Variability of Conifers Annual Increment. *Russian Journal of Ecology* **24**: 275–280.
Shatar TM, McBratney AB. **2004**. Boundary-line analysis of field-scale yield response to soil properties. *Journal of Agricultural Science* **142**: 553–560.
Shishov V V., Tychkov II, Popkova MI, Ilyin VA, Bryukhanova M V., Kirdyanov A V. 2016. VS-oscilloscope: A new tool to parameterize tree radial growth based on climate conditions. *Dendrochronologia* **39**: 42–50.
Simard S, Giovannelli A, Treydte K, Traversi ML, King GM, Frank D, Fonti P. **2013**. Intra-annual dynamics of non-structural carbohydrates in the cambium of mature conifer trees reflects radial growth demands. *Tree Physiology* **33**: 913–923.
Sitch S, Huntingford C, Gedney N, Levy PE, Lomas M, Piao SL, Betts R, Ciais P, Cox P, Friedlingstein P, *et al.* 2008. Evaluation of the terrestrial carbon cycle, future plant geography and climate-carbon cycle feedbacks using five Dynamic Global Vegetation Models (DGVMs). *Global Change Biology* **14**: 2015–2039.
Smith DM, Allen SJ. **1996**. Measurement of sap flow in plant stems. *Journal of Experimental Botany* **47**: 1833–1844.
Soja AJ, Tchebakova NM, French NHF, Flannigan MD, Shugart HH, Stocks BJ, Sukhinin AI, Parfenova EI, Chapin III FS, Stackhouse Jr. PW. **2007**. Climate-induced boreal forest change: Predictions versus current observations. *Global and Planetary Change* **56**: 274–296.
Song X, Barbour MM, Farquhar GD, Vann DR, Helliker BR. **2013**. Transpiration rate relates to within- and across-species variations in effective path length in a leaf water model of oxygen isotope enrichment. *Plant, Cell and Environment* **36**: 1338–1351.
Souto-Herrero M, Rozas V, García-González I. **2017**. A 481-year chronology of oak earlywood vessels as an age-independent climatic proxy in NW Iberia. *Global and Planetary Change* **155**: 20–28.

Sperry JS, Love DM. **2015**. What plant hydraulics can tell us about responses to climate-change droughts. *New Phytologist* **207**: 14–27.

Sperry JS, Meinzer FC, Mcculloh KA. **2008**. Safety and efficiency conflicts in hydraulic architecture: scaling from tissues to trees. *Plant, Cell and Environment* **31**: 632–645.

Sprintsin M, Chen JM, Desai A, Gough CM. **2012**. Evaluation of leaf-to-canopy upscaling methodologies against carbon flux data in North America. *Journal of Geophysical Research* **117**: 1–17.

Steltzer H, Post E. **2009**. Seasons and Life Cycles. *Science* **324**: 886–888.

Steppe K, De Pauw DJW, Doody TM, Teskey RO. **2010**. A comparison of sap flux density using thermal dissipation, heat pulse velocity and heat field deformation methods. *Agricultural and Forest Meteorology* **150**: 1046–1056.

Steppe K, Lemeur R, Vanrolleghem A. **2005**. A mathematical model linking tree sap flow dynamics to daily stem diameter fluctuation and radial stem growth. *Tree Physiology* **26**: 257–273.

Steppe K, Lemeur R. **2007**. Effects of ring-porous and diffuse-porous stem wood anatomy on the hydraulic parameters used in a water flow and storage model. *Tree Physiology* **27**: 43–52.

Steppe K, Pauw DJW De, Lemeur R. **2008**. A step towards new irrigation scheduling strategies using plant-based measurements and mathematical modelling. *Irrigation Science* **26**: 505–517.

Steppe K, Pauw DJWDE, Lemeur R, Vanrolleghem A. **2005**. A mathematical model linking tree sap flow dynamics to daily stem diameter fluctuations and radial stem growth. *Tree Physiology* **26**: 257–273.

Steppe K, Sterck F, Deslauriers A. **2015**. Diel growth dynamics in tree stems: Linking anatomy and ecophysiology. *Trends in Plant Science* **20**: 335–343.

Steppe K, Vandegehuchte MW, Tognetti R, Mencuccini M. **2015**. Sap flow as a key trait in the understanding of plant hydraulic functioning. *Tree Physiology* **35**: 341–345.

Steppe K, von der Crone JS, De Pauw DJW. **2016**. TreeWatch.net: A Water and Carbon Monitoring and Modeling Network to Assess Instant Tree Hydraulics and Carbon Status. *Frontiers in Plant Science* **7**: 1–8.

Sultan SE. **2000**. Phenotypic plasticity for plant development, function and life history. *Trends in Plant Science* **5**: 537–542.

Sun H, Aubrey DP, Teskey RO. **2012**. A simple calibration improved the accuracy of the thermal dissipation technique for sap flow measurements in juvenile trees of six species. *Trees - Structure and Function* **26**: 631–640.

Sutanto SJ, Van Den Hurk B, Dirmeyer PA, Seneviratne SI, Röckmann T, Trenberth KE, Blyth EM, Wenninger J, Hoffmann G. **2014**. HESS Opinions 'a perspective on isotope versus non-isotope approaches to determine the contribution of transpiration to total evaporation'. *Hydrology and Earth System Sciences* **18**: 2815–2827.

Sutera SP, Skalak R. **1993**. The History of Poiseuille Law. *Annual Review of Fluid Mechanics* **25**: 1–19.

Swanson RH. **1994**. Significant historical developments in thermal methods for measuring sap flow in trees. *Agricultural and Forest Meteorology* **72**: 113–132.

Swetnam TW, Allen CD, Betancourt JL. **1999**. Applied Historical Ecology: Using the Past to Manage for the Future. *Ecological Applications* **9**: 1189–1206.

Taneda H, Sperry JS. **2008**. A case-study of water transport in co-occurring ring- versus diffuse-porous trees: Contrasts in water-status, conducting capacity, cavitation and vessel refilling. *Tree Physiology* **28**: 1641–1651.

Tardieu F. **2010**. Why work and discuss the basic principles of plant modelling 50 years after the first plant models? *Journal of Experimental Botany* **61**: 2039–2041.

Teepe R, Dilling H, Beese F. **2003**. Estimating water retention curves of forest soils from soil texture and bulk density. *Journal of Plant Nutrition and Soil Science* **166**: 111–119.

Tei S, Sugimoto A, Yonenobu H, Matsuura Y, Osawa A, Sato H, Fujinuma J, Maximov T. **2017**. Tree-ring analysis and modeling approaches yield contrary response of circumboreal forest productivity to climate change. *Global Change Biology* **23**: 5179–5188.

Thornton PE, Running SW, White MA. **1997**. Generating surfaces of daily meteorological variables over large regions of complex terrain. *Journal of Hydrology* **190**: 214–251.

Thuiller W, Albert C, Araújo MB, Berry PM, Cabeza M, Guisan A, Hickler T, Midgley GF, Paterson J, Schurr FM, *et al.* 2008. Predicting global change impacts on plant species' distributions: Future challenges. *Perspectives in Plant Ecology, Evolution and Systematics* **9**: 137–152.

Tor-ngern P, Oren R, Ward EJ, Palmroth S, Mccarthy HR, Domec J. **2014**. Rapid report Increases in atmospheric CO_2 have little influence on transpiration of a temperate forest canopy. *New Phytologist* **205**: 518–525.

Trotsiuk V, Svoboda M, Weber P, Pederson N, Klesse S, Janda P, Martin-Benito D, Mikolas M, Seedre M, Bace R, *et al.* 2016. The legacy of disturbance on individual tree and stand-level aboveground biomass accumulation and stocks in primary mountain Picea abies forests. *Forest Ecology and Management* **373**: 108–115.

Tuominen H, Puech L, Fink S, Sundberg B. **1997**. A Radial Concentration Gradient of Indole-3-Acetic Acid Is Related to Secondary Xylem Development in Hybrid Aspen. *Plant physiology* **115**: 577–585.
Turchin P, Wood SN, Ellner SP, Kendall BE, Murdoch WW, Fischlin A, Casas J, McCauley E, Briggs CJ. **2003**. Dynamical effects of plant quality and parasitism on larch budmoth. *Ecology* **84**: 1207–1214.
Tuzet A, Perrier A, Leuning R. **2003**. A coupled model of stomatal conductance, photosynthesis. *Plant, Cell and Environment* **26**: 1097–1116.
Tyree MT, Zimmermann M. **2002**. *Xylem structure and the ascent of sap*. New York, USA: Springer.
Tyree T. **1988**. A dynamic model for water flow in a single tree: evidence that models must account for hydraulic architecture. *Tree Physiology* **4**: 195–217.
Uggla C, Moritz T, Sandberg G, Sundberg B. **1996**. Auxin as a positional signal in pattern formation in plants. *Proceedings of the National Academy of Sciences of the United States of America* **93**: 9282–9286.
Vaganov EA, Hughes MK, Shashkin A V. **2006**. *Growth dynamics of conifer tree rings: images of past and future environments*. Berlin, Germany: Springer-Verlag Berlin Heidelberg.
Vaganov EA. **1990**. The tracheidogram method in tree-ring analysis and its application. In: Cook ER, Kairiukstis LA. Eds. Methods of dendrochronology: applications in the environmental sciences. Dordrecht, The Netherlands: Kluwer Academic Publishers, 63–76.
Valladares F, Matesanz S, Guilhaumon F, Araújo MB, Balaguer L, Benito-Garzón M, Ernesto WC, van Kleunen GM, Naya DE, Nicotra AB, *et al.* 2014. The effects of phenotypic plasticity and local adaptation on forecasts of species range shifts under climate change. *Ecology Letters* **17**: 1351–1364.
Van de Wal BAE, Guyot A, Lovelock CE, Lockington DA, Steppe K. **2015**. Influence of temporospatial variation in sap flux density on estimates of whole-tree water use in *Avicennia marina*. *Trees - Structure and Function* **29**: 215–222.
van den Honert TH. **1948**. Water transport in plants as a catenary process. *Discussions of the Faraday Society* **3**: 146–153.
van der Sleen P, Groenendijk P, Vlam M, Anten NPR, Boom A, Bongers F, Pons TL, Terburg G, Zuidema PA. **2014**. No growth stimulation of tropical trees by 150 years of CO_2 fertilization but water-use efficiency increased. *Nature Geoscience* **8**: 24–28.
van Genuchten MT. **1980**. A closed-form equation for predicting the hydraulic conductivity of unsaturated soils. *Soil science society of America journal* **44**: 892–898.
Vandegehuchte MW, Steppe K. **2012**. Sapflow+: A four-needle heat-pulse sap flow sensor enabling nonempirical sap flux density and water content measurements. *New Phytologist* **196**: 306–317.
Venables WN, Ripley BD. **2002**. *Modern Applied Statistics with S*. New York, USA: Springer.
Verbeeck H, Steppe K, Nadezhdina N, De Beeck MO, Deckmyn G, Meiresonne L, Lemeur R, Čermák J, Ceulemans R, Janssens IA. **2007a**. Model analysis of the effects of atmospheric drivers on storage water use in Scots pine. *Biogeosciences* **4**: 657–671.
Verbeeck H, Steppe K, Nadezhdina N, De MOP, Deckmyn G, Meiresonne L, Lemeur R, Čermák JANÈ, Ceulemans R, Janssens IA. **2007b**. Stored water use and transpiration in Scots pine: a modeling analysis with ANAFORE. *Tree Physiology* **27**: 1671–1685.
Vergeynst LL, Vandegehuchte MW, McGuire MA, Teskey RO, Steppe K. **2014**. Changes in stem water content influence sap flux density measurements with thermal dissipation probes. *Trees - Structure and Function* **28**: 949–955.
Verhoef A, Egea G. **2014**. Agricultural and Forest Meteorology Modeling plant transpiration under limited soil water: Comparison of different plant and soil hydraulic parameterizations and preliminary implications for their use in land surface models. *Agricultural and Forest Meteorology* **191**: 22–32.
Villalba R, Lara A, Masiokas MH, Urrutia R, Luckman BH, Marshall GJ, Mundo IA, Christie DA, Cook ER, Neukom R, *et al.* 2012. Unusual Southern Hemisphere tree growth patterns induced by changes in the Southern Annular Mode. *Nature Geoscience* **5**: 793–798.
von Arx G, Carrer M. **2014**. Roxas-A new tool to build centuries-long tracheid-lumen chronologies in conifers. *Dendrochronologia* **32**: 290–293.
von Arx G, Crivellaro A, Prendin AL, Čufar K, Carre M. **2016**. Quantitative Wood Anatomy - Practical Guidelines. *Frontiers in Plant Science* **7**: 1–13.
von Arx G, Dietz H. **2005**. Automated image analysis of annual rings in the roots of perennial forbs. *International Journal of Plant Science* **166**: 723–732.
Vysotskaya LG, Vaganov EA. **1989**. Components of the variability of radial cell size in tree-rings of conifers. *IAWA Bulletin* **10**: 417–428.
Ward EJ, Domec JC, King J, Sun G, McNulty S, Noormets A. **2017**. TRACC: an open source software for processing sap flux data from thermal dissipation probes. *Trees - Structure and Function* **31**: 1737–1742.
White AC, Rogers A, Rees M, Osborne CP. **2016**. How can we make plants grow faster? A source-sink perspective on growth rate. *Journal of Experimental Botany* **67**: 31–45.

Wiedemann A, Marañón-Jiménez S, Rebmann C, Herbst M, Cuntz M. **2016**. An empirical study of the wound effect on sap flux density measured with thermal dissipation probes. *Tree Physiology* **36**: 1471–1484.

Wieser G, Leo M, Oberhuber W. **2014**. Transpiration and canopy conductance in an inner alpine Scots pine (*Pinus sylvestris* L.) forest. *Flora* **209**: 491–498.

Wieser G. **2007**. Limitation by insufficient carbon assimilation and allocation. In: Wieser G, Tausz M. Eds. Trees at their upper limit - treelife limitation at the Alpine timberline. Dordrecht, The Netherlands: Springer, 79–129.

Wightman MG, Martin TA, Gonzalez-Benecke CA, Jokela EJ, Cropper WP, Ward EJ. **2016**. Loblolly pine productivity and water relations in response to throughfall reduction and fertilizer application on a poorly drained site in northern Florida. *Forests* **7**.

Wilson BF, Wodzicki TJ, Zahner R. **1966**. Differentiation of Cambial Derivatives - Proposed Terminology. *Forest Science* **12**: 438–440.

Wilson KB, Hanson PJ, Mulholland PJ, Baldocchi DD, Wullschleger SD. **2001**. A comparison of methods for determining forest evapotranspiration and its components: Sap-flow, soil water budget, eddy covariance and catchment water balance. *Agricultural and Forest Meteorology* **106**: 153–168.

WMO. **2008**. *Guide to Meteorological Instruments and Methods of Observation, Appendix 4B, WMO-No. 8 (CIMO Guide)*. Geneva, Switzerland: World Meteorological Organization.

Wolkovich EM, Cook BI, Allen JM, Crimmins TM, Betancourt JL, Travers SE, Pau S, Regetz J, Davies TJ, Kraft NJB, *et al.* 2012. Warming experiments underpredict plant phenological responses to climate change. *Nature* **485**: 494–497.

Wood SN. **2006**. *Generalized additive models: an introduction with R*. Boca Raton, USA: Chapman and Hall/CRC.

Woodruff DR, Meinzer FC. **2011**. Water stress, shoot growth and storage of non-structural carbohydrates along a tree height gradient in a tall conifer. *Plant, Cell and Environment* **34**: 1920–1930.

Wronski J, Holmes JW, Turner NC. **1985**. Phase and amplitude relations between transpiration, water potential and stem shrinkage. *Plant, Cell and Environment* **8**: 613–622.

Wu C, Hember RA, Chen JM, Kurz WA, Price DT, Boisvenue C, Gonsamo A, Ju W. **2014**. Accelerating Forest Growth Enhancement due to Climate and Atmospheric Changes in British Colombia, Canada over 1956-2001. *Scientific Reports* **4**: 1–5.

Wullschleger SD, Childs KW, King AW, Hanson PJ. **2011**. A model of heat transfer in sapwood and implications for sap flux density measurements using thermal dissipation probes. *Tree Physiology* **31**: 669–679.

Wullschleger SD, Meinzer FC, Vertessy RA. **1998**. A review of whole-plant water use studies in trees. *Tree Physiology* **18**: 499–512.

Yamori W, Noguchi K, Hikosaka K, Terashima I. **2010**. Phenotypic plasticity in photosynthetic temperature acclimation among crop species with different cold tolerances. *Plant Physiology* **152**: 388–399.

Zhang Z, Babst F, Bellassen V, Frank D, Launois T, Tan K, Ciais P, Poulter B. **2017**. Converging climate sensitivities of European forests between observed radial tree growth and vegetation models. *Ecosystems* **21**: 410–425.

Zhao M, Running SW. **2010**. Drought-Induced Reduction in Global Terrestrial Net Primary Production from 2000 through 2009. *Science* **329**: 940–943.

Zheng H, Wang Q, Zhu X, Li Y, Yu G. **2014**. Hysteresis responses of evapotranspiration to meteorological factors at a diel timescale: Patterns and causes. *PLoS ONE* **9**: 1–10.

Zuidema PA, Baker PJ, Groenendijk P, Schippers P, van der Sleen P, Vlam M, Sterck F. **2013**. Tropical forests and global change: filling knowledge gaps. *Trends in plant science* **18**: 413–419.

Zurell D, Thuiller W, Pagel J, Cabral JS, Münkemüller T, Gravel D, Dullinger S, Normand S, Schiffers KH, Moore KA, *et al.* 2016. Benchmarking novel approaches for modelling species range dynamics. *Global change biology* **22**: 2651–2664.

Zuur AF, Ieno EN, Elphick CS. **2010**. A protocol for data exploration to avoid common statistical problems. *Methods in Ecology and Evolution* **1**: 3–14.

Zweifel R, Haeni M, Buchmann N, Eugster W. **2016**. Are trees able to grow in periods of stem shrinkage? *New Phytologist* **211**: 839–849.

Zweifel R, Häsler R. **2001**. Dynamics of water storage in mature subalpine *Picea abies*: temporal and spatial patterns of change in stem radius. *Tree Physiology* **21**: 561–569.

Zweifel R, Item H, Hasler R. **2001**. Link between diurnal stem radius changes and tree water relations. *Tree Physiology* **21**: 869–877.

Zweifel R, Steppe K, Sterck FJ. **2007**. Stomatal regulation by microclimate and tree water relations: interpreting ecophysiological field data with a hydraulic plant model. *Journal of Experimental Botany* **58**: 2113–2131.

Zweifel R, Zimmermann L, Zeugin F, Newbery DM. **2006**. Intra-annual radial growth and water relations of trees: Implications towards a growth mechanism. *Journal of Experimental Botany* **57**: 1445–1459.

Summary

Conifers show a biogeographical distribution across a wide range of contrasting environmental conditions, stretching from the Arctic Circle to the equator and Southern Hemisphere. In mountainous ecosystems, conifers can dominate at high elevations with low temperatures severely limiting tree growth and survival. Conifers growing at sites with temperature limiting conditions are highly sensitive to ongoing climatic change, where warmer and drier conditions will impact their growth. Understanding how high-elevation conifers will respond to these changes in climate is critical, as they play a role in regulating terrestrial carbon storage (facilitated by the formation of woody tissue) and water balance (by releasing water to the atmosphere via transpiration). The environmental regulation of wood formation (i.e., tracheid development in conifers), which dictates annual ring-width patterns, is commonly associated with the tree's photosynthetic activity, while other growth-limiting factors might also be relevant. For example, tree growth requires turgidity in the cambium to exert the pressure necessary for cell expansion, assimilates to lengthen and thicken cell walls, warmth to allow the metabolic reactions to take place, and time for these processes to be completed. Yet, an in-depth study on how important tree hydraulics (i.e., transpiration dynamics) are in regulating "turgor-driven" growth in high elevation forests is lacking.

As part of the LOTFOR project, the general objective of this work is to develop a better mechanistic understanding on how tree hydraulics and environmental factors interact in regulating wood formation and shaping tree rings in high-elevation conifer trees. More specifically, the coupling between stem hydrological cycles and structural carbon dynamics is investigated in the context of increasing temperature and water scarcity. This thesis combines multi-annual records of both intra-annual wood formation data and high-resolution hydraulic measurements within a mechanistic growth model to explain inter- and intra-annual tree growth patterns. To simulate the impact from recent climate change on these mechanisms, a space-for-time experimental setting is applied within the Lötschental, located in the Swiss Alps, where we collected data of two commonly occurring conifer species (*Larix decidua* Mill. and *Picea abies* Karst. L.) along an elevation/thermal gradient and contrasting wet and dry sites. Additionally, evaluations are performed on existing methodologies for measuring sap flow and handling large wood anatomical datasets.

Analysing how climate affects tree growth at high elevations requires measurements on inter- and intra-annual growth, frequently obtained from tree rings and wood formation observations, respectively. In CHAPTER 2 of this thesis, more than 150 years of inter-annual growth dynamics along the elevational gradient (derived from tree rings) are assessed in relation to temperature, precipitation and insect activity. An analysis of the recent forest biomass increment increase, derived from the tree-ring width measurements, indicates that the absence of insect outbreaks (since 1981) has caused an equal or even greater impact on carbon sequestration compared to the observed warmer summer temperatures. The presented analysis reveals the relevance of including such biotic drivers and their interactions with climate in models assessing the future productivity and carbon sink capacity of forests. In CHAPTER 4, using the algorithms presented in CHAPTER 3, we monitored intra-annual tracheid development across an 8 °C thermal gradient including two elevational transects (in the Lötschental and Vosges Mountains in France) to investigate cell enlargement and wall thickening dynamics in relation to environmental conditions. Results show that at colder sites, differentiating tracheids compensate for lower rates of cell enlarging and wall thickening by increasing the cell development time, except for the wall-thickening latewood cells. This compensation allows conifer trees to mitigate the influence of temperature on the final tree-ring structure, with important implications for the ring's size and functioning.

The production of carbohydrates and generation of turgidity in the cambium to initiate growth are tightly linked to the way a tree regulates the flow of water through the soil-plant-atmosphere continuum. For high elevation conifers, the regulation of the stomatal conductance in the leaves is important, as transpiration has to be optimised for minimal water losses during winter and maximum photosynthetic yield during the short vegetative season. Interestingly, sap flow (measured with thermal dissipation probes installed into the water-conducting wood) can be used to derive stomatal conductance, although this application requires proper data processing of raw sap flow measurements to reduce uncertainties. CHAPTER 5 presents a quantification of the uncertainties generated by commonly applied data-processing methods for conifer sap flow measurements. The uncertainty analysis reveals the importance of performing species-specific calibrations of the sap flow probes, determining zero sap flow conditions with environmental measurements, and applying a dampening correction for better estimates of both the variability and absolute values of whole-

tree water use. The processed sap flow measurements are used in CHAPTER 6 to address the ability of *L. decidua* and *P. abies* in the Lötschental to adjust their conductance response to environmental conditions when growing under persistently colder and drier conditions. The results indicate that the pioneer *L. decidua* is more plastic in optimizing its conductance response to temperature with increasing elevation, compared to *P. abies*. Surprisingly, drought sensitive *P. abies* did not show a stronger downregulation of its stomatal conductance during drought episodes compared to *L. decidua*. The stronger plasticity of stomatal conductance response to environmental conditions and the higher water-conductance efficiency of *L. decidua*, compared to *P. abies*, provides a new insight into how trees differ in water-use strategies and indicates that *L. decidua* may be well equipped to function under changing future climatic conditions, compared to a climax species such as *P. abies*.

While mechanistic models can now simulate turgor-driven growth and potentially improve current growth predictions, they lack validation on annual timescales. CHAPTER 7 uses the processed intra-daily sap flow together with site-specific environmental measurements in a mechanistic whole-tree model. The simulated growth dynamics show good agreement with the observed inter- and intra-annual growth in high-elevation conifers (obtained from tree-ring width and xylogenesis observations, respectively). Four years of high-resolution measurements on sap flow and diameter variations were used to apply the mechanistic model for *L. decidua* or *P. abies* trees growing along the elevational gradient and in contrasting dry and wet sites in the Lötschental. Good agreement was found between the simulated and observed radial stem growth. Growth was unlikely to occur at temperatures below 2 °C (which is above the photosynthetic minimum) or soil water potentials lower than -0.6 MPa. These results suggest that turgor and its environmental drivers are important for regulating radial growth and should be considered when assessing forest productivity under changing environmental conditions.

If one message becomes clear from this thesis, it is that elevational transect studies provide crucial insights into the effect of persistent changes in growing season temperature (as induced by climate change) on annual tree growth patterns, wood formation dynamics and tree hydraulics. Furthermore, collecting a large variety of tree physiological measurements is vital for testing and validating the mechanisms that regulate tree growth and forest productivity patterns.

Acknowledgements

Doing a PhD on wood formation and tree hydraulics in high-elevation forests is not a walk in the park. Besides enjoying the scenic views in the Lötschental for nearly four years, I had to conquer many steep slopes and deal with the occasional boulder falling on my desk. This thesis would probably have never been printed, on the material obtained from tree corpses, without the influence of many people. In this section I would like to thank those who have contributed to making this "hike" both possible and enjoyable.

I would like to thank my supervisors Patrick Fonti and David Frank for introducing a clumsy lowlander into mountainous ecosystems. Patrick, you have always given me the freedom to explore many research paths, even if these would run along steep cliffs. Your engaged supervision and critical view on the results I dumped on your desk were crucial in shaping me as a research enthusiast. David, thank you for always taking the time to guide/force me to look beyond my 'virtual' trees and equations and see the forest. Even if it was written on the back of a crumbled piece of paper, your advice was always valuable and inspiring

External forcing impacts both tree rings and PhDs. This project would not have been possible without the support from Ansgar Kahmen and Kathy Steppe. Ansgar, thank you for your engaging physiological view on my work and valuable tips and tricks for shaping my academic career. Kathy, thank you for the support and exciting discussions on how we could make trees grow virtually. I look forward to continue our collaboration in the future.

The success of any hike depends on the right environmental conditions. During my PhD I had the pleasure to work together with an army of successful and inspirational "youngsters". Stefan Klesse and Jesper Björklund, better known as the "cabinet folk", it has been a great pleasure to share the office with you at the WSL. Thank you so much for the laughs, beers, inspiration, support and never-ending scientific discussions. I also had the pleasure to share fieldwork, ideas and analyses with several interns, PhDs and postdocs: Daniel Balanzategui, Flurin Babst, Henri Cuny, Lars Dietrich, Alex Hurley, Chris Pappas, Annika Oertel, Giulio Perulli, Angela Prendin, Leonie Schönbeck, Matthias Speich and Ana Stritih. We shared exciting times together, either in the field, in a bar or behind a laptop. Thank you for sharing these moments, excitement, support and passion.

During my PhD and my journey through the complex scientific world, I was supported by many engaging, inspiring and passionate researchers: Georg von Arx, Alan Crivellaro, Ingo Heinrich, Elisabeth Graf Pannatier, Rafael Poyatos, Cyrille Rathgeber, Marcus Schaub and Kerstin Treydte. Thank you for helping me to develop my academic skills and for being role model scientists. A special thanks goes to thank Pieter Zuidema and Peter Groenendijk for introducing me into the wonderful world of trees and allowing me to be involved in their tropical adventures.

To Ulf Büntgen, Paolo Cherubini, Marina Fonti, Holger Gärtner, Daniel Nievergelt, Lenka Matéju, Frederick Reinig, Kristina Seftigen, Loïc Schneider, Ruedi Seiler, Anne Verstege and other colleagues at the Dendrosciences group, thank you for creating an enjoyable and productive atmosphere at the WSL. Our shared scientific discussions, fieldwork and social events were of great value to me.

It is no secret that I enjoyed my time outside the research bubble. The reason for this is simple: I have met too many amazing people. The only way to start this list is by thanking Stefan, Robbie and Ana. Your friendship, love and support during this four year lasting adventure was invaluable. Without you guys I would have never been able to finish this project and enjoy my life in Switzerland. To Adrian, Angela, Amelie, Andi, Anil, Emily, Isabelle, Joep, Jose, Jürgen, Leonie, Marco, Manuel, Matias, Matthias, Milica, Natasha, Nemanja, Sandra, Sia, Sonia, Tessa, Rick, Ruedi and many more, thank you all for your friendship and the times we shared (in the pub).

Despite being abroad, I was always supported by my friends and family up North to do the things I love. To Anne, Bart, Corine, Fani, Gideon, Laurens, Jan, Jeffrey, Nanette, Nirja and Yorick, thank you for your unconditional friendship and the frequent visits. To Djarno, Joey, Keje and Roy, thank you for the inspirational time we had playing in ‘Johnny Park’ and beyond. A special thanks goes to my parents and my brothers, Theo, Els, Wouter, Daniel and Maarten. Your love and support always helped me to stay positive, even during tough times. Finally, I would like to thank my great-uncle Piet for inspiring me to pursue the things I love doing in life.

PhD training and education

Activity	Date	Location	Description
Education			
COST training school	26/05/2014 - 28/05/2014	Ghent, Belgium	COST-action STReESS training school on Modelling drought stress responses in trees.
European Dendroecological Fieldweek	31/08/2014 - 06/09/2014	Oviedo, Spain	Fieldweek covering the full spectrum of dendrochronological issues.
Rigi-workshop	18/01/2015 - 20/01/2015	Rigi-Kulm, Switzerland	Interdisciplinary workshop on Mathematical and Computational modelling in Life Science.
Advanced statistics course	13/11/2015 - 04/12/2015	Birmensdorf, Switzerland	Course on advanced statistics, linear mixed-effects models and Bayesian statistics.
PSC Colloquium	28/09/2016 - 03/11/2016	Zürich, Switzerland	Plant Science Center's PhD program on Challenges in Plant Sciences.
Presentations			
Eurodendro	08/09/2014 - 12/09/2014	Lugo, Spain	Poster on Alpine forests and climate change: Coupling stem water flow and structural carbon allocation.
TRACE	11/05/2016 - 15/05/2016	Bialowieza, Poland	Poster on Assessing the impact of larch budmoth outbreak on tree biomass growth along an Alpine elevational gradient.
EcoSummit	29/08/2016 - 01/09/2016	Montpellier, France	Poster on Modelling ecohydrological processes on landscape scale: A ground trothing on Alpine forests.
EGU	23/04/2017 - 28/04/2017	Vienna. Austria	Presentation on How to make a tree ring: Coupling stem water flow and cambial activity in mature Alpine conifers.
Teaching experience			
ETH Dendroecology	09/10/2014 - 10/10/2014	Zürich, Switzerland	Teaching detrending, chronology building and statistics in dendroecology.
European Dendroecological Fieldweek	12/09/2016 - 18/09/2016	Kransjka Gora, Slovenia	Teaching on dendroclimatology and statistics.
Advanced data management and manipulation using R	29/05/2017 - 30/05/2016	Birmensdorf, Switzerland	Teaching data management and processing in R software.

Curriculum Vitae

Personal information

Name	Peters, Richard Louis
Address	Alfred Escher-Strasse 76 8002 Zürich, Switzerland
Telephone	+31 61 3106161
Email	richard.peters@wsl.ch
Date of Birth	6th of October, 1987
Nationality	Dutch
Gender	Male

Research interests

Tree physiology; Forest ecology; Mechanistic growth modelling; Tree hydraulics; Wood anatomy; Stable isotopes; Dendrochronology

Education

2014 – Present **PhD candidate in Dendrosciences**

Forest Dynamics Unit, Swiss Federal Research Institute for Forest, Snow and Landscape Research (WSL), Birmensdorf (Switzerland) / Department of Environment, Basel University, Basel (Switzerland)

Topic: Mechanistic understanding of tree hydraulics and wood formation under changing environmental conditions.

PhD thesis: Transpiration, Tracheids and Tree rings: Linking stem water flow and wood formation in high-elevation conifers (Defence: May 2018).

2009 – 2011 **MSc in Environmental Biology**

Department of Biology, Utrecht University,
Utrecht (the Netherlands)

Master thesis: The effect of priming and temperature on the decomposition of labile and recalcitrant litter.

Major: Ecology and Natural Resource Management

2006 – 2009 **BSc in Biology**

Department of Biology, Utrecht University,
Utrecht (the Netherlands)

Bachelor thesis: Effect of abiotic conditions on plant growth in turf ponds: A theoretical study on the terrestrialization process.

Interest: Theoretical Ecology, Tropical Ecology, Applied Biostatistics

2000 – 2006 **High School Graduate (Matura)**
Erfgooiers College, Huizen (the Netherlands)
Profile: Nature & Health with economics, geography and physics

Work experience

2016 – 2017 **Teaching assistant at the WSL**
Assisting at the European Dendroecological Fieldweek in Slovenia and France and Advanced Data Management and Manipulation in R courses. Supporting interns and master students within the Dendrosciences group.

2012 – 2014 **Visiting researcher in Tropical Forest Ecology**
Working within the Forest Ecology and Forest Management group at the Wageningen University (the Netherlands) on testing different statistical models to determine long-term growth changes in tropical trees from Thailand and Cameroon.

2011 – 2014 **Consultant in Ecology and Nature Conservation**
Working as an ecological consultant and model developer for ARCADIS Belgium/Nederland BV performing and managing national (Dutch and Belgium government) and international (European Commission) projects.

2010 – 2011 **Voluntary worker in Nature Conservation**
Voluntary work for the conservation of the Iberian wolf at the Iberian Wolf Recovery Centre (Portugal).

Personal skills

Language Dutch (native), English (full professional) and German/French (elementary).

Computer MS Office, Geographic Information Systems (IDRISI Andes, ArcGIS, ERDAS), statistical software (SPSS, R) and modelling software (STELLA, GRIND, Berkeley Madonna, MATLAB, R, Phytosim and Python).

Other Experience with teaching, spatial modelling, mechanistic growth modelling, programming in R, fieldwork, remote sensing and laboratory research.

Driving license In the possession of a class B driver's license.

Hobbies Playing guitar and piano, hiking, bouldering

Publication record

Accepted papers

Peters RL, Fonti P, Frank DC, Poyatos R, Pappas C, Kahmen A, Carraro V, Prendin AL, Schneider L, Baltzer JL, Baron-Gafford GA, Dietrich L, Heinrich I, Minor RL, Sonnentag O, Matheny AM, Wightman MG, Steppe K. In press. Quantification of uncertainties in conifer sap flow measured with the thermal dissipation method. *New Phytologist*

Peters RL, Balanzategui D, Hurley AG, von Arx G, Prendin AL, Cuny HE, Björklund J, Frank DC, Fonti P. 2018. RAPTOR: Row and position tracheid organizer in R. *Dendrochronologia* **47**: 10–16. doi: 10.1016/j.dendro.2017.10.003

Peters RL, Klesse S, Fonti P, Frank DC. 2017. Contribution of climate vs. larch budmoth outbreaks in regulating biomass accumulation in high-elevation forests. *Forest Ecology and Management* **401**: 147–158. doi: 10.1016/j.foreco.2017.06.032

Peters RL, Groenendijk P, Vlam M, Zuidema PA. 2015. Detecting long-term growth trends using tree rings: a critical evaluation of methods. *Global Change Biology* **21**: 2040–2054. doi: 10.1111/gcb.12826

Sánchez-Salguero R., Hevia A., Camarero JJ., Treydte K, Frank DC, Crivellaro A, Domínguez-Delmás M, Hellmann L., Kaczka RJ, Kaye M, Akhmetzyanov L, Ashiq MW, Bhuyan U, Bondarenko O, Camisón Á, Camps S, Constante García V, Costa Vaz F, Gavrila IG, Gulbranson E, Huhtamaa H, Janecka K, Jeffers D, Jochner M, Koutecký T, Lamrani-Alaoui M, Lebreton-Anberrée J, Martín Seijo M, Matulewski P, Metslaid S, Miron, S, Morrisey R, Opdebeeck J, Ovchinnikov S, **Peters RL**, Petritan AM, Popkova M, Rehorkova S, Rodríguez Ariza MO, Sánchez-Miranda A, Van der Linden M, Vannoppen A, Volařík D. 2017. An intensive tree-ring experience: connecting education and research during the 25th European Dendroecological Fieldweek (Asturias, Spain). *Dendrochronologia* **42**: 80–93. doi: 10.1016/j.dendro.2016.12.005

Lintunen A, Paljakka T, Jyske T, Peltoniemi M, Sterck F, von Arx G, Cochard H, Copini P, Caldeira MC, Delzon S, Gebauer R, Grönlund L, Kiorapostolou N, Lechthaler S, Lobo-do-Vale R, **Peters RL**, Petit G, Prendin AL, Salmon Y, Steppe K, Urban J, Roig Juan S, Robert EM, Hölttä T. 2016. Osmolality and Non-Structural Carbohydrate Composition in the Secondary Phloem of Trees across a Latitudinal Gradient in Europe. *Frontier in Plant Science* **7**: 1–15. doi: 10.3389/fpls.2016.00726

Petit G, von Arx G, Kiorapostolou N, Lechthaler S, Prendin AL, Anfodillo T, Caldeira MC, Cochard H, Copini P, Crivellaro A, Delzon S, Gebauer R, Gričar J, Grönholm L, Hölttä T, Jyske T, Lavrič M, Lintunen A, Lobo-do-Vale R, Peltoniemi M, **Peters RL**, Robert EMR, Juan SR, Senfeldr M, Steppe K, Urban J, Van Camp J, Sterck F. In press. Tree differences in biomass allocation and growth rate drive universal scaling in leaf area to sapwood area across Europe. *New Phytologist*

Ongoing papers

Peters RL, Speich M, Pappas C, Treydte K, Graf-Pannatier E, Kahmen A, Steppe K, von Arx G, Fonti P. In preparation. Contrasting plasticity of stomatal conductance to temperature and drought in high-elevation *Larix decidua* and *Picea abies*. *Plant, Cell & Environment*

Peters RL, Steppe K, Cuny HE, de Pauw D, Frank DC, Schaub M, Rathgeber CBK, Fonti P. In preparation. Turgidity, the engine behind radial wood growth in mature Alpine conifers. *New Phytologist*

Peters RL, Oertel A, Fonti P, Kahmen A, Frank DC, Saurer M, Graf-Pannatier E, Speich M, Treydte K. In preparation. Long-term intra-annual $\delta^{18}O$ transfer and fractionation from source to leaf water in mature *Picea abies* and *Larix decidua* trees.

Cuny HE, Fonti P, Rathgeber CBK, von Arx G, **Peters RL**, Frank DC. In review. Couplings in cell kinetics mitigate temperature influence on conifer wood anatomy. *Plant, Cell & Environment*

Pappas C, Fonti P, **Peters RL**, Frank DC. In preparation. Cross-scale patterns of temporal variability in tree-level carbon- and water-dynamics.

Books

Werner S, Szalai S, Kőpataki É, Kondor AC, Musco E, Koch H, Zsuffa I, Trombik J, Kuras K, Koeck M, Lakatos M, **Peters R**, Lambert S, Hlásny T, Adriaenssens V. 2014. Future imperfect: Climate change and adaptation in the Carpathians. UNEP, ISBN: 978-82-7701-145-5

Presentations

Peters RL, Frank DC, Treydte K, Steppe K, Kahmen A, Fonti P. 2017. How to make a tree ring: Coupling stem water flow and cambial activity in mature Alpine conifers. *EGU oral presentation.*

Peters RL, Klesse S, Fonti P, Frank D. 2016. Assessing the impact of larch budmoth outbreaks on tree biomass growth along an Alpine elevational gradient. *TRACE poster presentation.*

Peters RL, Frank DC, Treydte K, Fonti P. 2014. Coupling stem water flow and structural carbon dynamics. *EuroDendro poster presentation.*

Peters RL, Groenendijk P, Vlam M, Zuidema PA. 2012. Methods for detecting long-term growth changes in tropical tree rings: a critical comparison. *TRACE poster presentation.*

Balanzategui D, Hurley A, **Peters RL**, Kuznetsova V, Helle G, Heinrich I. 2018. Climate response of Scots pine tracheid cells across the European-Eurasian maritime-continental climate gradient. *TRACE poster presentation.*

Balanzategui D, Heußner KU, Wazny T, Helle G, **Peters RL**, Hurley A, Heinrich I. 2017. Wood anatomical proxies from lowland European oak and Scots pine for climate reconstructions. *TRACE oral presentation.*

Fonti P, Bryukhanova M, Sviderskaya I, **Peters RL**, von Arx G. 2017. Tracheid anatomical changes of Larix siberica under drought stress. *TRACE poster presentation.*

Zuidema PA, Groenendijk P, Vlam M, van der Sleen P, **Peters RL**. 2016. Reconstructing growth trends from tree-ring data: can we account for biases. *ATBC oral presentation.*

Speich MJR, **Peters RL**, Zappa M, Fonti P, Frank D, Treydte K, Kahmen A, Lischke H. 2016. Modelling ecohydrological processes on landscape scale: A ground truthing study on Alpine forests. *EcoSummit poster presentation.*

Groenendijk P, **Peters RL**, van der Sleen P, Vlam M, Bongers F, Zuidema PA. 2014. Tree-ring analysis to detect centennial-scale growth changes in tropical tree species. *TRACE oral presentation.*

Reviewer

Agricultural and Forest Meteorology; Dendrochronologia; PLOS ONE; Annals of Forest Science; Journal of Biogeography; Climate of the Past, Tree Physiology

The research described in this thesis was financially supported by the Swiss National Science Foundation, grant number 150205.

Printed by:
Swiss Federal Research Institute for Forest, Snow and Landscape Research (WSL), Zürcherstrasse 111, CH-8903 Birmensdorf, Switzerland